A study of Benguela Niños and Niñas from 1958 to 2015

By

Rodrigue Anicet IMBOL KOUNGUE

Department of Oceanography

University of Cape Town

This thesis is submitted for the degree of

Doctor of Philosophy

University of Cape Town April 2018

Dedication

I dedicate this thesis to my parents, Koungue Paul Benjamin and Koungue Jeanne, to my brother and sisters Ilik Arnaud Fabien, Mone Koungue Rosine Pamela and Ongtha Koungue Marlene Theophanie and my niece Ongbel Koungue Jessica Maelle. For all the support you have brought into my life during my academic journey.

Plagiarism declaration

I, **Rodrigue Anicet Imbol Koungue**, hereby declare that the work in this thesis is original and has been written by myself upon guidance of my supervisors Prof. Mathieu Rouault and Dr. Serena Illig (except where acknowledgement is made to the work of others) and that neither the content of this thesis nor any part of it has been submitted for another degree in this or any other university. I authorise the University to reproduce for the purpose of research either the whole or any portion of the contents in any manner whatsoever.

Signature: Signed by candidate Date: 6th April 2018

Declaration for inclusion of Publication

I confirm that I have been granted permission by the University of Cape Town's Doctoral Degrees Board to include the following publication in my thesis, and where co-authorships are involved, my co-authors have agreed that I may include the publication:

Imbol Koungue, R. A., S. Illig, and M. Rouault (2017), Role of interannual Kelvin wave propagations in the equatorial Atlantic on the Angola Benguela Current system, *J. Geophys. Res. Oceans*, 122, 4685–4703, doi:10.1002/2016JC012463.

Signature: Signed by candidate Date: 6th April 2018

Student name: Rodrigue Anicet Imbol Koungue Student number: RDRIMB001

Acknowledgements

First of all, I would like to thank the Almighty God for the strength and health he gave me to accomplish this Thesis.

I am extremely grateful to my supervisors Prof. Mathieu Rouault and Dr Serena Illig for their useful advice and guidance throughout this thesis. They were always available for me and it meant a lot to me.

I am grateful to all the Members and academic staff from the Department of Oceanography at the University of Cape Town. In particular, many thanks to Cashifa Karriem and Sharon Bosma for their helpful administrative work done during my studies at the University of Cape Town.

I would like to acknowledge the Nansen TuTu Centre for having trust in me and for giving me the opportunity to start my PhD project.

I would like to thank the investigators of the project PREFACE through which, I gained additional knowledge and established collaborations for the future.

I am very grateful to ICEMASA project for the funding I received to attend conferences overseas. It gave me opportunities to present my work and have good exposure to the scientific community.

I would like to express my appreciation to Dr Bernard Bourlès, through who I have been aware of this PhD project and who supported me during the application process.

I thank Professor Peter Brandt, who invited me in 2016 to participate in the research cruise M131 onboard of the German research vessel METEOR. It was a wonderful experience for me.

I am grateful to Dr Marek Ostrowsky, who invited me at the Institute of Marine Research (IMR) in Bergen, Norway and guided me on my project during my stay.

I would like to thank Dr Julien Jouanno from the University of Toulouse (LEGOS) who provided part of the model outputs used in this thesis.

A special thank you to Arielle Stela Nkwinkwa Njouodo for all the support, discussions we had, and good time spent together while doing our PhD at the University of Cape Town.

I express my gratitude to Mr Ngueti Joseph for the encouragements and support I received during this PhD project.

Abstract

Prediction and Research Moored Array in the Tropical Atlantic (PIRATA) records in combination with outputs from an Ocean Linear Model (OLM) and altimetric data are used to investigate the link between the equatorial Atlantic Ocean dynamics and the variability in the coastal region of Angola-Namibia at interannual timescales over 1998 to 2012. The PIRATA records help to define an index of equatorial Kelvin wave activities in the Equatorial Atlantic. There is a good agreement between PIRATA monthly dynamic height anomalies, altimetric monthly sea surface height anomalies (SSHA), and sea level anomalies calculated with an OLM at interannual time scales. This allows the interpretation of PIRATA records in terms of equatorial Kelvin wave propagations. Extreme warm or cold events in the Angola – Namibia area lag strong anomalous eastward equatorial propagations by 1–2 months. Remote equatorial forcing via equatorial Kelvin waves which propagate poleward along the west African coast as coastal trapped waves is at the origin of their developments. Results show a seasonal phasing, with significantly higher correlations between the equatorial index and coastal sea surface temperature anomalies (SSTA) off Angola-Namibia in October - April season. Then, a systematic study of all the Benguela Niño and Benguela Niña events before 1982 is done using an Ocean general circulation model in combination with the OLM outputs from 1958 to 2015. 26 anomalous strong coastal events (16 warm and 10 cold) are identified. The analysis of their evolution confirms the remote equatorial origin of most of these coastal anomalous strong events. Modelled meridional transport anomalies across the Angola Benguela Front (ABF) contribute to the development of these anomalous coastal warm events. Across the ABF, the results obtain with the net temperature transport are similar to the ones with net mass transport. Most anomalous events peak in October - April season. Lagged composites of surface temperature and wind stress anomalies in the equatorial and southeastern Atlantic reveal that both local and remote forcings develop simultaneously 1-2 months before the peak of Benguela Niño or Niña. At the monthly scale, local atmospheric forcing is more correlated with anomalous coastal events occurring in Southern Angola which is a non-wind-upwelling driven region. The results from this thesis open the possibility to predict Benguela Niño and Benguela Niña events using an index depicting the equatorial interannual variability associated with Interannual Equatorial Kelvin Wave propagation, especially from October to April when the coastal stratification is favourable to the imprint of coastal trapped waves in the surface layer.

TABLE OF CONTENTS

LIST OF FIGURES

LIST OF TABLES

LIST OF ACRONYMS

ABA: Angola Benguela Area

ABUS: Angola Benguela Upwelling System

ABF: Angola Benguela Front

AC: Angola Current

ADCP: Acoustic Doppler Current Profiler

AG: Angola Gyre

AVHRR: Advanced Very High-Resolution Radiometer

AVISO: Archiving, Validation and Interpretation of Satellite Oceanographic Data.

BC: Benguela Current

BUS: Benguela Upwelling System

CalUS: California Upwelling System

CTW: Coastal Trapped Waves

CUS: Canary Upwelling System

DFS: DRAKKAR Forcing Set

DFS5: DRAKKAR Forcing Set version 5

DFS5.2: DRAKKAR Forcing Set version 5.2

DYNH: Dynamic Height

EBUS: Eastern Boundary Upwelling System

EKW: Equatorial Kelvin Wave

EUC: Equatorial Under Current

GC: Gabon Current

HUS: Humboldt Upwelling System

IEKW: Interannual Equatorial Kelvin Wave

IRI: Institute for Climate and Society

ITCZ: Intertropical Convergence Zone

KW: Kelvin Wave

NOAA: National Oceanic and atmospheric Administration

NBUS: Northern Benguela Upwelling System

NN: Northern Namibia

OGCM: Ocean General Circulation Model

OI-SST: Optimum Interpolation Sea Surface Temperature

OI-SST v2: Optimum Interpolation Sea Surface Temperature version 2

OLM: Ocean Linear Model

PIRATA: Prediction and Research Moored Array in the Tropical Atlantic

RMSD: Root-Mean-Square Difference

SA: Southern Angola

SAA: South Atlantic Anticyclone

SECC: South Equatorial Counter Current

SEUC: South Equatorial Under Current

SLA: Sea Level Anomaly

SSH: Sea Surface Height

SSHA: Sea Surface Height Anomalies

SST: Sea Surface Temperature

SSTA: Sea Surface Temperature Anomalies

STD: Standard Deviation

T10: Temperature at 10 m

T10A: Temperature at 10 m Anomalies

TRMM TMI: Tropical Rainfall Measurement Mission's Microwave Imager

WOA: World Ocean Atlas

WOA13 v2: World Ocean Atlas 2013 version 2

Z20: Depth of the isotherm 20°C

ZWS: Zonal Wind Stress

CHAPTER 1

1 INTRODUCTION

Eastern Boundary Upwelling Systems (EBUS) are among the most productive marine ecosystems in the world ocean supporting important fisheries [*Bakun et al.,* 2015]. While EBUS cover less than 1% of the world ocean surface, they provide around 20% of the fish catch [*Fréon et al.,* 2009]. They are present on both hemispheres in the Pacific Ocean (Peru/Chile or the Humboldt Upwelling System (HUS, **Figure 1.a**) in the south and the California Upwelling System (CalUS, **Figure 1.b**) in the north) and in the Atlantic Ocean (the Canary Upwelling System (CUS, **Figure 1.c**) along the northwest African coast and the Benguela Upwelling System (BUS, **Figure 1.d**) in the south Atlantic). The four major EBUS are subject to the atmospheric circulation associated with the subtropical gyres of the Atlantic and the Pacific Oceans. EBUS are located on the eastern side of the quasi-stationary high-pressure cells, where their dynamics is driven by the prevailing equatorward winds of the eastern flanks of the subtropical high pressure system (**Figure 1.1,** top panels). In association with the Coriolis force and the presence of the coastal boundary, coastal alongshore winds blowing equatorward induce an offshore surface Ekman flow. Following the principle of mass conservation, this offshore advected surface water is replaced by deeper, cold, nutrient-rich waters with high CO_2 concentrations, low pH, and low oxygen concentrations [*Garcia-Reyes et al.*, 2015]. This mechanism, called coastal upwelling, is responsible for surface cooler than normal temperature (**Figure 1.1,** top panels) and high chlorophyll concentrations (**Figure 1.1,** bottom panels) in the sunlit layer of the coastal fringe. Many factors can modulate the intensity of the coastal upwelling most notably the slope of the continental shelf, the shape of the coast, the intensity or direction of the wind, and the water column stratification. One of the most important features of the EBUS is that there is an enhanced biological production with high primary production (**Figure 1.1,** bottom panels) in these zones. Therefore, an important pelagic fish stock is found in the EBUS. During the upwelling season, upwelling regions show important primary production, therefore planktonic organisms, including larval fish and invertebrates, grow in the coastal

productive habitat [*Chavez et al.,* 2009]. The economy of countries neighbouring EBUS areas rely considerably on these marine resources for food and employment. There is an urgent need to increase capacity to predict changes in ecosystem structures as they are vital for the neighbouring societies.

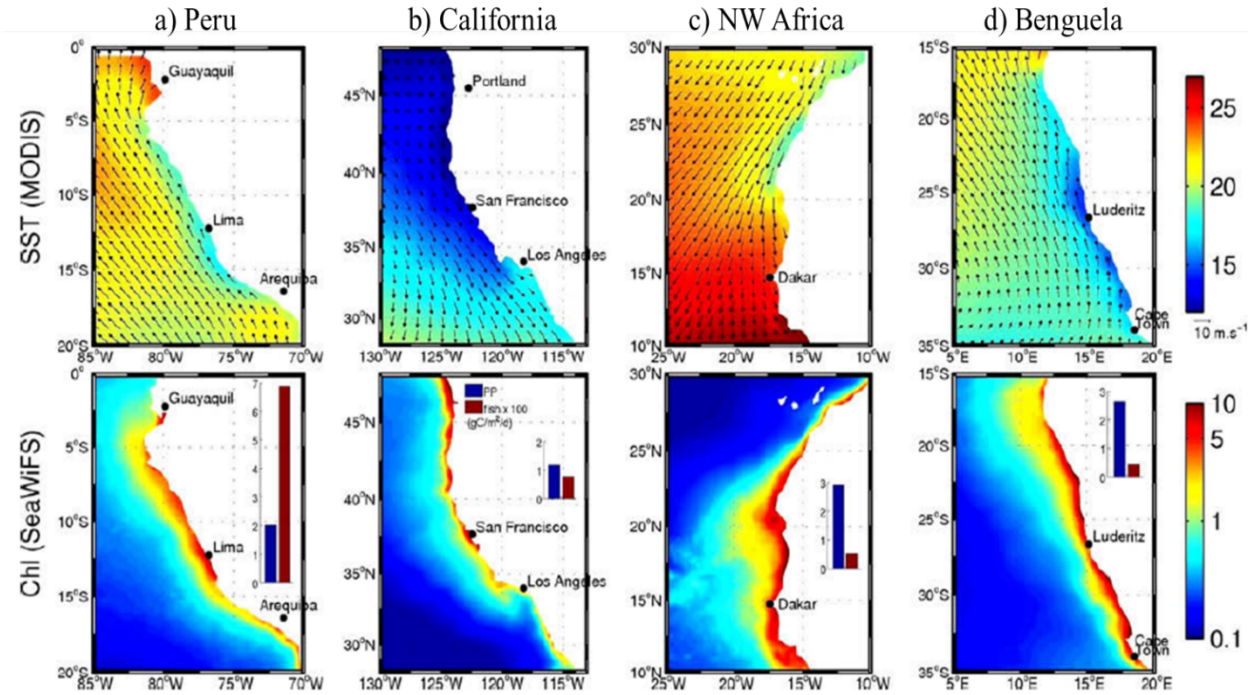

Figure 1.1: High resolution maps of Sea Surface Temperature (SST), winds and chlorophyll-a for the four major EBUS. SST (colour shading in top panels) were estimated using MODIS monthly data (ftp://podaac.jpl.nasa.gov/OceanTemperature) and averaged from July 2002 to April 2008; chlorophyll-a concentrations (colour shading in bottom panels) were estimated from SeaWiFS monthly data (https://oceancolor.gsfc.nasa.org) and averaged from September 1997 to September 2007; surface winds are estimated from QuikSCAT weekly scatterometer data [*Liu et al.,* 1998] and averaged from July 1999 to July 2008. All products were regridded on the QuikSCAT grid (0.25°×0.25°). Inserts in the chlorophyll-a maps show the mean primary productivity (blue bar) and fish catch (red bar) averaged over the 1998–2005 period. Figure from *Chavez et al. [*2009].

After a brief overview of EBUS worldwide, the introduction will now focus more specifically on the dynamic of southeast Atlantic region where the BUS is located. This chapter will be organized in four sections: Section 1.1 describes the mean atmospheric and oceanic features as well as the surface and subsurface circulation in the Angola-Benguela Upwelling System (ABUS). Section 1.2 describes the major interannual warm and cold events in the ABUS also called Benguela Niños or Niñas respectively. Section 1.3 will focus on the description of the main forcing mechanisms responsible for the generation of Benguela Niño or Niña events. Section 1.4 will then present the objectives and outline of this thesis.

1.1 PRESENTATION OF THE STUDY AREA: THE SOUTHEASTERN ATLANTIC OCEAN

1.1.1 Mean atmospheric and oceanic key features, surface and subsurface currents

Compared to the other EBUS, one of the main specific features of the BUS is that it is encircled by warm waters at his northern and southern boundaries: tropical water from the equatorial Atlantic in the north and warm-water coming from the Agulhas Current in the south. This is well observed in **Figure 1.2** (left panel) which illustrates the SST and wind stress in austral summer in the southeast Atlantic Ocean. The convergence zone between the warm equatorial waters and the cold upwelled waters from the BUS form a well-defined meridional thermal front called Angola-Benguela Front (ABF) [*Shannon et al.,* 1987; *Mohrholz et al.,* 2001; *Veitch et al.,* 2006] as observed in **Figure 1.2.** Temperature values across the ABF (difference between the northern and southern boundaries of the frontal zonal) are 2.4°C in austral winter and 4.2°C in austral summer [*Veitch et al.,* 2006]. *Veitch et al.* [2006] also found a meridional SST gradient of 1°C per 34 km across the ABF in austral summer, whereas a 4°C per degree latitude meridional gradient was estimated by *Colberg and Reason* [2006] in the middle of the ABF. The location of the ABF changes seasonally: ~16°S in austral winter [*Veitch et al.,* 2006] and further south at ~17.5°S in austral summer [*Shannon et al*., 1986; *Colberg and Reason,* 2006, 2007; *Veitch et al.,* 2006; *Veitch et al.,* 2010]. The ABF zone is also presented as a transition zone between the north tropical ecosystem in Angola and the Northern Benguela Upwelling System (NBUS, from 19°S to 24°S). The ABF is a challenging area to model. The ABF zone is indeed a zone of strong

warm SST bias in numerical model especially in coupled ocean-atmosphere model [*Richter and Xie,* 2008; *Li and Xie,* 2012; *Richter et al*., 2012; *Toniazzo and Woolnough,* 2014; *Richter et al.,* 2014] which can peak up to 8°C [*Koseki et al.,* 2017].

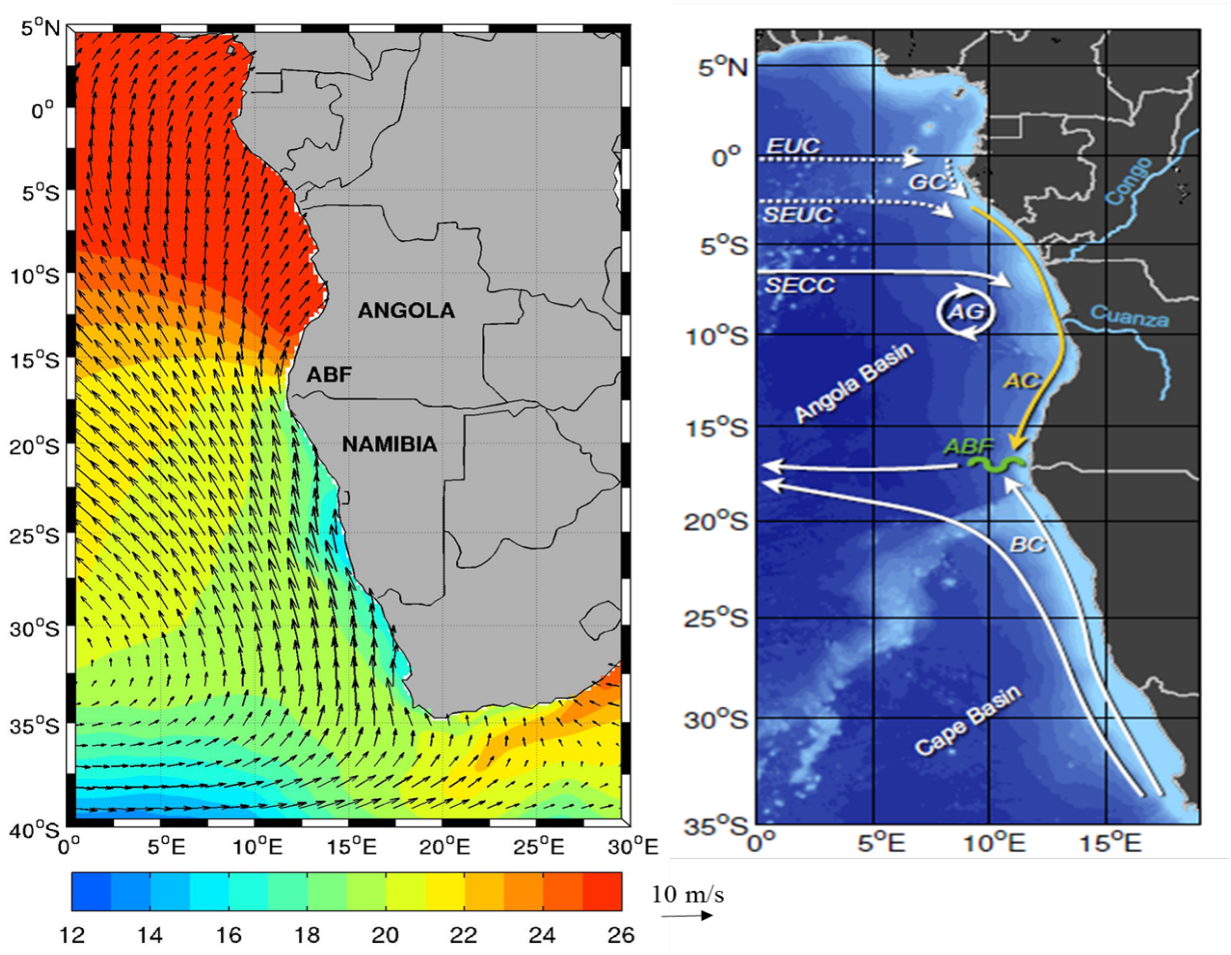

Figure 1.2: Left panel: AVHRR SST [*Riesen and Chelton*, 2008] and SCOW wind stress [*Risien and Chelton*, 2008] averaged in austral summer (October to March) from September 1999 to October 2009. Right panel: Schematic representation of ocean currents in the southeastern Atlantic Ocean. Main features are the Equatorial Undercurrent (EUC), the South Equatorial Undercurrent (SEUC), the South Equatorial the Counter Current (SECC), the Gabon Current (GC), the Angola Gyre (AG), the Angola Current (AC), the Benguela Current (BC), and the Angola-Benguela Frontal (ABF). Figure from *Kopte* [2017].

The causes of the large warm SST biases in the ABF zone are still under debate. *Meeuwis and Lutjeharms* [1990] observed that the southeast Atlantic was under the influence of the seasonal shift of the South Atlantic Anticyclone (SAA) which also influences the location of the ABF. **Figure 1.2** (left panel) shows that along the west African coast, the wind stress is mostly southerly (alongshore). The wind stress is stronger south of the ABF where it drives a strong upwelling mainly south of 15°S up to the southern tip of Africa [*Rouault et al.,* 2007]. North of the ABF, the wind stress is weaker throughout the year [*Ostrowski et al.,* 2009]. Another key feature in the southeast Atlantic is the presence of the Angola Gyre (AG) north of the ABF, illustrated in **Figure 1.2**, right panel. The AG is a cyclonic gyre [*Mercier et al*., 2003] and was for the first time described in detail by *Moroshkin et al.* [1970] during an oceanographic survey from in 1968. During this survey, the cyclonic gyre was visible through maps of dynamic topography. These maps revealed a cyclonic motion from surface to 300 m depth, located ~14°S and 4°E, in which the sea surface height is about 8 dynamic centimeters lower than the surrounding region, and a spatial extension of ~1000 km [*Moroshkin et al*., 1970; *Gordon and Bosley* 1991]. The center of the cyclonic gyre is characterized by high salinity surface water caused by a regional excess of evaporation [*Gordon and Bosley,* 1991] and by low oxygen thermocline water [*Bubnov,* 1972; *Gordon and Bosley,* 1991]. This might result from the high productivity caused by a shallow thermocline and nutricline [*Voituriez and Herbland,* 1982] and a regeneration of water mass in this zone which is a slow process [*Poole and Tomczak,* 1999].

In the southeastern Atlantic Ocean, the variability of the ABUS is under the influence of different type of currents flowing either at the surface or in the subsurface (counter currents or poleward currents) as illustrated in **Figure 1.2,** right panel [*Rouault et al.*, 2007; *Kopte,* 2017]. The oceanic circulation is shown in **Figure 1.2** (right panel) for the late austral summer based on cruise datasets from past studies [*Gordon and Bosley***,** 1991; *Shannon and Nelson,* 1996; *Gammelsrød et al.,* 1998; *Stramma and Schott,* 1999; *Lass et al*., 2000; *Mercier et al.,* 2003; *Schott et al.,* 2004]. This includes from the equator to the south Pole: The Equatorial Under Current (EUC) which is an eastward flowing subsurface current (it flows opposite to the trade winds following the depth-dependent eastward pressure gradient [*Brandt et al.,* 2014]). The EUC is mainly fed by the waters coming from the north Brazil Current which flows northward along the Brazilian coast in the western part of the Atlantic Ocean [*Hazeleger et al.,* 2003]. The EUC transports high-saline and oxygen-rich water masses eastward along the equatorial Atlantic from

the western boundary. Further East, from 1°S to ~6°S the poleward Gabon Current (GC) is a subsurface flowing current, fed partly by the EUC [*Wacongne,* 1988; *Verstraete,* 1992]. South of the EUC, the South Equatorial Under Current (SEUC) flows eastward below the thermocline between 3°S to 5°S [*Mercier et al*., 2003]. South of the SEUC, between 7°S and 9°S [*Gordon and Bosley,* 1991], there is a remarkable eastward flowing current called the South Equatorial Counter Current (SECC) which turns southward towards the African coast. Like the EUC, relative maxima in salinity or oxygen characterize the SECC and SEUC. The SECC contributes to the northern limb of the AG [*Mercier et al*., 2003]. The southward-flowing warm Angola Current (AC) is found on the eastern limb of the AG. Past studies suggested that the AC is fed by the equatorial current system composed of the EUC, SEUC and the SECC [*Peterson and Stramma,* 1991; *Wacongne and Piton,* 1992]. Past studies described the AC in terms of current velocity and transport using synoptic hydrographic measurements [*Moroshkin et al.*, 1970; *Dias, 1983a,b*; *Mercier et al.,* 2003]. The AC is a fast current flowing along the west African coast of Southern Africa with velocities between 30 and 50 cm s^{-1}. The AC flows between the surface and ~300 m - 400 m depth and advects tropical warm, saline, low oxygen and nutrient-rich water southward. The AC is shown to be a subsurface geostrophic southward current [*Moroshkin et al.*, 1970; *Dias, 1983a,b*; *Mercier et al.,* 2003] between 9°S and 16°S. Transport values of the AC of 1.2 Sv and 3.7 Sv were calculated by *Dias* [1983] during cruises in September 1970 and July 1971 respectively at 12°S. Sometimes, the AC breaks through the ABF and continues flowing as poleward undercurrent below the thermocline [*Lass et al.,* 2000; *Mohrholz et al*., 2001]. *Nelson* [1989] has reported the poleward undercurrent as an extension of the AC which is stronger (weaker) in austral summer (winter). Modelling study of *Veitch et al.* [2010] showed that the poleward undercurrent flows north of 28°S and is mainly driven by the wind stress curl via the Sverdrup relation. Recently, *Kopte et al.* [2017] provided useful information of the mean properties and variability of the AC using for the first time ~2.5 years (July 2013 to October 2015) velocity observations around 11°S from a mooring array. This is a good starting point to give useful insights into the AC variability and transport and to help comparing and validating ocean model simulations. In combination with other ship measurements, *Kopte et al.* [2017] found that the AC core ranges between 50 m - 100 m depth with the mean southward alongshore velocity (~8 $cm.s^{-1}$) located between 50 m - 60 m depth. *Kopte et al.* [2017] estimated a mean southward transport in the AC of 0.32 ± 0.05 Sv using 13 shipboards velocity sections. At

seasonal timescales, this southward transport showed bimodal variations with maxima in March-April and September/October at 11°S.

In the Angola basin, other features likely to be considered are the Congo River and the Cuanza River runoffs. The Congo River has the second largest worldwide annual discharge in the ocean [*Materia et al*., 2012]. According to *Eisma and Van Bennekom* [1978], Congo River runoff (~6°S) varies seasonally between 2.90×10^4 m^3/s in austral winter (July–August) and 6.0×10^4 m^3/s in austral summer (December). During the austral summer (December/January), the Cuanza River (~9°S) runoff reaches its maximum freshwater discharge along the coast of Angola [*Mohrholz et al.,* 2001]. High precipitation rate occurs at the African coast in the eastern equatorial Atlantic in austral summer. In the upper layers, strong stratified water column is observed at the locations of the Congo and Cuanza River runoffs and in the surrounding areas. *Eisma and Van Bennekom* [1978] showed that strength in runoffs from Congo and Cuanza Rivers depends on the precipitation rate at the African coast and in the respective drainage areas. *Berrit and Dias* [1977] observed from their hydrographic section a decrease in sea surface salinity off Lobito (Angola) ~1psu between December and March before becoming high again in May up to rest of the year. This decrease in sea surface salinity was confirmed on the sea surface salinity charts of *Merle* [1978] in which a poleward advection of freshwater along the African coast from Congo River was observed.

South of the ABF, the northwestward flowing cold geostrophic Benguela Current is represented. The Benguela Current is an eastern boundary current linked to the BUS, (**Figure 1.1d**). Benguela Current is part of the eastern limb of the anticyclonic gyre in the southern Atlantic and flows along the continental shelf of South Africa (~35°S) up to ~14°S off Angola [*Field and Shillington,* 2006]. The width of Benguela Current varies spatially. The Benguela Current appears to be 200-300 km wide at its southern part and ~750 km wide at its northern part **[***Wedepohl et al.,* 2000] and is found in the upper 1000 m [*Garzoli and Gordon,* 1996]. *Lass and Mohrholz* [2008] observed that around 19°S, Benguela Current bends westward or northwestward and feeds the South Equatorial Current. But part of its flow continues northward along the coast and enters in the Angolan waters. A transport of 28 ± 4 Sv of the Benguela Current feeding the South Equatorial Current was estimated by *Mercier et al.* [2003]. From 500 m – 1200 m, past studies estimated the volume transport in the Benguela Current between 13 - 31 Sv [*Fu,* 1981; *Shannon,* 1985; *Stramma and Peterson,* 1989; *Garzoli and Gordon,* 1996]. The

Benguela Current is formed from water masses coming from the South Atlantic Current, the Agulhas Current and the southeast coastal current that flow along the African coast [*Mercier et al.*, 2003], but the sharing amounts from these different sources are still under debate [*Lass and Mohrholz*, 2008]. In the BUS, the coastal variability is also associated with the strong oceanic intrinsic variability, characterized by a large variety of meso- and submeso-scales features (eddies, filaments, fronts), observed in the distribution of the physical and biogeochemical tracers. Some of these eddies are locally generated via horizontal and vertical shear between the Benguela Current and the alongshore undercurrent [*Marchesiello et al.,* 2003; *Penven et al.*, 2005]. This creates a baroclinic instability which leads to the formation of mesoscale eddies propagating westward and transporting coastal physical and biogeochemical properties into the open Ocean. Some of the meanders encountered in the BUS are originating from the retroflection of the Agulhas Current in the south Atlantic. These large eddies, the Agulhas rings, coming from the retroflection of the Agulhas Current are composed of warm, salty and oxygen-rich waters from the Indian Ocean. During their intrusion in the South Atlantic, the warm, salty and oxygen-rich waters transported in the rings are mixed with the cold and oxygen-poor waters from the BUS.

1.2 DESCRIPTION OF BENGUELA NIÑO/NIÑA INTERANNUAL EVENTS

The BUS is one of the most productive marine ecosystems in the world supporting a large marine ecosystem (**Figure 1.1d**). It undergoes important variability at a wide range of frequencies and in particular at interannual timescales. Every few years, the BUS is indeed subject to the intrusion of anomalously warm waters from the tropical Atlantic. These events are called Benguela Niños [*Shannon et al.,* 1986]. Benguela Niños typically manifest along the coast of Angola and Namibia in the southeast Atlantic Ocean. They are similar to El Niño phenomenon along the equatorial Pacific Ocean and along the coast of Peru, but with less intensity and they are less frequent than El Niño events. These anomalously warm events tend to reach their maximum during the late austral summer mainly during March-April and originate from the relaxation of zonal wind stress in the western part of the equatorial Atlantic in January-February [*Florenchie et al.*, 2003, 2004; *Rouault et al.,* 2007; *Lübbecke et al.*, 2010]. During a Benguela Niño event, sea surface temperature (SST) can peak up to 4°C more than the seasonal

average [*Rouault et al.*, 2017]. These extreme coastal events can last from few months to half a year or more [*Rouault at al*., 2003; *Florenchie et al*., 2004; *Rouault,* 2012].

Figure 1.3 illustrates the evolution of the 2010/2011 Benguela Niño using SST anomalies (SSTA) from monthly climatology derived from Tropical Rainfall Measurement Mission's (TRMM) Microwave Imager (TMI). The 2010/2011 Benguela Niño reaches its

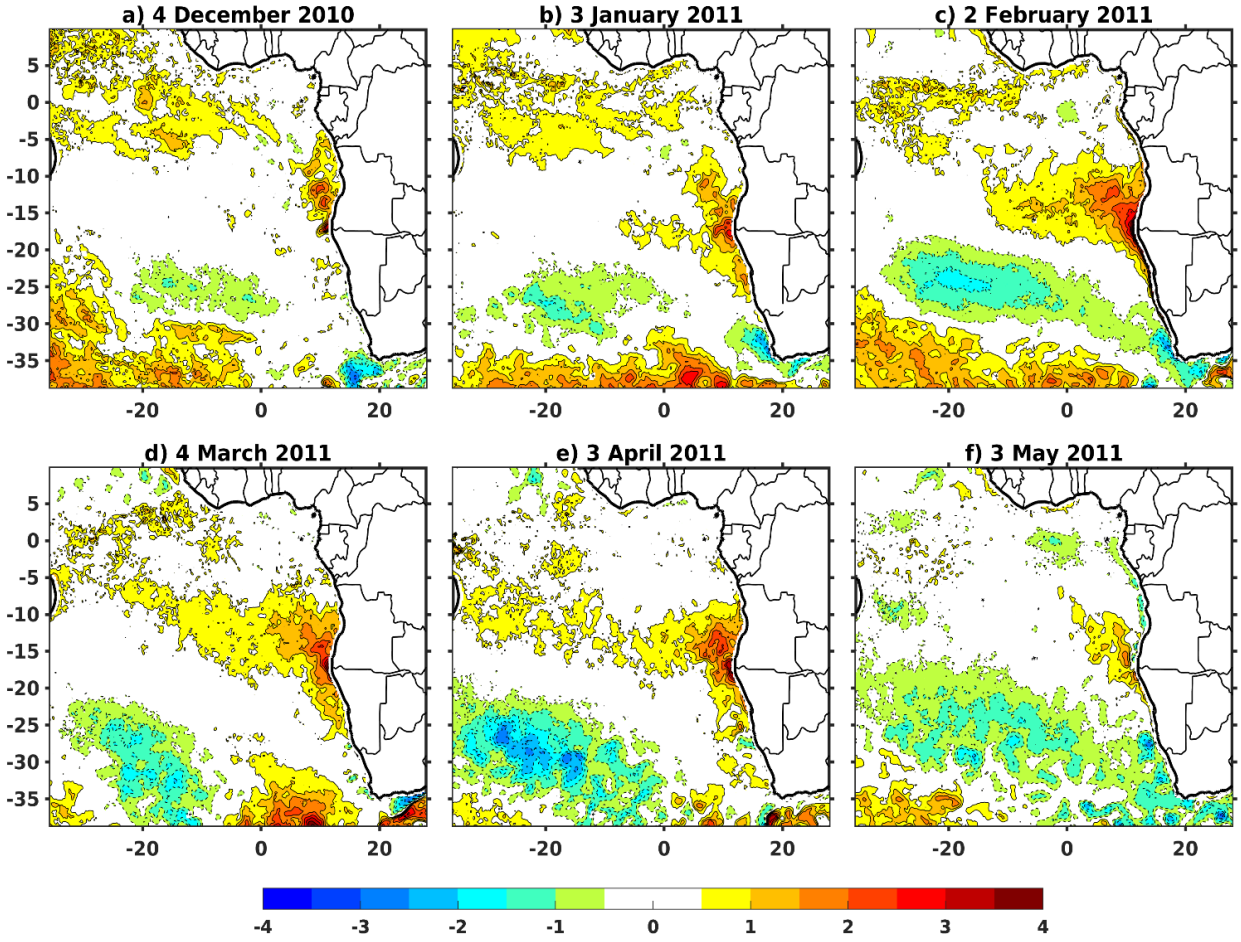

Figure 1.3: From top to bottom and left to right: TRMM TMI SST interannual anomaly from December 2010 to May 2011. Dates correspond to the middle of the monthly time period considered for averaging. Anomalies are departures from the 1998-2011 monthly climatology. Figure from *Rouault et al.* [2017].

maximum in February 2011 along the Angola – Benguela Current system. SSTA persist till April 2011 and propagate poleward (**Figure 1.3**). May 2011 marks the demise of the warm event. The

2010/2011 Benguela Niño is different from the other Benguela Niños as it does not peak in March-April, but in January and it starts in October 2010. The inverse of the Benguela Niño event is the Benguela Niña event [*Florenchie et al.,* 2004] and Benguela Niña has not been extensively studied in the literature. Benguela Niño event is associated with an anomalously poleward transport of warm waters in the Northern Benguela Upwelling system (NBUS) [*Rouault,* 2012] which could lead to a reduction of the local upwelling [*Bachèlery et al.,* 2016a] or could be linked to local upwelling of warm nutrient-poor tropical waters as in 2001 [*Rouault et al.,* 2007]. Couple of major warm or cold events have been documented in the literature. For instance, the first warm event described was the one occurring between March and July 1934. This warm event was first reported by *Walter* [1937] and cited by *Shannon et al.* [1986]. During the 1934 warm event, SST was 2 - 3°C above the climatological mean at Swakopmund (23°S) located north of Walvis Bay in Namibia. *Shannon et al.* [1986] also reported the occurrence of Benguela Niño events in 1949, 1963 and 1984. *Gammelsrød et al.* [1998] observed that the upper ocean temperature anomalies were high (up to 8°C above the seasonal mean) along the coast of Angola and Namibia in March 1995. The 1995 Benguela Niño was the warmest coastal event since 1984 [*Gammelsrød et al.,* 1998]. According to *Gammelsrød et al.* [1998], the 1995 Benguela Niño was associated with negative sea surface salinity anomalies along the Angolan coast and positive subsurface salinity anomalies along the Namibian coast. *Mercier et al.* [2003] estimated 11 Sv of transport in the AC using the World Ocean Circulation Experiment (WOCE) line A13 sampling from January to March 1995 corresponding to the Benguela Niño year reported by *Gammelsrød et al.* [1998] and others. Poleward undercurrent plays an important role during Benguela Niño in austral summer by advecting more tropical water into the NBUS [*Bachèlery et al.,* 2016a]. Also, based on their modelling study in the NBUS, *Muller et al.* [2014] suggested that during the austral summer (DJF), a strong poleward undercurrent combined with an on-shelf transport leaded to an increased upwelling between 22°S and 25°S. *Rouault et al.* [2007] described the major warm event 2001 using TMI SST. They observed the presence of warmer than normal SST along the Angola – Namibian coastlines between February and April 2001. The strongest Benguela Niño since 1995 occurred in 2010/2011 (**Figure 1.3**) and it has been studied recently by *Rouault et al*., [2017]. Besides Benguela Niño events, quick coastal events with less intensity occur along the Angola – Benguela Current system and are categorized as minor (moderate) coastal event or less intense events. According to the literature, the study by

Reason et al., [2006] using extended SST from National Oceanic and Atmospheric Administration (NOAA) averaged in the Angola – Benguela Area (ABA, 8°E - 15°E; 10°S – 20°S) revealed that minor coastal warm events were observed in 1986, 1988, 1991, 1996, 1997/98 [*Boyd et al.,* 1987; *Carton and Huang,* 1994; *Reason et al.* 2006]. Extreme cold events or Benguela Niñas occurred in 1978, 1982, 1983, 1991/92, 1997 and 2004 [*Florenchie et al.,* 2004; *Reason et al*., 2006]. According to *Florenchie et al.* [2004], on average, Benguela Niña events seem to last longer than Benguela Niños along the Angola – Benguela Current system. *Lübbecke et al*. [2010] using interannual times series analysis of SST averaged along the equatorial Atlantic (ATL3 box, [20°W - 0°E; 3°S – 3°N]) and in the ABA box, suggested that the Benguela Niño (Niña) was followed by strong warming (cooling) in the eastern equatorial Atlantic called Atlantic Niño (Niña). The time lag ranged between one to three months due to the difference in thermocline depth in the 2 regions consistent with *Rouault et al.* [2009]. This tendency of Atlantic Niño to follow Benguela Niño was confirmed by *Richter et al.* [2010] using composite maps of a coupled ocean–atmosphere model in the tropical Atlantic. Moreover, *Lübbecke et al*. [2010] argued that these two types of events (Atlantic and Benguela events) should be seen as one phenomenon due to the observed high correlations. Forcing related to Benguela Niños or Niñas will be discussed further below in **section 1.3**. Past studies reported that Benguela Niño events have a strong impact on the local marine ecosystem [*Binet et al.,* 2001; *Boyer and Hampton,* 2001] as the BUS is one of the most productive marine ecosystems in the world. During a Benguela Niño event, anomalously warm, poor–oxygen and nutrients tropical waters penetrate into the NBUS and affect primary productivity and thus the food availability to higher trophic levels [*Chassot et al.,* 2010]. The presence of low nutrients and oxygen waters in the NBUS can lead to devastating consequences on the distribution of marine species and on the marine ecosystems in the Angola Benguela upwelling system (ABUS) [*Monteiro and van der Plas, 2006*]. During the 1963 Benguela Niño off Namibia coast, temperature and salinity peaked in June 1963 [*Shannon et al.,* 1986]. According to *Schülein et al*. [1995], no sardine eggs were present during the main spawning months in NBUS [*Stander and De Decker* 1969]. The 1984 Benguela Niño was marked by a major poleward transport of the sardine stocks which leads to low level of abundance of fish stocks in the Namibian waters [*Le Clus* 1985]. Between 1993 and 1996, poor recruitment and decreasing catch rates of sardine stocks in the NBUS were attributed to low level of oxygen during 1993/1994 and the occurrence

of a Benguela Niño in 1995 [*Boyer et al.*, 2001].

Benguela Niño events have a significant influence on the southern African rainfall [*Rouault et al.*, 2003; 2009; *Lutz et al.,* 2015]. The occurrence of the warm events along the Angola – Benguela Current system in late austral summer concomitantly with the maximum of the annual cycle of SST and rainfall there, leads to an increase in atmospheric instability, evaporation and coastal rainfall [*Hirst and Hastenrath*, 1983]. Benguela Niño events are associated with floods mainly along the western coast of Angola and Namibia [*Hirst and Hastenrath*, 1983] and above average rainfall in the Namib Desert [*Shannon et al.,* 1986; *Rouault et al.,* 2003]. These anomalous coastal warm events can also influence rainfall further inland [*Rouault et al.*, 2003]. According to the significant impacts (societal, environmental and economic) associated with the development of these extreme warm events mostly on the marine ecosystem in the BUS and on the southern Africa climate, it would be useful to forecast these extreme coastal warm events and implement an early warning system.

1.3 FORCING MECHANISMS LINKED TO BENGUELA NIÑOS/NIÑAS

The forcing mechanisms responsible for the interannual variability of SST in Angola – Benguela Current system are discussed in this section and are still under debate. Two principal forcings are mentioned in the literature: Firstly, the local atmospheric forcing mainly explained by variations in the coastal wind stress along the coast of Angola and Namibia. Secondly, the remote oceanic forcing mainly explained by the propagation of interannual equatorial Kelvin waves (IEKW) along the equatorial Atlantic, which then, at the African coast, propagate poleward as Coastal Trapped Waves (CTW) [*Hardman-Mountfjord et al.,* 2003; *Schouten et al.,* 2005; *Polo et al.*, 2008].

1.3.1 Role of the local forcing along the Angola – Benguela Current system

In the literature, some studies emphasized that at interannual timescales, Benguela Niño events along the Angola – Benguela Current system are locally driven by local alongshore wind

anomalies categorized as the local atmospheric forcing. Strong or weak alongshore wind enhance or decrease the upwelling of subsurface cold waters and will cool or warm the BUS.

At interannual timescales, *Richter et al.* [2010] showed using observations and a coupled ocean–atmosphere simulation that local alongshore wind modulations (local atmospheric forcing) are responsible for the coastal SST variability in the southeast Atlantic Ocean. They further emphasized that alongshore wind anomalies generated by a basin-scale weakening of the South Atlantic Anticyclone (SAA) started ~3 months before the peak of SST anomalies (**Figure 1.4**).

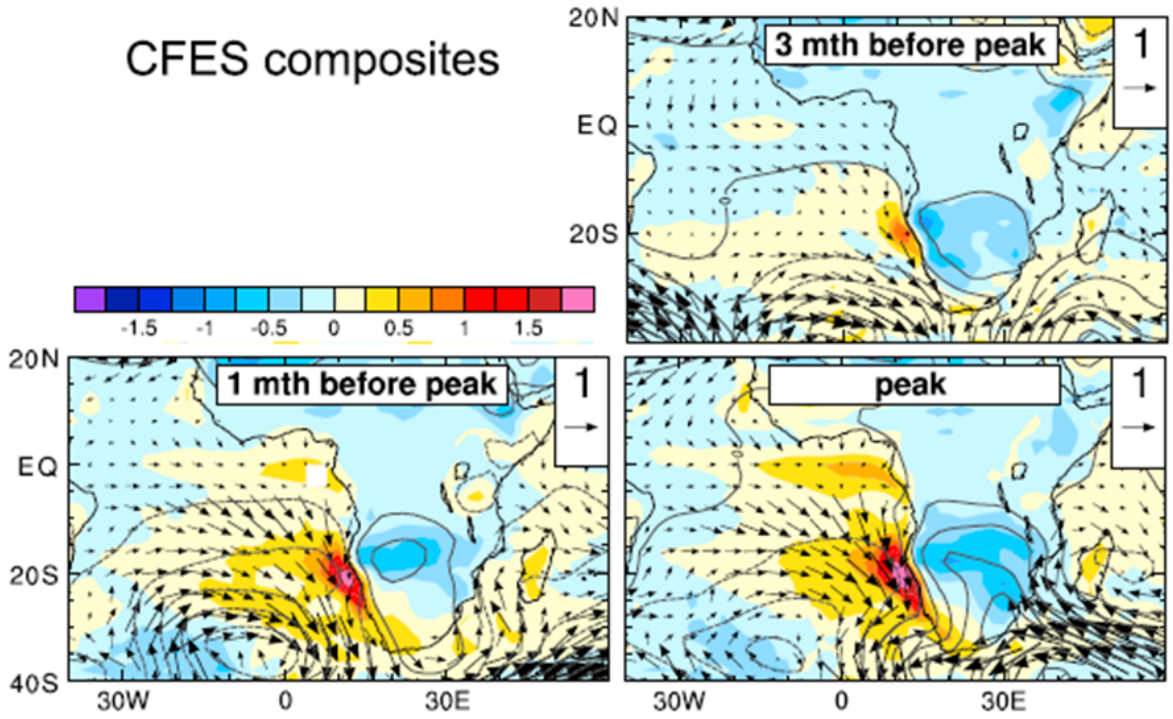

Figure 1.4: Simulated anomalous SST (colour; °C; land areas indicate ground temperature), surface wind stress (arrows; N m^{-2}*100), and sea level pressure (contours; 0.25 hPa interval) composited on the ABA SST index. Only events with standard deviations greater than 2 are selected. Dashed contour lines indicate negative values. Figure from *Richter et al*. [2010].

Results from the regression analysis performed by *Richter et al.* [2010] using daily mean of SST

and wind field in the South Atlantic suggested that SST responded to individual wind anomalies within a couple of days, mostly around 20°S. These individual wind bursts could be further enhanced by local air–sea interactions [*Richter et al.,* 2010]. Using an atmospheric general circulation model coupled to an ocean model in the Atlantic Ocean, *Trzaska et al.* [2007] showed that at interannual timescales, SST variability in the South Atlantic is primarily modulated by the intensity of the basin scale variations of the SAA which is consistent with the findings of *Richter et al.* [2010]. At interannual timescales, weakening of the SAA could be attributed to climate conditions over the adjacent continents [*Seager et al.,* 2003; *Richter and Xie,* 2008], the position of the Atlantic Intertropical Convergence Zone (ITCZ) and influences from the Indian and Pacific Oceans variability. As an example, *Richter et al.* [2010] using satellite data of SST and Sea Surface Height (SSH) during the 1995 Benguela Niño, showed that there was no evidence for the propagation of equatorial Kelvin waves prior to the onset of this extreme event.

Recently, *Junker et al.* [2015] using a regional ocean circulation model investigated the link between the wind stress curl and the meridional transport in the BUS during the period 2000 – 2008. They showed that south of the ABF between 20°S and 25°S in the NBUS, along the west African coast, the annual and semi-annual cycles of the local forcing through the wind stress curl is important for the poleward transport of warm tropical waters in the NBUS which is one of the key elements for the development of Benguela Niño [*Rouault,* 2012]. However, due to the limited length of the time series of available observations (January 2004 to September 2005), they were not able to properly validate the meridional transport calculated from their regional model over the study period which is from 2000 – 2008 (9 years) at interannual timescales. They further concluded that at interannual timescales, meridional transport along the west African coast cannot be explained by wind stress curl variations in their study and suggested that the connexion with the equatorial Atlantic (*cf.* **section 1.3.1**) might play a role on the interannual fluctuations of the meridional transport.

Besides the role played by local alongshore wind anomalies in the southeast Atlantic discussed by *Richter et al.* [2010] at interannual timescales during the onset of Benguela Niño, past studies such as *Florenchie et al.,* [2004] and *Rouault et al.,* [2007] have looked at the possible contribution of local ocean–atmosphere exchanges during the coastal warm or cold events. *Florenchie et al.,* [2004] using the reanalysis NCEP-NCAR [*Kalnay et al.,* 1996] for sea surface heat fluxes and Optimum Interpolation SST [*Reynolds and Smith,* 1994] for SST in the

ABA box found that the latent heat flux which is the main contributor to the sea surface heat fluxes, played a passive role and acted like a thermostat cooling warm events or warming cool events. The same conclusion was stated in a study of *Rouault et al.,* [2007] who found that cooling effect of heat fluxes during some coastal warm events including the 1995 and 2001 ones, contributed to the demise of these events. *Rouault et al.* [2007] also argued that the cooling effect at the surface during the 1995 and 2001 coastal events was enhanced by lower than normal incoming shortwave radiation due to the presence greater than normal cloud cover and rainfall along the Angola Benguela area. Modelling study of *Bachèlery et al.* [2016a] also showed that positive or negative anomalies of nearshore wind stress (local atmospheric forcing) modulated the signature of the coastal interannual anomalous events as wind stress could be in or out of phase leading to an increase or decrease of the intensity of the coastal interannual events respectively.

1.3.2 Remote oceanic forcing

At interannual timescales, many studies suggested that Benguela Niño events along the coasts of Angola and Namibia are originated from the equatorial Atlantic via eastward propagation of IEKW along the equatorial wave guide [*Florenchie et al.*, 2003, 2004; *Rouault et al.*, 2007; *Lübbecke et al.,* 2010; *Bachèlery et al.,* 2016a*; Rouault et al.*, 2017] and similarly for Benguela Niñas [*Florenchie et al.*, 2004]. Once the IEKW reaches the African coast, the IEKW reflects westward as Rossby wave and a substantial amount of its energy is transmitted poleward as CTW [*Clarke*, 1983; *Enfield et al*., 1987].

Long equatorial Kelvin and Rossby waves play a key role on the oceanic equatorial adjustment to wind forcing at interannual timescales and in the three equatorial basins. IEKWs are forced by trade wind variations in the western part of the equatorial Atlantic and propagate eastward along the equatorial Atlantic. Note that the annulation of the Coriolis force along the equatorial band, sets the equator as a wave guide and allows faster propagations of equatorial waves compared to other latitudes (**Figure 1.5a,** 3rd panel). Long IEKWs are non-dispersive waves, meaning that they travel with a constant phase speed and are independent of the wave frequency. Thus, the dispersion relation associated with IEKWs can be written as $\omega = k \times c$ where

ω is the frequency of the wave and *c* the phase speed of the wave. The vertical structure of the long IEKWs and their phase speed are controlled by the vertical stratification of the Ocean.

The triggering mechanism of long Equatorial Kelvin Waves (EKW) is attributed to the modulation of the easterly wind in the western part of the equatorial Atlantic leading to vertical displacements of the thermocline and modification of the current intensity. Weakening of easterlies in the western part of the equatorial Atlantic triggers a convergence of local zonal currents rising the sea level. This deformation of the sea surface induced by weakening of the easterlies triggers a downwelling Kelvin wave that propagates to the east rising the sea level (**Figure 1.5a**, 1st panel) and deepening the thermocline. The downwelling Kelvin wave is associated with a reduction of the equatorial upwelling and warmer SST in the Gulf of Guinea.

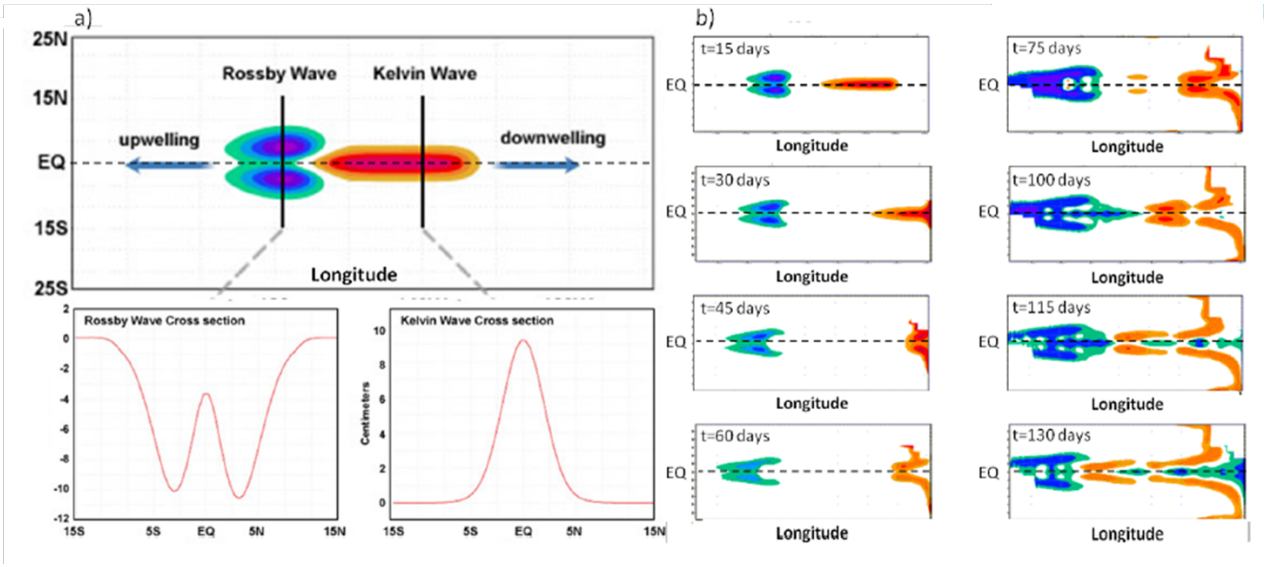

Figure 1.5: (a) Response of sea level (cm) to weakening of easterlies in the tropical Atlantic. Figure from *Laing and Evans* [2011] (b) Downwelling Kelvin wave (orange to red) and upwelling Rossby wave (green to blue) propagations along the equatorial wave guide in the Atlantic Ocean. Figure from International Research Institute for Climate and Society (IRI, https://iri.columbia.edu).

At the same time, the weakening of the easterlies in the western part of the equatorial Atlantic triggers an upwelling Rossby wave which propagates westward (**Figure 1.5a**) up to the Brazilian

coast and reflects eastward as an upwelling equatorial Kelvin wave. The reflection mechanism of the equatorial waves is well illustrated in **Figure 1.5b**. Conversely, the strengthening of easterlies in the western part of the equatorial Atlantic triggers an upwelling equatorial Kelvin wave and a downwelling Rossby waves. Note that the term upwelling is related to a divergence of local zonal currents leading to a depression of the sea level associated with a shallowing of the thermocline.

Along the equatorial Atlantic, in a stratified oceanic environment, the equatorial wave propagations induce vertical movements of the water column which might create a contact between the different density layers. The solutions of the equations of motion over the vertical component with consideration of some simplifications that can be found in *Illig et al.* [2004], yield the introduction of the equatorial baroclinic modes, such as the vertical structure variability of the ocean can be represented by the summed-up contributions of the gravest baroclinic modes. As introduced in *Illig et al.* [2004], the baroclinic mode decomposition can be performed on an Ocean General Circulation Model (OGCM). For each baroclinic mode, the later will provide the vertical structure of the waves, their phase speed, the Rayleigh coefficients and the wind projection coefficients. Then the amplitude of the long equatorial waves can be estimated by projecting the baroclinic mode contribution onto the theoretical meridional structures of the waves. *Cane and Sarachik* [1976] were the first to study the linear theory of horizontal equatorial wave propagations setting up the tropical Pacific Ocean as an infinite basin in the meridional direction. *Cane and Sarachik,* [1979] adapted the previous linear theory in the tropical Atlantic Ocean. The presence of the coastlines in the eastern side (Gulf of Guinea) and western side (Brazilian coast) of the Atlantic basin, lead them to add supplementary boundary conditions at the northern and southern boundaries of the tropical Atlantic. Moreover, a multi-mode Ocean Linear Model (OLM) can be set up using the inferred wave parameters. The single-mode equatorial OLM was developed by *Cane and Patton* [1984] and *du Penhoat and Treguier* [1985]. *Zebiak* [1993] adapted the coupled model of *Zebiak and Cane* [1987] in the tropical Atlantic. The OLM used in *Zebiak* [1993] had one baroclinic mode which characteristics were chosen between the first and the second baroclinic mode. For the first time in the Tropical Atlantic, *Illig et al.* [2004] used a high resolution OGCM from 1981–2000 to study the equatorial wave propagations. They performed a baroclinic mode decomposition using the vertical density profile of the tropical Atlantic and compared the results with the solution of a multi-mode ocean

linear model. They quantified the contributions of the gravest baroclinic modes to sea level anomalies and surface zonal currents at interannual timescales. Each mode has its own vertical structure, the n^{th} baroclinic mode which crosses the zero n^{th} times and which amplitude decreases with depth. In the equatorial Atlantic, the first baroclinic mode is the fastest mode of Kelvin waves and the second baroclinic mode the most energetic mode [*Illig et al.,* 2004]. According to *Illig et al.* [2004], the phase speed of the first baroclinic mode of equatorial Kelvin wave ranges between 2.4 m/s and 3 m/s which is 3 times the phase speed of Rossby waves. Similarly, the phase speeds of the second and third baroclinic modes of Kelvin waves are ~1.4 m/s and 0.9 m/s respectively.

Part of the incoming eastward equatorial wave energy is transmitted southward along the southwestern African coast as CTW. CTW keeps the same properties as EKW with similar dynamic effects (effect on SLA and thermocline depth as described earlier for IEKW) and thermodynamic effects (through thermocline feedback changing the diapycnal heat flux below the mixed layer which indirectly impacts the SST) on the coastal water column in terms of downwelling or upwelling during its poleward propagation along the west African coast. CTW triggers vertical displacements of the thermocline which can modulate the surface and subsurface temperature ~ 2°C and imprint the Sea Level Anomaly (SLA) by several centimeters [*Pizarro et al.*, 2001, 2002; *Leth and Middleton*, 2006; *Colas et al.,* 2008; *Polo et al.,* 2008; *Richter et al*., 2010; *Belmadani et al.,* 2012; *Bachèlery et al.,* 2016a]. As illustrated in **Figure 1.6a**, during their propagation along the southwest coast of Africa, downwelling CTWs induces an increase of sea level, deepens the thermocline and triggers coastal warm temperature anomalies detectable at the sea surface which could be at the origin of Benguela Niño. Past authors [*Ostrowski et al*., 2009; *Bachèlery et al.,* 2016a] suggested that CTW partly controlled the strength of the variability of the poleward undercurrent. Based on experimentation with a regional ocean model, *Bachèlery et al.* [2016a] quantified that over the 2000 – 2008 period, 89% of the coastal SST interannual variability off Angola and Namibia is explained by the remote oceanic forcing via equatorially-forced CTW propagations, while they attributed 29% for the interannual coastal fluctuations to the local atmospheric forcing. They concluded that the remote oceanic forcing is the main forcing mechanism of the coastal SST variability in the southeast Atlantic.

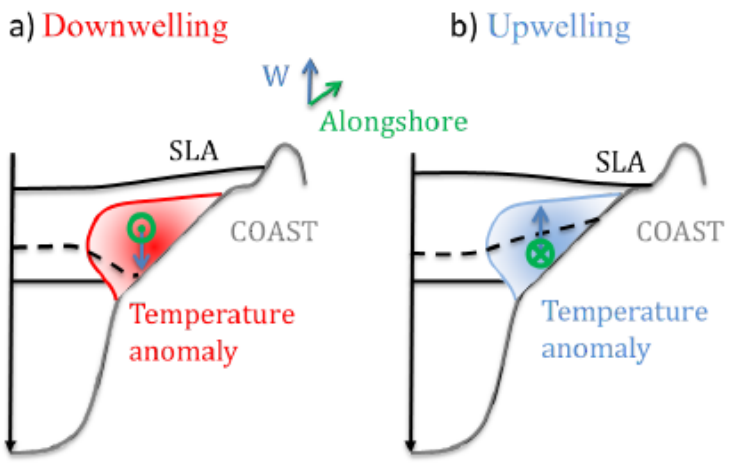

Figure 1.6: a) Illustration of the influence of downwelling CTW along the coast which generate positive SLA, deepening of the thermocline (dashed line), leading to warm temperature anomaly (red shading), poleward current (green circle) and reduced vertical current (blue arrow). b) Influence of upwelling CTW along the coast which trigger negative SLA, shallowing of the thermocline, leading to cold temperature anomaly (blue shading), equatorward current (green circle) and strong vertical current (blue arrow). Figure from *Bachèlery* [2016].

Bachèlery et al. [2016a] found that at interannual timescales, the signature of CTWs on coastal temperature is detectable up to ~26°S and their effects on the subsurface coastal currents and density can be observed up to ~30°S when removing the effect of local atmospheric forcing. They further suggested that at interannual timescales, the CTW signature on coastal SST is not observable south of 26°S due to the low stratification associated with the strong upwelling dynamic regime located there. The efficiency by which CTW could trigger temperature anomalies through vertical advection process is controlled by the vertical stratification of the water column along the southwest African coast as suggested by *Bachèlery et al.* [2016a]. According to the study of *Tchipalanga et al.* [2018], off Angola, the upper-ocean stratification increases in austral summer and decreases in austral winter. Moreover, *Bachèlery et al.* [2016b] using a coupled physical-biogeochemical model from 2000-2008 showed that at interannual timescales, 85% of the nitrate and oxygen coastal variability from Angola to the BUS, is explained by remote forcing via CTW propagations. The latter impacts the primary production

along the coast of southwestern Africa. According to previous studies [*Polo et al.,* 2008; *Ostrowski et al*., 2009], March-April and September/October corresponding to the periods of maxima of the velocity of the Angola Current and occurred at the same time as the semi-annual downwelling CTWs. The inverse effect is observed during the propagation of an upwelling CTW (**Figure 1.6b**). The upwelling CTW decreases the sea level, shallows the thermocline and induces cold temperature anomaly which could be at the origin of moderate cold event and Benguela Niña. The subsequent CTW has also a significant influence on the coastal current circulation. According to the modelling study of *Bachèlery et al.* [2016a], during the mature phase of the downwelling event in February 2001 (**Figure 1.7a**), the downwelling CTW at the origin of this major event strengthens the poleward alongshore current in the upper 200 m associated with reduced equatorward flow in the upper 40 m and strong poleward flow in between 120 – 200 m. In February 2001, a decrease of the upward vertical current and cross-shore current leads to an important reduction of the coastal upwelling. Conversely, during the

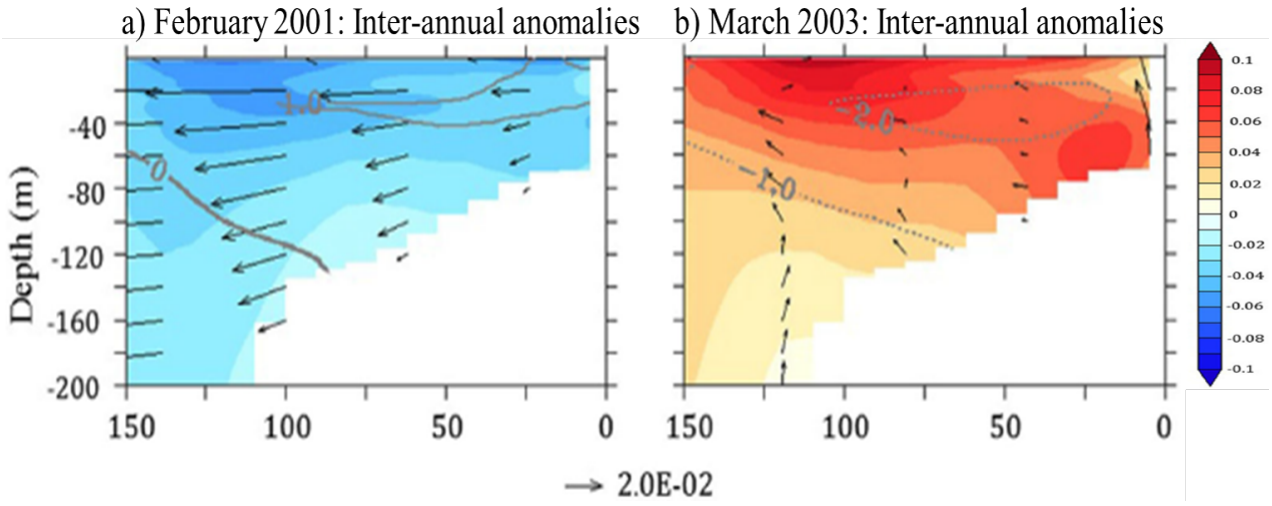

Figure 1.7: Interannual anomalies of temperature (contours, °C), alongshore currents (colour, m/s), cross-shore (arrows, m/s) and vertical currents (arrows, 2000* m/s) averaged between 18°S – 25°S during the mature phase of a) coastal downwelling in February 2001 and b) coastal upwelling event in March 2003 based on model outputs from *Bachèlery et al.* [2016a]. Data are shown within the 150 km coastal band in the upper 200 m. Figure from *Bachèlery et al.* [2016a].

mature phase of the upwelling event in March 2003 (**Figure 1.7b**), the local current circulation

associated with the passage of the upwelling CTW increases the equatorward and upward vertical current flows in the upper 200 m associated with strong coastal upwelling of cold nutrient-rich waters along the coast and the appearance of coastal cold temperature anomalies.

1.4 OBJECTIVES AND OUTLINE

Our understanding of the functioning of the tropical Atlantic climate and our ability to forecast its impacts on the Atlantic fishing communities constitute an important research topic for the scientific community, objectives of the international projects such as PREFACE. Thus, the motivations of this thesis lie in the framework of understanding the mechanisms associated with the development of the extreme warm and cold events at interannual timescales called Benguela Niños and Niñas, their links with the equatorial Atlantic variability and the contribution of the local forcings in the southeast Atlantic Ocean.

1.4.1 Objectives of this study

Past studies mainly used satellite data or models [*Florenchie et al.,* 2004; *Richter et al.,* 2010; *Bachèlery et al.,* 2016a], to document and study the dynamics of the Benguela Niño and Benguela Niña events. Here, for the first time, I use real-time buoy records from the Prediction and Research Moored Array in the Tropical Atlantic (PIRATA) program to describe the Benguela Niños and Niñas and their connexion with the equatorial Atlantic at interannual timescales. Additionally, an OLM is used to interpret these observations along the equatorial Atlantic as IEKW propagations.

The objectives of this thesis will consist to:

- Investigate at interannual timescales, the different processes responsible for the onset and development of Benguela Niños and Benguela Niñas along the southeast Atlantic Ocean.

- Investigate the connection between the coastal and the equatorial Atlantic variability.

- Investigate the role of the large-scale and local wind forcing, along with the modulation of the vertical oceanic stratification during the interannual coastal events.

1.4.2 Outline of the thesis

In this context, I will first document the connection between the equatorial Atlantic and the coastal variability and using the PIRATA records from 1998 to 2012 as well as altimetric SSH data and outputs from the equatorial OLM. Having validated the OLM outputs from 1998 to 2012, I will use it with an OGCM from 1958 to 2015 to investigate past Benguela Niños and Niñas that occured before 1982.

The outline of the thesis will consist on:

- Chapter 2 will give an overview of the different products used for this study (observations, satellite and model outputs). I will present the different methods implemented for this study and the validations of the OLM and the OGCM outputs at seasonal and interannual timescales.
- Chapter 3 will document the link between the equatorial Atlantic and the Angola Benguela coastal variability at interannual timescales from 1998 to 2012. In this section, I will: 1) Use a combination of PIRATA data, AVISO and the OLM to identify equatorial propagations of abnormal Sea Surface Height Anomalies (SSHA). 2) Define an equatorial oceanic index of interannual equatorial Kelvin wave amplitude using the OLM outputs and link this proxy to the coastal variability off Angola and Namibia in order to forecast the Benguela Niños or Niñas. This study was published in *Imbol Koungue et al*. [2017].
- Chapter 4 will study all the Benguela Niños and Niñas that occurred from 1958 to 2015. Little information exists before the satellite era on Benguela Niños or Benguela Niñas that occurred before 1982. In this chapter, I will: 1) Identify and classify all the SST coastal events in terms of extreme and moderate warm and cold coastal events along the Angola Benguela Current system from 1958 to 2015. 2) Compute the coastal net mass transport and the associated temperature transport across the ABF using the OGCM and investigate its contribution to the development of the coastal events. 3) Illustrate some composite maps of Benguela Niños and Niñas during the austral summer in the South Atlantic.
- Chapter 5 will document other potential processes that can play a role during the development of the coastal events. 1) The large-scale wind influence during the onset of

Benguela Niños and Niñas using lagged composite analysis of Temperature at 10 m and surface wind stress anomalies. 2) The role played by local atmospheric forcing (alongshore wind stress anomalies) along the Angola Benguela Current system. 3) The modulation of the CTW signature to the sea surface temperature by the local vertical stratification depending on the season.

- Chapter 6 will provide a discussion of the results, conclusions and perspectives of this work.

CHAPTER 2

2 DATA AND METHODS

2.1 DATA

To describe the equatorial variability, records from equatorial Atlantic PIRATA moorings (Dynamic Height (DYNH) and depth of thermocline (Z20)) are used and compared with outputs from an OLM and Sea Surface Height (SSH) derived from altimetry. Comparison allows to understand the equatorial dynamics signature and to interpret the data in terms of linear propagations. Along the ABUS, OGCM outputs are compared in surface and subsurface with available observational datasets, such as Optimum Interpolation Sea Surface Temperature (OI-SST), the World Ocean Atlas 2013 version 2 (WOA13 v2). OI-SST and OGCM were then used to document the coastal variability off Angola and Namibia. OGCM allows calculation of the net subsurface ocean transport at 17°S which is a key factor during the development of Benguela Niños [*Rouault,* 2012]. The data and details of the characteristics of the linear equatorial model and the tropical Atlantic simulation are described below.

2.1.1 Observations

2.1.1.1 PIRATA moorings

PIRATA buoys have been deployed in the tropical Atlantic since September 1997 [*Servain et al.*, 1998; *Bourlès et al.*, 2008]. PIRATA program is composed of an array of moorings in the Atlantic Ocean (**Figure 2.1,** left panel). PIRATA moorings record and sample the water column with five temperature/conductivity sensors deployed at depths of 1, 10, 20, 40, and 120 m, five

temperature sensors positioned at depths of 60, 80, 100, 140, and 180 m, and two temperature/pressure sensors positioned at 300 and 500 m along the equatorial Atlantic (**Figure 2.1,** right panel).

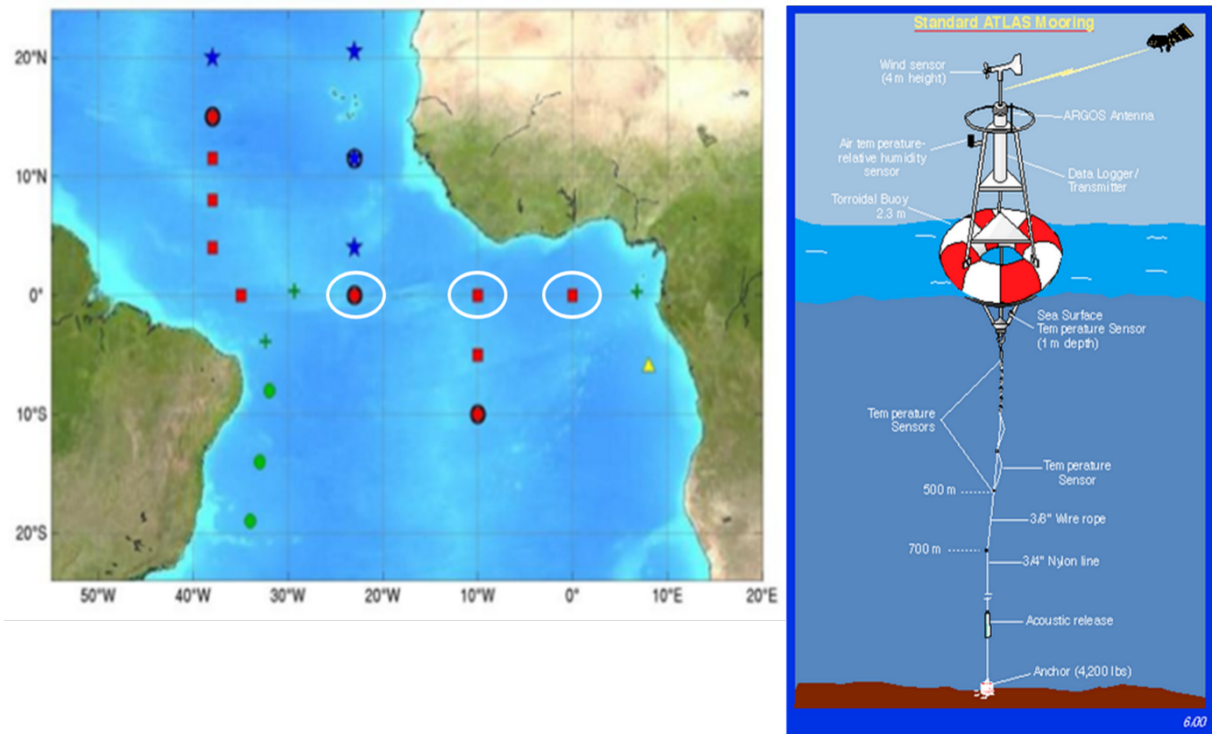

Figure 2.1: Left panel: The PIRATA backbone of ATLAS buoys (red squares), northeast extension (blue stars), southwest extension (green circles), southeast extension pilot project (yellow triangle), and island-based observation sites (green crosses).. Positions of the moorings used in this thesis are represented by white circles. Figure modified from *Bourlès et al.* [2008]. Right panel: Vertical presentation of a PIRATA ATLAS buoy with the positions of its temperature sensors between the surface and 500 m depth (https://wwww.pmel.noaa.gov/gtmba/moorings).

Data display, download, climatology estimations and more details are available on the dedicated website http://www.pmel.noaa.gov/tao/disdel/. Interannual anomalies of parameters can also be downloaded from the website. These interannual anomalies are computed by subtracting the climatology from the daily data. Climatology sources are different depending on the parameter.

For example, in the Atlantic Ocean, to compute interannual anomalies of dynamic height and depth of the 20°C isotherm (identified by the position of the 20°C isotherm, Z20, positive downward), the climatology of the World Ocean Atlas 2009 (https://www.nodc.noaa.gov/OC5/WOA09/pr_woa09.html) is used.

The equatorial variability is documented using PIRATA data which help to detect and monitor the propagation of Kelvin waves along the equatorial Atlantic. Note that one of the goals of PIRATA project is to study the ocean-atmosphere interactions aiming to monitor the interannual activity of the long equatorial waves (*cf.* **section 1.3.2**). PIRATA data are also used to validate the OLM and the tropical Atlantic OGCM simulation. This validation is done using monthly dynamic height and anomalous depth of the thermocline from 3 PIRATA's buoys located along the equator at 23°W, 10°W, and 0°E at 0°N (white circled buoys, **Figure 2.1,** left panel) over the 1998 to 2015 period. It is worth to mention that sometimes, PIRATA records have gaps at various locations due to vandalism or data failure. Quantification of gaps for the 3 PIRATA moorings circled in white in **Figure 2.1** (left panel) is done in **chapter 3** over the period 1998 to 2012. Results show 35%, 41%, and 50% of missing values are encountered in the dynamics height interannual anomalies estimation at [23°W; 0°N], [10°W; 0°N], and [0°E; 0°N], respectively. Note that from 2006 to 2012, gaps are less frequent with only 22%, 15% and, 16% of missing data at the same equatorial mooring locations. 5 day means from PIRATA buoys data interpolated between different mooring locations along the equator are also used to illustrate some particular eastward propagations (*cf.* **Chapter 3**) using Hovmöller diagram of depth of the thermocline along the equatorial Atlantic. This Hovmöller diagram of depth of the thermocline allows the estimation of the speeds of identified Kelvin waves that are estimated by calculation (*cf.* **section 2.2.3**).

2.1.1.2 Optimum Interpolation Sea Surface Temperature version 2 (OI-SST v2)

In other to identify and classify interannual warm and cold events in the Angola-Benguela Current system, as well as validate the tropical Atlantic simulation (OGCM) in the same area at the surface, monthly Optimum Interpolation Sea Surface Temperature version 2 (OI-SST v2) [*Reynolds et al.,* 2002] is used and is available at 1°×1° horizontal resolution available since 1982. Data can be downloaded from the NOAA website

https://www.esrl.noaa.gov/psd/data/gridded/. This dataset is derived from daily merged, in situ data (ship measurements, buoys (moored and drifting)) and high resolution (9 km) infrared satellite observations from the AVHRR (Advanced Very High-Resolution Radiometer, https://podaac.jpl.nasa.gov/AVHRR-Pathfinder) instrument on board NOAA. The description of the different sources of in situ data can be found in *Reynolds et al.* [2002]. The OI-SST v2 dataset is used to assess the interannual SST coastal variability along the western coast of Africa within 3 zones of interest taken within the 1°-width coastal band (**Figure 2.2**). As coastal zones of interest, from the North to the South, the Southern Angola domain, where data are averaged

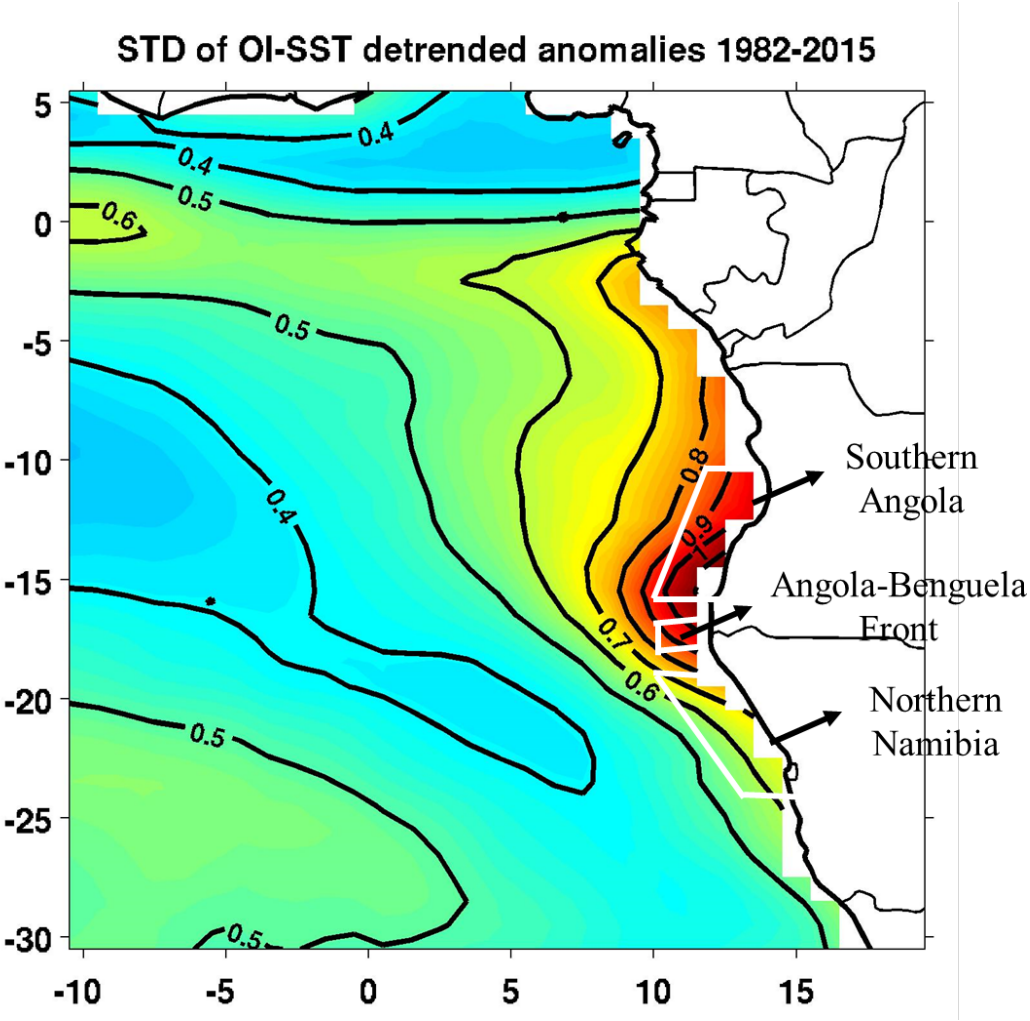

Figure 2.2: Standard deviation (STD) of monthly detrended anomalies of OI-SST v2 from 1982-2015 (°C). White boxes represented the 3 zones of interest.

from 10°S to 15°S, is a tropical warm water region; the ABF zone, where data is averaged from 16.5°S to 17.5°S, is a transition region between warm tropical water and cold upwelling water and the Northern Namibia domain also called NBUS where data is averaged from 19°S to 24°S, is a region of cold upwelled waters. The Southern Angola and Northern Namibia domains are similar to the ones used in *Rouault* [2012] and *Rouault et al.* [2017]. The Northern Namibia domain is in a wind driven upwelling while the Southern Angola domain is affected by the Angola Current and coastal trapped waves with low wind speed. The ABF zone just defines the transition between Angola and Namibia and the latitudinal extension is quite similar to the one of *Rouault* [2012] who used 17°S for his meridional transport proxy.

2.1.1.3 World Ocean Atlas 2013 version 2 (WOA13 v2)

The World Ocean Atlas (WOA) 2013 version 2 (WOA13 v2) allows to evaluate the OGCM skills in the tropical Atlantic in representing the mean vertical structure of temperature along the equatorial Atlantic wave guide and at 23°S in the southeast Atlantic Ocean. WOA13 v2 monthly climatology is then chosen from 1955 until 2012 (an average of six decadal means) in the upper 28 vertical levels. WOA13 v2 monthly climatology is a gridded product derived from in situ measurements (for example ship-deployed Conductivity-Temperature-Depth (CTD), Expendable Bathythermographs (XBT), gliders, moored and drifting buoys), interpolated and produced at a 0.25×0.25 degree resolution. It contains 102 vertical levels from the surface (0 m) to 5500 m [*Locarnini et al.,* 2013]. The data is processed by NOAA and archived at the National Oceanographic Data Center (NODC). The data is available on the website http://www.nodc.noaa.gov/OC5/woa13/.

2.1.1.4 Sea level anomalies from AVISO

The reference altimetric SSH gridded product distributed by the Archiving, Validation and Interpretation of Satellite Oceanographic Data (AVISO) merges data from TOPEX/Poseidon and Jason-1/2/3 altimeters. These data are used to document the interannual equatorial variability of SSH and to fill gaps in PIRATA time series (*cf.* **Chapter 3**). The data are also compared to the

tropical Atlantic OGCM for the purpose of model validation **(***cf.* **section 2.3).** Data are distributed by CLS on a weekly (7 days) temporal resolution available on a 1/4° horizontal resolution grid. The error made by altimeters (for example TOPEX/Poseidon) while calculating the sea level anomalies is ~2 cm [*Le Traon et al*., 1998]. Refer to *Le Traon et al*. [1998] and *Ducet et al.* [2000] for more details on data and gridding procedures.

2.1.2 Model outputs

2.1.2.1 Tropical Atlantic Simulation (TATLT025).

The OGCM numerical model used in this study is the oceanic component of the Nucleus for European Modelling of the Ocean program (NEMO3.6) [*Madec,* 2014]. It solves the Navier-Stokes primitive equations under spherical coordinates discretized on a C-grid and fixed vertical levels (z-coordinate). The parameterization and the physical parameters are similar to those of *Hernandez et al.* [2016, 2017]. The regional grid has ¼° horizontal resolution and extends from 98.50°W to 19.80°E, and from 34.05°S to 33.73°N. There are 75 vertical levels, with 12 levels within the first 20 m and 24 levels within the first 100 m. The momentum advection scheme is the third-order upstream biased. Tracers are advected with a total variance dissipation scheme and a Laplacian isopycnal diffusion is applied with a diffusion coefficient of 300 m^2/s. The model time step is 1200s. The vertical diffusion coefficient is estimated using the generic length scale scheme with a k-epsilon turbulent closure [*Umlauf and Burchard*, 2003]. More details can be found in *Reffray et al.* [2015] and *Maraldi et al.* [2013]. Daily outputs from MERCATOR global reanalysis GLORYS2V3 were used to force the model at its lateral boundaries. The atmospheric fluxes of momentum, heat, and freshwater at the surface are given by bulk formulae [*Large and Yeager,* 2009] using 3h fields of wind speed, atmospheric temperature and humidity, and daily fields of long wave, short wave radiation and precipitation from the DRAKKAR Forcing Set (DFS) version 5.2 (DFS5.2) [*Dussin et al.,* 2016]. DFS5.2 is actually a corrected forcing for DRAKKAR simulation using ERA-Interim atmospheric reanalysis [*Dee et al.,* 2011]. The shortwave radiation forcing is modulated on-line by an analytical diurnal cycle. A monthly climatological runoff based on the dataset of *Dai and Trenberth* [2002] is prescribed near the

river mouths as a surface freshwater flux with increased vertical mixing in the upper 10 m. There is no explicit restoring of the SST, but the specification of atmospheric conditions (air temperature, humidity, and wind speed) when forcing the ocean model with the bulk formulae in the simulation acts to restore the SST toward prescribed air temperature. This may participate to counterbalance model biases in reproducing the Benguela upwelling variability. Note that there is no restoring toward observed or climatological sea surface salinity [*Hernandez et al.,* 2016] and similarly for SST. The OGCM is integrated over the long period 1958 – 2015 and monthly averages where provided for this work. I received the OGCM outputs from Dr Julien Jouanno from University of Toulouse in France.

2.1.2.2 Ocean Linear Model (OLM)

Outputs of a simulation carried out with the equatorial Atlantic OLM is used. The OLM was developed by *Illig et al.* [2004] and was used in *Rouault et al.* [2007] to understand the mechanisms linked to long equatorial wave propagations. It is also used to interpret OGCM outputs and altimetric data in terms of equatorial wave propagations. The OLM allows me to interpret local observations measured by PIRATA buoys (DYNH and Z20) and altimeter data into basin-scale Interannual Equatorial Kelvin Wave (IEKW) dynamics. The simulation of the westward and eastward propagations of equatorial Rossby and Kelvin waves respectively in the equatorial band is performed within a domain extending from 50°W to 10°E and from 28.875°S to 28.875°N, with a horizontal resolution of 2° in longitude and 0.25° in latitude. Ocean vertical movement decompositions include six baroclinic modes together with phase speed, wind-stress projection coefficient, and friction derived from a high-resolution OGCM [*Illig et al.,* 2004]. The OLM wind stress forcing is provided by 2 day-averaged DRAKKAR Forcing Set version 5 (DFS5) [*Dussin et al.,* 2016]. It is important to mention that DFS wind stress is similar to ERA-Interim reanalysis [*Dee et al.,* 2011] wind stress with a horizontal resolution of 0.75°. The OLM is forced by 2-day wind stress averages obtained by cubic interpolation of monthly means. Model wind stress forcing is first detrended and monthly interannual anomalies (*cf.* **section 2.2.1**) are calculated over the periods of interest. The OLM is run over 2 periods of interest: Firstly from 1980 – 2012 because the PIRATA program started in September 1997 and the DFS5

wind stress at our disposal was available up to the end of 2012. Secondly, a longer period from 1958 – 2015 (OGCM period) is used because OGCM wind stress forcing (*cf.* **section 2.1.2.1**) is used to force the OLM in order to characterize equatorial Kelvin waves propagations occurring before 1980 (*cf.* **Chapter 4**). I received the OLM outputs from Dr Serena Illig who is one of my PhD co-advisors.

2.2 METHODOLOGY

2.2.1 Interannual monthly anomalies

First, the high-frequency variability (at least sub-monthly) is filtered by averaging all data and model outputs on a monthly resolution. To compute the interannual monthly anomalies, monthly climatology (estimated over the period of interest) is removed from the initial monthly time series. Since interannual variability is my timescale of interest and there is a linear trend or decadal variability in SST over the Angola-Benguela current system, it is important to remove the linear trend before computing the anomalies. To do so, the linear least square regression fit is estimated and is removed from the original time series.

2.2.2 Normalization of Anomalies

In this study, 2 methods are used for the normalization of the monthly anomalies time series: either by dividing the monthly anomalies by the mean standard deviation or by dividing each monthly anomaly by the standard deviation of that month as done in *Rouault* [2012].

2.2.3 Wave speed calculation

In this study, the phase speed of the interannual Kelvin waves along the equatorial Atlantic is estimated using the ratio between the travelled distance by the Kelvin waves along the equator

based on Hovmöller diagram and the elapsed time. The phase speed is given by:

$$\boldsymbol{v = \frac{d}{t}}$$

The estimated phase speeds will be compared to the theoretical values from *Illig et al.* [2004].

2.2.4 Taylor Diagram

Taylor diagrams are used to compare the OGCM outputs to available observation datasets such as PIRATA, WOA and AVISO over the period 1958 - 2015. Taylor diagram provides the degree of correspondence between observations and simulation in terms of four statistics: the Pearson correlation coefficient (R) between observations and simulation, the root-mean-squared difference (RMSD), and the standard deviations (σ) of observations and simulation. The Pearson correlation coefficient R expresses the pattern resemblance between observations and simulation. R varies between -1 and 1, meaning that if R is less than 0, observations and simulation are negatively associated (if the observed parameters increase, simulated one decreases). A value of R = 0 means that there is no resemblance in the variation between observations and simulation. A value of R greater than 0 indicates that observations and simulation are positively associated. When it comes to looking at the differences between observations and simulation, root-mean-squared difference (RMSD) is used. If the RMSD is close to 0, this means that observations and simulation look quite alike. Since the first two statistics provide a significant information quantifying the correspondence between 2 patterns, the variances or standard deviations of observations and simulation are needed for a complete characterization. According to *Taylor* [2001], the relationship between these four statistics is given by:

$$\boldsymbol{E'^2 = \sigma_f^2 + \sigma_r^2 - 2\sigma_f\sigma_r R}$$

Where E' is the RMSD, σ_f and σ_r are respectively the variances of simulation (OGCM) and observations respectively. Taylor made an analogy using the triangular geometric relationship given by the law of cosines ($\mathbf{c^2 = a^2 + b^2 - 2ab\cos\varphi}$, with a, b, c the lengths of the sides of the triangle and φ the angle formed between sides a and b) shown in **Figure 2.3**.

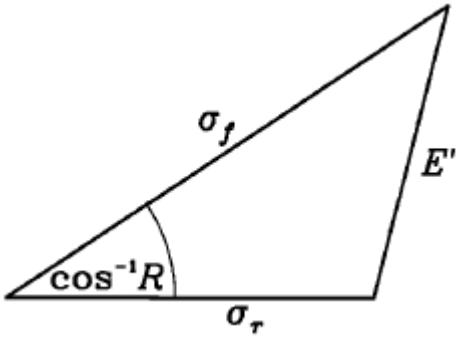

Figure 2.3: Geometric representation of the relationship between the four statistics: R (correlation coefficient), the E' (RMSD) and the standard deviations of observations and simulation σ_r and σ_f respectively.

Where c = E', a = σ_f , b = σ_r and R is cos φ meaning that φ = $\cos^{-1}R$ as observed in **Figure 2.3**. The Taylor diagram [*Taylor* 2001] is then a summary polar plot in which correlation coefficients between observations and simulations are given by the azimuthal angles. The Taylor diagrams used in this thesis are customized such that the radial distance from the origin is proportional to the standard deviation of a pattern (normalized by the standard deviation of the observations) and the green dashed lines measure the distance from the reference point (Black point, Ref) and indicate the RMSD.

2.2.5 Composite and bootstrap

Compositing is the process of averaging field over some identified occurrences of particular events or periods. I select extreme coastal warm or cold events defined when interannual temperature at 10 m (T10) anomalies exceed ±1 standard deviation for at least 2 of the coastal zones of interest (**Figure 2.2**) and for at least 3 months (*cf.* **Chapter 4**). For instance, over the 1958-2015 period, 16 extreme warm events and 10 extreme cold events are identified. In this study, compositing is performed for the extreme coastal warm T10 interannual events (*cf.* **section 1.2**) that peak in March/April [*Florenchie et al*., 2003, 2004; *Rouault et al.,* 2007; *Lübbecke et al.,* 2010; *Rouault* 2012]. The same method is used for extreme coastal cold events. 5 extreme warm and cold coastal events are identified. Composite or lagged composite analysis

can then be performed over T10 and wind stress anomalies.

The bootstrap method is used to test the statistical significance of composite maps. This method allows to calculate the statistically significant areas in composite maps of T10 anomalies. The bootstrap technique is a nonparametric test which is independent of the distribution of the data. The bootstrap method was for the first time introduced by *Efron* in 1977 [*Diaconis and Efron,* 1983]. The basic idea when performing the bootstrap is to construct a large collection of artificial data group having the same size as the target group. For this study, the target group corresponds to the occurrences of anomalous extreme warm or cold events called Benguela Niños or Niñas leading to a composite map for each category of events. 10.000 artificial data groups are randomly generated from the initial dataset. Note that there are two different ways to perform the bootstrap test: with or without replacement [*Grotjahn and Faure* 2008]. For this study, the bootstrap testing without replacement is chosen meaning that the months among each randomly picked group are all different. In this case, the initial dataset is resampled 10.000 times to form 10.000 artificial averages. These 10.000 artificial averages are sorted in an ascending order. Therefore, each grid point of my composite map will be statistically significant at 90% (using p-value statistical test from *Best and Roberts* [1975]) if its value can be classified as an" extreme outlier", meaning that this value is located in the upper 5% or lower 5% of the artificial group distribution.

2.3 MODEL VALIDATION

This part of the thesis is dedicated to the validation of the two model outputs (OLM and OGCM), which are used in this thesis with available observation datasets.

2.3.1 OLM validation

The OLM used here was validated in *Illig et al.* [2004] over the period 1992 – 2000 using altimetric SSHA from TOPEX/POSEIDON+ERS1/2 missions (T/P+ERS1/2) and it showed good skill in reproducing equatorial Atlantic dynamics. Here the OLM outputs are used over a longer period and validated over the period 1993 – 2015 using a map correlation shown in

Figure 2.4. **Figure 2.4** represents correlation map between monthly detrended SSHA from AVISO and SSHA from OLM statistically significant at 95% (using p-value statistical test from *Best and Roberts* [1975])**.** As expected, OLM SSHA and AVISO SSHA agree well in the equatorial wave guide along which the Kelvin and Rossby waves are propagating. There correlations are statistically significant and larger than 0.5. For instance, statistically significant

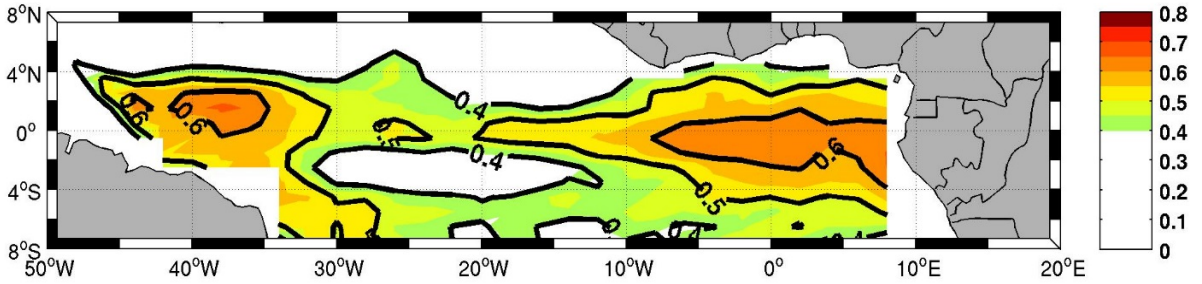

Figure 2.4: Correlation map between monthly detrended AVISO SSHA and OLM SSHA over the 1993 - 2015 period in the tropical Atlantic Ocean. Correlations statistically significant at the 95% level are greater than 0.4. Black lines represented 0.1 correlation contours.

correlations of 0.5, 0.56 and 0.63 are observed between the AVISO SSHA and OLM SSHA at [23°W; 0°N], [10°W; 0°N] and [0°E; 0°N] respectively. These positions correspond to 3 PIRATA mooring locations (**Figure 2.1,** left panel). The pattern of low correlation coefficients along the equator between 30°W and 12°W corresponds to place where the seasonal thermocline displacements change in sign from west to east (pivot of the thermocline) leading to small amplitude of interannual anomalies of SSH [*Illig et al.* 2004].

2.3.2 OGCM validation

This section is dedicated to the validation of the OGCM tropical Atlantic simulation. Firstly, comparison between the equatorial mean structure (1958 to 2015) of the tropical Atlantic simulation (OGCM) temperature and the WOA13 v2 (1955 - 2012) temperature in the upper

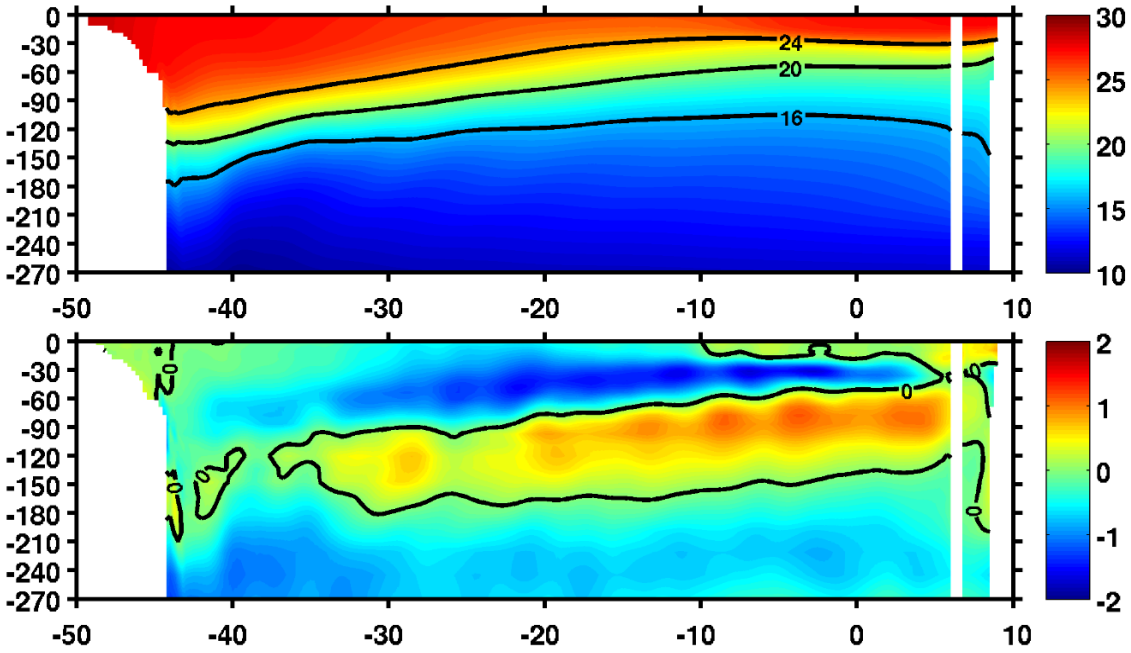

Figure 2.5: Top: Longitude-depth section of OGCM mean vertical temperature at the equator (0°N) from 1958 to 2015. The black contours represent the mean position of the 16°C, 20°C and 24°C isotherms respectively. Bottom: Difference between mean longitude-depth sections of temperature from OGCM and WOA13 v2. Black contour represents 0°C.

270 m (**Figure 2.5**) from 50°W to 10°E at 0°N is done. The simulated thermocline depth is well represented along the equatorial Atlantic being deeper in the western side and shallower in the eastern part of the equatorial Atlantic with warm waters in the upper layers and cold waters below the thermocline (**Figure 2.5,** top panel). Moreover, the simulated thermocline appears to be too diffuse compared to the observations. The map of the difference between the mean OGCM and WOA13 v2 temperature shown in (**Figure 2.5,** bottom panel) reveals that OGCM appears to be cooler than the observations in the surface layer (from 44°W to 10°W) and above the thermocline where the difference is less than -1°C. Within the thermocline, the difference between the OGCM and WOA13 v2 is larger than 1°C, meaning that the OGCM simulated

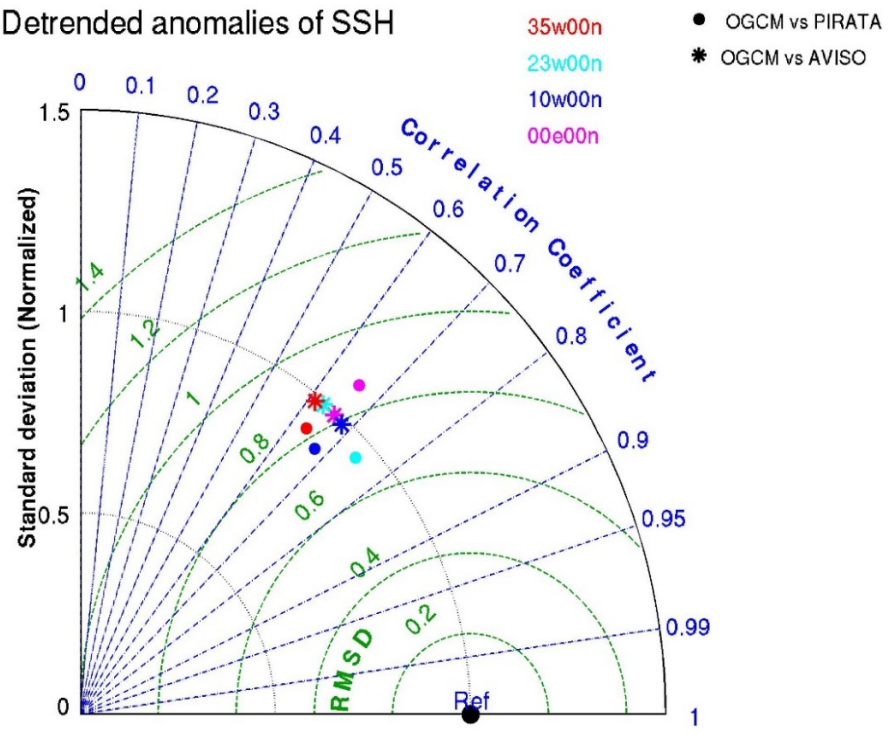

Figure 2.6: Taylor diagram (*cf.* **section 2.2.4**) comparing OGCM detrended anomalies of SSH with PIRATA observation data (points) and AVISO (stars). Data are averaged at 0°N along the equatorial Atlantic (35°W, 23°W, 10°W, 0°E.) over the period 1998 – 2015.

temperature above the thermocline is warmer than the observed one. Same biases were mentioned by *Illig et al.* [2004] when validating their OGCM simulated temperature at the surface and subsurface along the equatorial Atlantic. The thermocline depth is well represented along the equatorial Atlantic being deeper in the western side than in the eastern part of the equatorial Atlantic.

Figure 2.6 shows a Taylor diagram (c*f.* **section 2.2.4**) of detrended anomalies of SSH, computed along the equatorial Atlantic (0°N) at the 4 locations (35°W, 23°W, 10°W, 0°E) of the PIRATA moorings. The period used here goes from 1998 to 2015. OGCM agrees best with the PIRATA observations at [23°W; 0°N] and [10°W; 0°N]. At these two locations, the RMSD is

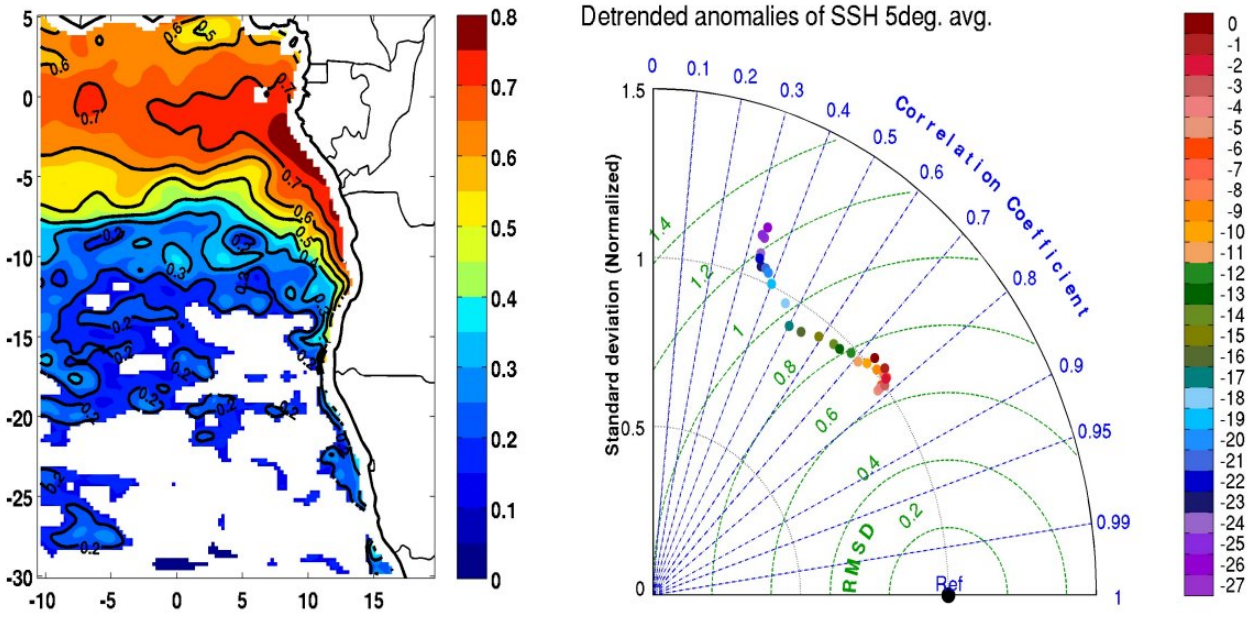

Figure 2.7: Left: Correlation map between observed monthly detrended interannual AVISO SSHA and model SSHA over the 1993 - 2015 period in the southeast Atlantic Ocean. The white area depicts non-significant correlations at 95% confidence level (using p-value statistical test from *Best and Roberts* [1975]). Black lines represented 0.1 correlation contours. Right: Taylor diagram (*cf*. **section 2.2.4)** for 5° running mean detrended anomalies of coastal SSH centred at each latitude from 0°S- 27°S showing the model skills estimated by comparing with AVISO data. Data are averaged within 1 coastal band over the period 1993 to 2015.

lower than 0.8 cm and correlation coefficients equal to 0.74 and 0.67 respectively. The OGCM has almost the same variability than AVISO SSHA. The normalized standard deviation is close to 1 for each PIRATA mooring location and the correlation range between 0.6 and 0.7 (statistically significant at 95% using p-value statistical test from *Best and Roberts* [1975]).

A correlation map between monthly interannual detrended anomalies of SSH using AVISO and the simulation is estimated (**Figure 2.7**, left panel). There is a good correlation between the simulation and AVISO SSHA statistically significant at 95% (using p-value statistical test from *Best and Roberts* [1975]), along the equatorial wave guide with correlation larger than 0.7 from 0°E towards the west African coast. Polewards, the zone of maximum correlation expands, trapped to the African coast. I report that the correlation decreases in the southward direction up to around 25°S. This suggests a dynamical connection between the

equatorial domain and the coastal domain southward up to ~ 25°S which seems to be the limit where the signature of the coastal trapped waves is observable [*Bachèlery et al.,* 2016a]. Offshore, the lack of significant correlation represented in white in **Figure 2.7** represents a mismatch between the OGCM and AVISO SSHA (non-significant correlation at 95%). This area corresponds to the area of high mesoscale activity (presence of eddies). Since there is no assimilation in the simulation, simulated and observed eddies are not collocated. A Taylor diagram (*cf.* **section 2.2.4**) summarizes the comparison between OGCM and AVISO SSH along the southwest African coast within a 1-degree coastal band and for various 5°-width latitudinal bands, centred at each point between 0°S and 27°S over the period of 1993 to 2015. Latitudes are shown by the color of points according to the colorbar on **Figure 2.7** on the right panel. This diagram is used to test the realism of simulated variability against observed AVISO SSHA variability. As observed in **Figure 2.7 (**right panel**)**, the correlation decreases, and the root mean square centred increases in a southward direction. This means that the disagreement between the model and the observations is much pronounced in the south. In the area between 0°S and 11°S, the simulated variability agrees well with the AVISO SSH because the amplitude or energy in the OGCM seems to be correct or comparable with the observed one (normalised standard deviation close to 1). Also, maximum correlation coefficients ranging between [0.7 – 0.8] are obtained between 0°S and 11°S.

Along the southwest African coast, from 7°E to 14°E, the mean simulated cross-shore vertical structure of the temperature in the upper 270 m at 23°S is presented along with the difference between the simulation and WOA13 v2 (**Figure 2.8**). The simulation represents quite well the signature of the coastal upwelling off Namibian coast with the isotherm 15°C position tilted upward and is close to the surface near the coast (**Figure 2.8,** left panel). The difference between the mean vertical section of temperature at 23°S from OGCM and WOA13 v2 is presented in **Figure 2.8** (right panel). The simulation is warmer than the observations in the surface layer (up to 30 m depth) over the 8° offshore. Above 30 m depth and offshore, the

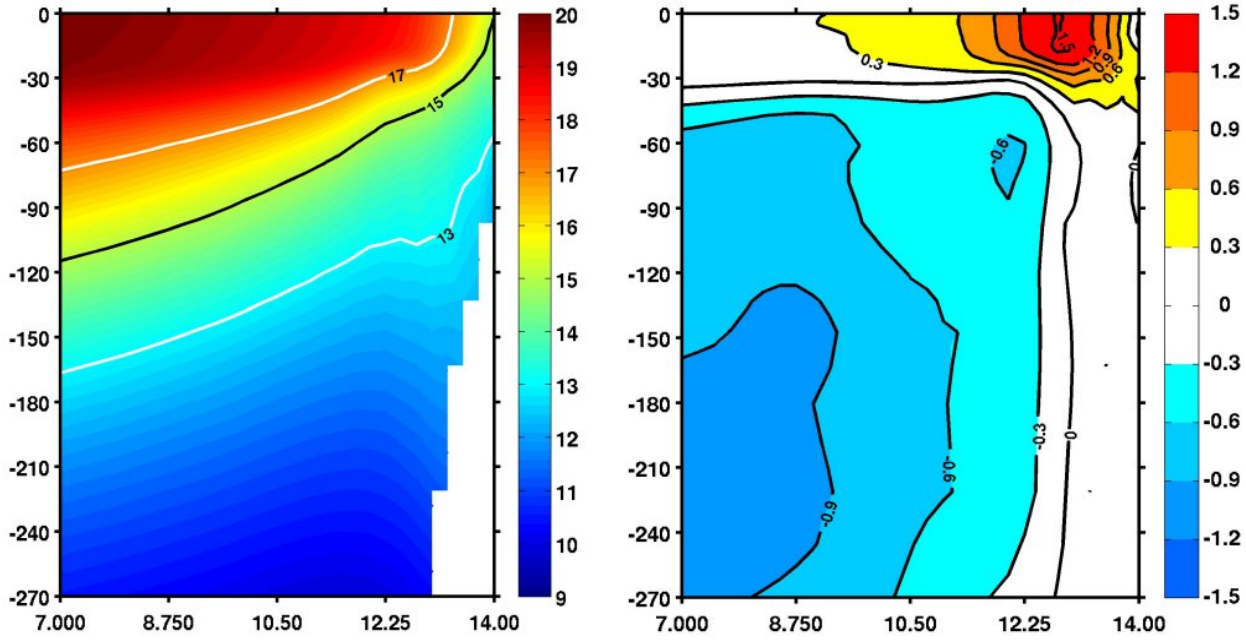

Figure 2.8: Left: OGCM mean vertical temperature section at 23°S (1958 - 2015) as a function of depth (meters) and longitude (degree E) and, right: Difference between model and WOA13 v2. The black (white) contours represent the mean position of the 15°C (17°C and 13°C) isotherms respectively. Black lines represent 0.2°C.

simulated temperature is cooler than the observed one. The large difference comprises between 1.4°C and 2°C appears close to the coast at the surface in the upper 30 m within around 400 km wide coastal band. The large differences observed between the OGCM and the observations refer to warm biases related to modelling problems encountered in the Angola-Benguela Current system. Similar results were obtained in the study by *Bachèlery et al.* [2016a] in the upper layer at the same position. Also, the simulation remains slightly warmer (less than 0.4°C) close to the coast and below 30 m compared to the observations.

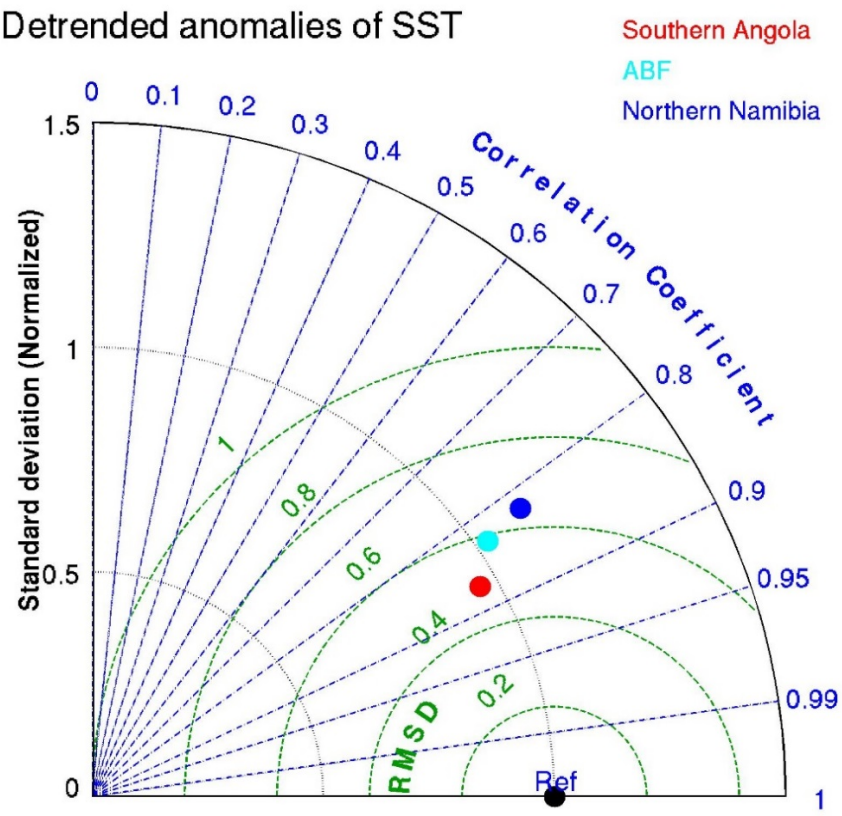

Figure 2.9: Taylor diagram (*cf.* **section 2.2.4**) comparing OGCM detrended anomalies of SST with OI-SST data. Data is averaged within 1 coastal band over 10° to 15°S (Southern Angola), 16.5°S to 17.5°S (ABF Zone) and 19°S to 24°S (Northern Namibia) representing the 3 coastal zones of interest (**Figure 2.2**) from the period 1982 - 2015.

Figure 2.9 shows a Taylor diagram of detrended SST anomalies averaged in Southern Angola (red dot), the Angola Benguela Front (light blue dot) and Northern Namibia (blue dot). The correlation range is quite good for the 3 coastal zones [0.8 - 0.9]. Correlation decreases, and the root mean square centred increases in a southward direction from the northernmost domain with tropical water to the southernmost domain, a wind-driven upwelling domain. This is also shown in **Figure. 2.7** (right panel).

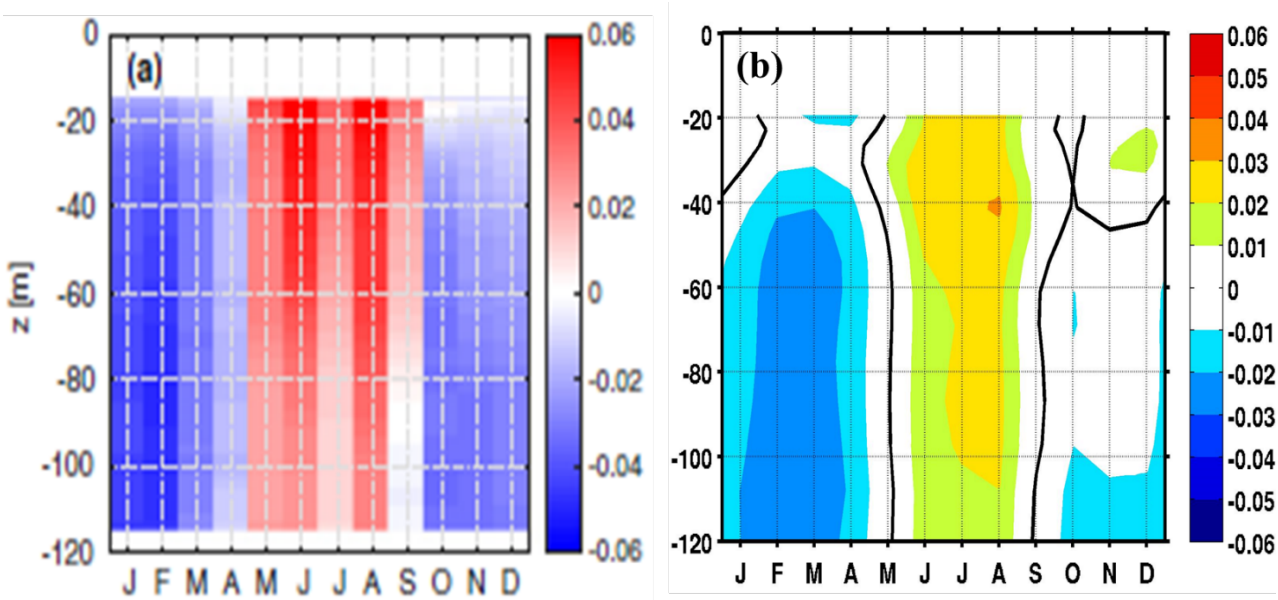

Figure 2.10: a) Monthly climatology of alongshore current velocities (cm/s) at 23°S from an Acoustic Doppler Current Profiler (ADCP) located at ~14°E. Figure from *Junker et al.* [2017]. b) OGCM mean vertical section of meridional current velocities averaged around the same position as the ADCP used in (a). For both figures, the monthly mean climatology is computed over the period 2003 – 2015. Positive (negative) current velocity values mean northward (poleward) directed currents.

As presented in **Chapter 1**, section 1.2, advection of warm Angolan tropical waters across the ABF into the Northern Namibia domain is a key element in the development of the Benguela Niño in the Angola – Benguela Current system [*Rouault* 2012]. Before using the OGCM to quantify the net mass transport across the ABF, a validation of OGCM meridional current velocities is performed and is presented in **Figure 2.10**. It was not possible to validate the OGCM at interannual timescales due to the scarcity of ocean current observations. This is the reason why validation is done at the seasonal scale. Such ADCP maps are the only one at hand to validate the model over this period (**Figure 2.10**). The seasonal cycle of OGCM vertical structure (from 20 - 120 m) of meridional velocities is compared to the observed meridional velocities measured with an ADCP located at around [~14°E; 23°S] from *Junker et al.* [2017] over the period 2003 – 2015.There is a quite good match in terms of representation of the

seasonal cycle of meridional currents between the OGCM and the ADCP currents from *Junker et al.* [2017]. Northward currents (positive values of meridional current velocities) are observed between May–September throughout the water column. Conversely, from October to April, the alongshore currents are mostly directed poleward (negative values of meridional current velocities). OGCM shows a weak equatorward flow (~0.01 cm/s) in the upper 45 m between October and December (**Figure 2.10b**) which was observed by *Junker et al.* [2017], but in the upper 16 m.

In conclusion, the mean state simulated by the OGCM is quite realistic along the equatorial Atlantic (temperature) and in the southeast Atlantic Ocean (temperature and alongshore currents). Furthermore, the OGCM (SSH and SST) and OLM (SSH) show good skills in representing interannual oceanic dynamics in the zones of interest of this study. OLM will allow to interpret altimetric data and OGCM SSH in terms of equatorial wave propagations. OGCM will provide a useful insight into the different surface and subsurface processes related to Benguela Niño and Niña interannual events in the Angola Benguela Current system especially before the satellite era (before 1982). After the description of the data and the methodology used for this study, the OLM is used in following chapter in combination with PIRATA moorings and AVISO SSH to investigate interannual equatorial Kelvin wave propagations along the Equatorial Atlantic and look at their link with the coastal warm or cold events along the Angola Benguela Current system.

CHAPTER 3

3 CONNECTION BETWEEN EQUATORIAL ATLANTIC AND ANGOLA BENGUELA CURRENT SYSTEM AT INTERANNUAL TIMESCALES

3.1 INTRODUCTION

Benguela Niños and Niñas are extreme interannual warm and cold respectively which happen along the coast of Angola and Namibia (*cf.* **section 1.2**). The prediction of these coastal extreme events is crucial for the southern African regions because of their significant impacts on the regional rainfall and marine ecosystem. To better understand the triggering mechanisms of Benguela Niños and Niñas, past studies highlighted the role played by two different forcings: the local atmospheric forcing, mainly through the modulation of the alongshore wind stress, and the remote oceanic forcing, associated with the propagation of EKW and CTW (*cf.* **section 1.3** for more details).

This part of my thesis focuses on the role of the remote oceanic forcing and is dedicated to the investigation of the relationship between the linear Equatorial Atlantic dynamics and the ocean variability along the coasts of Angola and Namibia. Past studies suggested that IEKW played a dominant role in the development of Benguela Niños and Niñas at interannual timescales [*Rouault et al.* 2007; *Bachèlery et al*. 2016a; *Rouault et al.* 2017]. Notably, one of the goals of PIRATA project (*cf.* **section 2.1.1**) is to study the ocean-atmosphere interactions aiming to monitor the interannual activity of the long equatorial waves, in my case the IEKW. Additionally, the OLM (*cf.* **section 2.1.2.2**) is used to simulate long interannual equatorial waves in the tropical Atlantic Ocean as the one used in *Rouault et al.* [2007] and *Rouault et al.* [2017]. This OLM is forced by interannual wind stress anomalies and allows interpreting observed sea level fluctuations as linear response to wind stress variations (*cf.* **section 2.1.2.2**). Different types

of datasets such as PIRATA dynamic Height and thermocline depth anomalies, AVISO SSHA and OLM SSHA are used to identify equatorial propagations related to IEKW activities and to define an oceanic index that we use to compare to SSTA along the Angola Benguela Current system.

3.2 ARTICLE'S RESULTS

Results from this work have been published in Journal of Geophysical Research Oceans (JGR-Oceans) in June 2017, as:

Imbol Koungue, R. A., S. Illig, and M. Rouault (2017), Role of interannual Kelvin wave propagations in the equatorial Atlantic on the Angola Benguela Current system, *J. Geophys. Res. Oceans*, 122, 4685–4703, doi:10.1002/2016JC012463.

The analysis and write up of this paper were done by myself under the guidance of my supervisors. All of the co-authors contributed to the writing, improvement and correction of the paper.

3.2.1 Identification of Abnormal SSH Propagations along the Equator

To identify abnormal equatorial propagations of SSH, we define a criterion which consists to detect DYNH and Z20 anomalies from PIRATA that exceed ± 1 standard deviation (green lines, **Figure 3.1**) for at least 2 months in a row at [0°E; 0°N] and at one other equatorial mooring location. When encountering missing values in monthly DYNH and Z20 PIRATA records, we search for 2-month abnormal altimetric SSHA at [0°E; 0°N] and at one other PIRATA mooring location. At the end, the detected abnormal episodes must always expect to be concomitant with eastward Kelvin propagation estimated from the OLM, in order to interpret local anomalies into basin scale IEKW. In order to document the link between equatorial Kelvin wave propagations and the Angola-Benguela Current system, we present in **Figure 3.1** the monthly normalized detrended interannual anomalies of dynamic height from PIRATA (blue line), along with monthly altimetry-derived and OLM-derived SSH anomalies (black line and red line,

respectively) from January 1998 to December 2012 at [0ºE; 0ºN] (top), [10ºW; 0ºN] (middle), and [23ºW; 0ºN] (bottom). The standard deviation of PIRATA-derived DYNH anomalies at [0ºE; 0ºN] is 2.83 cm, 2.76 cm at [10ºW; 0ºN], and 2.33 cm at [23ºW; 0ºN]. In **Figure 3.1**,

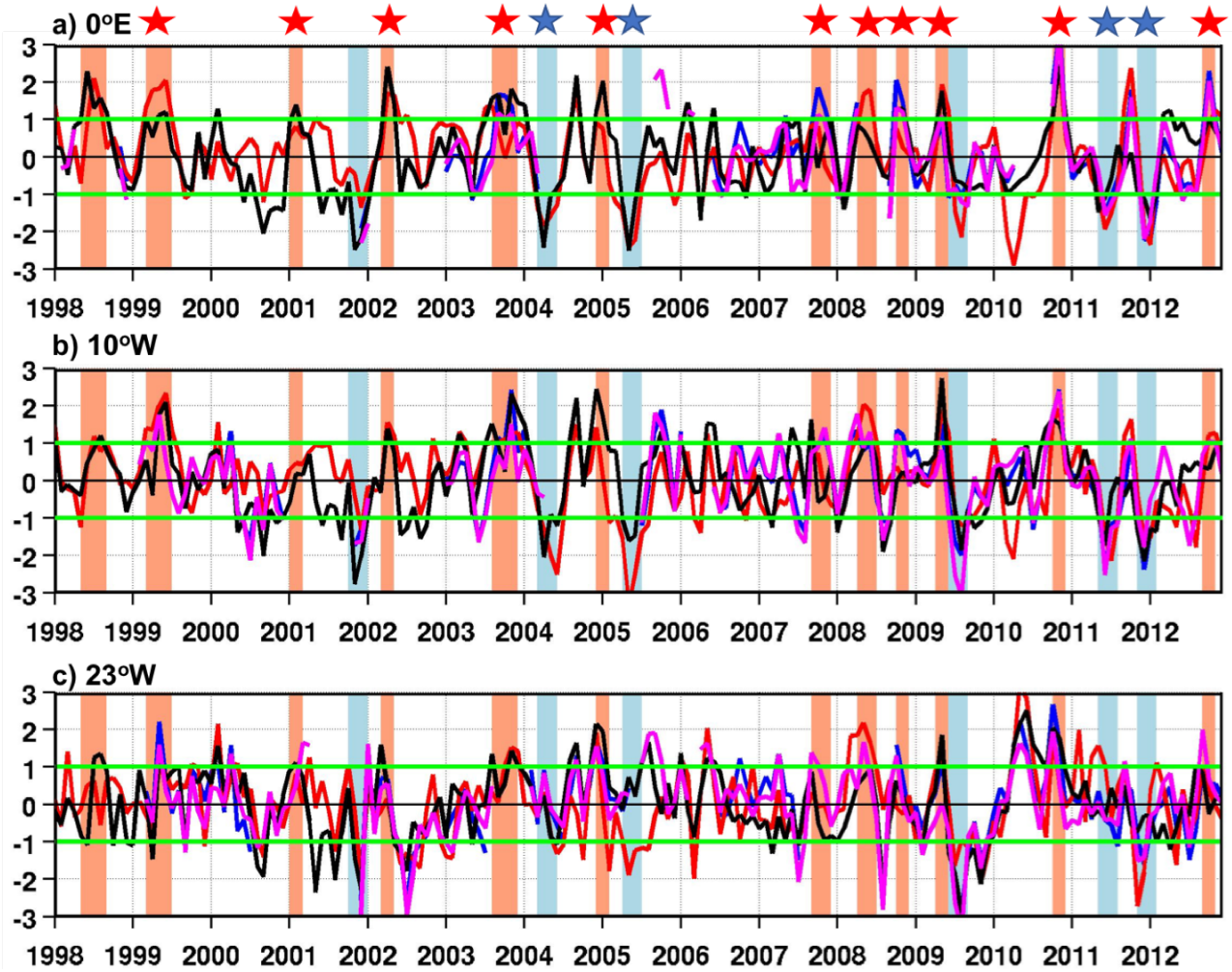

Figure 3.1: Monthly detrended normalized interannual anomalies of DYNH and depth of isotherm 20ºC from PIRATA in blue and magenta lines respectively, AVISO SSH in black line, and OLM SSH in red line; top, at [0ºE; 0ºN]; middle, at [10ºW; 0ºN], and bottom, at [23ºW; 0ºN]. Green horizontal lines indicate thresholds (± 1 standard deviation) to detect abnormal equatorial episodes. Abnormal positive and negative SSHA propagation episodes are represented by red and blue rectangles, respectively. Red and blue stars above the top plot highlight abnormal positive and negative SSHA propagation episodes associated with wind-forced IEKW (as opposed to IEKW trigged by Rossby wave reflection).

abnormal positive and negative SSH anomalies episodes in the eastern equatorial Atlantic are highlighted by red and blue rectangular shadings, respectively, which width is function of the duration of the episode. These coloured rectangles constitute our equatorial variability index. This proxy will be used throughout this chapter and the rectangles will be reproduced in the subsequent figures.

At a monthly resolution, there is a good agreement between PIRATA-DYNH, AVISO SSH, and OLM SSH interannual anomalies (*cf.* **Table 3.1**). At [0ºE; 0ºN], there is a correlation of 0.68 between altimetry-derived SSH anomalies and PIRATA DYNH anomalies, while correlation between the OLM SSHA and PIRATA DYNH anomalies is 0.65, both being significant at 95% level (using p-value statistical test from *Best and Roberts* [1975]). The same analysis is also conducted using the Z20 from PIRATA moorings. Results show that, even if numerous gaps are presents in PIRATA Z20 data, correlation between PIRATA Z20 and PIRATA DYNH remains larger than 0.8 for the three equatorial moorings and 2-month lag peaks identified in DYNH are also captured in the subsurface PIRATA Z20 measurements (*cf.* **Table 3.2**). Gaps occur occasionally in PIRATA at different locations, so we are also using altimetry to verify the robustness of our results and extend our analysis to period where no PIRATA data are available. Interannual OLM SSH outputs compare well with equatorial observations emphasizing the dominance of the equatorial wave propagation signal on the equatorial variability over the 1998 - 2012 period, extending the results from *Illig et al.* [2004] over a more recent period. Thus OLM outputs are used here to interpret local observations in terms of basin-scale variability associated with IEKW.

Correlation	[23°W; 0°N]	[10°W; 0°N]	[0°W; 0°N]
PIRATA DYNH – OLM SSHA	0.59	0.53	0.65
PIRATA DYNH – AVISO SSHA	0.75	0.67	0.68
OLM SSHA – AVISO SSHA	0.51	0.59	0.62

Table 3.1: Correlation between PIRATA DYNH, OLM SSH and AVISO SSH monthly detrended interannual anomalies at [23°W; 0°N], [10°W; 0°N], and at [0°E; 0°N] over the 1998 - 2012 period. Correlations are statistically significant at 95% (using p-value statistical test from *Best and Roberts* [1975]).

downwelling episodes	PIRATA DYNH			PIRATA Z20			Altimetry			OLM	Literature
	23°W	10°W	0°E	23°W	10°W	0°E	23°W	10°W	0°E		
1998 (May-Sep)							✓	✓	✓	✓	
1999 (Mar-Jul)	✓			✓	✓		✓	✓	✓	✓	Doi2007
2001 (Jan-Mar)				✓			✓	✗	✓	✓	Rouault2001
2002 (Mar-May)	✗			✗			✓	✓	✓	✓	HB2009
2003 (Aug-Dec)		✓	✓		✓	✓	✓	✓	✓	✓	
2004/2005 (Dec-Feb)	✓			✓			✓	✓	✓	✓	
2007 (Sep-Dec)		✓	✓	✓	✓	✓	✗	✓	✓	✓	
2008 (Apr-Jul)		✓	✓	✓	✓		✓	✓	✗	✓	
2008 (Oct-Dec)	✓	✓	✓	✓	✓	✓	✗	✗	✓	✓	
2009 (Apr-Jun)	✓	✓	✗	✗	✗	✓	✓	✓	✓	✓	
2010 (Oct-Dec)	✓	✓	✓	✓	✓	✓	✓	✓	✓	✓	
2012 (Sep-No)	✗		✓	✓	✓	✓	✓	✗	✓	✓	

Upwelling episodes											
2001/2002 (Oct-Jan)	✓	✓	✓	✓	✓	✓	✓	✓	✓	✓	
2004 (Mar-Jun)	✗			✗			✓	✓	✓	✓	
2005 (Apr-Jul)				✗	✓		✗	✓	✓	✓	Marin2009+HB2009
2009 (Jun-Sep)	✓	✓	✓	✓	✓	✓	✓	✓	✗	✓	FM2010b+BUR2016
2011 (May-Aug)	✓	✓	✓	✗	✓	✓	✗	✓	✓	✓	
2011/2012 (Nov-Feb)	✓	✓	✓	✓	✓	✓	✗	✓	✓	✓	

Table 3.2: List of abnormal downwelling and upwelling propagations as detected in detrended interannual PIRATA dynamics height (DYNH), depth of 20°C isotherm (Z20), altimetric signal at [23°W; 0°N], [10°W; 0°N] and [0°E; 0°N], with outputs from the Ocean Linear Model (OLM) showing concomitant anomalous propagations. Grey cell shading corresponds to missing data in PIRATA records. Green check symbols correspond to 2-month abnormal episodes captured by time series analysis. Orange check symbols correspond to 1-month abnormal episodes. Red cross symbols depict anomalies that do not exceed our predefined threshold. In agreement with our criterion to depict strong equatorial propagations (priority to in situ PIRATA data over altimetry, and peaks detected concomitantly at [0°E; 0°N] and at one of the other mooring location, see **section 2.5.3** in *Imbol Koungue et al.* [2017] for more details), green cell shading highlight the decisive information used to catalogue strong downwelling and upwelling episodes. The last column recapitulates the studies which mention these abnormal propagations: *Foltz and McPhaden* [2010b] (FM2010b), *Doi et al.* [2007] (Doi2007), *Rouault et al.* [2007] (Rouault2007), *Hormann and Brandt* [2009] (HB2009), *Marin et al*. [2009] (Marin2009), and *Burmeister et al.* [2016] (BUR2016).

A combined analysis of PIRATA, altimetry, and OLM time series allows us to identify numerous significant upwelling and downwelling IEKW over the 1998 - 2012 period. The criterion used consists to look at the PIRARA DYNH or Z20 or altimetric SSHA respectively that exceed the ± 1 standard deviation for at least 2 months at 0°E; 0°N and at another mooring location. Our results are summarized in **Table 3.2** which is presented above. According to our criterion, abnormal downwelling IEKW SSH signatures (positive SSH episodes) occurred in 1998 (May - September), 1999 (March - July), 2001 (January - March), 2002 (March - May), 2003 (August - December), 2004/2005 (December - February), 2007 (September - December), 2008 (April - July), 2008 (October - December), 2009 (April - June), 2010 (October - December), and 2012 (September - November). Negative SSH episodes (abnormal upwelling IEKW SSH signatures) occurred in 2001/2002 (October - January), 2004 (March - June), 2005 (April - July), 2009 (June - September), 2011 (May - August), and 2011/2012 (November - February). These anomalies are also clearly detected earlier in time in the other mooring locations (**Figure 3.1** middle and bottom plots) at [10°W; 0°N] and [23°W; 0°N] confirming a propagation in SSH from West to East. Note that the linear model shows a significant eastward SSH propagation from February to June 2010, which is not captured by the observations (**Figure 3.1**). Thus, it is not taken into account in our equatorial index, whereas a Benguela Niña was observed along the western African coast afterwards. Some of these episodes were described in the literature. For instance, the 2001 propagation episode was extensively reported in *Rouault et al.* [2007] and linked to a warm event in the Angola-Benguela Current system in late austral summer 2001. The propagation of positive SSH in 1999 described here corresponds to a coastal warm event at the Angola Benguela front reported by *Mohrholz et al.* [2001] and *Doi et al.* [2007]. Furthermore, the austral fall 2002 abnormal positive propagation episode SSH is described in the study of *Hormann and Brandt* [2009], who mentioned intense downwelling Kelvin wave activities in 2002 along the equator. Upwelling Kelvin waves were already identified along the Equator at the origin of the negative SSH propagation episode in 2005 [*Hormann and Brandt*, 2009; *Marin et al.,* 2009]. More details are given in the **section 3.2.2** concerning the 2009 abnormal negative SSH episode which has been documented by *Foltz and McPhaden* [2010b] and *Burmeister et al*., [2016]. Note that during the 2001 downwelling propagation episode, no data are available from PIRATA equatorial dynamic height (DYNH). However, the 2001 event is well captured by PIRATA anomalous depth of the thermocline (Z20)

at [23°W; 0°N] (**Figure 3.1**). Normalized Altimetry monthly SSHA also capture strong abnormal episode at [0°E; 0°N]. In *Rouault et al.* [2007], the PIRATA records (depth of the isotherm 20°C) were available in 2001 and allowed detecting the eastward propagation of higher than normal SSHA in early 2001. For our study, for most of the year 2001, low quality data is recorded with several measuring depths having low quality number 4 meaning questionable data. Therefore, no DYNH data are now available for download to sample the 2001 downwelling propagation, and only time series of Z20 at [23°W; 0°N] is available.

3.2.2 Forcing and propagation of Equatorial Kelvin Waves From 1998 to 2012

In order to interpret the local in situ signal from PIRATA records in terms of linear propagations, and better describe the propagating characteristics of the equatorial dynamics as sampled by PIRATA along the equator, we analyze now the equatorial wave propagation signature and the associated forcing.

To do so, we have detrended and averaged the OLM key forcing parameter, viz., the zonal wind stress interannual anomalies over the ATL4 domain (i.e., [50°W–25°W; 3°S–3°N], *Illig and Dewitte* [2006]). This time series is displayed on **Figure 3.2** (top). Most of the SSH positive and negative propagations described earlier (shaded rectangles) are associated with weaker and stronger than normal easterly wind stress anomalies, respectively. Following the decrease or the increase of the easterly wind stress in the western equatorial Atlantic, positive or negative SSHA episodes, respectively, propagate eastward through the PIRATA array of moorings (**Figure 3.1**). Close inspection of lag correlation (not shown) between zonal wind stress anomalies and OLM SSH anomalies reveals a 95% significant correlation of 0.6 when the western equatorial zonal wind stress anomalies in ATL4 lead the OLM SSH anomalies at [0°E; 0°N] by a month. This lag of 1 month corresponds to a propagation speed of 1.6 m/s which is consistent with the propagation phase speed of Kelvin wave mode 2, in agreement with the study of *Illig et al.* [2004]. This leads to focus on IEKW and examine the outputs of the OLM in order to characterize the role of equatorial wave dynamics in the propagations of the SSH across the basin.

Figure 3.2 (bottom) presents the first three gravest baroclinic modes of equatorial Kelvin wave contributions to SSH variation from 1998 to 2012. The summed-up contribution is

averaged between 20°W and 0°E, at 0°N. The second baroclinic mode of IEKW is the most energetic mode, followed by the first one in agreement with *Illig et al*. [2004] and *Bachèlery et al*. [2016a]. As in *Illig et al.* [2004], the linear dynamics controls the equatorial variability as the correlation between OLM outputs and altimetric interannual anomalies remain significant at 95% level along the whole equatorial waveguide (**Figure 2.3**). The amplitude of IEKW averaged

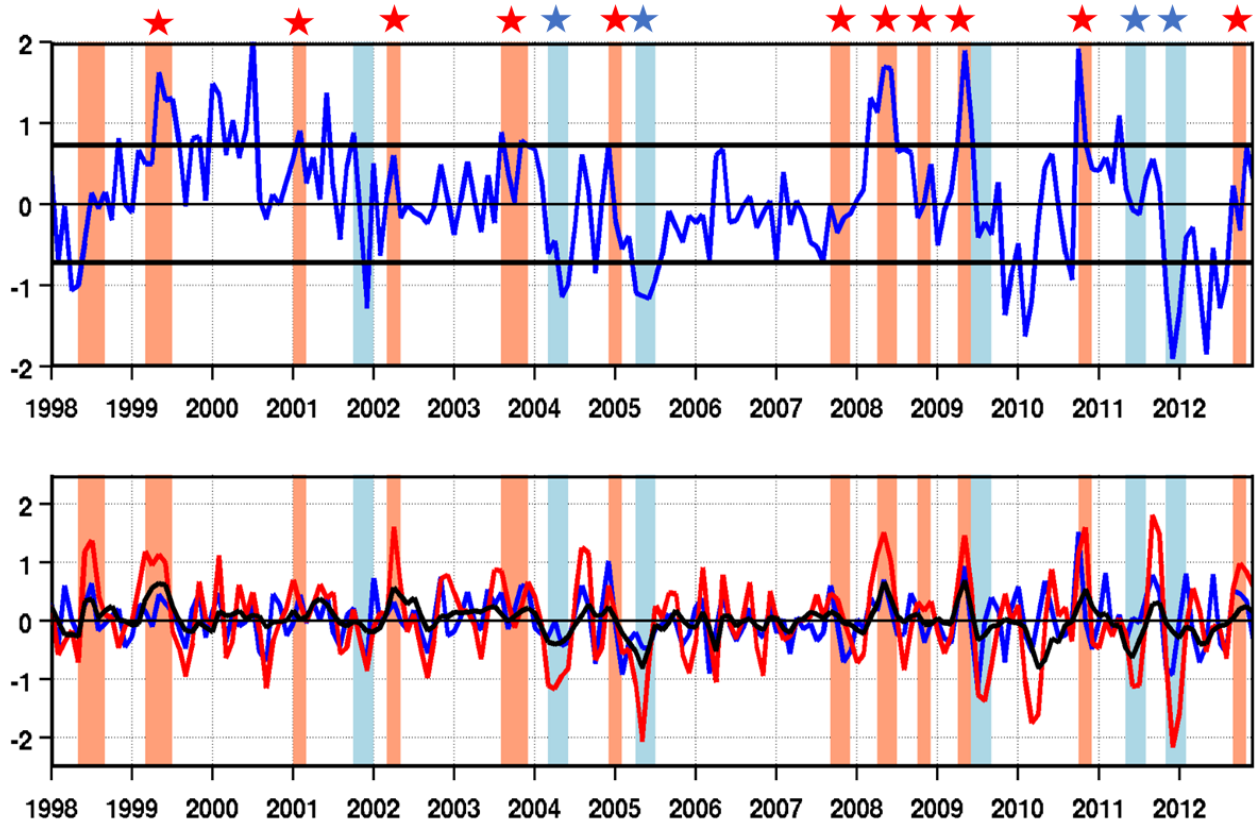

Figure 3.2: (Top) Detrended monthly anomalies of zonal wind stress (N.m^{-2}) averaged over ATL4 (50°W–25°W, 3°S–3°N). Black horizontal lines indicate ±1 standard deviation. Bottom, OLM detrended anomalies of Kelvin wave monthly contribution to SSHA (cm): first baroclinic mode in blue, second baroclinic mode in red, and third baroclinic mode in black, averaged over (20°W–0°E, at 0°N). Abnormal equatorial positive and negative SSHA propagation episodes identified in **Figure 3.1** are represented by red and blue rectangles, respectively. Red and blue stars highlight abnormal positive and negative SSHA propagation episodes associated with wind-forced IEKW (as opposed to IEKW trigged by Rossby wave reflection).

between 20°W and 0°E, at 0°N (**Figure 3.2**, bottom) is compared with the equatorial index (**Figure 3.1**) and results show a good agreement. Thus, the OLM represents well the equatorial variability of IEKW propagations over the 1998 - 2012 period. Most of the western zonal wind stress anomalies are related to propagation of downwelling or upwelling IEKW, respectively. These waves propagate eastward and are observed through positive or negative abnormal SSH in the Eastern equatorial Atlantic (**Figure 3.1**, top). According to what is expected from Kelvin wave dynamics in connection with the modulation of the forcing, for some particular years, 1998 (from May to September), 2001/2002 (from October 2001 to January 2002), and 2009 (from June to September), the direction of zonal wind stress anomalies (**Figure 3.2**, top) does not match the sign of abnormal SSH propagations. In agreement with *Foltz and McPhaden* [2010a], the analysis of the wave sequence (not shown) reveals that for the year 1998, negative zonal wind stress interannual anomalies force preferentially westward propagating downwelling Rossby waves, rather than upwelling Kelvin waves. This is more likely due to the spatial pattern of the wind stress anomalies that is maximal off equator. At the Brazilian coast, these Rossby waves reflect into eastward propagating downwelling Kelvin waves. Symmetrically, for years 2001/2002 and 2009, decreased easterly winds in the western tropical Atlantic, through the propagation and reflection of upwelling Rossby waves, yield to upwelling IEKW signal in the Eastern Atlantic. According to *Foltz and McPhaden* [2010b] and *Burmeister et al*. [2016], the observed 2009 negative abnormal SSH anomalies results from a wave reflection process. The latter is related to anomalous northwesterly wind in the Equatorial Atlantic associated with strong negative Atlantic meridional mode in boreal spring 2009. This mechanism explains the apparent inconsistency between the sign of the wind stress anomalies in the western Atlantic and the equatorial SSHA in the Gulf of Guinea. This supports our idea of defining an index based on the IEKW activity in the Eastern Atlantic as monitored by PIRATA, rather than using wind stress amplitude in the western Tropical Atlantic, in order to forecast SST anomalies along the coasts of Angola and Namibia, which will be done in the following.

Over 1998 - 2012, when we compare OLM second mode of IEKW (averaged within [20°W– 0°E; 0°N]) and wind index (averaged within ATL4 box), the 95% significant correlation between IEKW and SSH anomalies along the Southern Angola coastline (averaged between 10°S and 15°S and within 1° coastal band) is significantly higher (~0.5, **Figure 3.3a**) than the one with the wind index (~0.25, **Figure 3.3b**), when both equatorial indexes lead coastal SSH

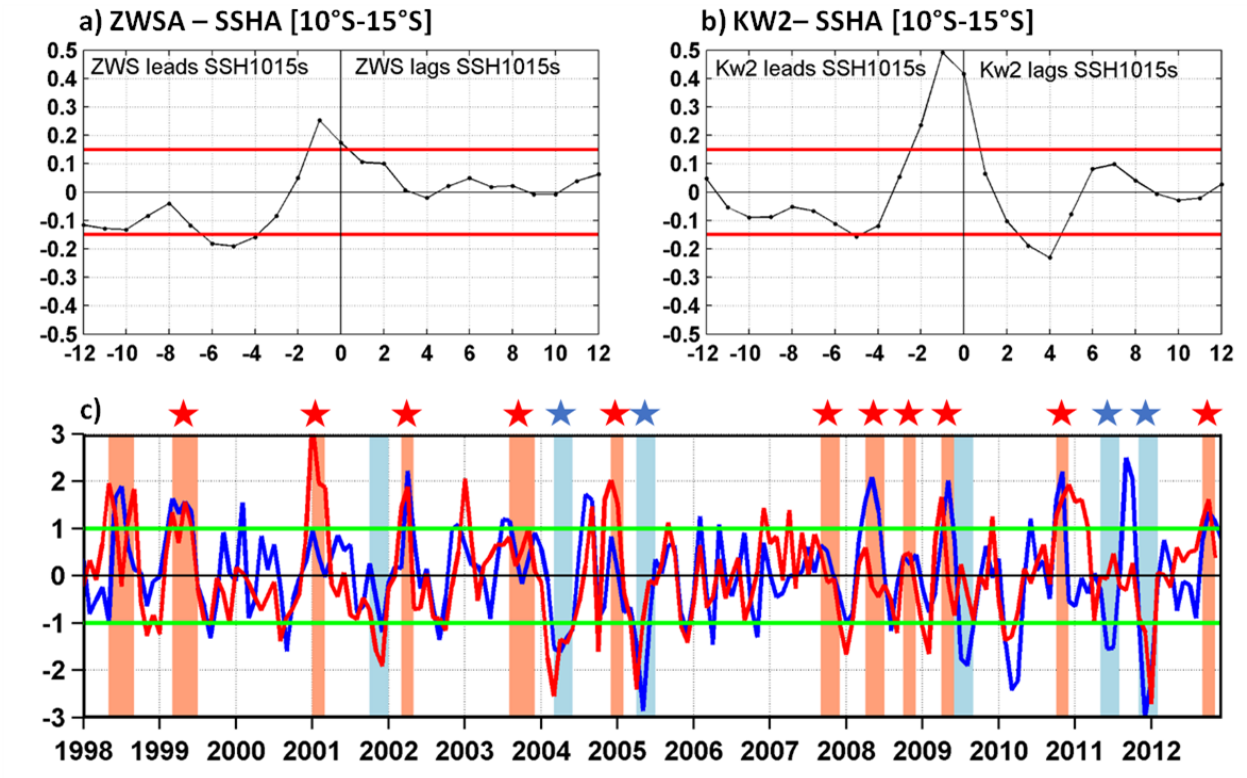

Figure 3.3: (a) Correlation analysis between monthly Zonal Wind Stress Anomalies (ZWSA) averaged in ATL4 (50°W - 25°W; 3°S - 3°N], and monthly SSH anomalies along the African coast in Southern Angola (averaged between 10°S and 15°S and over 1° coastal fringe), in function of the Lag (in months). Negative lags indicate that ZWS leads. (b) Same but with correlation between monthly OLM IEKW second mode averaged between 20°W and 0°E at 0°N and monthly SSH anomalies along the African coast. Negative lags indicate that IEKW leads. The 95% significant correlation threshold is indicated by red lines. (c) Monthly OLM IEKW second mode in blue averaged between 20°W and 0°E at 0°N and 1 month lagged detrended normalized monthly SSH anomalies averaged between 10°S and 15°S and from the coast to 1° offshore according to the maximum of correlation that appears at lag -1. Green horizontal lines represent the ±1 standard deviation. Abnormal equatorial positive and negative SSHA propagation episodes identified in **Figure 3.1** are represented by red and blue rectangles, respectively. Red and blue stars highlight abnormal positive and negative SSHA propagation episodes associated with wind-forced IEKW (as opposed to IEKW trigged by Rossby wave reflection).

variability by 1 month. Noteworthy, when we remove periods during which the sign of the wind does not match (according to what is expected from the linear theory) with the sign of the OLM second mode IEKW SSH anomalies (i.e., May - September 1998, October 2001 to January 2002, and June - September 2009), the correlation between the wind index and coastal SSH anomalies increases to reach a value of 0.4. Also, we notice that in **Figure 3.3b**, the significant correlations with IEKW leading coastal SSH anomalies occur over a broad lag interval, ranging from 0 to 2 months, highlighting the duration of interannual events. It most likely also reflects the change in IEKW phase speed associated with each peculiar event and which depends on the southeastern Atlantic vertical structure variability and baroclinic mode contribution that will be discussed in detail at the end of section 3.4. **Figure 3.3c** presents the IEKW mode 2 time series (averaged within [20°W–0°E; 0°N]) and the coastal SSHA time series (averaged between 10°S and 15°S and within 1° coastal band) shifted ahead in time by one month. It allows appreciating the dynamical coherence between equatorial and coastal domains when the equatorial (IEKW mode 2) leads the Southern Angola coastal SSH by 1 month according to the maximum of correlation obtained in **Figure 3.3b**.

3.2.3 Propagations of Kelvin Waves in PIRATA Z20

Figure 3.4 further illustrates the signature of eastward propagations in PIRATA records. It presents some specific cases used to estimate the speed of abnormal propagations as observed by 5-day means of Z20 anomalies from PIRATA records and altimetry. This also allows us to calculate, for some specific strong eastward propagations, the time lags at different longitudes and compare estimated phase speed values to the speed of each baroclinic modes. Uncertainties in the estimates of propagation phase speeds using the PIRATA records are also evaluated as some noise could be superimposed on the peaks. We focus here on PIRATA Z20 interannual anomalies because fluctuations of the thermocline depth of about 15 m (deepening or shoaling) are also an important signature of the IEKW, which is also captured by altimetry (SSHA).

In **Figure 3.4a**, we observe from the 22 October 2003, a clear eastward propagation of a deepening of the thermocline starting at 35°W which takes 32 days to reach the eastern part of the equatorial Atlantic (0°E) on the 22 November 2003. The maximum deepening of the thermocline is larger than 15 m, located between 15°W and 10°W. Thus, this propagation agrees

with a free propagating second baroclinic mode downwelling Kelvin wave with a phase speed of 1.4 ± 0.15 m/s, in agreement with the study of *Illig et al.* [2004]. The associated anomalies (SSH

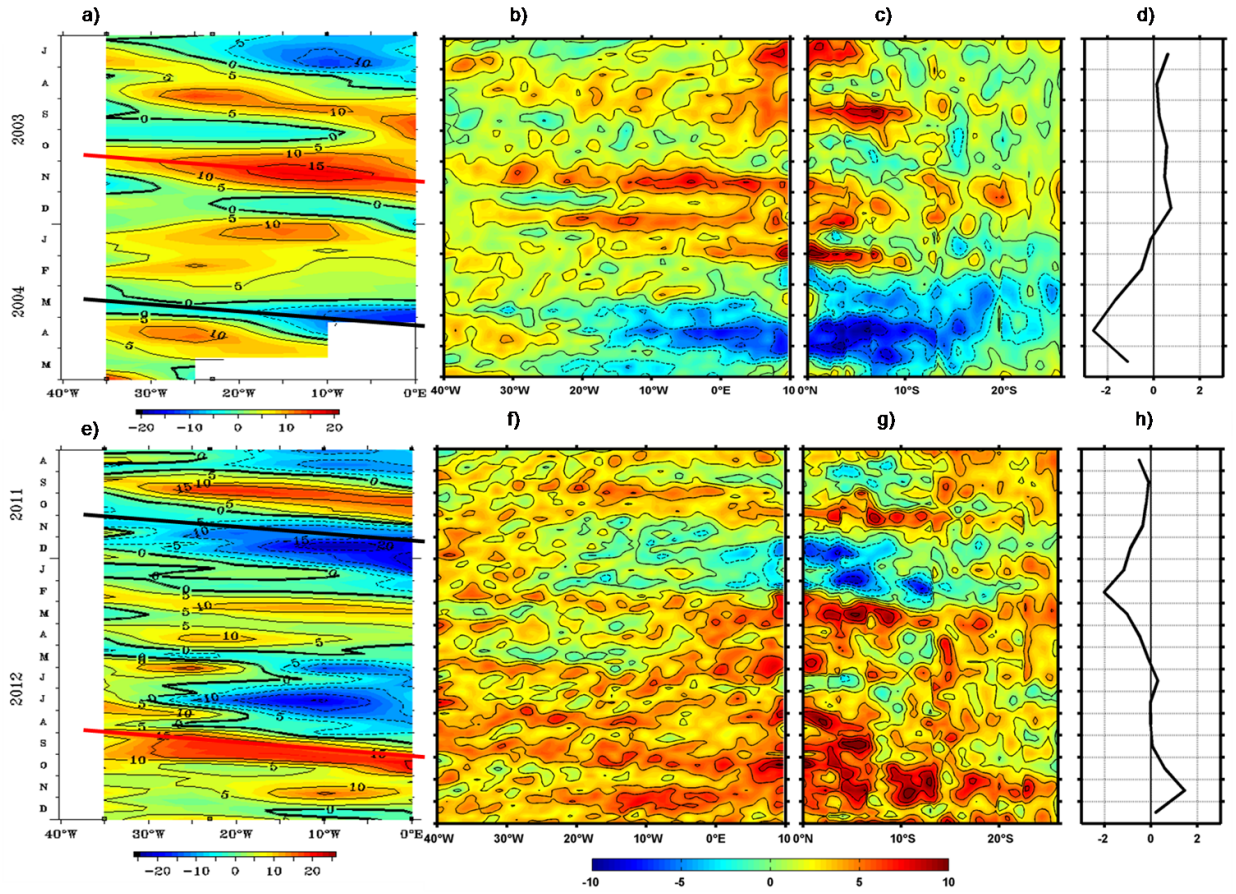

Figure 3.4: (top: from left to right, a) Longitude time Hovmöller diagram of 5 day means of Z20 anomalies (m) along the equator inferred from PIRATA moorings and interpolated between mooring locations, (b) SSH anomalies (cm) inferred from AVISO along the equator averaged between 1°S and 1°N, (c) latitude time Hovmöller diagram of SSH anomalies (cm) inferred from AVISO averaged within 1° coastal fringe, and (d) time series of SST anomalies (°C) averaged from 10°S to 15°S within 1° coastal fringe for the period July 2003 to May 2004. Bottom, the same plots are represented, but for the period August 2011 to December 2012. The red and black tick straight lines represent eastward phase speed estimates (m/s).

and Z20) last for about 3 months at 0°E, as illustrated in **Figures 3.4b** and **3.1** (top). The associated SSH anomalies are consequently captured by our equatorial criterion based on

PIRATA DYNH and classified as strong abnormal equatorial SSH episodes (see red rectangle in **Figure 3.1** and **Table 3.2**). The thermocline depth, (Z20) remains deeper than normal up to September 2003, when an upwelling negative propagation develops. Equatorial propagating anomalies are also captured by altimetry (**Figure 3.4b**). Similarly, in 2012 a clear eastward propagation of positive anomalies of Z20 larger than 10 m is observed basin wide from the 30 August to the 27 September 2012 with a maximum deepening larger than 15 m at 0°E in early October 2012 (**Figure 3.4e**). The thermocline remains deeper by about 15 m during the propagation of the IEKW along the equator. An eastward phase speed of 1.6 ± 0.15 m/s is estimated using the abovementioned methodology. It suggests that a strong downwelling IEKW mode 2 was triggered in the west by a relaxation of the equatorial Trade wind (**Figure 3.2** top plot).

In austral autumn 2004, from 35°W toward the African coast along the equatorial wave guide, we observe a rapid eastward propagation of negative anomalies of Z20 from around the 15 March 2004 and reaching 0°E around the 6 April 2004, with a maximum shoaling located East of 10°W. Despite the lack of data in the Eastern part of the equatorial Atlantic records by the PIRATA buoys in April and May 2004 (also summarized in **Table 3.2)**, this eastward propagation is well observed in the altimetric signal (**Figure 3.4b**). It suggests that shoaling of the thermocline takes ~15 days to travel eastward from 35°W to 0°E. The corresponding wave speed is around 2.00 ± 0.15 m/s and corresponds to the first baroclinic mode. Similarly, around the 30 October 2011 from 35°W, an eastward propagation of negative anomalies of Z20 is observed in the PIRATA records along the equator. It reaches 0°E around the 2nd December 2011, characterized by a maximum shoaling of the thermocline of ~15 m at 0°E. The eastward IEKW speed associated is ~1.4 ± 0.15 m/s. This propagation corresponds to a second baroclinic mode of IEKW. This eastward propagation of SSHA is also observed in altimetry (**Figure 3.4f**). These estimated phase speed and baroclinic mode are consistent with the study of *Illig et al.* [2004].

In **Figures 3.4c** and **3.4g**, we observe that the anomalous equatorial propagations identified in **Figures 3.4b and 3.4f** are consistent with southward propagations along the African coast up to 25°S. However, the coastal anomalies are less intense than the anomalies along the equator and decrease as they propagate further South, in agreement with the modelling results of *Bachèlery et al.* [2016a].

Furthermore, **Figures 3.4d** and **3.4h** which present the interannual coastal SST anomalies in Southern Angola, highlight that the equatorial wave propagation identified in the observations (PIRATA and altimetry) are subsequently associated with extreme cold or warm SST events along the western coast of Africa. Indeed, downwelling propagations in austral spring 2003 and 2012 are associated with warmer than usual SST in the coastal [10°S - 15°S] box. Conversely, upwelling equatorial propagations are subsequently followed by negative anomalous SST larger than 2°C. These preliminary results suggest that the oceanic teleconnection with equatorial dynamics as observed by PIRATA moorings plays an important role in the coastal interannual SST variability along west Africa. This will be addressed in more detail in the **section 3.2.4**.

3.2.4 Link between equatorial variability and the Angola Benguela system

In order to document the link between the equator and the Angola Benguela Current system, **Figure 3.5** presents normalized coastal detrended OI-SST along the Angola Benguela Current system averaged in the 3 coastal zones of interest. On top, we show the time series of the Southern Angola domain ([10°S–15°S]); in the middle, the Angola Benguela Frontal zone ([16.5°S–17.5°S], and at the bottom, the Northern Namibia upwelling domain ([19°S–24°S]) as shown in **Figure 2.2**. Here, we define an extreme warm or cold event as a period during which the normalized detrended SST anomalies exceed one standard deviation for at least 3 months in a row and for at least two of the three coastal zones. Also, when normalized detrended SST anomalies exceed one standard deviation for less than 3 months in a row within two of the three coastal zones, we distinguish the event as a moderate coastal event. Identified major SST events are denoted with dark red or blue triangles above the time axis on the bottom plot. Results show that most major warm and cold events along the African coast, especially in Southern Angola and Angola Benguela front domains, are linked to the equatorial variability index associated with IEKW propagations which are triggered by zonal wind stress anomalies in the western equatorial Atlantic. Based on the criterion above defined for abnormal coastal SST events, we identified seven major warm events: in 1998 (August - November), 1999 (March - August), 2001 (January - May), 2003 (July - December), 2008/2009 (November - January), 2010/2011 (November - April), and 2012 (October - December), and six cold events in 2001/2002 (October - March), 2002 (July - December), 2004 (January - April), 2005 (April - June), 2010 (February - May), and

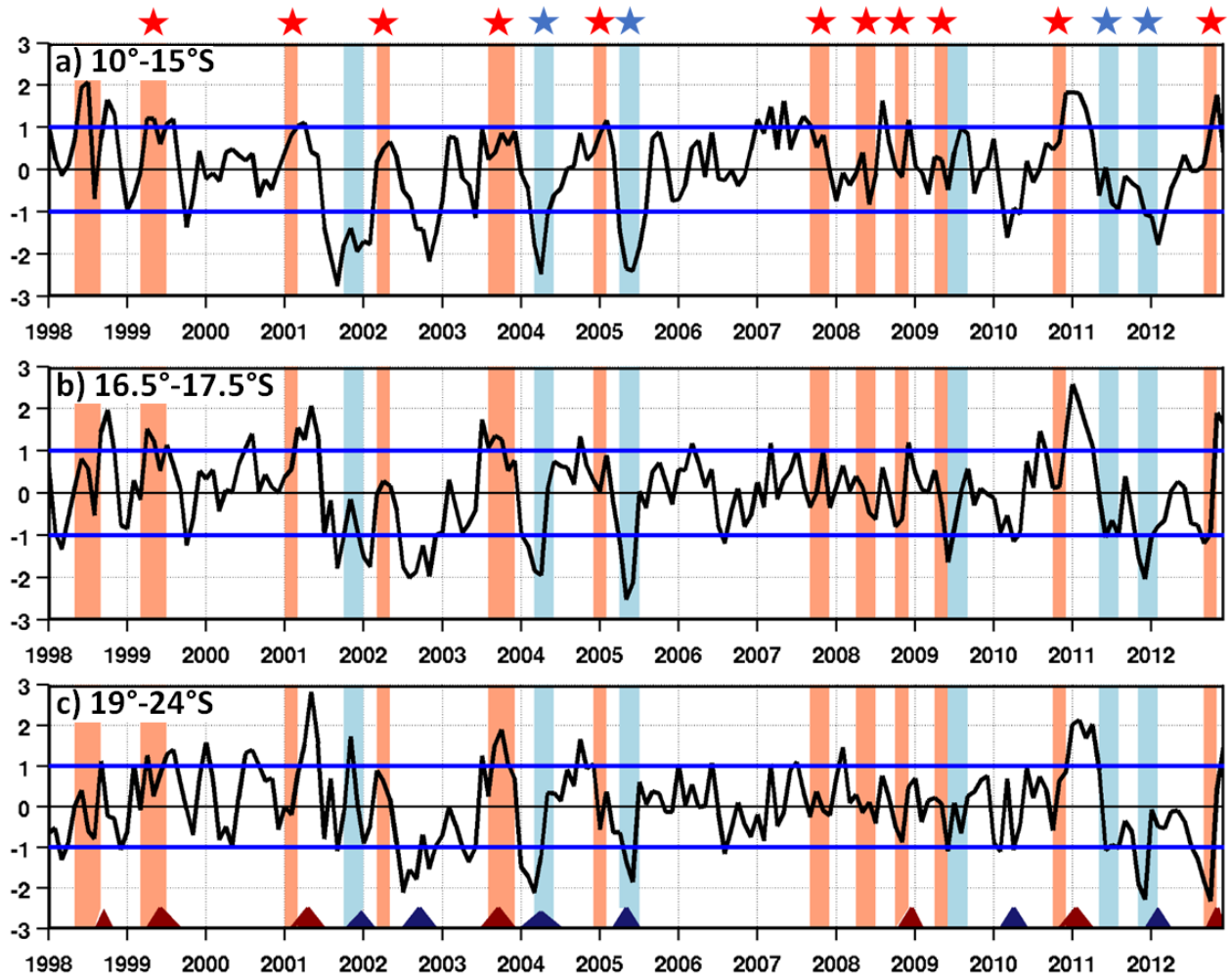

Figure 3.5: Monthly detrended normalized anomalies of SST in (top) Southern Angola averaged from 10°S to 15°S and from the coast to 1° offshore, (middle) Angola Benguela Front region averaged from 16.5°S to 17.5°S and from the coast to 1° offshore, and (bottom) Northern Namibia averaged from 19°S to 24°S and from the coast to 1°offshore. Blue horizontal lines represent the threshold (±1 standard deviation) used to detect abnormal coastal SST events in the three domains. Dark red and blue triangles on the bottom plot represent extreme warm and cold events, respectively, along the Angolan-Namibian coastlines. Abnormal equatorial positive and negative SSHA propagation episodes identified in **Figure 3.1** are highlighted with red and blue rectangles, respectively. Red and blue stars highlight abnormal positive and negative SSHA propagation episodes associated with wind-forced IEKW (as opposed to IEKW trigged by Rossby wave reflection).

2011/2012 (November - March). Major warm events 2003 and 2012, as well as major cold events 2004 and 2011, are clearly seen in **Figures 3.4c**, **3.4d**, **3.4g**, and **3.4h**.

	Whole 15-year period	Strong equatorial propagation periods
[10°S-15°S]	0.40	0.60
[16.5°S-17.5°S]	0.27	0.49
[19°S-24°S]	0.16	0.68

Table 3.3: Correlation between monthly detrended IEKW mode 2 anomalies averages between [20°W-0°W] at 0°N and monthly detrended normalized anomalies of SST in Southern Angola ([10°S-15°S]; 1° coastal band), in the Angola Benguela Front region ([16.5°S-17.5°S]; 1° coastal band), and in the Northern Namibia area ([19°S-24°S]; 1° coastal band). Correlations are performed over the 1998 - 2012 period (1st column) and only during identified strong equatorial propagation episodes (2nd column), with IEKW mode 2 leading SST anomalies by 1 month. Correlations are statistically significant at 95% (using p-value statistical test from *Best and Roberts* [1975]).

Some of these warm events were identified previously by couple of authors [*Rouault et al.,* 2007; *Ostrowski et al.,* 2009; *Lübbecke et al.,* 2010; *Rouault* 2012]. There is little in the literature concerning cold events after 2002. The 1999 Benguela Niño at the Angola Benguela Front was described by *Mohrholz et al*. [2001] and *Doi et al.* [2007]. A 0.4 (0.27) lag correlation (*cf.* **Table 3.3**), statistically significant at 95%, is estimated when normalized detrended anomalies of IEKW mode 2 averaged between 20°W and 0°E at 0°N leads normalized detrended anomalies of SST in the Southern Angola (ABF) domains by 1 month over the whole (15 years) period. There is no significant correlation with Northern Namibia domain. Significantly higher values of correlations are estimated when only considering periods of strong equatorial propagations (*cf.* **Table 3.3**). Over the periods of strong equatorial propagations, we find a higher correlation of 0.6 (0.49) statistically significant at 95% when OLM IEKW mode 2 leads detrended normalized anomalies of SST by 1 month in Southern Angola (ABF zone).

Noteworthy, these values are dependent on the prescribed lag, with in particular higher correlations with Northern Namibia domain when a 2-month lag is used (not shown). We

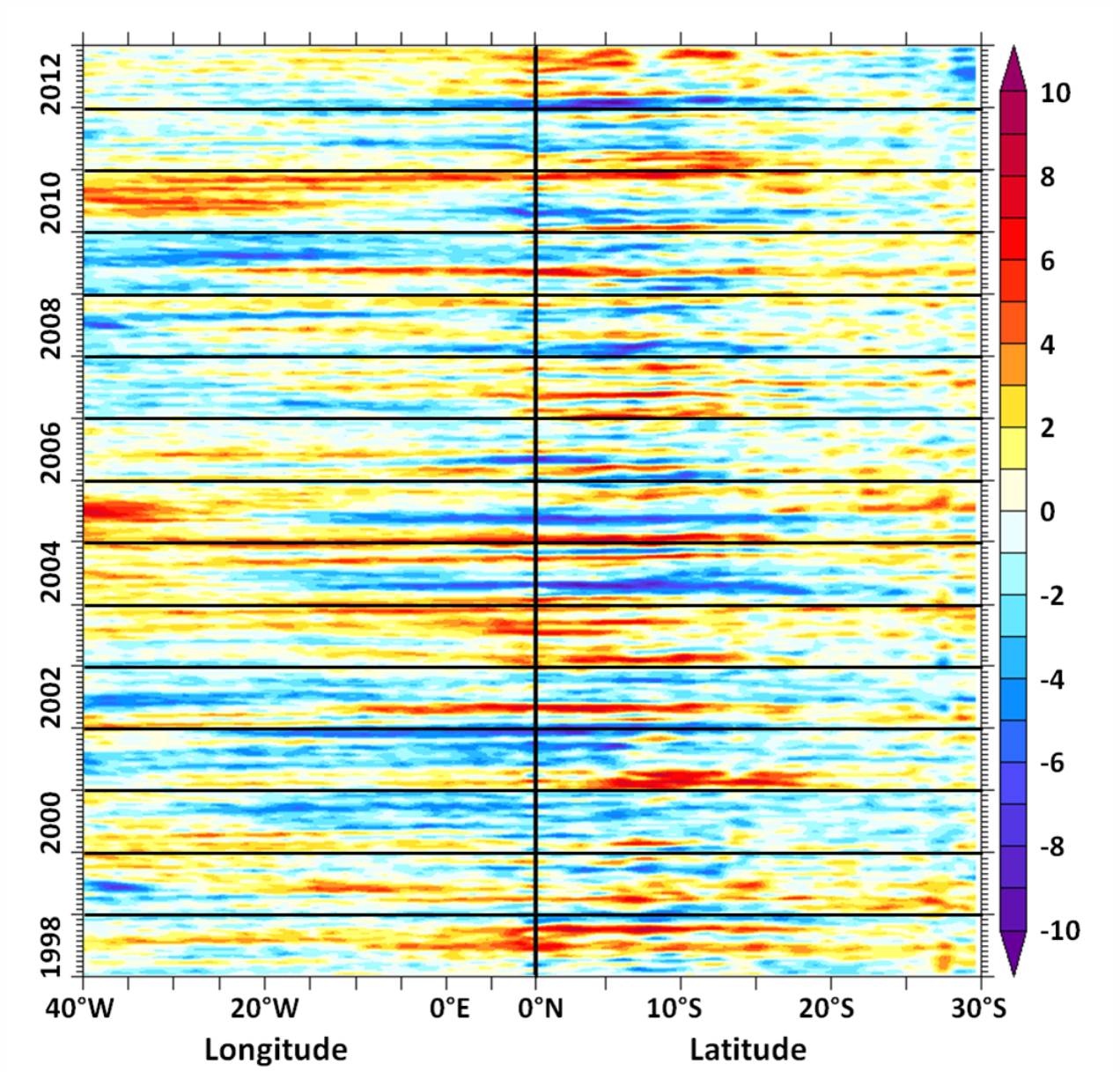

Figure 3.6: Longitude-time and latitude-time Hovmöller diagrams of monthly detrended SSH anomalies in cm, left plot averaged between 1°S and 1°N along the equator, and right plot along the African coast from 0°S to 30°S and averaged from the coast to 1° offshore.

observe in **Figure 3.5**, slow propagations of SST anomalies as we move from Southern Angola to Northern Namibia. A sensitivity to the speed of propagation of coastal SSTA is observed, revealing that each coastal event develops differently. The persistence and slow propagation of SST anomalies from Southern Angola to Northern Namibia in these domains, already mentioned

in *Rouault* [2012], were attributed to advection of warm tropical waters in the Northern Benguela upwelling domain. He found a significant lag correlation coefficient between the two domains when Southern Angola SST anomalies lead Northern Namibia SST anomalies by 1 - 4 months.

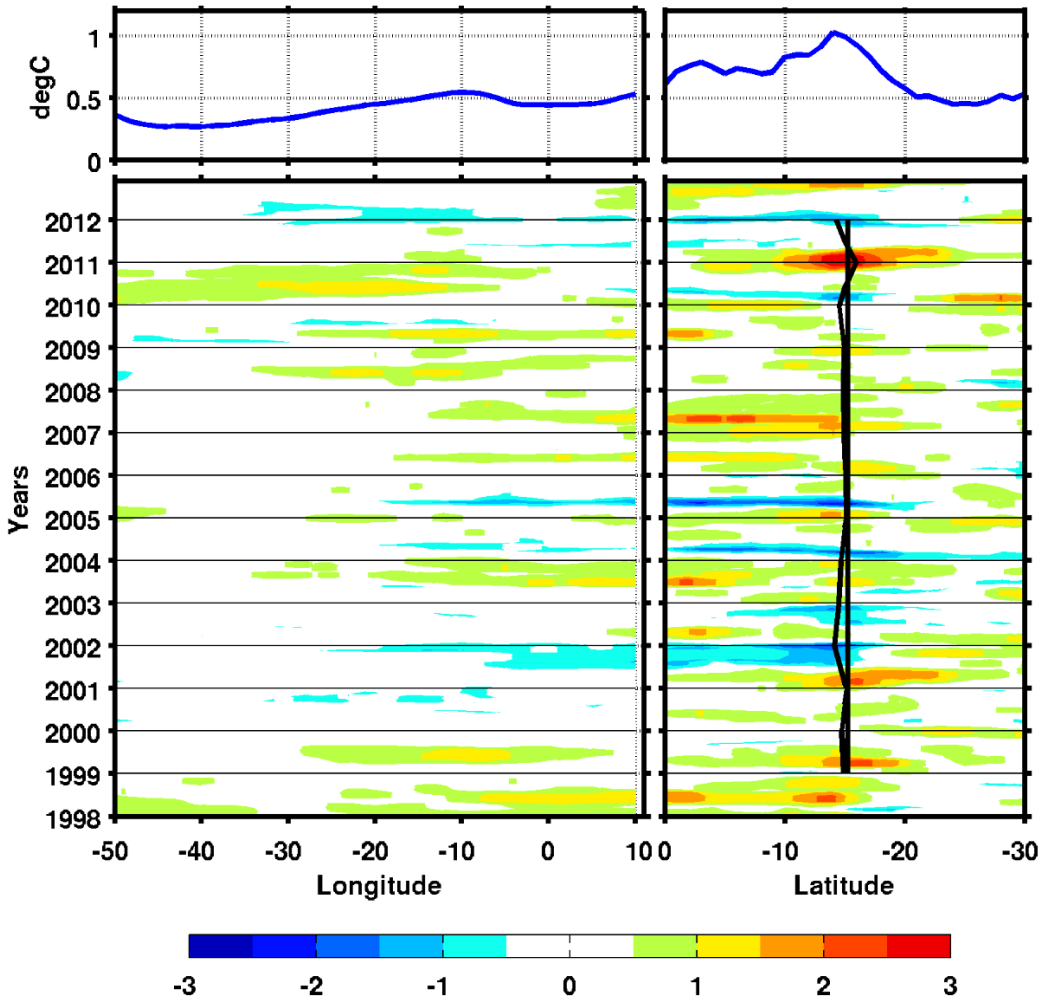

Figure 3.7: (Left; top) Standard deviation) and (bottom) Hovmöller diagram of monthly detrended OI-SST anomalies (°C) along the equator and averaged between 1°S and 1°N, and for (top) the right plot standard deviation and (bottom) Hovmöller latitude-time diagram of monthly detrended but along the African coast from 0°S to 30°S and averaged from the coast to 1°offshore. The yearly mean latitude from 1998 to 2012 over the October to April season of the isotherm 22°C is represented by the black line and its averaged position by the straight line along the African coast.

Also, local effects (coastal wind stress anomalies) could modulate the SSTA magnitude of these events south of the ABF zone [*Richter et al.,* 2010; *Bachèlery et al.,* 2016a].

Most of the abnormal positive and negative propagation episodes described above in **Figure 3.1** are clearly observed in **Figure 3.6**. **Figure 3.6** is a Hovmöller diagram of monthly detrended altimetry derived SSH anomalies along the equator and along the African coast all the way to the Angola Benguela (17°S) or further South.

Hovmöller diagram shown in **Figure 3.7** illustrates the propagation of monthly detrended SST and shows the connection between the equatorial domain and the African coastline but with less success than altimetry. The main altimetry-derived propagations along the coast (**Figures 3.6** and **3.4c** and **3.4g**) correspond to the main IEKW identified previously. Recently, using modelling approach, *Bachèlery et al.* [2016a] argued that the propagations along the coast were due to Coastal Trapped Kelvin Waves (CTW), also mentioned in *Ostrowski et al.* [2009]. This suggests that the main IEKW and SSHA propagation episodes that we have identified propagate along the coast as CTW (*cf.* **section 1.3**).

We summarized our equatorial variability index in relation with the major warm and cold events in **Figure 3.8a**. The red (blue) rectangles describe the positive (negative) equatorial propagation episodes and their duration identified in **Figure 3.1** and **Table 3.2**. Tick symbols inside rectangles mean that equatorial propagations precede coastal warm or cold events in the Angola-Benguela Current system, while cross symbols indicate a mismatch. Results show that over the 1998 - 2012 period, 12 out of 18 IEKW identified episodes match coastal SSTA events. From October to April, 10 out of 12 equatorial SSHA episodes match coastal events, while from May to September 4 out of 6 equatorial propagations are not followed by coastal events along western Africa. Furthermore, we note that all 11 extreme coastal events (identified with contours on **Figure 3.8a**) are associated with preceding equatorial propagating signal. Also, particular IEKW propagation episodes in 1998, 2001/2002, and 2009 associated with Rossby wave reflection, show a good match with coastal SST events, which, as pointed out previously, give more credit to an IEKW index, rather than wind stress amplitude in the western Tropical Atlantic. In addition, as illustrated in **Figures 3.3c** and **3.5**, periods with no strong interannual equatorial Kelvin wave episode (from July 1999 to February 2001 and from July 2005 to September 2007 for instance) also correspond with periods without extreme coastal SSH and SST event. However, the cold coastal events in August 2002 and May 2010 (**Figure 3.5**) are not

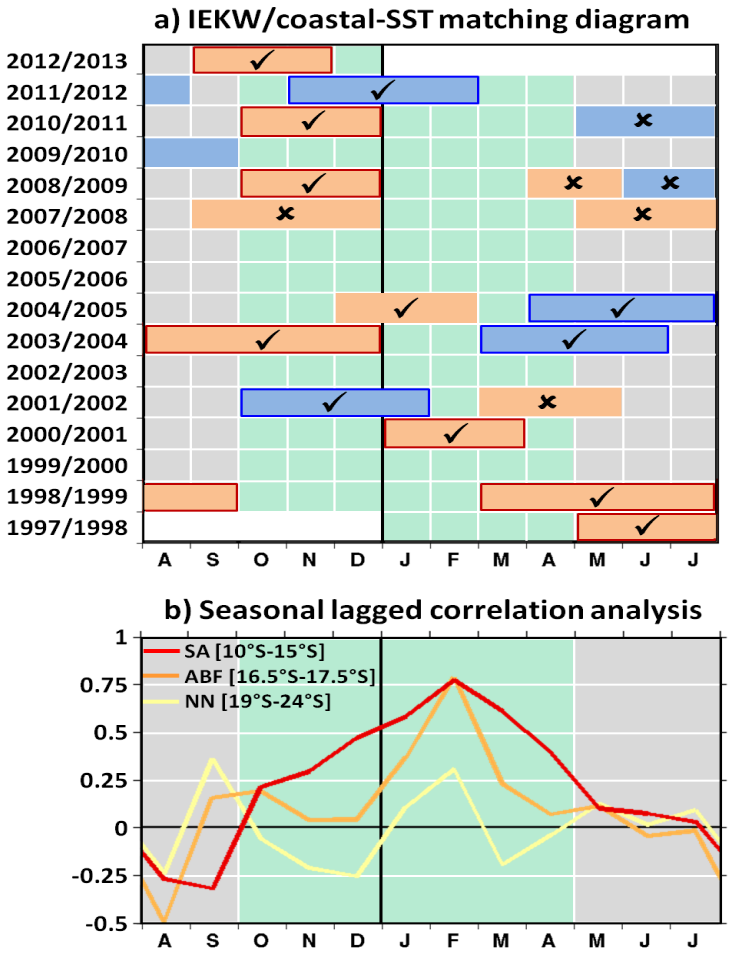

Figure 3.8: a) Prediction score of the coastal warm and cold events using the equatorial variability index from 1998 to 2012. Red and blue rectangles represent abnormal positive and negative equatorial SSH propagation identified in **Figure 3.1**. Tick symbols (✓) inside rectangles mean that equatorial propagations precede coastal warm or cold events, while cross symbols (×) indicate a mismatch. Bold red and blue contours of rectangles stand for extreme coastal warm events (see section 2.5c in *Imbol Koungue et al.* [2017]). b) Seasonal cycle of 5 months running correlation between IEKW mode 2 anomalies averaged between [20°W-0°E] at 0°N and monthly detrended normalized SSTA in Southern Angola (red), Angola Benguela Front region (orange) and Northern Namibia (yellow). Correlations are performed only over the strong equatorial propagation periods (blue and red rectangles in top panel) with equatorial index leading coastal SSTA by one month. Green background shading indicates the best forecasting period from October to April.

preceded by strong upwelling equatorial waves as depicted by our criterion. Notably, the linear model shows strong anomalous negative SSHA at 0°E and 10°W preceding the cold coastal event in May 2010. For the cold coastal event in August 2002, only PIRATA buoy located at 23°W shows strong negative SSHA, no data are available at the other moorings locations and altimetric SSHA peaks do not fulfil the criterion. Following our methodology, both SSH signals are not classified as strong equatorial propagations.

To better appreciate the link between the interannual equatorial and coastal variability, we computed a 5-month running correlation between IEKW mode 2 anomalies averaged between [20°W and 0°E; 0°N] and monthly detrended normalized anomalies of coastal SSTA in the three regions. We only selected period of strong equatorial SSH propagations (shading rectangles) when the equatorial index (IEKW mode 2) is leading coastal SSTA by 1 month. The seasonal cycle of the corresponding correlation is presented in **Figure 3.8b**. We observe that the maximum lag-correlation (statistically significant at 95%) occurs during austral summer. The peak is observed in February, when lag correlation coefficients between equatorial variability and SSTA in Southern Angola (red line) and in the Angola Benguela Front region (orange line) reach 0.75. A sensitivity to the value of the prescribed lag is observed, with, in particular, larger correlation values (> 0.7) for the Southern domain (Northern Namibia) when a lag of 2 months is considered (not shown). Over the mid-October to April period (green shading in **Figure 3.8**), the correlation in the Northern domain is significantly higher than in the other regions. In general, October to April seems the best season for the successful prediction of the warm and cold events in the Angola Benguela Current system. Notably, this good correlation highlighted in **Figures 3.8a** and **3.8b** does not take into account the local effects (local upwelling induced by alongshore wind stress variability, vertical density stratification efficiency, cloud cover fluctuations, and turbulent heat flux forcing), which can modulate the signature of the remote equatorial forcing along the western coast of Africa. Our study is thus consistent with the modelling study of *Bachèlery et al*. [2016a], who observed that at interannual timescales, remote equatorial forcing is more efficient to trigger coastal SSH and SST events than the local atmospheric forcing along the Angola Benguela coasts. But the alongshore wind forcing, with unfavourable or favourable local upwelling wind, is not negligible since its effects on temperature interannual anomalies can superimpose on the remotely forced CTW. Also, of particular interest is the vertical stratification of the water column which can modulate the signature in SST of CTW propagations. In

agreement with our results, vertical stratification will modulate the efficiency of vertical current anomalies to imprint the SST [*Goubanova et al.,* 2013], and thus austral summer stratified surface layer will be more prone to SST anomalies than mixed winter conditions. Also, *Polo et al.* [2008a] studied the intraseasonal EKW and highlighted two dominant periods for the emergence of Kelvin Waves (KW): Austral Spring (September - December) for downwelling KW and Austral summer (November - January) for upwelling KW. The favourable season when a potential propagation of the second baroclinic mode IEKW could trigger a warm or a cold event 1 month later would be mostly between October and April.

3.3 SUMMARY

In this chapter, we used a simple methodology, based on monthly anomaly time series at particular locations along the equator where real-time in *situ* data from PIRATA moorings are available and satellite SST along the southwestern coast of Africa. An OLM is used to better characterize the IEKW propagations along the equatorial wave guide. The relationship between equatorial Atlantic Ocean variability and the coastal region of Angola-Namibia is then investigated at interannual time scales from 1998 to 2012. Results show that over the 1998-2012 period, the interannual OLM SSH outputs compare well with the equatorial observations emphasizing the dominance of the equatorial wave propagation signal on the equatorial variability over this period. The OLM outputs along with a methodology based on temporal and spatial coherence allow depicting 18 strong eastward equatorial Kelvin wave episodes in PIRATA and altimetric observations: 12 strong downwelling and 6 strong upwelling waves. An index of equatorial Kelvin wave activity is defined based on Prediction and Research Moored Array in the Tropical Atlantic (PIRATA). Significant correlations statistically significant at 95% are found along the equatorial wave guide between PIRATA monthly dynamic height anomalies, altimetric monthly SSHA and SSHA derived from the OLM. These significant correlations allow us to interpret PIRATA records in terms of equatorial Kelvin waves. We found that the second baroclinic mode of IEKW is the most dominant mode. Systematic analysis of all strong interannual equatorial SSHA showed that they precede by 1–2 months extreme interannual SSTA along the African coast, which confirms the hypothesis that major warm and cold events in the Angola-Benguela Current system are remotely forced by ocean-atmosphere interactions in

the equatorial Atlantic. Wind anomalies in the western Equatorial Atlantic force equatorial downwelling and upwelling Kelvin waves that propagate eastward along the equator and then poleward along the African coast triggering extreme warm and cold events, respectively. A proxy index based on linear ocean dynamics appears to be significantly more correlated with coastal variability than an index based on wind variability. Modest values of 0.4 (0.27) of the lagged correlation between the IEKW mode 2 and the SSTA in the SA (ABF) domains are found when equatorial Kelvin wave mode 2 activity leads Southern Angola (Angola Benguela Front) SSTA by 1 month. Furthermore, we have performed the seasonal cycle of the 5-month running correlation between equatorial activity and coastal variability over the identified strong equatorial propagation periods. Results show that the values of the lag correlation between equatorial variability and SSTA in Southern Angola and in the Angola Benguela Front region reach 0.75 in austral summer from October – April (**Figure 3.8b**). This season corresponds to the period when equatorial variability could be successfully linked to coastal SST interannual events. It is also a good start to set up an early warning system for the Benguela Niño and Niña along the west African coast between Angola and Namibia.

As mentioned in this chapter, the study of the role of the local variability was not the scope of this research, and we were also limited on time with a period of 15 years. The agreement between the OLM and PIRATA records from 1998 to 2012 leads to extend the OLM solution over the period 1958 to 2015 (58-years) concomitantly with the outputs of an OGCM from 1958 to 2015 (*cf.* **section 2.1.2**). This will be done in the next chapter which will allow to study the mechanisms associated with past extreme Benguela Niños and Benguela Niñas events before 1982, such as the 1963 extreme warm event and the extreme cold event in 1958.

CHAPTER 4

4 BENGUELA NIÑO AND BENGUELA NIÑA EVENTS AND THEIR CONNEXION WITH THE EQUATORIAL VARIABILITY FROM 1958 TO 2015

4.1 INTRODUCTION

In the previous chapter, 15 years (1998 - 2012) of PIRATA data, altimetry, and OLM outputs is used to show that EKW propagations in the equatorial Atlantic played a major role for the onset of the Benguela Niño and Benguela Niña events in the Angola-Benguela Current system. In this chapter, a numerical simulation over the period 1958 - 2015 (58 years) is used to study the coastal interannual events including the ones that developed before the 80's when satellite remote sensing of SST was not available. Most Benguela Niño and Niña studies found in the literature started in 1982 with the use of OI-SST. Before the satellite era and the advent of ocean modelling, the state of the ocean was not well known and poorly understood. Global Ocean measurements were not as well developed as now and were mostly done using in situ observations (ship measurement along sections, tide gauges, dedicated cruise). Nowadays, with the use of satellite estimates, state of the art models with data assimilation and observations (Argo floats, buoys, and gliders), oceanic processes are better understood at a global scale. The results obtained in this chapter focus on extreme warm and cold coastal events including the ones that occurred during the 60's and 70's (Benguela Niño 1963) and are compared with a paucity of available papers by previous authors such as *Stander and De Decker* [1969]; *Shannon et al.* [1986].

In this chapter, I will firstly classify the different types of coastal events using the 58 years long time series of the validated OGCM in terms of extreme or moderate coastal events. Secondly, since the meridional advection of equatorial warm waters at 17°S associated with the

passage of a CTW is a good indicator in the development of Benguela Niño and Niña in the NBUS according to *Rouault* [2012], I will also calculate the coastal net mass transport and the net temperature transport at 17°S within 1° coastal band using the OGCM outputs. Thirdly, February-March-April composite maps of some well-known extreme coastal events are illustrated and compared with the newly identified extreme coastal events. Please, note that in this chapter, all the monthly detrended anomalies will be normalized with respect to their seasonal standard deviation (*cf.* **section 2.2.2**) as in *Rouault* [2012].

4.2 CLASSIFICATION OF DIFFERENT TYPE OF COASTAL EVENTS

Before starting the description of the results, I want to highlight the fact that the OGCM temperature a 10 m (hereafter T10) is used instead of OGCM SST for the rest of this thesis. The reason being that the OGCM SST could be impacted by turbulent heat fluxes and related net heat budget at the surface in the OGCM which could influence the SST. However, there is no difference between the two simulated OGCM temperature at surface and at 10 m (not shown), because both levels are found within the model mixed layer depth. In order to identify and classify the coastal warm and cold events along the Angolan - Namibian coastlines, **Figure 4.1** represents the normalized detrended anomalies of model T10 along the Angolan - Namibian coastlines averaged in the 3 coastal zones of interest as shown in **Figure 2.2**, between 10°S to 15°S from the coast to 1° offshore (top), between 16.5°S to 17.5°S within 1°coastal band (middle), and between 19°S to 24°S within 1° coastal band (bottom). Data are detrended, but this does not significantly affect the identification and classification of the different events. I will comment on the detrending of the data further below. Criteria are used to identify coastal extreme or moderate warm or cold events. I define an extreme warm or cold event when T10 anomalies exceed the threshold of ±1 standard deviation (STD) for at least 3 months for at least 2 domains. I define a moderate warm or cold event when T10 anomalies exceed the threshold of ±1 STD for at least 2 months in one domain and 1 month in another domain. Note that differences (in terms of duration) could occur between some previous identified coastal events using OI-SST in chapter 3 and the ones identified in this chapter due to the fact that the criteria are not fulfilled here. These differences could be attributed to the use of a longer time series (58

years) which give a slightly different monthly climatology and different standard deviations with weaker variability and therefore different normalized T10 anomalies. Also, the OGCM outputs can differ from observations or satellite estimates, the latest having also their shortcoming.

Based on these criteria above defined, a total of 55 anomalous coastal events shown in **Figure 4.1** with coloured rectangles are identified and classified into 26 extreme coastal events (16 extremes warm and 10 extreme cold events) and 29 moderate coastal events (13 moderate

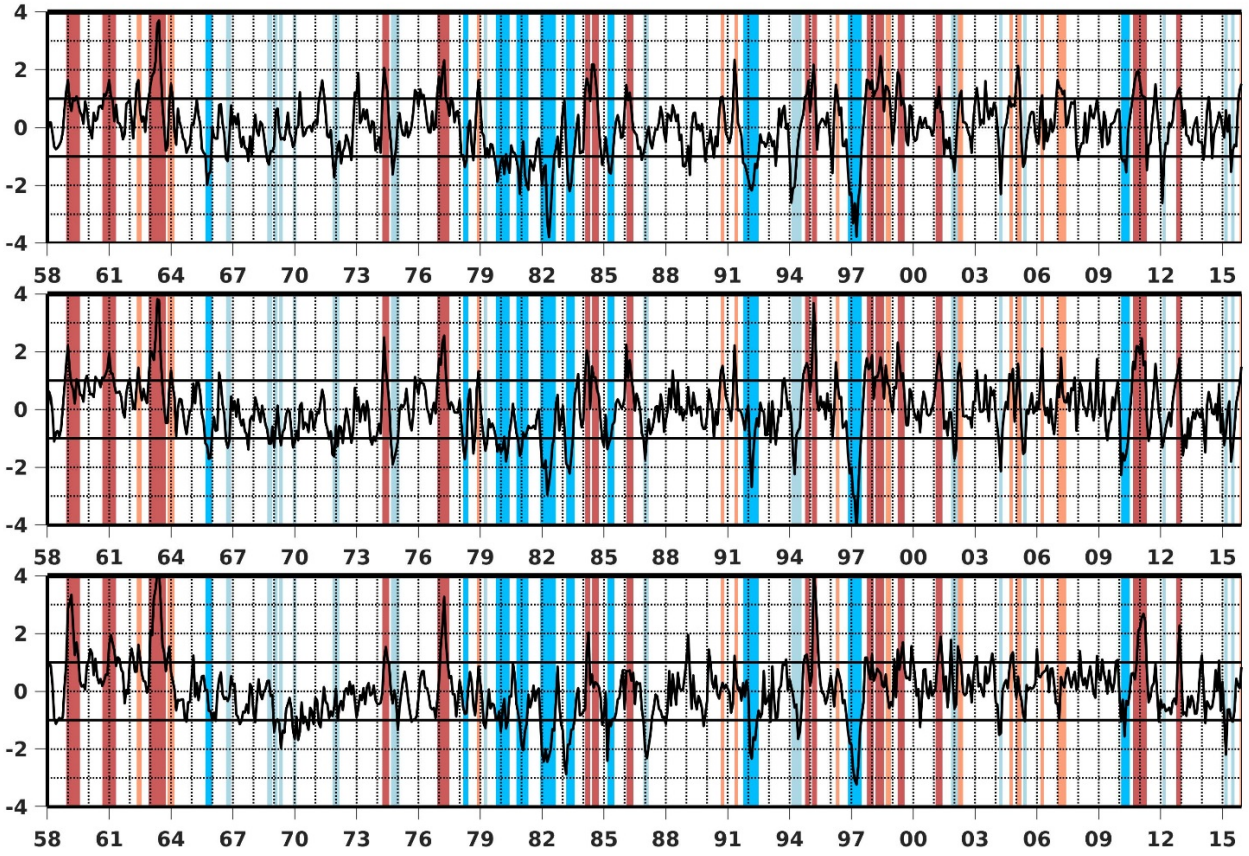

Figure 4.1: Monthly detrended normalized anomalies of T10 in (top) Southern Angola averaged from 10°S to 15°S and from the coast to 1°offshore, (middle) Angola Benguela Front region averaged from 16.5°S to 17.5°S and from the coast to 1° offshore, and (bottom) Northern Namibia averaged from 19°S to 24°S and from the coast to 1° offshore. Black horizontal lines represent the threshold (±1 standard deviation) used to detect extreme and moderate coastal T10 events in the three domains. Red (blue) and light red (light blue) rectangles represent extreme warm (cold) and moderate warm (cold) coastal events respectively along the Angolan-Namibian coastlines.

	Events (Beginning-end)	Southern Angola (SA)		Angola Benguela Front (ABF)		Northern Namibia (NN)	
		Peak month	Duration (month)	Peak month	Duration (month)	Peak month	Duration (month)
Extreme coastal warm events (16)	1958/12 – 1959/07	Jan	2	Jan	3	Mar	8
	1960/09 – 1961/04	Jan	5	Jan	7	Feb	4
	1962/12 – 1963/09	June	8	May	8	June	9
	1974/04 – 1974/07	May	4	May	2	June	3
	1976/12 – 1977/06	Apr	5	Apr	5	Apr	5
	1984/02 – 1984/05	Mar	3	Mar	3	Apr	2
	1984/06 – 1984/09	July	4	June	3	N/A	0
	1986/02 – 1986/05	Feb	3	Feb	4	N/A	0
	1994/10 – 1994/12	Dec	3	Nov	4	Nov	2
	1995/02 – 1995/04	Mar	3	Mar	3	Mar	3
	1997/10 – 1998/01	Oct	4	Jan	5	Oct	2
	1998/02 – 1998/07	June	5	June	5	N/A	0
	1999/04 – 1999/07	Apr	4	Apr	4	July	4
	2001/02 – 2001/05	Apr	3	Apr	3	May	4
	2010/09 – 2011/04	Dec	8	Feb	8	Mar	5
	2012/10 – 2012/12	Dec	3	Dec	3	Dec	2
Extreme coastal cold events (10)	1965/09 – 1965/12	Oct	3	Nov	3	N/A	0
	1978/03 – 1978/05	Apr	3	Apr	3	N/A	0
	1979/10 – 1980/05	Nov	8	Apr	8	Jan	8
	1980/10 – 1981/04	Dec	12	Dec	5	Feb	5
	1981/12 – 1982/08	May	9	Apr	9	Apr	9
	1983/03 – 1983/07	May	4	May	5	Mar	6
	1985/03 – 1985/06	May	4	Mar	3	Mar	4
	1991/10 – 1992/06	Mar	9	Mar	3	Mar	5
	1996/11 -1997/06	Apr	8	Apr	8	Apr	8
	2010/02 – 2010/06	May	5	Feb	5	N/A	0

Table 4.1: Extreme coastal warm and coastal cold events along the southeastern Atlantic Ocean, showing the event periods, peak month of the event and their duration in each of the 3 coastal zones of interest.

warm and 16 moderate cold events). Extreme warm and cold events are summarized in **Table 4.1,** whereas the moderate warm and cold ones are summarized in **Table 4.2.** Indeed, over the period 1958 to 2015, for both type of coastal events, 29 warm events and 26 cold ones in total are identified. The number of warm events would dominate the number of cold events, which is

to be expected since the equatorial T10 signal is actually positively skewed, with more strong positive events and less weak and long negative events. For instance, the skewness of T10 anomalies in the ABF zone (**Figure 4.1,** middle panel) is 0.1 and in the Northern Namibia (**Figure 4.1,** bottom panel) zone is 0.5. Past studies identified some of these warm and cold events in the southeast Atlantic Ocean [*Stander and De Decker* 1969; *Shannon et al.,* 1986; *Walker* 1987; *Florenchie et al*. 2004; *Reason et al.,* 2006; *Rouault et al.,* 2007; *Ostrowski et al.,* 2009; *Lübbecke et al.*, 2010; *Rouault,* 2012; *Imbol Koungue et al.,* 2017; *Rouault et al*., 2017]. However, new extreme coastal events which are not described in the previous studies are identified; namely, the extreme warm events 1958/1959 (December – July), 1960/1961 (September - April), 1974 (April - July). Similarly, undocumented extreme cold events are identified in 1965 (September - December), 1978 (March – May), 1979/1980 (October - May), 1980/1981 (October - April), 1985 (March - June). Most of these extreme warm and cold events occurred in the 3 coastal zones of interest excluding extreme cold events 1965 (September - December), 1978 (March – May) which develop only in Southern Angola and ABF zone. There is a long cooling period (1980 to 1983) composed of four successive extreme cold coastal events occurring at the same time in the three coastal zones of interest (**Figure 4.1**). The coastal warm events in 1984 (February - April) and 1984 (June - September) identified by the OGCM are described as one single event 1984 in the literature [*Rouault et al.,* 2003; *Florenchie et al.,* 2003,2004; *Lübbecke et al.*, 2010; *Rouault,* 2012]. Similarly, the extreme coastal events 1994 (October - December) and 1995 (February - April) identified with the OGCM are described as one single event 1994/1995 (December - July) by *Rouault* [2012]. The reason for splitting these two events is based on the abovementioned criteria that are used to identify the different events. Also, *Rouault* [2012] only used OI-SST and the Northern and Southern domains for his criteria. Monthly T10 anomalies indeed drop suddenly in May 1984 (January 1995) and are below +1 STD in the 3 domains before increasing again in the following month (**Figure 4.1**). *Lutz et al*. [2013], based on SST only found a major warm event in from January 1963 to March 1964 that is represented in the OGCM as a moderated coastal warm event in 1963/1964 (November – February). The duration of the warm and cold coastal events (**Table 4.1**), varies from a couple of months to half a year or more (for example the Benguela Niños 1995 and 2010/2011) consistent with findings of *Florenchie et al.* [2004]. The periods during which anomalous coastal events occur in **chapter 3** (PIRATA period 1998 - 2012) are sometimes different from the events

	Events Beginning-end	Southern Angola (SA)		Angola Benguela Front (ABF)		Northern Namibia (NN)	
		Peak month	Duration (month)	Peak month	Duration (month)	Peak month	Duration (month)
Moderate coastal warm events (13)	1962/05 – 1962/07	June	2	June	1	June	2
	1963/11 – 1964/02	Jan	2	Jan	1	Dec	2
	1978/11 – 1978/12	Dec	2	Dec	2	N/A	0
	1990/09 – 1990/10	Oct	2	Oct	2	N/A	0
	1991/05 – 1991/06	May	2	May	2	May	1
	1996/04 – 1996/05	Apr	2	Apr	2	N/A	0
	1998/09 – 1998/11	Sept	3	Sept	2	N/A	0
	2002/03 – 2002/05	May	2	Apr	3	Mar	2
	2004/09 – 2004/10	Sept	2	Sept	2	Oct	2
	2005/01 – 2005/03	Feb	3	Feb	1	N/A	0
	2006/03 – 2006/04	Apr	1	Apr	2	N/A	0
	2007/01 – 2007/05	Jan	5	Mar	1	N/A	0
	2015/11 – 2015/12	Dec	2	Dec	1	N/A	0
Moderate coastal cold events (16)	1966/09 – 1966/11	Oct	2	Oct	3	N/A	0
	1968/09 – 1968/11	Oct	2	Nov	2	N/A	0
	1969/01 – 1969/02	Jan	2	Jan	2	Jan	2
	1969/04 – 1969/05	May	2	May	2	May	2
	1969/12 – 1970/01	Dec	2	Dec	2	Jan	2
	1971/11 – 1972/02	Dec	3	Dec	2	Feb	1
	1974/09 – 1975/01	Nov	2	Oct	5	Jan	1
	1979/03 – 1979/04	Apr	2	Apr	2	Apr	2
	1986/12 – 1987/02	N/A	0	Jan	2	Feb	3
	1994/02 – 1994/07	Feb	4	Apr	2	June	2
	2001/11 – 2002/02	Jan	3	Jan	2	N/A	0
	2004/03 – 2004/04	Apr	1	Apr	2	Mar	2
	2005/05 – 2005/06	May	2	May	2	June	1
	2012/02 – 2012/03	Feb	2	Feb	2	N/A	0
	2015/02 – 2015/03	N/A	0	Feb	1	Mar	2
	2015/06 – 2015/07	June	1	June	2	July	2

Table 4.2: Classification of moderate coastal warm and coastal cold along the southeastern Atlantic Ocean, showing the event periods, peak month of the event and their duration in each of the 3 coastal zones of interest.

reported in this chapter. For instance, the extreme warm event 2010/2011 (November–April)

reported in chapter 3 or by *Rouault et al*. [2017] is here September 2010 – to April 2011. Some previous identified coastal events using OI-SST in chapter 3 such as coastal warm events 2003 (July–December), 2008/2009 (November–January) do not fulfil the criteria here.

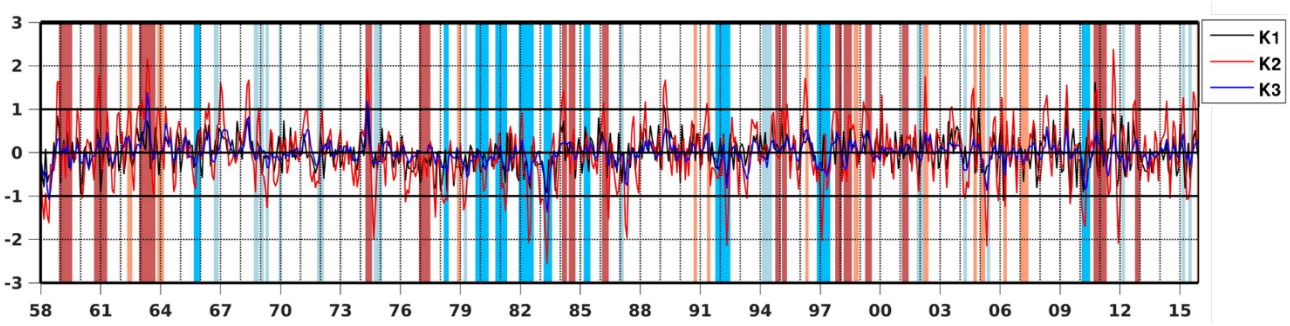

Figure 4.2: OLM detrended anomalies of Kelvin wave monthly contribution to SSHA (cm): first baroclinic mode (K1) in black, second baroclinic mode (K2) in red, and third baroclinic mode (K3) in blue, averaged over (20°W–0°E, at 0°N). Coastal warm or cold events identified in **Figure 4.1** are represented by red and blue rectangles, respectively.

According to the good agreement observed in **Figure 3.1** between PIRATA Dynamic Height and the OLM SSHA in the monitoring of the IEKW (statistically significant correlation at 95% of 0.65 at [0°E; 0°N]) along the equatorial wave guide, OLM outputs are used to characterize the long IEKW propagations along the equatorial Atlantic that occur between 1958 – 2015 (**Figure 4.2)**. Before 1980, many assumptions or suggestions were made *Shannon et al.* [1986] to link the various observed extreme warm coastal events (1963) to remote forcing in the western part of the equatorial Atlantic. For example, *Shannon et al.* [1986] found that the 1963 Benguela Niño was associated with low, westward wind-stress off Brazil. Using DFS wind stress to force the OLM, most of the coastal warm (cold) events are preceded by downwelling (upwelling) EKW propagations. This means that the remote oceanic forcing is at the origin of most of the coastal events along the Angola Benguela Current system as it was the case for PIRATA period (1998 – 2012). For example, the linear model shows that positive IEKW mode 2 (in red) anomaly along the equatorial Atlantic occurs ~1 month before the extreme warm coastal event 1962/1963 along the Angola – Namibia coastline. Therefore, remote oceanic forcing though propagation of downwelling IEKW mode 2 (most energetic mode) could have triggered

the 1963 Benguela Niño reported by *Shannon et al.* [1986].

Figure 4.3a illustrates the number of occurrences of the calendar month at which the events peak. Top panel presents this distribution for the sum of extreme warm and cold events for the 3 different coastal zones (Southern Angola in red, ABF in blue and Northern Namibia in black), whereas the bottom panel presents the occurrences for the total moderate events. **Figure 4.3a** shows that for all the coastal zones, most of the occurrences happens from Austral spring to late summer (October to April) with a maximum of 5 occurrences in April and May (Southern Angola, zone 1), 7 in April (ABF, zones 2) and 6 in March (Northern Namibia, zones 3) for the total extreme coastal events (cold + warm). Late summer season (February to April) seems to be the peak season for Benguela Niño which agrees with the literature. This period (February – April) belongs to the October – April season which seems to be the best period for an IEKW mode 2 to be linked to Benguela Niño or Niña event along the Angola Benguela Current system (*cf.* **section 3.2.4**). There are 18 of 26 occurrences of extreme events (69%) in Southern Angola, 21 out of 26 occurrences of extreme events (80%) in ABF zone and 16 out of 20 occurrences of extreme events (80%) in Northern Namibia occurring between October and April along the Angola – Benguela Current system. Notably, October - April was the best season for an Equatorial Kelvin wave mode 2 to be linked to a Benguela Niño or Niña in the Angola Benguela Current system [*Imbol Koungue et al*. 2017]. This will be discussed later in **Chapter 5**. Outside this period (October – April), the number of occurrences of extreme coastal events is low or null for Southern Angola (August and September), ABF (July, August, September) and Northern

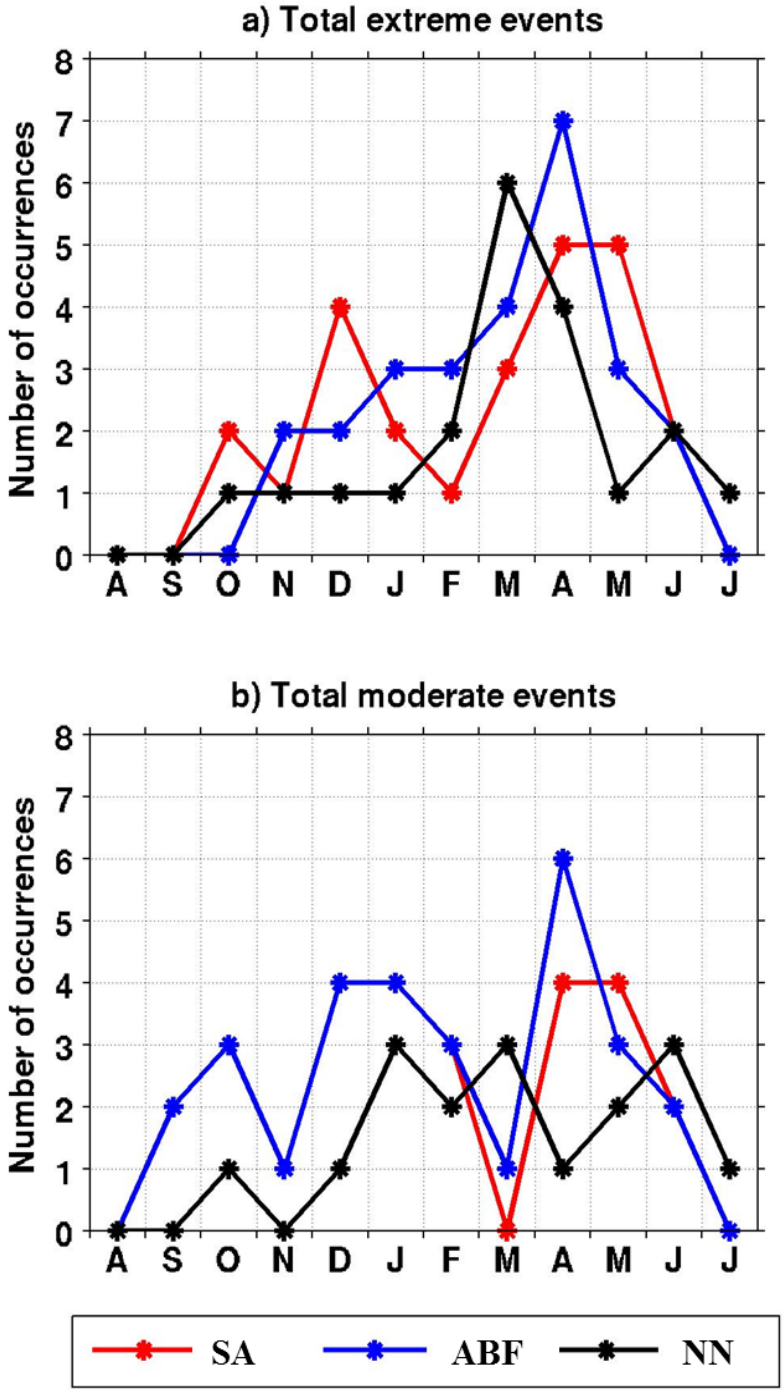

Figure 4.3: Number of occurrences of the peak month of each event with respect to the calendar months. a) Sum of extreme warm and cold coastal events for the different zones (Southern Angola (SA) in red, ABF in blue and Northern Namibia (NN) in black). b) The same as in a), but for the sum of moderate warm and cold events.

Namibia (August and September). In **Figure 4.3b**, October to April seems to be the favourable period for the development of moderate coastal events for Southern Angola and ABF zones despite the fact that the number of occurrences of moderate coastal events is lower than the number of occurrences of extreme events obtained in **Figure 4.3a**. In terms of percentage for the occurrence of a peak during October - April season using the total moderate events (**Figure 4.3b**), 19 out of 27 (70%) in Southern Angola, 22 out of 29 (75%) in ABF and 11 out of 17 (65%) in Northern Namibia. The percentages of occurrences of moderate coastal events in the three zones of interest remain high.

Figure 4.4 shows all the 55 anomalous T10 coastal events sorted from the warmest to the coolest in the 3 coastal zones of interest (**Figure 2.2**, SA (a), ABF (b), NN (c)), and their associated intensities in IEKW mode 2. The intensity of each event is calculated as the sum of the T10 anomalies during the event divided by the duration of the event (number of months). The same method is used for estimated the intensity of IEKW mode 2 with IEKW mode 2 leading T10 anomalies by 1 month, this means that the time series of IEKW mode 2 is shifted forward by one month to be in advance on T10 anomalies before computing its intensity.

Results show that although the intensities of the coastal events associated with IEKW mode 2 are smaller compared to the T10 anomalies one (red line), there is a quite good agreement between the intensity in T10 anomalies (°C/month) and the intensity of IEKW mode 2 (cm/month). Both time series seem to vary together meaning in that the coastal warm and cold events are related to positive and negative intensities of IEKW mode 2 respectively, except for the extreme warm coastal event 1976/1977 (December – June) where the intensity of the IEKW mode 2 is below 0. This suggests that the remote equatorial forcing is not at the origin of the 1976/1977 extreme coastal warm event, while it seems to trigger the undocumented extreme coastal warm events with positive IEKW mode 2 anomalies during the 1958/1959, 1960/1961, 1974 events and upwelling IEKW mode 2 during extreme coastal cold events in1965, 1970, 1979/1980, 1980/1981 and 1985. For most of the moderate warm and cold events, the intensity of IEKW mode 2 along the equatorial Atlantic is very weak and around 0 respectively. Over the period 1958 to 2015, the warmest coastal event occurring in the three coastal domains is 1962/1963 (December – September) and the coolest coastal events are 1981/1982 (December – August) and 1996/1997 (November – June) respectively.

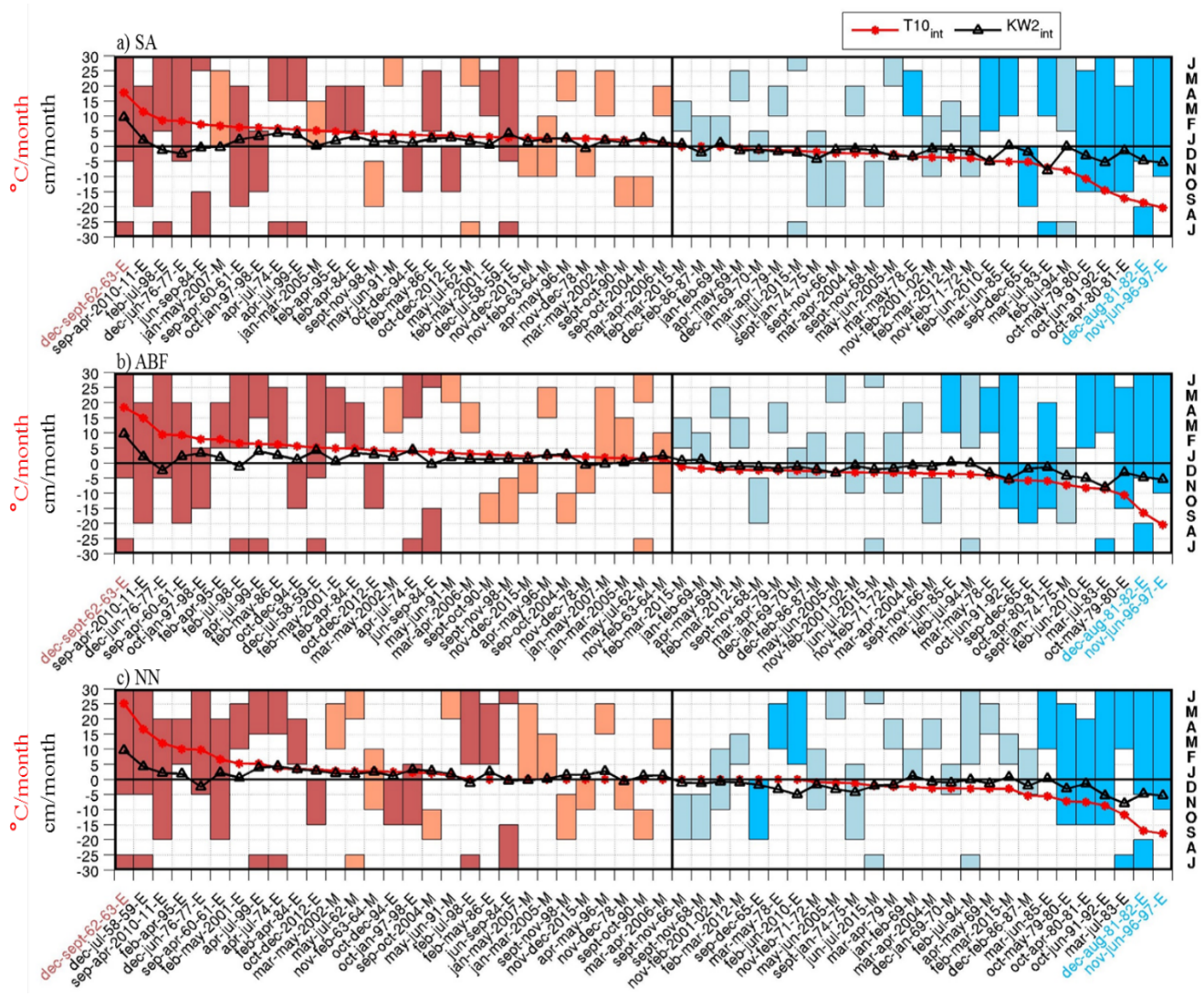

Figure 4.4: Classification of the coastal events from the warmest to the coolest using OGCM T10 from 1958 to 2015 in the: (a) Southern Angola, (b) Angola-Benguela Front, (c) Northern Namibia. Dotted red line represents the T10 anomaly intensities ($T10_{int}$ from OGCM, °C/month) of each coastal event. The black line with triangles represents the intensities of IEKW mode 2 ($KW2_{int}$ from OLM, averaged within [20°W-0°E; 0°N], cm/month) shifted forward by 1 month (leading T10 by 1 month, in agreement with **Figure 4.5**) and averaged over the duration of the coastal event. The height (start and end) of the bar corresponds to the period when the event occurs which is represented on the right y-axis. The black vertical line separates the warm from the cold events. The labels in red (blue) highlight the warmest (coolest) coastal events observed in the 3 coastal domains.

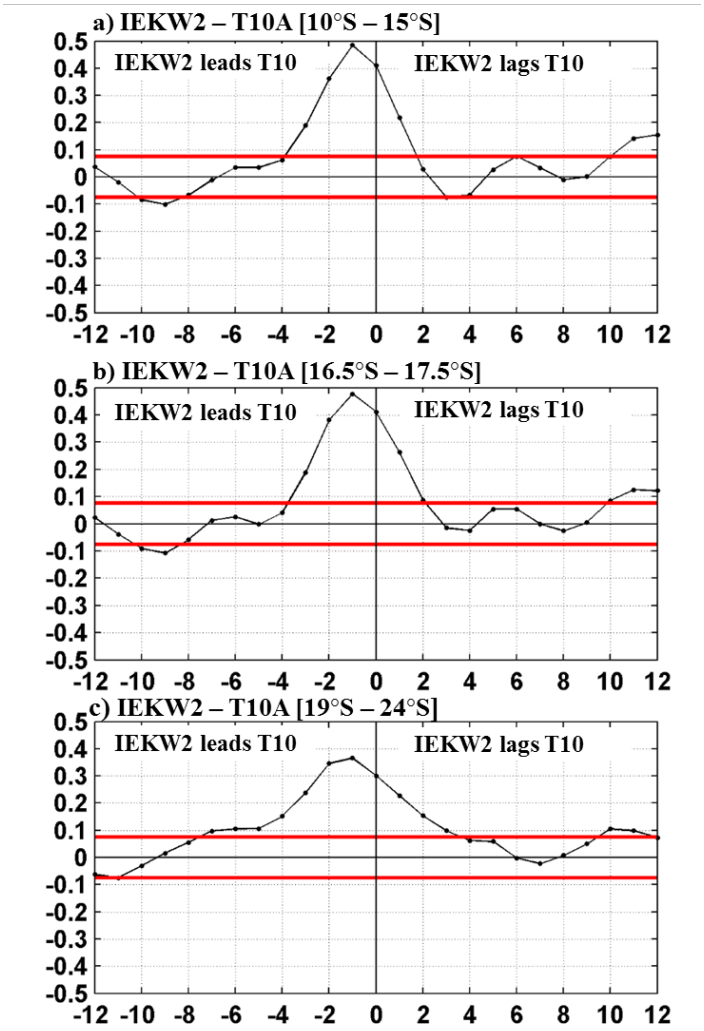

Figure 4.5: Correlation analysis over 1958 - 2015 between monthly OLM IEKW second mode (IEKW2) averaged between 20°W and 0°E at 0°N, and monthly OGCM T10 anomalies (T10A) along the African coast in a) Southern Angola (averaged between 10°S and 15°S and over 1° coastal fringe), b) Angola-Benguela Front (averaged between 16.5°S and 17.5°S and over 1° coastal fringe) and c) Northern Namibia (averaged between 19°S and 24°S and over 1° coastal fringe) in function of the Lag (in months). Negative lags indicate that IEKW2 leads. The 95% significant correlation threshold is indicated by red lines.

To confirm the relationship between the remote oceanic forcing (EKW) and the coastal events along the southwest African coast, lag correlation analysis is performed (**Figure 4.5**) between coastal OGCM T10 detrended anomalies and OLM IEKW mode 2 detrended anomalies over 1958 to 2015 (58 years). There is a maximum correlation of ~0.5 statistically significant at

95% when detrended anomalies of IEKW mode 2 averaged along the equatorial Atlantic lead detrended anomalies of T10 in Southern Angola (**Figure 4.5a**) and the ABF zone (**Figure 4.5b**) by 1 month. Similarly, maximum correlation statistically significant at 95% of ~0.4 (0.35) is found when IEKW mode 2 anomalies lead T10 anomalies in Northern Namibia (**Figure 4.5c**) by 1 (2) month(s). The significant correlations between the IEKW mode 2 and T10 anomalies mean that downwelling or upwelling IEKW mode 2 which are triggered by change in the easterlies in the western equatorial Atlantic, are linked to positive or negative coastal events along the Angola – Benguela Current system respectively with IEKW mode 2 leading coastal T10 anomalies by 1 month. There is a significant correlation at lag 0 between IEKW mode 2 and T10 anomalies in the 3 coastal zones. Significant correlations when IEKW mode 2 is leading T10 anomalies appear in the range [1 - 3] months for Southern Angola and ABF and [1 – 7] months in Northern Namibia. The broad range of lags between IEKW mode 2 and T10 anomalies could be attributed to the changes of IEKW phase speeds which are associated with each particular coastal event and which could depend on the local vertical stratification and baroclinic mode contributions. It could also be attributed to persistence of warm events after their onset. For northern Namibia it is consistent with lag correlation between Angola and Namibia fund by *Rouault* [2012] due to slow advection of warm anomalies by transport. Maximum correlation (~0.5) statistically significant at 95% is obtained in **Figure 4.5b** which is similar to the correlation obtained in **Chapter 3** (**Figure 3.3b)** between IEKW mode 2 and SSTA in Southern Angola when using the PIRATA's period (1998 – 2012).

Equatorially-forced coastal trapped waves interact with the alongshore currents along the Angola – Benguela Current system depending on their characteristics. During its passage, a downwelling (upwelling) coastal trapped wave could strengthen (decelerate) local coastal currents along the Angola-Benguela coast [*Ostrowski et al*. 2009]. This interaction between the coastal trapped waves and the current could impact on the meridional transport across the ABF. According to *Rouault* [2012], there is a relationship between anomalies of near meridional transport across the ABF (17°S) and the SST anomalies in Northern Namibia. In the following section, I will assess the contribution of modelled coastal net transport at the Angola - Benguela front to investigate the connection between the Angola – Benguela Front zone and the Northern Namibia zone from 1958 - 2015.

4.3 COASTAL NET MASS TRANSPORT AT 17°S AND ITS LINK WITH THE WARM OR COLD EVENTS IN NORTHERN NAMIBIA

According to the previous studies [*Rouault,* 2012; *Rouault et al*. 2017], warm or cold coastal events are related to southward or northward transport anomalies along the southwest African coastline respectively. Therefore, assessing the advection of warm or cold waters in the NBUS (from 19°S to 25°S) or further south, is a key element for the development of the Benguela Niños or Niñas. This meridional transport at 17°S is taken as a proxy as in *Rouault* [2012]. A detailed circulation at the ABF to better understand how representative is the meridional transport at a single latitude (17°S) for the cross-frontal transport would be more representative, but this is beyond the scope of this study.

Figure 4.6 presents the annual cycle of the meridional volume transport at 17°S across the ABF averaged in the upper 120 m within 1° coastal band. Throughout the year, across the

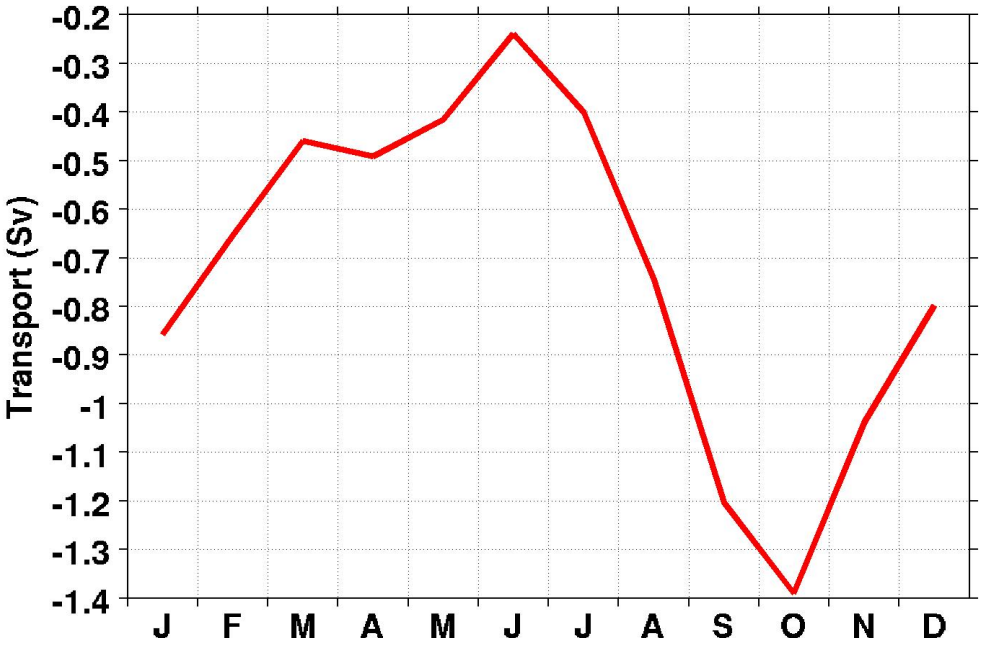

Figure 4.6: Mean annual cycle from 1958 - 2015 of the modelled meridional volume transport at the Angola - Benguela front (17°S) averaged between the surface and 120 m and from the coast to 1 degree offshore in Sv (Sverdrup, 1 Sv = 10^6 m^3/s).

ABF, the volume transport is poleward. The poleward transport is minimum in June (austral

winter) with a value of 0.2 Sv. The poleward flow starts to intensify in July and peaks in October (1.4 Sv). Afterwards, the poleward flow decreases again until December. These results agree partially with modelled transport reported in *Rouault* [2012] who found a bimodal behaviour of the meridional transport across the ABF with maxima in February and October and minima in austral winter and in December using an OGCM with a lower resolution than here from 1982 – 2002. However, the first maximum in February observed by *Rouault* [2012] is not represented by the present simulation. Also, *Rouault* [2012] found a reversal flow (equatorward flow) in June which is not observed in my estimated meridional transport as well. All these points will be discussed further below in the general discussion.

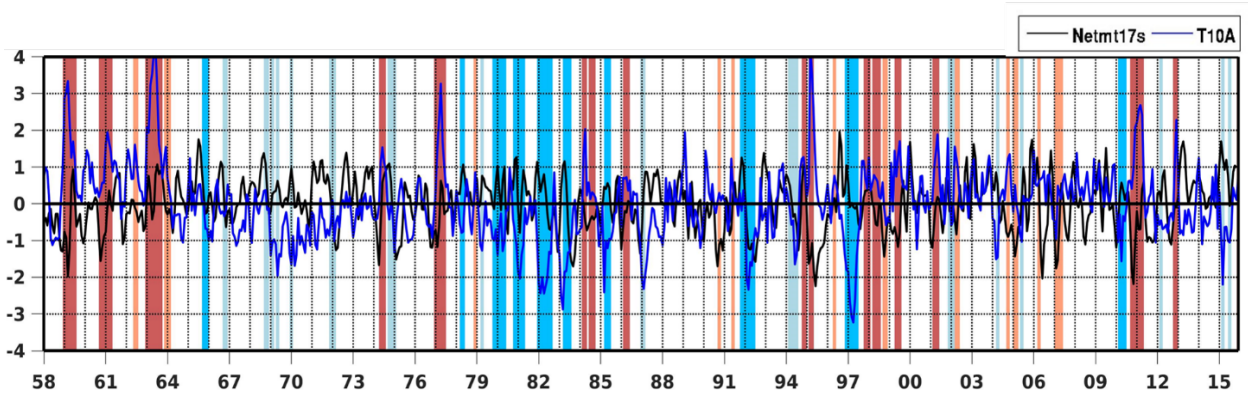

Figure 4.7: Monthly detrended normalized anomalies of meridional volume transport (Netmt17s in blue) at the Angola - Benguela front (17°S) averaged between the surface and 120 m (black line) and monthly detrended normalized anomalies of T10 (in black)) averaged in the Northern Namibia domain (19°S – 24°S). Data are averaged from the coast to 1 degree offshore. Positive values of transport indicate reduced poleward flow or equatorward flow whereas negative values of transport indicate strong poleward flow. Coastal warm or cold events identified in **Figure 4.1** are represented by red and blue rectangles, respectively.

Figure 4.7 presents a comparison between the monthly detrended normalized anomalies of meridional volume transport across the ABF located around (17°S) and the monthly detrended normalized anomalies of T10 downstream (in Northern Namibia) calculated over 1958 to 2015. High-frequency fluctuations being observed in the time series of normalized detrended anomalies of meridional transport across the ABF, for display purposes only, the detrended

normalized anomalies of meridional volume transport were smoothed with a 3-month running windows as in *Rouault* [2012]. Positive anomaly of meridional volume transport accounts for reduced poleward flow or equatorward flow and negative anomaly of the meridional volume transport depicts a stronger poleward transport than the seasonal average (**Figure 4.6**). The volume transport across the ABF seems to mirror the identified coastal warm and cold events. Interestingly, most of the warm or cold events are associated with a stronger or weaker poleward flow across the ABF respectively. Results also indicate that the Benguela Niño 2010/2011 is associated with a strong poleward transport of warm tropical waters in Northern Namibia at the beginning of the event. This result is in agreement with *Rouault et al.* [2017] which highlighted the role played by the poleward subsurface current by advecting warm tropical waters in the Northern Namibia. During the long cooling period (1980 to 1983), positive anomalies of meridional transport are observed (weaker than normal poleward transport in 1979/1980, 1980/1981, 1981/1982; and equatorward flow in 1983) which could enhance the local cooling by advecting cold Benguela waters. The warmest coastal event (1962/1963) is linked to a less strong poleward flow compared to other extreme coastal warm events (1958/1959, 1960/1961, 1974, 1976 /1977, 1995, 2010/2011) where considerable strong poleward transport is observed (transport anomalies below -1 standard deviation). The strongest poleward transport anomaly occurs in June 1995 (-2.2 standard deviation), 3 months after March 1995, peak month of the 1995 extreme coastal warm event. A strong poleward flow in February 1995 (1 month before the peak month of the 1995 warm event) is still observed which could partly favour the warming in the Northern Namibia in 1995. Conversely, for the coolest coastal event in 1996/1997 where detrended normalized anomalies of T10 reach -3.2 standard deviation in April 1997, a weak poleward flow (above 1 STD) is observed with two peaks of 1.95 (1) standard deviation in August 1996 (December 1996) respectively 9 (4) months before the peak in T10 anomalies in April 1997 (**Table 4.1**)). Over 1958 to 2015, the maximum meridional transport anomaly occurs in August 1996 (~1.95 standard deviation) corresponding to an equatorward flow which could partially explain the coolest coastal event 1996/1997 (November – June). However, some coastal events like the 1991/1992 (October - June) do not seem to be linked to the meridional transport anomalies across the ABF domain. For the case of the 1991/1992 extreme coastal cold event, strong poleward transport anomalies occurred during the extreme coastal cold event. This means that transport anomalies across the ABF do not contribute to the development of the 1991/1992

extreme coastal cold event in Northern Namibia.

Figure 4.8 is an update of **Figure 4.4** and illustrates the intensities of the equatorial forcing (IEKW mode 2) and the meridional transport anomalies across the ABF (Netmt17S) with respect to each of the anomalous coastal T10 anomalies events that develop in Northern Namibia. The method used to calculate the intensity of an event is stated in **section 4.2**. Note that the original time series of anomalies of IEKW mode 2 along the equatorial Atlantic and meridional transport anomalies across the ABF are shifted forward by 1 and 2 months respectively to lead the T10 anomalies in Northern Namibia before computing the intensities with respect to the period when the coastal events occur. In many cases, positive or negative intensities of T10 anomalies are associated with negative intensities (stronger poleward transport than the seasonal average) or

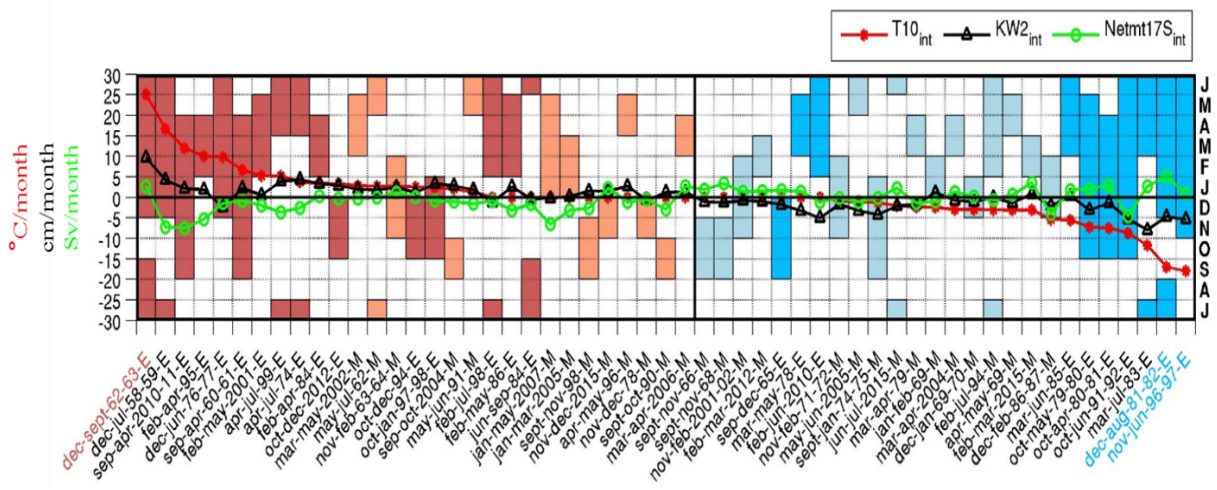

Figure 4.8: Same as **Figure 4.4c**, with an additional green line with open dots that represents the intensities of OGCM meridional transport à 17°S ($Netmt17S_{int}$, averaged with the 1°-width coastal fringe, Sv/month) shifted forward by 2 months (leading T10 by 2 months, in agreement with **Figure 4.9**) and averaged over the duration of the coastal event.

positive intensities (reduced poleward flow or equatorward flow) intensities of meridional transport anomalies across the ABF concomitantly with positive or negative intensities of IEKW mode 2 along the equatorial Atlantic. For example, it is the case for the newly identified extreme warm events 1958/1959, 1974, which are linked to a poleward transport with intensities of -7.3

Sv/month and -2.6 Sv/month respectively associated with downwelling IEKW mode 2 propagations. The intensity of the meridional transport across the ABF associated to the third new extreme event (1960/1961) is slightly negative, indicating a weak reduced poleward flow across the ABF. Also, intensities of other extreme warm events for example (1995 and 2010/2011 extreme warm events) are well related to poleward transport across the ABF. However, some anomalous warm events are associated with reduced poleward flow or equatorward flow. That was the case of the 1962/1963 Benguela Niño which is instead linked to downwelling EKW mode 2 propagations. The 1976/1977 extreme warm event is not remotely forced as this extreme warm event is concomitant with the propagation of an upwelling IEKW mode 2 (*cf.* **Section 4.2**). However, the weak poleward transport across the ABF could have contributed to the advection of warm waters in Northern Namibia during the 1976/1977 extreme warm event.

All the undocumented extreme cold events (1965, 1978, 1979/1980, 1980/1981, 1985) and other anomalous coastal events are associated with a reduced poleward flow or equatorward flow across the ABF even though the intensities of transport anomalies are weak and propagation of upwelling EKW mode 2 are recorded. An exception is observed for the 1991/1992 extreme cold event (as observed in **Figure 4.7**) and 1986/1987 moderate cold event which are related to poleward flow (negative intensity of meridional transport) across the ABF. This suggests that poleward transport develops across the ABF which is not favourable for the advection of cold waters in Northern Namibia.

Over the period 1958 to 2015, the strongest poleward flow across the ABF occurs during the 2010/2011 Benguela Niño (September – April) with a meridional transport intensity of -7.5 Sv/month. The weakest poleward flow (5.1 Sv/month) occurs during the extreme cold coastal events in 1981/1982 (December – August) which is the second coolest event over the 58 years.

Over 1958 - 2015, a modest but significant correlation at 95% occurs when the detrended anomalies of the meridional transport (not smoothed) across the ABF lead the interannual detrended anomalies of T10 in the Northern Namibia domain by 1 to 6 months with a maximum anti-correlation of -0.2 at 2-month lag (**Figure 4.9**). Note that the correlation observed at 1-month lag (**Figure 4.9**) is of the same order of magnitude. The timing between IEKW mode 2, meridional transport, and T10 anomalies will be further discussed in Chapter 6. Significant correlation at 95% of 0.35 also occurs when the detrended anomalies of IEKW mode 2 lead the

interannual detrended anomalies of T10 in the Northern Namibia domain by 2 months (**Figure 4.5c**). This means that over the whole study period, in absolute value, modest but statistically significant correlation (-0.2) at 95% between anomalies of meridional transport across the ABF 2 months ahead of T10 anomalies in Northern Namibia is smaller than the one obtained with anomalies of IEKW mode 2 and T10 anomalies in Northern Namibia (0.35) at 2 month lags (**Figure 4.5c**). However, considering only the periods of when moderate or extreme coastal events occur and by shifting forward the meridional transport and IEKW mode 2 anomalies time series by 2 months, improve the correlation up to -0.32 and 0.55 statistically significant at 95%. Therefore, this emphasizes the fact that the remote oceanic forcing via IEKW propagations is the leading mechanism on the onset and development of most of the anomalous coastal events in Northern Namibia in agreement with results in **Chapter 3**. Then, meridional transport anomalies contribute to the development of these

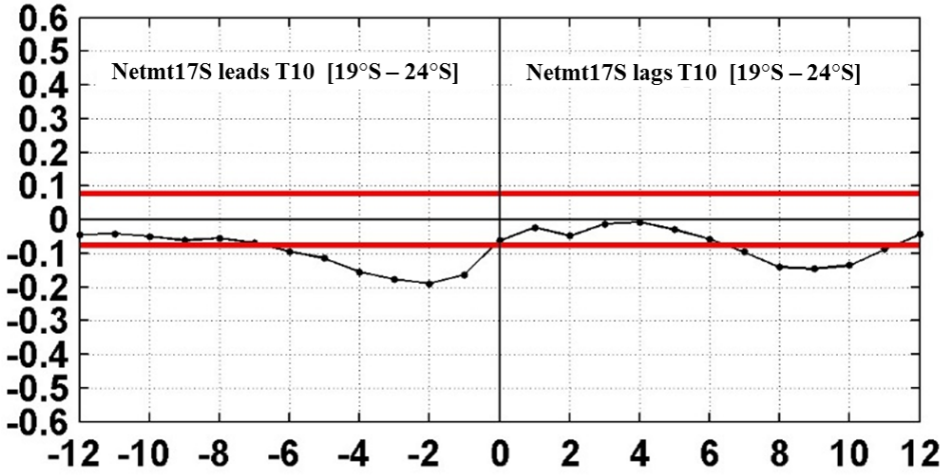

Figure 4.9: Correlation analysis between monthly meridional net mass transport anomalies across the ABF (Netmt17s) averaged in the upper 120 m and from the coast to 1° offshore , and monthly T10 anomalies along the African coast in Northern Namibia (averaged between 19°S and 24°S and over 1° coastal fringe), in function of the Lag (in months). Negative lags indicate that Netmt17s leads. The 95% statistically significant correlation threshold is indicated by red lines.

anomalous coastal events. There is also a lag correlation at 8 to 10 months also statistically

significant at 95% when the detrended normalized anomalies of T10 in the Northern Namibia domain lead the detrended normalized anomalies of transport across the ABF. The study of these lags of 7 to 11 months where the minimum correlation is ~ -0.15 statistically significant at 95% is beyond the scope of this thesis. There is no correlation at lag 0. This range of lags (1 to 6 months) between the net meridional transport across the ABF and the T10 anomalies in the Northern Namibia domain will be discussed in more detail further below.

The following section will assess the temperature transport anomalies at 17°S in order to observe if the correlation reported previously (-0.2) between meridional transport anomalies across the ABF and T10 anomalies will increase and look at a potential role of temperature transport across the ABF on the T10 anomalies in Northern Namibia.

4.4 COASTAL NET MERIDIONAL TEMPERATURE TRANSPORT ACROSS THE ABF (17°S)

Since meridional transport across the ABF zone is a key factor in the development of Benguela Niño and Niña, the net meridional temperature transport across the ABF is calculated here to check if the correlation between net mass transport anomalies across the ABF and T10 anomalies in Northern Namibia could be improved when using temperature transport. The net meridional temperature transport defines the amount of heat carried by the meridional currents over a defined area. By considering this definition, the net meridional temperature transport (Q) at 17°S integrated over depth (0 – 120 m) and within 1° coastal band is defined as the product of the meridional velocity field V = V(x, y, z, t) with the temperature field T = T(x, y, z, t) integrated zonally and over depth at 17°S as illustrated in the equation below:

$$\boldsymbol{Q(y,t) = \iint \rho\, C_p\, T\, V\, dx\, dz}$$

Where ρ is the reference density of seawater taken at 1025 kg.m^{-3}, C_p represents the specific heat capacity constant of seawater equal to 4.18 J/kg/°C. The seasonal cycle of the estimated meridional temperature transport across the ABF is presented in **Figure 4.10**. Across the ABF, the variations in the annual meridional temperature transport mimics the meridional volume transport shown in **Figure 4.6**. The seasonal cycle of temperature transport reveals that there is a

strong poleward transport of heat across the ABF which remains poleward (negative values) throughout the year. The temperature transport across

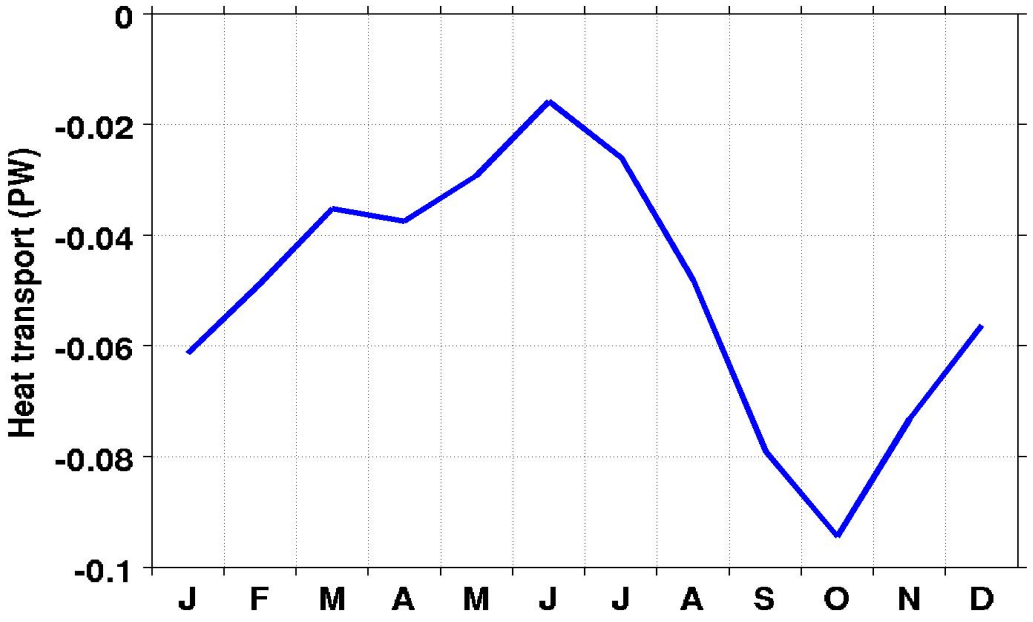

Figure 4.10: Same as **Figure 4.6**, but for the meridional temperature transport (in petawatt (PW), 1 PW = 10^{15} W).

the ABF is minimum in June (0.015 PW) and begins to strengthen in July (0.026 PW) and peaks in October (0.09 PW) where the maximum is observed. A decrease in the poleward temperature transport is observed until December. The same conclusions as for the meridional transport anomalies can be drawn using monthly detrended normalized anomalies of temperature transport across the ABF (**Figure 4.11**).

Figure 4.11 represents both time series of monthly detrended normalized anomalies of meridional temperature transport and meridional volume transport across the ABF averaged in the upper 120 m. There is no difference in variation between the two time series. This is expected since both parameters have the same variation for the seasonal cycle (**Figures 4.6** and **4.10**). However, small differences can be observed in terms of amplitude. Note that a Reynolds decomposition of the meridional temperature transport anomalies reveals that the term transport of the mean temperature times current anomalies largely controls the temperature transport

anomalies across the ABF compared to the transport of temperature anomalies times mean current and transport of temperature anomalies times current anomalies.

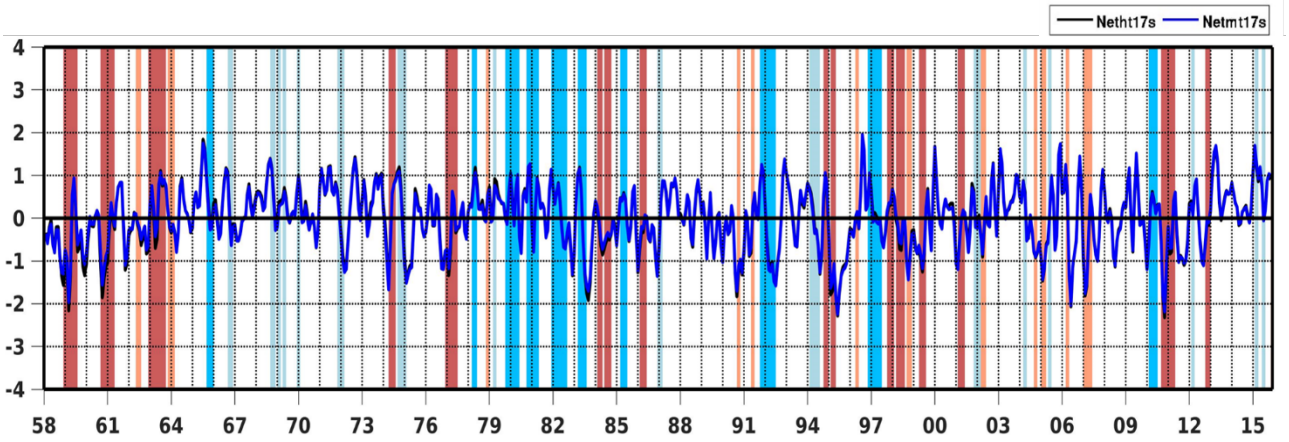

Figure 4.11: Monthly detrended normalized anomalies of meridional volume transport (Netmt17s in blue) and detrended normalized anomalies of meridional temperature transport (Netht17s, in black, in petawatt (PW), 1 PW = 10^{15} W) at the Angola - Benguela front (17°S) averaged between the surface and 120 m. Positive values of transport indicate reduced poleward flow or equatorward flow whereas negative values of transport indicate strong poleward flow. Coastal warm or cold events identified in **Figure 4.1** are represented by red and blue rectangles, respectively.

Correlations between temperature transport anomalies across the ABF and T10 anomalies downstream in Northern Namibia are estimated. Previously in **section 4.3**, correlation of -0.2 statistically significant at 95% were reported when detrended normalized anomalies of meridional transport lead T10 anomalies in Northern Namibia by 2 months. For the case of temperature transport, statistically significant correlation at 95% of -0.22 when the detrended normalized anomalies of temperature transport lead detrended normalized anomalies of T10 by 2 months (**Figure 4.12**). The correlations remain the same as the difference is around 0.02. Also, significant correlation lags range between 0 to 7 months with the temperature transport anomalies instead of 0 to 6 months previously found with the transport anomalies (**Figure 4.9**). No differences are observed in terms of lags and correlation values when temperature transport anomalies lag T10 anomalies in Northern Namibia compared to (**Figure 4.9**). In conclusion,

using the meridional temperature transport anomalies across the ABF do not improve the level of correlation between meridional transport across the ABF and warm or cold events along the coast of western Africa. The use of meridional temperature transport anomalies across the ABF does not improve the contribution of the advection of waters across the ABF in Northern Namibia.

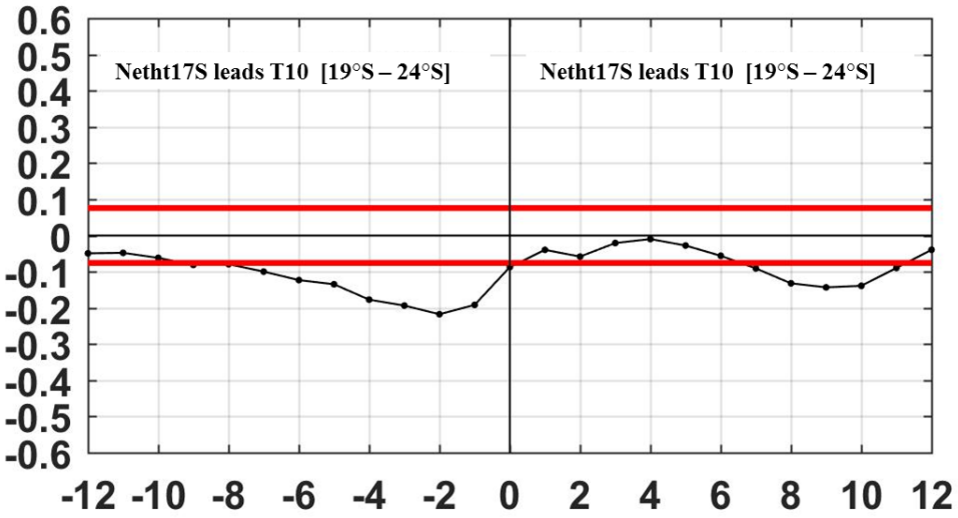

Figure 4.12: Correlation analysis between monthly meridional temperature transport anomalies across the ABF (Netht17s) averaged in the upper 120 m and from the coast to 1° offshore , and monthly T10 anomalies along the African coast in Northern Namibia (averaged between 19°S and 24°S and over 1° coastal fringe), in function of the Lag (in months). Negative lags indicate that Netht17s leads. The 95% statistically significant correlation threshold is indicated by red lines.

4.5 ILLUSTRATIONS OF SOME BENGUELA NIÑOS AND NIÑAS IN THE ATLANTIC OCEAN

4.5.1 Benguela Niño events

In this section, 8 different extreme warm coastal events that peak in February March or April (FMA) (*cf.* **Table 4.1**) in one of the coastal zones of interest (*cf.* **Figure 2.2**) are described and

inter-compared. For each of these 8 different extreme warm coastal events averaged in FMA, the corresponding detrended anomalies of IEKW mode 2 and detrended anomalies of meridional transport across the ABF are then averaged from January to March (JFM) and from December to February (DJF) respectively as shown in **Tables 4.3** and **4.4** as they lead T10 anomalies (FMA) by 1 month (**Figure 4.5**) and 2 months (**Figure 4.9**). Note that the 1962/1963 Benguela Niño shown in **Figure 4.13c** and the 1974 Benguela Niño (**Figure 4.13d**) peak either in May or June in the three coastal zones of interest (*cf.* **Table 4.1**). Results are shown in **Figure 4.13**. New extreme warm events (1958/1959, 1960/1961, 1974) are displayed in **Figure 4.13a, b** and **d**.

In late austral summer (February-March-April, FMA), during the 1958/1959 extreme event (**Figure 4.13a**), T10 anomalies are observed along the west African coast with T10 anomalies larger than 1°C along Southern Angola and Northern Namibia. Maximum warming (T10 anomalies > 2°C) is found in NBUS up to ~25°S. In January 1959 peak month of the 1958/1959 Benguela Niño in Southern Angola and ABF (*cf.* **Table 4.1**), maximum warming spreads from 11°S to ~22°S encompassing T10 anomalies exceeding 3°C (not shown). This pool of warm water progresses further south (~25°S) in March 1959 and decreases in intensity in Southern Angola (<1.5°C). In April 1959, the pool of warm waters is considerably reduced and T10 anomalies greater than 1°C is observed along the west coast of Africa with another maximum (>2°C) just north of Angola. The 1959 JFM (1 month before FMA 1959) average of detrended anomalies of IEKW mode 2 along the equatorial Atlantic is -0.13 cm. This corresponds to the propagation of an upwelling EKW mode 2 along the equatorial Atlantic in late austral summer 1959. But the downwelling EKW mode 2 observed in November 1958 (**Figure 4.2**) is enough to trigger the 1958/1959 extreme coastal warm event. The averaged anomalies of meridional transport across the ABF during the 1958/1959 DJF (December 1958 to February 1959, 2 months before FMA 1959) is -0.32 Sv (*cf.* **Table 4.3**) which is higher than the DJF climatology average (-0.77 Sv). This means that a strong poleward transport takes place across the ABF 2 months before the peak of the warm event. This poleward flow strengthens in the southward direction (**Figure 4.7**) during late austral summer 1959 with meridional transport anomaly of ~-2 standard deviations in March 1959. The 1959 late austral summer poleward flow could be linked to poleward advection of T10 anomalies in the Northern Namibia region during the 1958/1959 Benguela Niño.

During the FMA 1961 (**Figure 4.13b**), positive T10 anomalies are observed along the

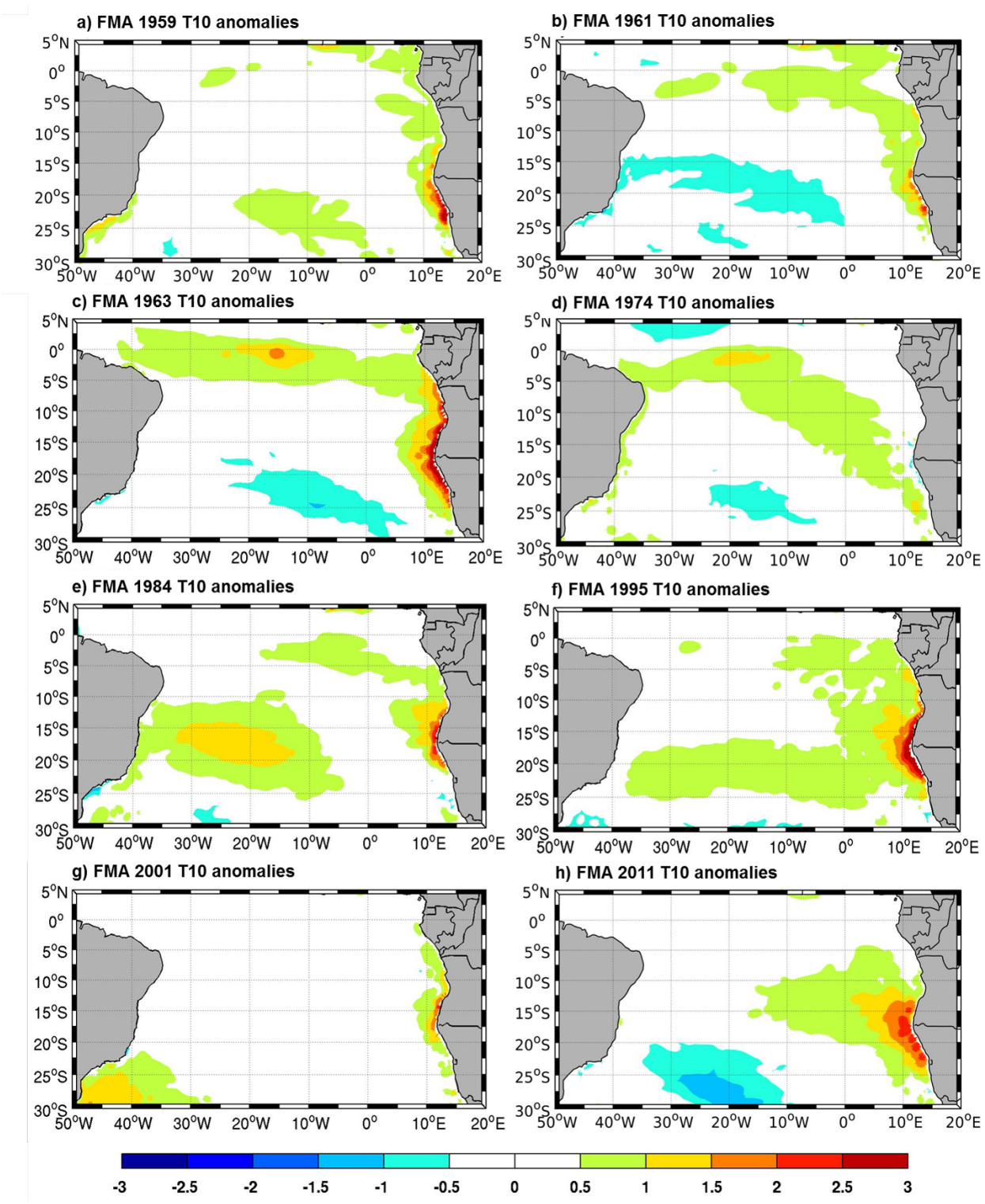

Figure 4.13: Monthly detrended anomalies of T10 (°C) averaged in February-March-April (FMA) during the Benguela Niños (a) 1958/1959, (b) 1960/1961, (c) 1962/1963, (d) 1974, (e) 1984, (f) 1995 (g) 2001 and (h) 2010/2011.

west African coast with maximum T10 anomalies (> 1°C) extending from 16°S to ~23°S. The warming pattern coverage extends north along the African coast and westward toward the equator up to around 18°W. In January 1961, peak month of the 1960/1961 Benguela Niño in Southern Angola and ABF (*cf.* **Table 4.1**), strong T10 anomalies (>2°C) are present from 12°S up to 18°S (not shown). In January 1961, the coastal warming pattern is observed along the African coast up to 5°N and westward along the equatorial Atlantic up to ~32°W. In February 1961, the T10 anomalies peak in Northern Namibia where the pool of warm water is now located (from 17°S to 22°S). In April 1961, T10 anomalies vanish north of the ABF along the west African coast and are present in Northern Namibia with less intensity (>0.5°C). The 1961 FMA average of T10 anomalies is less intense than the FMA 1959 (**Figure 4.13a**) even though these two extreme coastal events, peak in January in Southern Angola and ABF. An upwelling EKW second mode signal along the equatorial Atlantic is observed in JFM 1961 (*cf.* **Table 4.3**) since detrended anomalies of IEKW mode 2 is slightly negative (-0.04 cm). But over the whole period of the 1960/1961 extreme warm event (September – April) shown in **Figure 4.4**, positive intensity of IEKW mode 2 prevails which means downwelling EKW is observed. The averaged anomalies of meridional transport across the ABF during DJF 1960/1961 is -0.21 Sv (*cf.* **Table 4.3**) corresponding to a poleward transport across the ABF. **Figure 4.7** shows strong poleward flow across the ABF (<-1 standard deviation) between September and December 1960 which weakens but remains poleward until January 1961. The 1961 austral summer poleward flow could contribute to advect T10 anomalies poleward in the Northern Namibia region during the development of 1960/1961 Benguela Niño.

Along the Angola-Benguela Current system, the OGCM solution shows that the 1962/1963 Benguela Niño (**Figure 4.13c)** is the most extreme coastal events in terms of T10 anomalies even though it peaks around May – June (*cf.* **Table 4.1)**. This is confirmed with previous results in terms of T10 intensities observed in **Figure 4.4**. Anomalies of T10 (up to 2°C) start to develop along the west African coast in December 1962 between 2°S and 20°S. In February 1963, anomalies of T10 up to 3°C, are observed confined along the western African coast and reach Northern Namibia. T10 anomalies extend northwestward along the equatorial Atlantic. Maximum of T10 anomalies (>3°C) is observed in May – June along the equatorial wave guide and the west African coast up to 25°S. This extreme coastal event is interrupted by a cold anomaly of T10 that starts along the Gabon – Congo coastlines in August 1963 (not shown).

In late austral summer, the maximum warming (>2.5°C) along the west African coast from Southern Angola up to Northern Namibia is detected. The warming area spreads westward from the coast to couple of degrees offshore in the southeast Atlantic. There is a pattern of warming (>2°C) that extends northwestward from the west African coast toward the Brazilian coast along the equatorial Atlantic. *Katz et al.* [1977] observed that zonal wind stress near the equator west of 10°W was considerably low during the EQUALANT I cruise period in 1963 (February – April). This band of low zonal wind stress could be associated with the equatorial warming pattern associated with an Atlantic Niño or even a Benguela Niño (**Figure 3.7**). The averages during JFM 1963 of detrended anomalies of IEKW mode 2 along the equatorial Atlantic and the DJF meridional volume transport across the ABF are 0.94 cm and 0.11 Sv respectively (*cf*. **Table 4.3**). The averaged value found for the IEKW mode 2 (0.94 cm) corresponds to a propagation of a downwelling equatorial Kelvin wave which is also observed in **Figure 4.2** at the end of 1962 and beginning 1963. The averaged anomalies of meridional transport during DJF 1962/1963 is 0.11 Sv which is larger than the DJF climatology average (-0.77 Sv). This indicates a weaker poleward flow across the ABF. Likely, the alongshore flow does not reverse during the 1962/1963 Benguela Niño (not shown). This means that the flow remains poleward and could advect warm Angolan waters in Northern Namibia during the 1962/1963 Benguela Niño.

FMA 1974 event (**Figure 4.13d**) is different from the previous ones due to the absence of positive T10 anomalies along the west African coast. Conversely, there is a presence of cold T10 anomalies from 15°S to ~22°S. The warming pattern encompassing T10 anomalies greater than 0.5°C extends from Northern Namibia northwestward up to the equatorial Atlantic and then westward toward the Brazilian coast where it is observed southward. The 1974 extreme coastal event is supposed to peak in May in Southern Angola and June in the ABF zone and Northern Namibia (*cf*. **Table 4.1**). The warming pattern observed in April 1974 (not shown) is similar to the one in FMA 1974, but with a presence of T10 anomalies greater than 1°C from 17°S to 0°N along the west African coast and south of the equator between 25°W and 8°W from 5°S to 0°N. The warming pattern intensify in May 1974 with T10 anomalies greater than 3°C extending from 21°S to 0°N along the west African coast and centered in the equatorial Atlantic (not shown). The equatorial warming pattern observed in May 1974 resembles to the one of an intense Atlantic Niño as the anomalously warm pool is also located in the ATL3 box [20°W-0°E; 3°S-3°N]. Strong T10 anomalies persist in June 1974 along the equator and the west African coast.

Table 4.3 shows that in JFM 1974, downwelling EKW signal is observed with amplitude of 0.41 cm, whereas across the ABF zone, a DJF average of meridional transport anomalies during 1973/1974 of 0.20 Sv is estimated. This means that weak poleward flow is observed across the ABF in austral summer 1973/1974 and will be linked to warming in Northern Namibia 2 months later.

In late austral summer 1984 (**Figure 4.13e)**, a maximum of T10 anomalies (~ 2.5°C) is observed between 15°S and 18°S. The warming area extends equatorward up to ~ 5°S and westward from the African coast up to ~18°W. Another warming pattern is observed from the Brazilian coast to 5°W between 10°S - 25°S. During the 1984 Benguela Niño, T10 anomalies up to ~ 2.5°C develop along the African coast from 10°S to 20°S. This extreme event reaches its maximum in March 1984 with T10 anomalies larger than 3°C along the Southern Angola and Northern Namibia (not shown) coastlines. A warming pattern greater than 0.5°C is also observed from the African coast toward the west along the equatorial Atlantic. In April 1984, the event started to decay and T10 anomalies greater than 1°C moved equatorward north of 10°S along the African coast. Similar interpretations were described by *Rouault et al*. [2003] for the 1984 event using OI-SST dataset from 1982 to 2001. Also, using a FOCAL buoy track, *Reverdin and McPhaden* [1986] showed that there was a near zero westward current flow (South Equatorial Current) in the Gulf of Guinea where positive anomalies of SST were ~2°C during the second and third quarters of 1984. Across the ABF, the averaged transport anomalies during DJF 1983/1984 is 0.1 Sv meaning that a weaker than normal poleward flow prevails in austral summer, which is similar to the one of DJF 1962/1963. Along the equatorial wave guide, the 1984 JFM average of anomalies of IEKW mode 2 reveals that downwelling Kelvin wave with amplitude of 1.10 cm propagates. This downwelling IEKW mode 2 seems to be the strongest one compared to the others JFM averages in **Table 4.3** and one of the strongest in general after the one observed in 1963 over the period 1958 – 2015 (**Figure 4.2**).

Over the late austral summer season 1995 (**Figure 4.13f),** T10 anomalies form an intense warming area (>2°C) between 13°S and 23°S which is quite similar to the 1963 coastal event (**Figure 4.13c**) in the same delimited area. The warming area (>0.5°C) extends offshore in the southeast Atlantic between the African coast and 38°W from 15°S to 25°S. This warming pattern is not observed in the other cases. The warming area (>0.5°C) extends also northward along the African coast and westward along the equator up to 10°W. During the onset of the 1995

Benguela Niño, positive anomalies of T10 (>1°C) start to develop along the west African coast (2°S - 18°S) and become stronger in February 1995 (>2°C) between 12°S and 18°S (not shown). The peak of the 1995 event is found in March 1995 with a broad band of intense T10 anomalies greater than 3°C between 12°S and 23°S (not shown). The T10 anomalies persisted in April 1995, but are located between 15°S and 23°S. The T10 anomalies decrease in May 1995 and are found between 20°S and 23°S. North of 20°S, the positive T10 anomalies has already disappeared. These results are consistent with the results of *Rouault et al*. [2003] who also observed that during the 1995 event, unfavourable upwelling wind were present and could have intensified the 1995 event. During the 1994/1995 DJF season, there is a negative transport anomaly across the ABF of -0.24 Sv (*cf*. **Table 4.3**), meaning that stronger than normal poleward transport occurs across the ABF during austral summer 1994/1995. This strong poleward transport could have advected anomalous warm waters in Northern Namibia and contributed to the development of the 1995 Benguela Niño. The 1995 extreme coastal warm event is associated with the propagation of a downwelling IEKW mode 2 along the equator during the 1995 JFM season. Amplitude of the detrended anomalies of IEKW mode 2 is 0.62 cm.

Over the late austral summer 2001 (**Figure 4.13g**), positive T10 anomalies are observed along the west African coast from the equator continuously up to 25°S. The maximum T10 anomalies (>1.5°C) are found between the 12°S and 18°S. *Rouault et al.* [2007] observed the presence of strong southerly wind and high values of latent heat flux anomalies in FMA 2001 which participated to cool down the 2001 event and favoured upwelling in Northern Namibia. In 2001, positive anomalies of T10 greater than 1°C, are observed in January 2001 along the Angolan coast. These positive anomalies propagate southward up to the ABF zone in February 2001 and intensify in April 2001 with anomalies greater than 1.5°C observed between Southern Angola and Northern Namibia from the African coast to ~2° offshore (not shown). During May – June 2001, the positive T10 anomalies are observed along the entire coasts of Angola – Namibia covering a broad area but with less intensities than the previous months. The 2001 extreme warm event stops in July 2001 with the appearance of cool anomalies of T10 along west African coast. Our results are consistent with the results of *Rouault et al.* [2003]. Along the equatorial Atlantic, over the 2001 JFM season, a downwelling IEKW mode 2 propagated with amplitude of 0.11 cm (*cf*. **Table 4.3**). A strong than normal poleward transport is observed across the ABF during DJF 2000/2001 which contributes to advect the warm T10 anomalies downstream in Northern

Namibia. Average value of transport anomalies is -0.43 Sv (*cf.* **Table 4.3**) which is the strongest poleward flow compared to the others DJF averages in **Table 4.3.**

Lastly, **Figure 4.13h** shows that during FMA 2011, positive T10 anomalies greater than 1°C are found in a broad area extending from the coast to couple of degrees offshore between ~25°S and 12°S. The maximum of T10 anomalies (>2°C) is observed between 22°S to 15°S along the west African coast. The warming area spreads northwestward but does not reach the African coast. Positive anomalies of T10 (>1°C) appear along the west African coast north of 18°S in October 2010 and reach the maximum in December in Southern Angola (>2.5°C). This maximum T10 anomalies propagated southward into the Northern Benguela upwelling in February 2011. *Rouault et al*. [2017] found that the 2010/2011 Benguela Niño started along off Angola in November 2010 and peaked in January (**Figure 1.3**). The T10 anomalies persist up to April 2011 where it is interrupted by a cold event in May 2011 consistently with the results of

	JFM IEKW2 (cm)	DJF Netmt17S (Sv)
Climatology	N/A	-0.77
1958/1959	-0.13	-0.32
1960/1961	-0.04	-0.21
1962/1963	0.94	0.11
1973/**1974**	0.41	0.20
1983/**1984**	1.10	0.10
1994/**1995**	0.62	-0.24
2000/**2001**	0.11	-0.43
2010/2011	-0.15	-0.24

Table 4.3: Detrended anomalies of IEKW mode 2 (IEKW2, in cm) along the equatorial Atlantic averaged between 20°W – 0°E at 0°N from January to March (JFM) and detrended anomalies of meridional volume transport (Netmt17S, in Sv) across the ABF averaged within 1° coastal band from December to February (DJF) during the extreme warm events 1958/1959, 1960/1961, 1962/1963, 1974, 1984, 1995, 2001 and 2010/2011 represented in bold. Climatology of IEKW mode 2 is not available from OLM outputs.

Rouault et al. [2017]. In JFM 2011, upwelling EKW signal prevails along the equatorial Atlantic with an amplitude of -0.15 cm similar to the one in JFM 1959 (*cf.* **Table 4.3**). However, **Figure 4.2** shows that a downwelling EKW mode 2 with an amplitude of ~1.5 cm propagates along the equatorial Atlantic in September 2010 and is linked to the 2010/2011 extreme event. *Rouault et al.* [2017] reported that the weakening of easterly winds in the western equatorial Atlantic in October 2010 triggered a downwelling EKW at the origin of the 2010/2011 Benguela Niño. As in DJF 1994/1995, a quite strong than normal poleward transport (-0.24 Sv) prevails across the ABF during DJF 2010/2011 (*cf.* **Table 4.3**). This is consistent with the findings of *Rouault et al.* [2017] who reported that a strong poleward flow developed across the ABF and advected warm tropical water into Northern Namibia.

4.5.2 Benguela Niña events

Figure 4.14 is similar to **Figure 4.13** but for 7 extreme cold coastal events in FMA 1978, 1980, 1981, 1985, 1992, 1997 and 2010. The first four figures are the newly identified extreme cold events (**Figures 4.13a-d**). Similar methodology as in **section 4.5.1** is used to comment detrended anomalies of IEKW mode 2 and meridional transport during each coastal cold event.

During the late austral summer 1978 (**Figure 4.14a**), cold T10 anomalies (<-0.5°) are found along the west African coast north of 20°S up to 5°S where they extend westward up to 18°W. In Southern BUS (from 25°S to 30°S), there is a warming pattern meaning that the upwelling favourable wind was weaker than normal. The cooling pattern associated with the 1978 extreme cold event does not reach the Northern Namibia domain. It is confirmed in **Table 4.1** the 1978 extreme cold event is not recorded in the Northern Namibia domain and has a duration of 0 month. The 1978 extreme cold event peaks in April 1978 in Southern Angola and ABF (**Table 4.1**) and the cooling pattern is the same as FMA 1978 but with more intensity (cold T10 anomalies <-1°C). Strong upwelling IEKW prevails during JFM 1978 with amplitude of -0.89 cm along the equatorial Atlantic also observed in **Figure 4.2** which could have triggered the 1978 extreme cold event along the Angola – Benguela Current system. Across the ABF, average transport anomalies during DJF 1977/1978 is around 0 Sv (**Table 4.4**). This is due to the variations in the meridional transport anomalies (**Figure 4.7**) which shows negative anomalies of transport in December 1977 which is compensated by positive anomalies of meridional transport in January and February 1978. This means that meridional transport anomalies in DJF 1977/1978

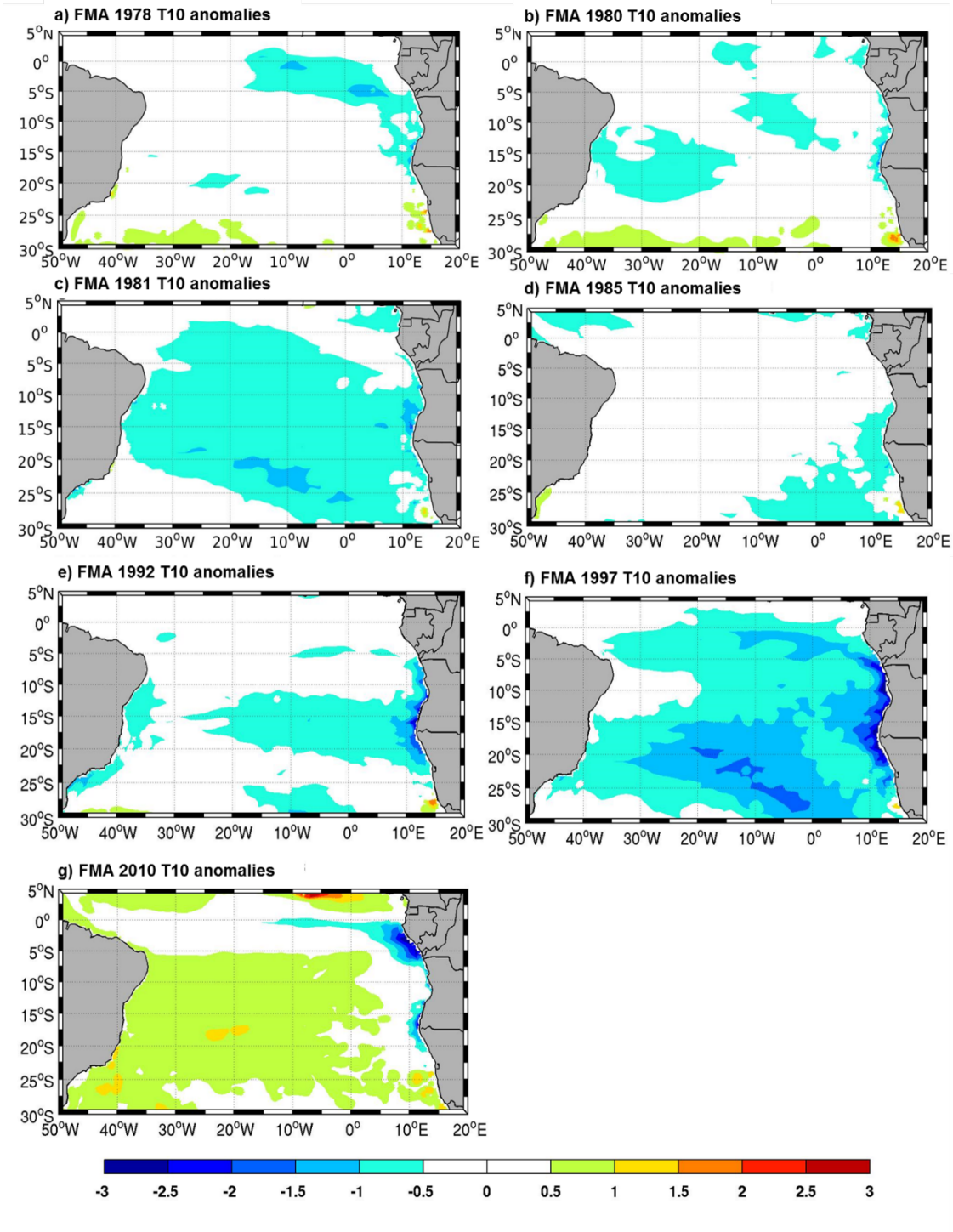

Figure 4.14: Monthly detrended anomalies of T10 (°C) averaged in February-March-April (FMA) during the Benguela Niñas (a) 1978, (b) 1980, (c) 1981, (d) 1985, (e) 1991/1992, (f) 1996/1997 and (g) 2010.

is not associated with the 1978 extreme cold event in the Northern Namibia. And as mentioned

previously, the 1978 extreme cold event does not reach the Northern Namibia (*cf.* **Table 4.1).**

In late austral summer 1980 (**Figure 4.14b**), cooling pattern (T10 anomalies <-0.5) is confined to the coast north of 20°S. As in FMA 1978, the cooling pattern shown in FMA 1980 does not reach Northern Namibia where a warming pattern takes place in the upwelling probably due to the weakening of upwelling favourable wind. In January 1980 (peak month of the 1978 extreme cold event in Northern Namibia), cold T10 anomalies are observed up to ~25°S. South of 25°S, positive T10 anomalies are present in the upwelling zone. An upwelling EKW signal in JFM 1980 with an amplitude of -0.54 cm (c*f.* **Table 4.4**) is associated with the 1980 extreme coastal

cold event. Across the ABF in DJF 1979/1980, the average meridional transport anomalies is 0.34 Sv leading to weaker than normal poleward flow as it does not reverse. This poleward meridional transport seems to be the weakest one compared to the others DJF averages in **Table 4.4**.

Cooling coverage observed in FMA 1981 (**Figure 4.14c**) is broader than the 2 previous extreme cold events and extends northwestward toward the Brazilian coast. Cold T10 anomalies (<-1°C) are present in Southern Angola. In February 1981, strong negative anomalies of T10 (<-1°C) are observed along the Northern Namibia coast (not shown). This pool of cold T10 anomalies progress northward along the Southern Angolan coast in March 1981 and extends to Northern Angola in April 1981 (not shown). An upwelling EKW mode 2 dominates in JFM 1981 with an amplitude of -0.36 cm along the equatorial Atlantic and is associated with an average meridional transport of -0.03 Sv across the ABF in DJF 1980/1981 (**Table 4.4**). The average meridional transport anomalies in DJF 1980/1981 is explained by the variations in the meridional transport anomalies show in **Figure 4.7** as in DJF 1977/1978.

Over the FMA 1985 (**Figure 4.14d**), cold T10 anomalies (~ -1°C) are observed between Southern Angola and Northern Namibia. South of 25°S, small warming area is observed along the coast. Cold T10 anomalies start to appear in March 1985 mostly in a broad area south of 10°S with a minimum (<-1.5°C) observed along the Northern Namibia coast. These cold anomalies propagate northward in April 1985 where they are visible from 4°S towards Northern Namibia (not shown). During the same month, the area of cold T10 anomalies shifts northward and is now located along Southern Angola. In May 1985, cold T10 anomalies persist in the southeast Atlantic Ocean and disappear in August 1985 with the presence of warm T10

anomalies along the west African coast (not shown). Across the ABF, there is a strong poleward flow (-0.21 Sv) prevailing in DJF 1984/1985 as the climatological average is -0.77 Sv. This strong poleward flow is not associated with advection of cold waters in Northern Namibia during the 1985 extreme cold event. Along the equatorial Atlantic, upwelling IEKW mode 2 propagate in JFM 1985 with an averaged amplitude of -0.01 cm which is quite weak.

Over the late austral summer 1992 (**Figure 4.14e**), minimum T10 anomalies (< -1°C) is confined to the west African coast between 6°S and 22°S. There is a cooling area from 5°S confined to the coast up to 11°S and extending from the African coast to around 30°W between 11°S and 20°S. This cooling pattern is similar to the one of March 1992 (not shown). Cold anomalies of T10 (~ -1°C) are observed north of 15°S covering a broad area in October 1991 (not shown). In December 1991, the cooling area is reduced and colder than normal T10 anomalies (< -1.5°C) are visible along the coast from 2°S to 15°S. In January 1992, the cold T10

	JFM IEKW2 (cm)	DJF Netmt17S (Sv)
Climatology	N/A	-0.77
1977/**1978**	-0.89	-0.004
1979/1980	-0.54	0.34
1980/1981	-0.36	-0.03
1984/**1985**	-0.01	-0.21
1991/1992	-0.10	0.12
1996/1997	-1.24	0.20
2009/**2010**	-0.99	-0.38

Table 4.4: Detrended anomalies of IEKW mode 2 (IEKW2, in cm) along the equatorial Atlantic averaged between 20°W – 0°E at 0°N from January to March (JFM) and detrended anomalies of meridional volume transport (Netmt17S, in Sv) across the ABF averaged within 1° coastal band from December to February (DJF) during the extreme cold events 1978, 1979/1980, 1980/1981, 1985, 1991/1992, 1996/1997 and 2010 represented in bold. Climatology of IEKW mode 2 is not available from OLM outputs.

anomalies persist in the same area, intensify and an extension of the cooling pattern (~ -1°C) is

observed from the coast westward up to 35°W along the equatorial Atlantic. In February 1992, the cold T10 anomalies propagate poleward along the west African coast and are now visible around 23°S before peaking in March 1992 with T10 anomalies observed around -2.5°C between Southern Angola and Northern Namibia. The cooling pattern extending from the coast to 30°W. Cold T10 anomalies persist along the west African coast until August 1992 and are stopped with the arrival of positive anomalies of T10 (not shown). In JFM 1992, an upwelling IEKW mode 2 propagates with an amplitude of -0.10 cm (**Table 4.4**). This upwelling IEKW mode 2 propagates the cold T10 anomalies along the west African coast. Meridional transport anomalies across the ABF during DJF 1991/1992 is 0.12 Sv leading to weaker than normal poleward transport in late austral summer 1992. As observed in **Figure 4.7** and **Figure 4.8**, over the 1991/1992 extreme cold event is related to poleward flow (negative intensity of meridional transport) across the ABF. This suggests that poleward transport develops across the ABF which cannot be linked to the advection of cold waters in Northern Namibia.

Over the FMA 1997 (**Figure 4.14f**), there is a presence of an intense cold pool of water covering almost the entire southern Atlantic with cold T10 anomalies less than -3°C confined along the African coast from 5°S to 22°S. Note that the 1996/1997 cold event is the coolest event observed over the period 1958 – 2015 (**Figure 4.4**). The 1996/1997 extreme cold event reaches its mature phase in April 1997 in the 3 coastal zones of interest (**Table 4.1**). This is consistent with the study of *Florenchie et al*. [2004]. This could also explain the similarities found in the cooling patterns in April 1997 (not shown) and FMA 1997. Quite strong upwelling IEKW mode 2 since propagates eastward in JFM 1997 along the equatorial Atlantic with an amplitude of -1.24 cm (**Table 4.4**). This upwelling IEKW mode 2 would have risen up the thermocline, then cools down the upper ocean and decreases the sea level. Along the Angolan coast, this decrease of sea level would lead to a decrease of the poleward geostrophic flow and could explain the low value of meridional transport anomalies that reach the ABF (0.20 Sv) shown in **Table 4.4** during DJF 1996/1997. The average meridional transport anomalies observed in DJF 1996/1997 represents the weakest poleward flow during extreme cold events in **Table 4.4**.

Over FMA 2010 (**Figure 4.14g**), the presence of cold T10 anomalies is observed along the equatorial Atlantic from 15°W toward the African coast and then from 0°N up to around 12°S but in a thin area confined to the coast from 7°S to 12°S along the African coast. Between 7°S and 2°S, minimum T10 anomalies forms a pool of cold water (<-1°C). A second cooling

pattern is observed between 13°S and 21°S with a minimum of -3°C located at the ABF at the zone and the rest of the southern Atlantic showed warming pattern which makes the FMA 2010 cold event is a bit different from the previous cold events. As shown in **Table 4.1**, the cold T10 anomalies do no reach Northern Namibia in 2010 (no peak and 0 month for duration of the event are recorded in Northern Namibia). In April 2010, there is a clear connection between the equatorial Atlantic and the west African coast (between 10°S and 0°N) up to 15°W visible where a large coastal cold pool of water with T10 anomalies less than -1°C is observed. During the same month, cold T10 anomalies are observed confined to the west African coast south of 10°S up to 23°S but with less intensity compared to the upstream cooling. Cold T10 anomalies persist until June 2010 and the demise of the event is observed with the arrival of a positive T10 event. During JFM 2010, strong upwelling IEKW mode 2 (-0.99 cm) signal prevails along the equator. Across the ABF, meridional transport anomalies are -0.38 Sv indicating a strong poleward flow during DJF 2009/2010 which is not associated with the advection of cold waters in Northern Namibia.

4.6 SUMMARY

In this chapter, an OGCM has been used to identify and classify the anomalous coastal warm and cold events along the southwest African coast using detrended normalized anomalies of temperature at 10 m over the period 1958 to 2015. 55 anomalous coastal events are identified in total, split up into 26 extreme events (16 warm, 10 cold) and 29 moderate events (13 warm and 16 cold) interannual events over the period 1958 to 2015. Strong correlation (0.65 statistically significant at 95%) between PIRATA dynamic height anomalies and OLM SSHA (c*f*. **Chapter 3**) leads me to use the OLM in the investigation of IEKW propagations and connection between equatorial region and the Angola Benguela Current system over 1958 to 2015. Results suggest the equatorial origin of most of these coastal anomalous events in agreement with results of **Chapter 3**.

Monthly distributions of peak of warming or cooling for of each coastal event occurring in each coastal zone reveal that the anomalous coastal events tend to peak during austral spring and late summer between October and April. Across the ABF poleward net transport dominates the annual cycle of meridional transport throughout the year, with a weak poleward flow in June

and a strong one in October. Most of the anomalous coastal events in Northern Namibia are mostly remotely forced via IEKW mode 2 propagations, but meridional transport anomalies across the ABF contribute to the development of these anomalous coastal warm events. Positive (weaker poleward flow than seasonal average or equatorward flow) or negative (stronger poleward transport than seasonal average) anomalies of meridional transport across the ABF are associated with negative or positive anomalies of T10 in Northern Namibia respectively. Lags of 1 to 6 months observed when net mass transport anomalies lead T10 anomalies in the Northern Namibia zone will be discussed later. The estimation of the net temperature transport across the ABF does not improve our results and correlations compared to the net mass transport across the ABF.

7 out of 8 newly extreme coastal events (3 warm: 1958/1959, 1960/1961, 1974 and 4 cold: 1978, 1979/1980, 1980/1981 and 1985) have been described during the FMA season along with 8 known extreme coastal events (5 Benguela Niños 1962/1963, 1984, 1995, 2001, 2010/2011 and 3 Benguela Niñas 1991/1992, 1996/1997, 2010). All the extreme warm or cold events are linked to downwelling or upwelling propagations of IEKW along the equatorial wave guide during JFM (1 month before FMA) except the extreme warm events 1958/1959, 1960/1961 and 2010/2011. However, the 1995 extreme coastal warm event is associated with the propagation of a downwelling IEKW mode 2 along the equator during the late austral summer season. This is not consistent with the study of *Richter et al.* [2010] which stated that no EKW propagated during the 1995 Benguela Niño. During DJF season (2 months before FMA), meridional transport anomalies across the ABF are not always consistent with the anomalies of T10 along the western coast of Africa. This was the cases for the Benguela Niña 1985 and 2010 where strong poleward flow is observed across the ABF instead of equatorward flow or weak poleward flow and Benguela Niños 1974 and 1962/1963 where equatorward flow or weak poleward flow prevails over DJF instead of strong poleward flow. This discrepancy between variations in the anomalies of T10 and meridional transport at 17°S could be at the origin of the low correlation (-0.2) reported in **Section 4.3** between the meridional transport anomalies across the ABF and the T10 anomalies in Northern Namibia. During the DJF season, the strongest poleward flow across the ABF for the extreme warm events occurs during DJF 2000/2001 (**Table 4.3**) for the extreme warm event 2001 and the strongest amplitude of downwelling EKW occurs in JFM 1984. Conversely, the weakest poleward flow across the ABF for the extreme

cold events occurs during DJF 1979/1980 and the strongest amplitude of upwelling EKW occurs in JFM 1997. Some extreme coastal events are not linked to equatorial propagations for example coastal cold event in 2002 (**Figure 3.5**) or warm event 1976/1977 (**Figures 4.2** and **4.4**). This means that other processes could have played a role on the onset or development of these coastal events, such as the role of the local forcing and the efficiency of the vertical stratification in the coastal fringe. In this context, the next chapter will focus on the computation of composite maps of wind stress and T10 anomalies in order to investigate the contribution of the large-scale wind stress. Also, analyses will be performed to investigate the role of the local forcing (alongshore wind-stress) during the onset of the anomalous warm and cold events at interannual timescales, and I will also discuss the contribution of the vertical stratification along the west African coastline.

CHAPTER 5

5 LARGE-SCALE WIND STRESS PATTERN OVER THE TROPICAL ATLANTIC, ROLE OF LOCAL WIND STRESS AND VERTICAL OCEAN STRATIFICATION DURING THE ONSET AND DEVELOPMENT OF THE INTERANNUAL COASTAL EVENTS

5.1 INTRODUCTION

The recent studies conducted by *Bachèlery et al.* [2016a] and *Imbol Koungue et al.* [2017] suggested that most of the important coastal warm and cold events along the Angola Benguela Current system are remotely forced via IEKW propagations which agrees with main findings of **chapter 4** for the 1958-2015 period. But they suggested that the role played by local variability (for instance wind stress, vertical stratification) is not negligible. Past study by *Richter et al.* [2010] suggested that Benguela Niños are locally forced via variations of alongshore coastal wind stress along the southwest coast of Africa. They also suggested that these coastal alongshore wind anomalies are part of a basin-scale weakening of the South Atlantic high variability that starts 3 months before SST anomalies peak along the coast of western Africa. Moreover, the role of the local stratification has been described as an efficiency coefficient which modulates the signature of the CTW on the temperature within the surface layer [*Goubanova et al*., 2013; *Bachèlery et al*., 2016a; *Imbol Koungue et al.*, 2017].

In this chapter, OGCM outputs and its wind-stress forcing are used between 1958 and 2015 to investigate the role of the atmospheric forcing and the characteristics of water column in the coastal fringe on the development and intensity of the Benguela Niño and Benguela Niña events. During the onset and the development of interannual coastal events, a lagged composite analysis will be performed to examine the contribution of the large-scale and local wind pattern. Cross and lagged correlation analysis will be calculated to explore the relationship between the coastal interannual temperature variations at 10-meter depth and the local and large-scale wind stress

anomalies in the southeastern Atlantic Ocean. Finally, vertical stratification of the water column within the coastal fringe will be estimated and discussed in the light of the modulation of the interannual coastal trapped wave signature on the SST.

5.2 ROLE PLAYED BY THE LARGE-SCALE WIND PATTERN DURING THE EXTREME OR MODERATE WARM OR COLD EVENTS

According to *Lübbecke et al.* [2010], the strength of the SAA given by the index in sea level pressure averaged between [30°W – 10°W; 40°S – 20°S], is linked to the development of the interannual southeastern Atlantic warm events. They reported lag of 1 month when the strength of the SAA leads SSTA in the ABA box in March. They also suggested that warming in the ABA box associated with Benguela Niño events, is also linked to the strength of the local wind stress which is also linked to the SAA position and intensity, also proposed by [*Richter et al.* 2010]. To better highlight the link between the large-scale wind and the interannual warming or cooling in the southeastern Atlantic Ocean, a lagged composite analysis of T10 detrended anomalies and wind stress over the tropical Atlantic domain (50°W - 20°E; 30°S - 20°N) at different lags for T10 anomalies and wind stress anomalies is performed. Only results for extreme coastal warm or cold events are presented. Here, a composite analysis by selecting all the extreme warm and cold coastal events summarized in **Table 4.1** which peak in March or April for at least 2 coastal zones of interest (*cf.* **Figure 2.2**) is performed. The result provides a composite map of detrended anomalies of T10 averaged during March – April season (late austral summer). Lagged composite maps are also presented in **Figure 5.1** and **5.2**, with a lag interval ranging from 3 months before the peak of the event to 2 months after the peak for both T10 and wind stress anomalies. 5 extreme warm coastal events (1976/1977; 1984; 1995; 1999 and 2001) and 5 extreme cold coastal events (1978; 1981/1982; 1985; 1991/1992 and 1996/1997) are then selected. Lagged composite maps of wind stress and T10 anomalies shown in **Figure 5.1** are performed by averaging for the 5 selected extreme warm events that peak in March – April, the wind stress and T10 anomalies 3 months before the peak (December – January), 2 months before the peak (January – February), 1 month before the peak (February – March), during the peak (March – April), 1 month after the peak (April – May), and 2 months

after the peak (May – June). Afterward, a bootstrap resampling technique on the T10 anomalies (*cf.* **section 2.2.5**) is applied to highlight only the statistically significant values at 90% on the composite maps. The results are presented in **Figure 5.1** and **5.2**.

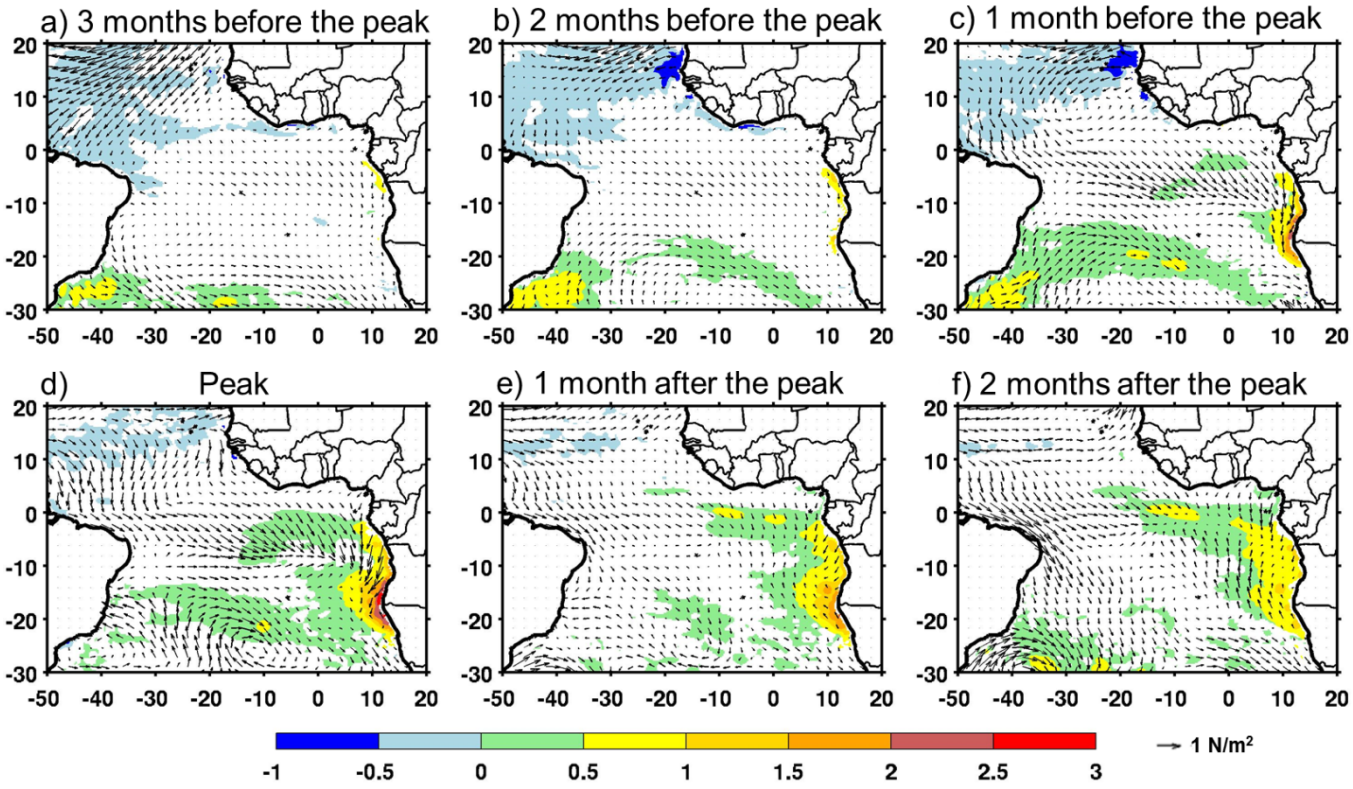

Figure 5.1: Composite maps of detrended anomalies of T10 (in colour, in °C) computed from 5 selected extreme warm coastal events and corresponding wind stress anomalies (arrows, $N.m^{-2}$) averaged in: a) December – January (3 months before peak); b) January – February (2 months before the peak); c) February – March (1 month before the peak); d) in March – April (peak); e) April – May (1 month after the peak); and May – June (2 months after the peak). The shaded areas (detrended anomalies of T10) represent the 90% statistically significant areas (using p-value statistical test from *Best and Roberts* [1975]).

3 months before the peak (**Figure 5.1a**), easterly wind stress anomalies are present in the western part of the equator. There is no significant warming along the coasts of Angola and Namibia.

Two months before the peak (**Figure 5.1b)**, there is a warming pattern observed along the southwest coast of Africa up to 18°S showing T10 anomalies greater than 0.5°C. Cooling pattern is observed in the northern tropical Atlantic with a minimum temperature at 10 m (<-0.5°C) observed along the Mauritania - Senegalese coastlines. Wind stress anomalies coverage can be well observed and spreads westward up to around 22°W along the equator and 10°S and comprises westerly anomalies along the equator, northwesterly anomalies and northerly anomalies which start to be noticeable close to the western African coast. This large coverage composed of weak wind stress anomalies forms the basin-scale weakening of SAA. Therefore, wind stress anomalies pattern observed in January – February (2 months before the peak) appear to be linked to the warming along the Angola – Benguela Current system [*Lübbecke et al.*, 2010; *Richter et al*., 2010] although these wind stress anomalies do not reach the western equatorial Atlantic a zone already shown to be important to force Kelvin waves (c*f.* **Chapter3**).

Figure 5.1c shows the anomalies of T10 and wind stress one month before the peak. Classical Benguela Niño signature is quite well observed from 5°S to 22°S with maximum (>2°C) between Southern Angola and the ABF zone (~17°S). The coastal warming extends from the west African coast to couple of degrees offshore. Cooling pattern persists in the North tropical Atlantic especially along the Senegalese – Mauritania coastline. The basin–scale weakening pattern of wind stress is well developed. As part of this large-scale weakening of wind stress, westerly wind stress anomalies are well observed in the western equatorial Atlantic which are the key forcing for downwelling IEKW that will be linked to a Benguela Niño one month later (*cf.* **Chapter 3**) corresponding to the peak of the event. At the same time, northwesterly wind stress anomalies south of the equator and northerly wind stress anomalies north of 20°S are well developed over the significant warming area. Strong northerly wind stress anomalies are also well developed over the Southern Angola domain where the maximum T10 anomalies occurs. Northwesterly wind stress anomalies (weakened southeasterly trade winds) observed south of the equator up to ~10°S East of 20°W over the warming area might be indicative of an ocean–atmosphere coupling, through Wind-Evaporation-SST feedback [*Lübbecke et al*., 2010], that would decrease the southerly wind stress along the Angolan coast. The SAA wind circulation weakens and shifts equatorward as an intensification of the cyclonic wind stress anomalies circulation south of 10°S over the significant warming area up to 10°W is observed.

The composite of the March – April extreme warm coastal events (**Figure 5.1d**), shows that the signature of Benguela Niño is noticeable with a maximum ~3°C between 15°S - 18°S along the Angola – Namibia coastlines. An interesting feature is that around 10°S to 18°S, the significant warming area spreads westward in a range of 10 to 12° offshore. The T10 anomalies extend further South continuously up to ~25°S, corresponding to the approximate maximum latitude where the signature of Benguela Niños and the interannual coastal trapped waves can be tracked [*Bachèlery et al*., 2016a]. In the southward direction, the significant warming area is confined to the coast. The significant warming area greater than 0.5°C extends northwestward into the eastern equatorial Atlantic region up to 15°W where the Atlantic cold tongue appears every year in Austral winter and where Atlantic Niño events develop in austral winter also [*Lübbecke et al.,* 2010]. This could be explained by the tendency of the Atlantic Niño to follow the Benguela Niño [*Richter et al*., 2010; *Lübbecke et al*., 2010] or they are the same phenomenon as proposed by *Lübbecke et al*. [2010]. Indeed, according to *Lübbecke et al.* [2010], there is a season lag between Benguela Niño and Atlantic Niño. The equatorial domain and the southeastern Atlantic domain share a considerable portion of variability [*Richter et al*., 2010]. The wind stress anomalies circulation during the peak (mature phase of the selected Benguela Niños) reveals that northerlies wind anomalies cover the whole warming area over the Southern Angola domain. The observed northerly anomalies persist over the warming along the Angolan coast. A convergence of weakened wind stress anomalies is observed over the significant warming area ~10°S which is also observed in **Figure 5.1c**. This could be explained by the coupling mechanism proposed by *Hu and Huang* [2007]. According to *Hu and Huang* [2007], coastal warming observed in austral fall in the southern tropic and equatorial Atlantic, is responsible of wind convergence over the basin causing westerly wind stress anomalies. South of 10°S, a divergence of wind stress anomalies is observed forming an anticyclonic wind stress anomalies circulation west of 25°W and a cyclonic wind stress anomalies circulation east of 25°W. The basin-scale weakening of wind stress persists.

One month after the peak (**Figure 5.1e**), along the west African coast, similar warming pattern is observed as in **Figure 5.1d** but with less intensity close to the Southern Angola and Northern Namibia coastlines. This suggests that the extreme coastal event is decaying. Westerly wind stress anomalies are still observed in the western part of the equatorial Atlantic.

2 months after the peak (**Figure 5.1f**), the intensity of the warming pattern observed in

Figure 5.1e decreases along Southern Angola and Northern Namibia, but the warming spreads northwestward along the equatorial Atlantic. This suggests that Atlantic Niño is taking place over the eastern equatorial Atlantic. Also, the presence of the westerly wind stress anomalies in the western equatorial Atlantic in May – June (2 months after the peak) could justify the onset of Atlantic Niño in the Eastern equatorial Atlantic.

Figure 5.2 presents the same analysis as **Figure 5.1,** but for the 5 extreme cold events abovementioned (1978; 1981/1982; 1985; 1991/1992 and 1996/1997). All these Benguela Niñas peak in March – April similar to the Benguela Niños composite detailed above. Compared to the

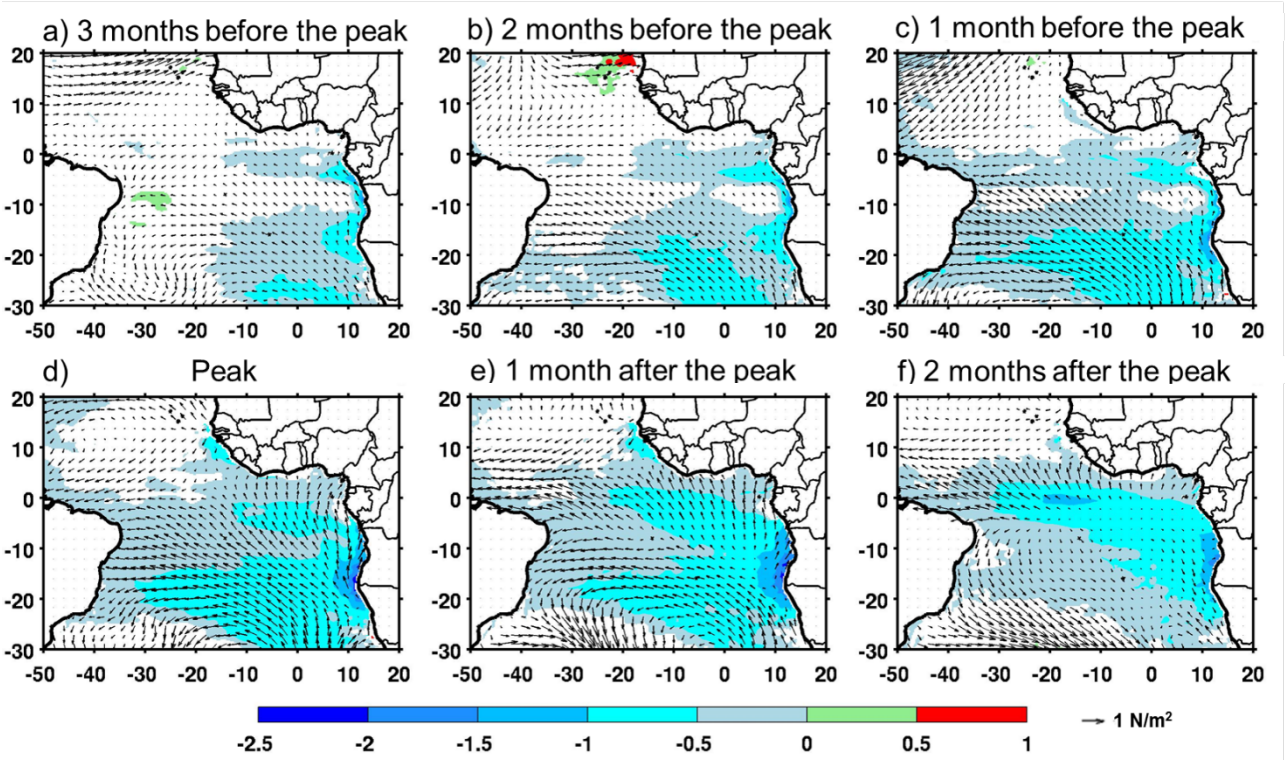

Figure 5.2: Composite maps of detrended anomalies of T10 (in colour, in °C) computed from 5 selected extreme cold coastal events and corresponding wind stress anomalies (arrows, $N.m^{-2}$) averaged in: a) December – January (3 months before peak); b) January – February (2 months before the peak); c) February – March (1 month before the peak); d) in March – April (peak); e) April – May (1 month after the peak); and May – June (2 months after the peak). The shaded areas (detrended anomalies of T10) represent the 90% statistically significant areas (using p-value statistical test from *Best and Roberts* [1975]).

extreme warm event composite maps (**Figure 5.1**), the 90% statistically significant cooling area is much broader and covers the south Atlantic Ocean for some cases (**Figures 5.2b** to **5.2f**). Cooling is more present along the northwestern coast of Africa, in the Gulf of Guinea and in the Atlantic cold tongue area. The composite maps do not portray the meridional dipole pattern of T10 anomalies depicted in **Figure 5.1** as no warming pattern is present in the north tropical Atlantic. 3 months before the peak of the selected Benguela Niñas (**Figure 5.2a**), cooling pattern appears east of 20°W south of the equator with minimum of T10 anomalies (<-0.5°C) observed between 20°S and 0°S. A second pattern of cold T10 anomalies (~-1°C to -0.5°C) is observed south of 20°S between 10°W and 10°E. No anomalous wind stress anomalies are observed in the western equatorial Atlantic and along the west African coast.

2 months before the peak (**Figure 5.2b**), the cooling coverage starts spreading along the equator and in the southeast Atlantic Ocean. At the same time, there is a warming pattern off Senegal – Mauritania coastlines. Along the west African coast, weak southerly anomalies develop. Strong southeasterly anomalies are present south of the equator between 25°S and 5°S and from 20°W to 10°E. These strong southeasterly anomalies associated with a larger cooling pattern compared to **Figure 5.2a**.

Figure 5.2c reveals cold T10 anomalies along the equatorial Atlantic almost connected with the cooling in the Southern Ocean. Cold T10 anomalies are also observed along the northwest coast of Africa. Minimum T10 anomalies are now observed between the Southern Angola and Northern Namibia and is now connected with the offshore cooling. In the western equatorial Atlantic, easterly wind stress anomalies are well observed 1 month before the peak of the event and constitute the perfect timing for the forcing of an upwelling IEKW that will be linked to a Benguela Niña event 1 month later (*cf.* **Chapter 3**) and observed in **Figure 5.2d**. There is an evidence of basin-scale strengthening of wind stress over the tropical Atlantic. Easterly wind stress anomalies observed in the western equatorial Atlantic are quite well connected with the southeasterly wind stress anomalies blowing over the cold T10 anomalies and forming the northeastern part of the anticyclonic circulation present south of 20°S in the southern tropic that could be attributed to the SAA circulation. The SAA circulation seems to have intensified compared to **Figure 5.2b**. Along the African coast, southerly wind stress anomalies are present over the cooling area and south of it. Similar to the Benguela Niño composite (**Figure 5.1c**), Wind-Evaporation-SST feedback might be at work, explaining the intensification

of the southeasterly winds north of 15°S.

During the peak (March – April), the Benguela Niña is at its mature phase (**Figure 5.2d**). Minimum T10 anomalies (<-1°C) are present between 22°S and 3°S along the west African coast. Intensified cooling is observed along the northwestern coast of Africa. Cold T10 anomalies ranging between -1°C and -0.5°C south of 10°S form with the coastal cooling area a broad pool of cold water in the south Atlantic. Similarly, to **Figure 5.1**, the tendency of Atlantic cold tongue events to follow Benguela Niña events could be argued here when the later occurs. The atmospheric circulation reveals a strong large-scale atmospheric circulation. This large-scale atmospheric circulation is formed by southerly wind stress anomalies over the cooling area along Angolan coast up to the ABF zone (~17°S), strong southeasterly anomalies offshore up to 30°W which gain a strong zonal component and become easterly wind anomalies toward the Brazilian coast and easterly wind stress anomalies in the western part of the equatorial Atlantic.

In **Figure 5.2e**, cold T10 anomalies persist but their coverage starts to diminish south of 20°S. Coastal cooling persists along the southwest African coast. Surprisingly, a broader cold pool of water is observed along the Angola and Northern Namibia with values of T10 anomalies quite similar to the ones observed in **Figure 5.2d**. Similar intensity observed between the coastal cooling during the peak and 1 month after it, reveals that the demise of the Benguela Niña takes longer compared to the demise Benguela Niño events. This is in agreement with the fact that the signature in the surface layer (SST) of Benguela Niña events last longer than Benguela Niño events as suggested by *Florenchie et al.* [2004]. In terms of wind stress anomalies, basin-scale strengthening of wind stress persists over the south Atlantic. South of the equator, an anticyclonic wind stress circulation is well represented and seems to have shifted northward prior to the development of the Atlantic cold tongue along the equatorial Atlantic in austral winter. Easterly wind stress anomalies coverage is reduced over the equatorial Atlantic and is present west of 20°W. This could be linked to the forcing of the Atlantic cold tongue which appears in austral winter in the eastern part of the equatorial Atlantic concomitantly with the northward shift of the SAA. Cross-equatorial southerly wind anomalies are present in the Gulf of Guinea east of 10°W and will lead to more cooling along the equatorial Atlantic through upwelling, entrainment and evaporation processes [*Okumura et Xie.,* 2004]. Convergence of southeasterly wind stress anomalies coming from the south Atlantic and northeasterly wind stress anomalies coming from the north Atlantic occurs in the North Atlantic ~5°N. Along the Angola – Benguela Current

system, southerly wind-stress anomalies are still observed along the Angolan coast (**Figure 5.2d** and **5.2e**).

2 months after the peak of Benguela Niña (**Figure 5.2f**), cold T10 anomalies coverage is reduced over the tropical Atlantic. The demise of the Benguela Niña along the coast of Angola and Namibia is remarkable. Northerly wind stress anomalies (weakened southerly or northerly wind stress) develop over the coastal cooling which can modulate the signature of the coastal cooling. Along the equatorial Atlantic, the ocean responds to the strong cross-equatorial southerly wind stress anomalies observed previously (**Figure 5.2e**) with an Atlantic cold tongue pattern well developed. Strong southeasterly and cross-equatorial southerly wind stress anomalies are located on the northern flank of the Atlantic cold tongue pattern whereas weaker wind stress than seasonal average on its southern flank. There is a convergence of the wind stress anomalies around 10°N which is fed by strong cross-equatorial southerly wind stress anomalies present on the northern flank of the Atlantic cold tongue. The wind stress anomalies forming the SAA are extended in the southwestern tropical Atlantic but are considerably weakened on its southeastern side over the cold waters.

In conclusion, at interannual timescales, Benguela Niño or Niña events are remotely forced via IEKW propagations along the equatorial Atlantic. IEKW are triggered by westerly or easterly wind stress anomalies in the western equatorial Atlantic well noticeable 1 month before the coastal events peak on the composite analysis presented in **Figure 5.1c** (**5.2c**). Benguela Niña events seem to last more than Benguela Niño events as little differences were observed between the peak and 1 month after the peak for the Benguela Niña. Ocean-atmosphere coupling seems to be active 1 month before the peak of the warm (cold) event (**Figure 5.1c** (**Figure 5.2c**)) with northwesterly (southeasterly) wind stress anomalies in the southern tropic East of 20°W and could have also amplified northerly (southerly) wind-stress anomalies along the Angola coast. Westerly and easterly wind stress anomalies in the western equatorial Atlantic were observed concomitantly with northerly and southerly wind stress anomalies along the Angola – Benguela Current system as part of the basin-scale weakening and strengthening of the wind stress observed 1-2 months before the peak and during the peak of the Benguela events. This leads to think that the local wind stress can probably contribute to the development of the Benguela events. This will be investigated in the following section of this chapter.

5.3 LOCAL WIND STRESS VARIABILITY IN THE SOUTHEAST ATLANTIC OCEAN

In the tropical Atlantic Ocean, the seasonal cycle dominates the variability [*Philander and Pacanowski*, 1986; *Ding et al*., 2009]. It is important to understand the annual cycle to better interpret the monthly interannual anomalies from monthly climatology. For this purpose, **Figure 5.3** presents the seasonal cycle of meridional wind stress averaged in 4 locations; namely, Southern Angola between 10°S to 15°S from the coast to 1° offshore), ABF (between 16.5°S to 17.5°S from the coast to 1° offshore), Northern Namibia (between 19°S to 24°S from the coast to 1° offshore) and Southern Namibia between 26°S to 30°S from the coast to 1° offshore. Note that Southern Namibia is an upwelling area. The prevailing climatological wind stress is directed equatorward (positive values) in the 4 zones. The lowest amplitude of wind stress is observed in Southern Angola (in red, **Figure 5.3**) throughout the year [*Rouault et al.,* 2007; *Lass et Mohrhorlz.* 2008; *Ostrowski et al.,* 2009; *Rouault.* 2012; *Rouault et al.*, 2017]. In Southern Angola, the wind stress values vary between 0.02 N.m^{-2} and 0.035 N.m^{-2}. In the ABF zone,

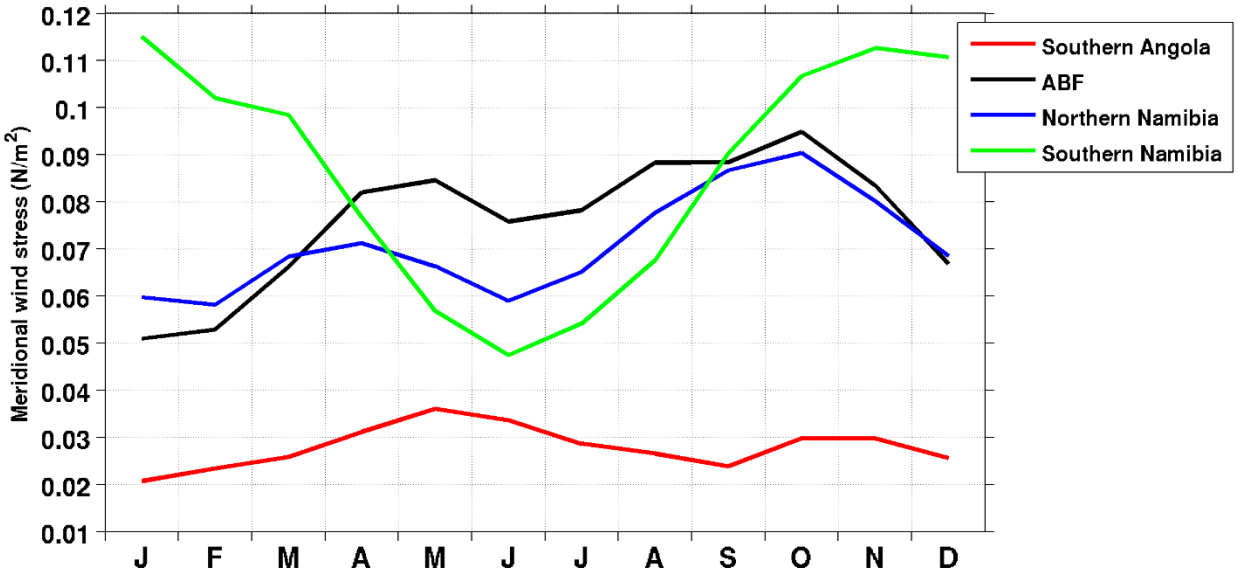

Figure 5.3: Annual cycle of OGCM meridional wind stress averaged in Southern Angola (10°S to 15°S from the coast to 1° offshore), in the ABF zone (16.5°S to 17.5°S from the coast to 1° offshore), in Northern Namibia (19°S to 24°S from the coast to 1° offshore) and in Southern Namibia (26°S to 30°S from the coast to 1° offshore). Positive values mean equatorward wind stress.

wind stress values range between 0.02 $N.m^{-2}$ and 0.095 $N.m^{-2}$. There is a bimodal variation of wind stress with maxima in April - May season (between 0.08 $N.m^{-2}$ - 0.09 $N.m^{-2}$) and in October (~ 0.095 $N.m^{-2}$) shown in **Figure 5.3** (in black). Low values of wind stress are found in austral summer between January and February. Upwelling favourable wind is found south of the ABF [*Hardman-Mountford et al.,* 2003; *Rouault et al.,* 2007; *Lass et Mohrhorlz.* 2008; *Rouault.* 2012]. Similar variations of the wind-stress is observed in Northern Namibia as in the ABF zone. Maxima in March – April (peak season of Benguela Niños and Niñas, *cf.* **Figures 5.1d** and **5.2d**) and in October in Northern Namibia are observed. Wind-stress in ABF zone is stronger than the one in Northern Namibia from March to November. This difference between the mean winter meridional wind stresses in the two zones could be explained by the seasonal shift of the St Helena High system which intensifies the wind-stress near the ABF zone (~17°S) in austral winter as shown by *Lass et al.* [2008]. In Southern Namibia, the wind stress is low in austral winter with a minimum in June most likely due to the seasonal shift of the Intertropical Convergence Zone (ITCZ) which is located further North in austral winter [*Boyd et al.,* 1987]. Conversely, the meridional wind stress in Southern Namibia is high in Austral spring/summer, period when the ITCZ is further south [*Boyd et al.,* 1987]. Wind stress in Northern Namibia and in the ABF zone are higher than in Southern Namibia, especially between April and September. This is due to the seasonal shift of the SAA which moves northwestward in Austral fall and winter and moves southward again around Austral summer, triggering weak upwelling favourable southeasterly wind in Northern Namibia and strong upwelling favourable southeasterly wind in South Africa.

Figure 5.4 shows the local interannual monthly detrended anomalies of OGCM meridional wind stress in Southern Angola (a), ABF zone (b), and Northern Namibia (c) from 1958 to 2015. The data are averaged within the 1° coastal fringe and smoothed with a 3-month running window (for display purpose only). Positive anomalies mean stronger than normal equatorward (southerly wind stress anomalies) wind stress, whereas negative anomalies mean weaker than normal equatorward wind stress (northerly wind stress anomalies). Climatology of wind stress from 1958 to 2015 reveals that the wind stress remains southerly especially in Angola, where weak wind stress is found throughout the year. The wind stress anomalies observed in the Southern Angola zone (**Figure 5.4a**) are weaker than the ones observed in the 2 other coastal zones. To better appreciate the local relationship between the T10 and meridional

wind stress anomalies, the identified anomalous coastal T10 events (*cf.* **section 4.2**) are represented by the coloured rectangles and overlaid to the panels of **Figure 5.4** (as in **Figure 4.1**). There is an opposite relationship between interannual coastal wind stress anomalies and anomalous coastal events. At interannual timescales, most of the local positive and negative coastal events might be associated with negative and positive wind stress anomalies. It means

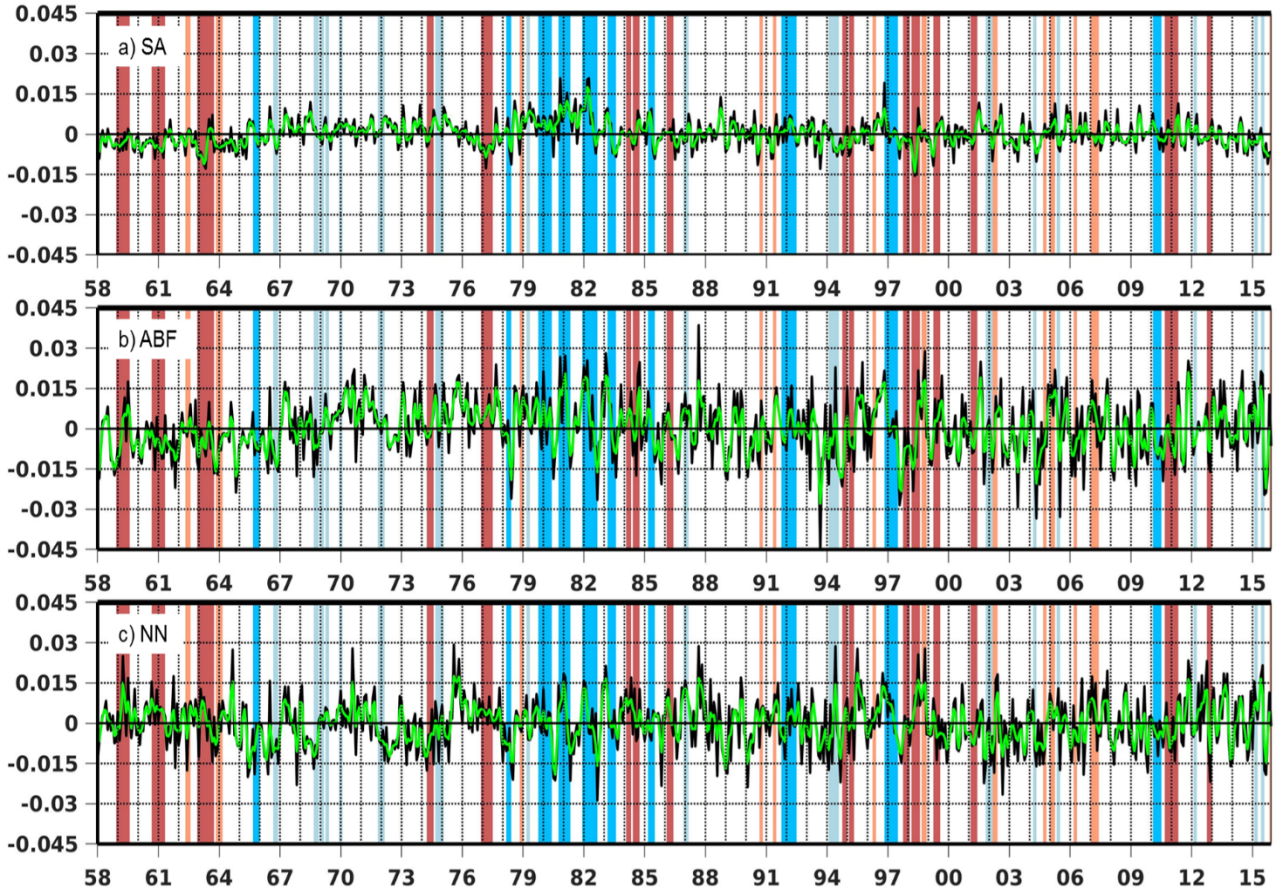

Figure 5.4: Monthly detrended anomalies of OGCM meridional wind stress (black line, $N.m^{-2}$) in (a) Southern Angola (SA) averaged from 10°S to 15°S and from the coast to 1°offshore, (b) Angola Benguela Front (ABF) region averaged from 16.5°S to 17.5°S and from the coast to 1° offshore, and (c) Northern Namibia (NN) averaged from 19°S to 24°S and from the coast to 1° offshore. Green line in each domain represents detrended anomalies of meridional wind stress smoothed with a 3-month running windows. Red (blue) and light red (light blue) rectangles represent extreme warm (cold) and moderate warm (cold) coastal events respectively along the Angolan-Namibian coastlines identified in **Figure 4.1**.

that northerly and southerly wind stress anomalies could trigger or favour warm and cold coastal events along the southwest African coast consistently with the composite maps of Benguela Niño (**Figure 5.1**) and Benguela Niña (**Figure 5.2**) events peaking in March – April. For instance, during the 2010/2011 Benguela Niño, low values of wind stress anomalies (~0.005 $N.m^{-2}$) are observed in the Southern Angola and the ABF zones in November 2010. In Northern Namibia, a reduction of upwelling favourable winds is observed in November 2010 (~ -0.005 $N.m^{-2}$), December 2010 (~ -0.01 $N.m^{-2}$), January 2011(~ -0.011 $N.m^{-2}$) and March 2011(~ -0.014 $N.m^{-2}$) before strengthening again in April and start cooling the event. Similar observations are found in *Rouault et al*. [2017] who observed that in Namibia lower than normal southeasterly upwelling favourable winds are observed in 2010/2011 especially in November 2010, December 2010 and March 2011. Northerly wind stress anomalies associated with the extreme coastal warm event in 1998. In this case, the wind stress along the southwestern coast of Africa will favour the positive T10 anomalies. The undocumented Benguela Niños 1958/1959 and 1974 are associated with northerly wind stress anomalies along the Angola – Namibia coastlines 1 month before their onsets. Whereas 1 month before the onset of the 1960/1961 Benguela Niño, northerly wind stress anomalies develop in Southern Angola and ABF, but southerly wind stress anomalies are observed in Northern Namibia. Conversely, 1 month before their onsets, undocumented Benguela Niñas 1979/1980, 1980/1981 and 1985 are associated with southerly wind stress anomalies along the southwest African coast. But 1 month before their onsets, the 1965 and 1978 undocumented Benguela Niñas are linked to southerly wind stress anomalies in Southern Angola and ABF and northerly wind anomalies in Northern Namibia. Surprisingly, absolute values of correlation between the local meridional wind stress and the anomalous coastal events are higher in Southern Angola than in the ABF zone or Northern Namibia (**Table 5.1**, 1st row) even though there are no upwelling favourable wind in Southern Angola. These correlations are confirmed in the composite maps in **Figures 5.1c** and **5.2c**, where the presence of the alongshore wind stress anomalies is observed mostly along the west African coast 1 month before the peak of the events for the 5-extreme events average. For example, in **Figure 5.1c**, strong northerly wind stress anomalies more developed in Southern Angola than northwesterly wind stress anomalies in Northern Namibia.

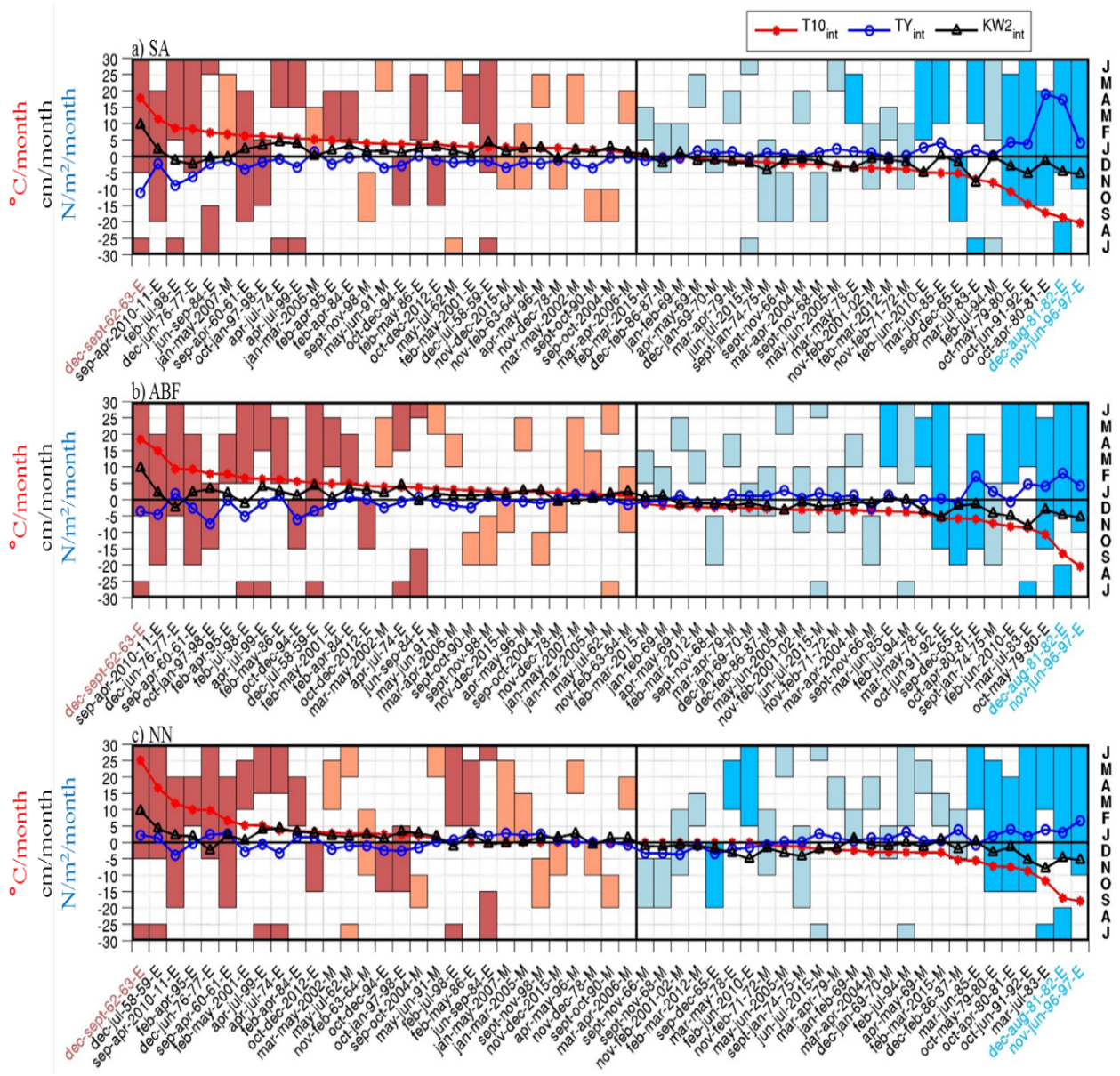

Figure 5.5: Same as **Figure 4.4**, with additional blue line with open circles that represents the surface coastal meridional wind stress (TY_{int} from OGCM, averaged within the same domains as T10, N/m^2/month) shifted forward by 1 month (leading T10 by 1 month, in agreement with **Figure 5.6**) and averaged over the duration of the coastal event.

Correlations	Southern Angola	ABF	Northern Namibia
T10 – TY	-0.82	-0.67	-0.36
T10 – EKW2	0.72	0.79	0.75
EKW2 - TY	-0.52	-0.58	-0.25 (x)

Table 5.1: Correlation between intensities of OLM IEKW mode 2 (EKW2) along the equatorial Atlantic and T10, TY (local meridional wind stress) calculated in the three coastal zones (Southern Angola, ABF and Northern Namibia). The cross in the last column means no statistically significant at 95%.

Also, during the extreme coastal warm events 1962/1963 and 1976/1977, northerly wind stress anomalies are associated with positive anomalies of T10 observed in the Southern Angola zone, but are not observed in the 2 other domains (**Figure 5.4**). This suggests that there was no upwelling favourable wind in Northern Namibia during the 1962/1963 and 1976/1977 extreme warm events. This means that these extreme coastal events are not associated with variations of the upwelling favourable wind stress in Northern Namibia but could be favoured by weaker than normal local wind stress along the Angola Coast. **Figure 5.5** is an update of **Figure 4.4** and illustrates the intensities of the equatorial forcing (IEKW mode 2) and the local forcing (TY) with respect to each of the anomalous coastal T10 anomalies events. Note that the original time series of anomalies of IEKW mode 2 along the equatorial Atlantic and local meridional wind stress anomalies are shifted forward to lead the T10 anomalies by 1 month before computing the intensities with respect to the period when the coastal events occur. **Figure 5.5** gives a better appreciation of this opposite relationship. In most of the coastal event cases, positive or negative T10 anomalies are associated with positive or negative intensities of IEKW mode 2 anomalies, concomitantly with negative or positive intensities of local meridional wind stress anomalies along the west coast of Africa. This confirms that both forcings could act concomitantly as part of a large-scale forcing during the onset of the coastal events for some specific cases as observed in **Figures 5.1c** and **5.2c**. For example, it is the case for the Benguela Niñas 1983, 1991/1992, 1996/1997 which are associated with negative intensity of IEKW mode 2 (upwelling equatorial Kelvin wave) and a positive intensity of local meridional wind stress anomalies (strong

alongshore wind stress than seasonal average), both forcing observed 1 month before the onset of the cold events. Conversely, Benguela Niño events 1995, 1997/1998, 2010/2011 are linked to positive intensity of IEKW mode 2 (downwelling equatorial Kelvin wave) and a negative intensity of local meridional wind stress anomalies (weak alongshore wind stress than seasonal average) observed 1 month before the onset of the cold events. For some coastal events, the intensity of T10 anomalies, IEKW mode 2 and local meridional wind stress anomalies can match only over one or two zones of interest as described previously. For example, **Figure 5.5c** reveals the presence of upwelling favourable wind stress in Northern Namibia (intensity of local meridional wind stress ~2 N/m^2/month) during the 1962/1963 Benguela Niño which could have stopped or damp the extreme warm event in Northern Namibia. However, in Southern Angola (**Figure 5.5a**) there is a link between intensities of T10 anomalies (~ 20°C/month), IEKW mode 2 (~ 10 cm/month) and local wind stress (~ -10 N/m^2/month). This means that 1 month before the onset of the coastal event, downwelling IEKW mode 2 propagates in phase with weaker than normal meridional wind stress along the Angolan coast. In the ABF zone (**Figure 5.5b**), intensities of T10 and IEKW mode 2 remain constant, but the wind stress start to become stronger than normal (~5 N/m^2/month). During the extreme warm coastal event 1976/1977, weaker than normal wind stress are present (intensity of ~ -3 N/m^2/month) in Southern Angola (**Figure 5.5a**). Surprisingly, this extreme warm coastal event is associated with an upwelling EKW mode 2 (intensity of ~-1 cm/month). At the same time, the wind stress becomes stronger than normal in the ABF zone (**Figure 5.5b**) and Northern Namibia (**Figure 5.5c)** leading to stronger than normal upwelling favourable wind stress. It means that the 1976/1977 extreme warm event might not have equatorial origin and could be locally forced in Southern Angola since alongshore wind stress is weaker than usual. T10 anomalies are then advected poleward across the ABF up to 24°S (*cf.* **Figures 4.7** and **4.8**) even though the upwelling favourable wind stresses are present in the ABF zone and Northern Namibia. Even though there is no wind driven upwelling in Southern Angola, the relationship between local wind stress and T10 anomalies seems to work well for the 1976/1977 extreme warm event. The local meridional wind stress in Southern Angola is also linked to the large-scale wind pattern as depicted in **Figures 5.1c** and **5.1d** as this event was used to composite the T10 anomalies. Correlation values shown in **Table 5.1** (1st row) mean that there is a negative correlation of -0.82 statistically significant at 95% between intensity of T10 anomalies and intensity of local meridional wins stress (TY). The

correlation between TY and T10 decrease in absolute value as we move polewards, but remains statistically significant at 95% (**Table 5.1,** 1st row). Statistically significant anti–correlations at 95% of -0.52 and -0.58 are found between intensities of IEKW mode 2 and TY from Southern Angola to ABF zone respectively (**Table 5.1**, 3rd row). It means that 1 month before the onset of a coastal warm or cold interannual events, downwelling or upwelling EKW propagate along the equatorial Atlantic whereas weaker or stronger than normal meridional winds are present in Southern Angola and the ABF zone respectively. It means that wind forced EKW in the western equatorial Atlantic could be part of the large-scale wind stress pattern as shown in **Figures 5.1** and **5.2**. In Northern Namibia, there is a non-significant correlation at 95% between intensities of IEKW mode 2 and TY anomalies. Moreover, **Figures 5.1c** and **5.2c**, **Table 5.1** (1st row) show that meridional wind stress anomalies in Northern Namibia domain are less correlated with T10 anomalies than in the two other zones. This could be explained by the fact that the Northern Namibia domain is more dynamic (upwelling zone) than the Southern Angola and ABF domains, which even makes the identification of anomalous event difficult. For example, in **Figure 4.3a**, out of 26 extreme events, only 17 were recorded in Northern Namibia while it was 26 for the each of the 2 other zones of interest.

Figure 5.6 shows lag correlations between local meridional wind stress (TY) and T10 anomalies in the three zones of interest respectively. Negative correlation ~-0.5 statistically significant at 95% occurs when the local meridional wind stress anomalies lead the T10 anomalies by 1 month in Southern Angola, in ABF zone (~-0.3), but by 0 to 1 month in Northern Namibia (~-0.3) for the period 1958 – 2015. This is expected in an upwelling region where coastal ocean responds rapidly to upwelling-favourable wind stress. This is also confirmed in the Southern Namibia upwelling region (25°S to 30°S), where the meridional wind stress anomalies and T10 anomalies are strongly anti-correlated (~-0.56) at lag 0 (not shown). Meridional wind stresses are weak throughout the year in Southern Angola (**Figure 5.3** and **5.4a**) where the highest correlation is found (**Table 5.1**, 1st row) and as discussed, some extreme coastal events (1962/1963 and 1976/1977) are not associated with northerly wind stress anomalies in the ABF zone and Northern Namibia. Statistically significant correlations at 95% are also observed when the detrended anomalies of meridional win stress lead the T10 by 0 and 10 months in Southern Angola (**Figure 5.6a**), 0 to 7 months in the ABF zone (**Figure 5.6b**) and 0 to 2 months in Northern Namibia (**Figure 5.6c**).

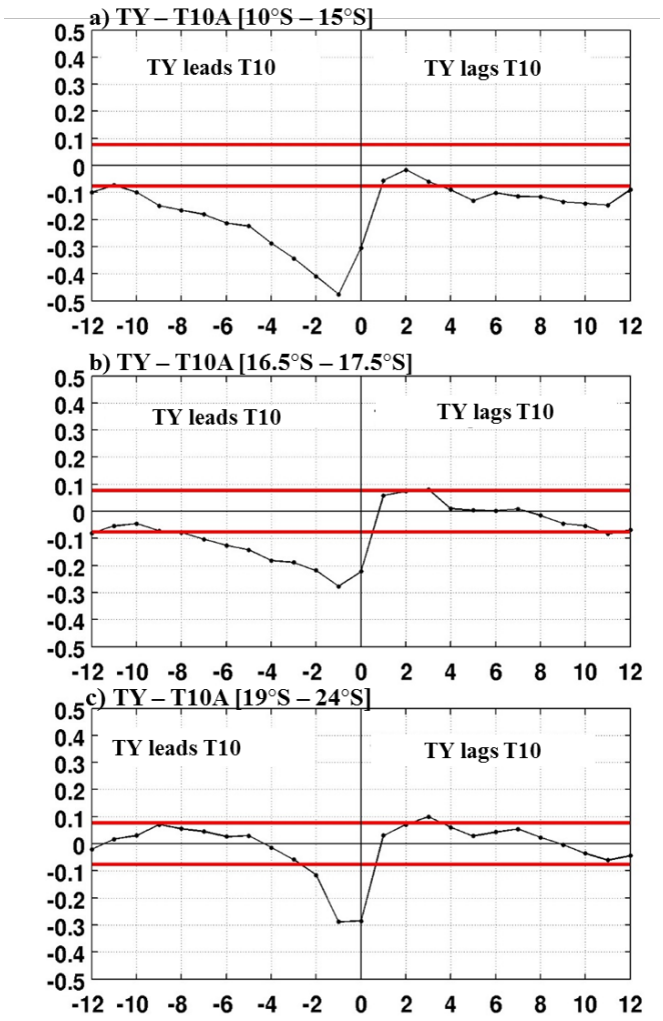

Figure 5.6: Local correlation analysis between monthly detrended normalized anomalies of OGCM meridional wind stress (TY) and T10 anomalies (T10A) in a) Southern Angola averaged from 10°S to 15°S and from the coast to 1°offshore in function of the Lag (in months); b) Angola Benguela Front region averaged from 16.5°S to 17.5°S and from the coast to 1° offshore in function of the Lag (in months); and c) Northern Namibia averaged from 19°S to 24°S and from the coast to 1° offshore in function of the Lag (in months). For all the panels, negative lags indicate that TY leads. The 95% statistically significant correlation threshold is indicated by red lines.

Lagged correlation for each calendar month between the two time series is performed in order to investigate in which month or season the best correlation occurs between the two

parameters. This lag correlation is presented in **Figure 5.7**. Results show negative correlation (statistically significant at 95%) of -0.64, -0.73 and -0.54 occurring in March-April-May (MAM) respectively when meridional wind stress anomalies (TY) lead T10 anomalies in Southern Angola by 1 month. There is also a high anti-correlation (statistically significant at 95%) of ~-0.6 occurring in April respectively when meridional wind stress anomalies (TY) lead T10 anomalies in Southern Angola by 2 months. These correlations indicate a strong link between austral fall T10 anomalies and meridional wind stress anomalies 1 month and 2 months earlier in Southern

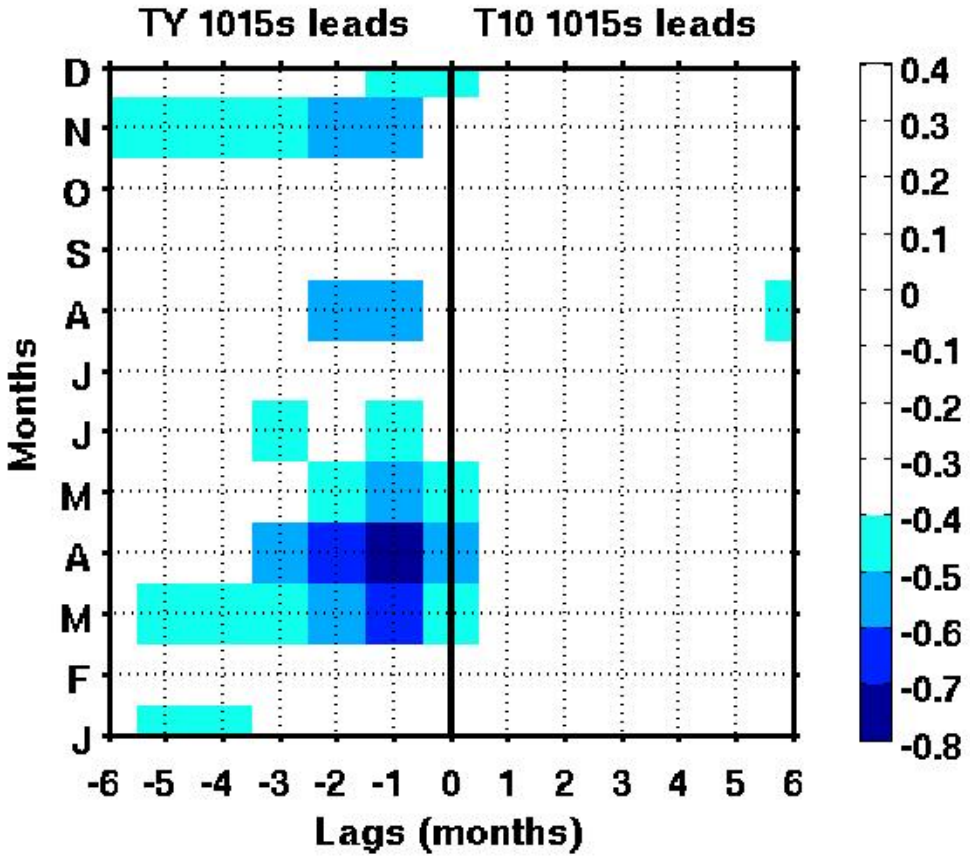

Figure 5.7: Lag correlation between detrended anomalies of OGCM meridional wind stress (TY) and T10 averaged in Southern Angola and presented at each month of the year. Correlations statistically significant at the 95% level are greater than 0.4 and lower than -0.4.

Angola mostly in March – April and April respectively. This is consistent with **Figures 5.1b, 5.1c,** and **Figures 5.2b, 5.2c** where extreme warm and cold coastal events peaking in March – April are associated with large-scale wind pattern encompassing northerly and southerly wind stress anomaly respectively. This large-scale wind stress pattern develops in January – February (2 months before the peak) and intensifies 1 month later (February – March) along the Angolan coast. The presence of these alongshore wind stress anomalies along the Angolan coast is also noticeable during the peak of the coastal events (March – April) and could justify the correlation

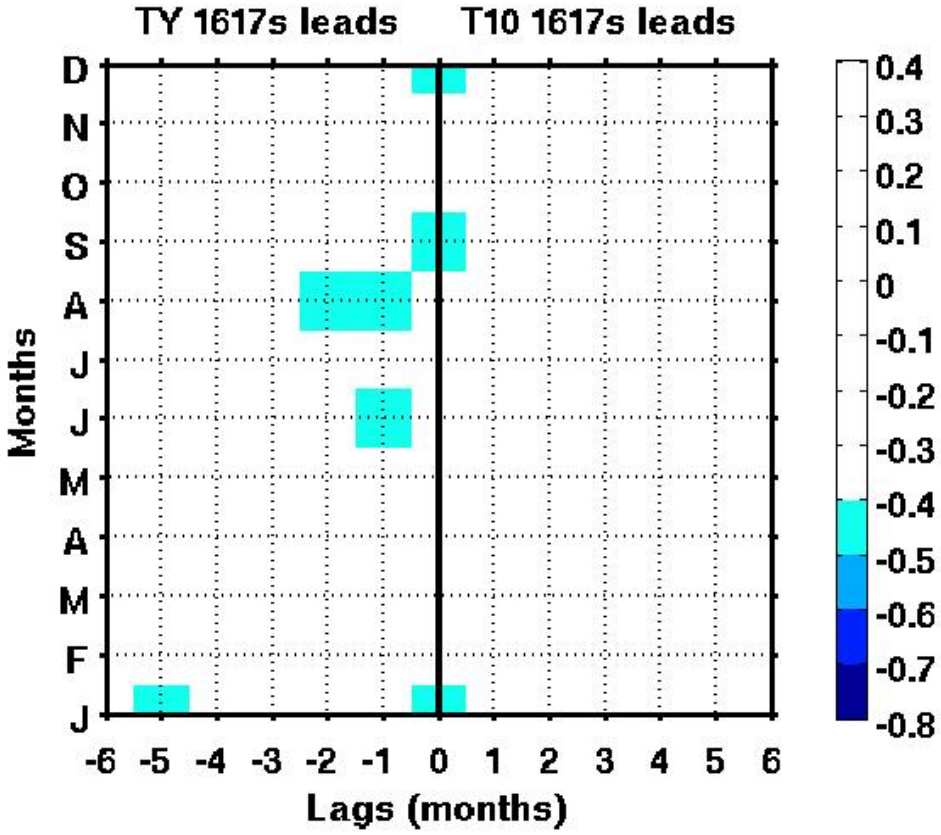

Figure 5.8: Lag correlation between modelled detrended anomalies of OGCM meridional wind stress (TY) and T10 averaged in the Angola Benguela Front zone and presented at each month of the year from 1958 - 2015. Correlations statistically significant at the 95% level are greater than 0.4 and lower than -0.4.

at lag 0 observed in April **(Figures 5.6 and 5.7)**. Moreover, the austral fall period corresponds to

the beginning of the northward migration of the SAA which could modify the local wind stress intensity during its ascension. Similar results were found by *Lübbecke et al.* [2010] who observed a correlation of -0.65 between the time series of interannual anomalies of February SAA index using sea level pressure averaged over 40°S to 20°S and 30°W to 10°W and SST in March averaged in the ABA box (10°S - 20°S and 8°E to the coast) between 1982 - 2007. Band of strong negative correlations (~ -0.5) appears in August (November) when the meridional wind stress anomalies lead the T10 anomalies by 1 to 2 (1 to 5) months. It means that austral winter/spring meridional wind stress anomalies influence T10 anomalies in the following season (or 1 to 2 seasons) later respectively.

Southward, in the ABF zone, the significant correlation shading areas are reduced compared to **Figure 5.7**. The same analysis presented in **Figure 5.7** is performed for the ABF zone in **Figure 5.8.** In August, correlation of ~-0.4 are reported when meridional wind stress anomalies (TY) lead T10 anomalies in the ABF zone by 1 to 2 months as in Southern Angola (**Figure 5.7**). At lag 0, correlation of ~-0.4 are also found in January, September and December between the two time series, meaning that the major warm or cold coastal events occur simultaneously with the weakening or strengthening of the local meridional wind stress which is part of the large-scale wind pattern. This result suggests that the anomalous events could be favoured by the local winds anomalies in the ABF zone since the coastal events are remotely forced by EKW from October to April [*Imbol Koungue et al.,* 2017]. However, meridional wind stress in the ABF zone could be linked to the major coastal events occurring in Austral winter (June and August) at lag -1. There is no correlation in austral fall (March-April-May) in the ABF zone. This is also observed in **Figures 5.1** and **5.2**, where there are no wind stress anomalies along the coast in the ABF zone for the composite of extreme warm and cold events.

Figure 5.9 shows that the two time series in Northern Namibia are correlated at lag 0 (from January to February and from August to December) and at lag -1 (in January, June, August - September and December). There is no statistically significant correlation between March and May, during the Benguela Niños and Niñas peak season [*Rouault et al*. 2017]. This is most likely due the weak vertical stratification of the ocean in austral autumn and winter (associated with a well-mixed surface layer, **Figure 5.10** and **Figure 5.11**), that inhibits the signature of the temperature vertical advection in the surface layer. But the highest anti–correlations (< -0.5) occur in January, September, November, December at lag 0 meaning that the local wind stress

anomalies could favour the development of the T10 anomalies in Northern Namibia. Correlations lesser than -0.5 are also observed in August - September at lag -1.

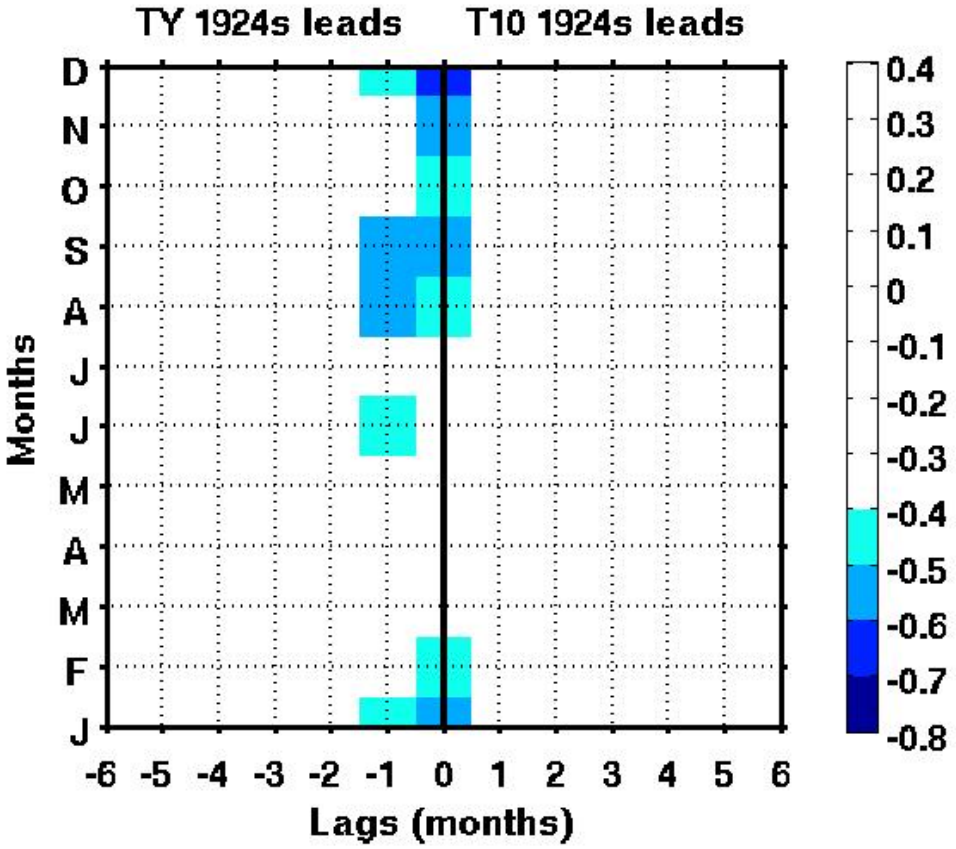

Figure 5.9: Lag correlation between modelled detrended anomalies of OGCM meridional wind stress (TY) and T10 averaged in the Northern Namibia zone and presented at each month of the year from 1958 - 2015. Correlations statistically significant at the 95% level are greater than 0.4 and lower than -0.4.

In conclusion, for most of the interannual coastal events, both remote oceanic and local atmospheric forcings are observed simultaneously being part of a large-scale forcing as concluded in **section 5.1**. At the monthly scale, local atmospheric forcing is more correlated with anomalous coastal events occurring in Southern Angola despite the total absence of upwelling favourable winds in Southern Angola mainly during March-April-May. Some anomalous coastal events are not identified in Northern Namibia most likely due to the upwelling dynamics. The

latter yields a well-mixed upper ocean that can reduce the signature of the anomalous coastal event. In this context, the following section will discuss the role of the local stratification in the coastal fringe during the interannual warm and cold coastal events.

5.4 MODULATION OF THE EVENT INTENSITY BY THE LOCAL VERTICAL STRATIFICATION

In the ocean, vertical density structure in water column is primarily controlled by ocean temperature and salinity. At interannual timescales, Benguela Niños or Niñas are mostly

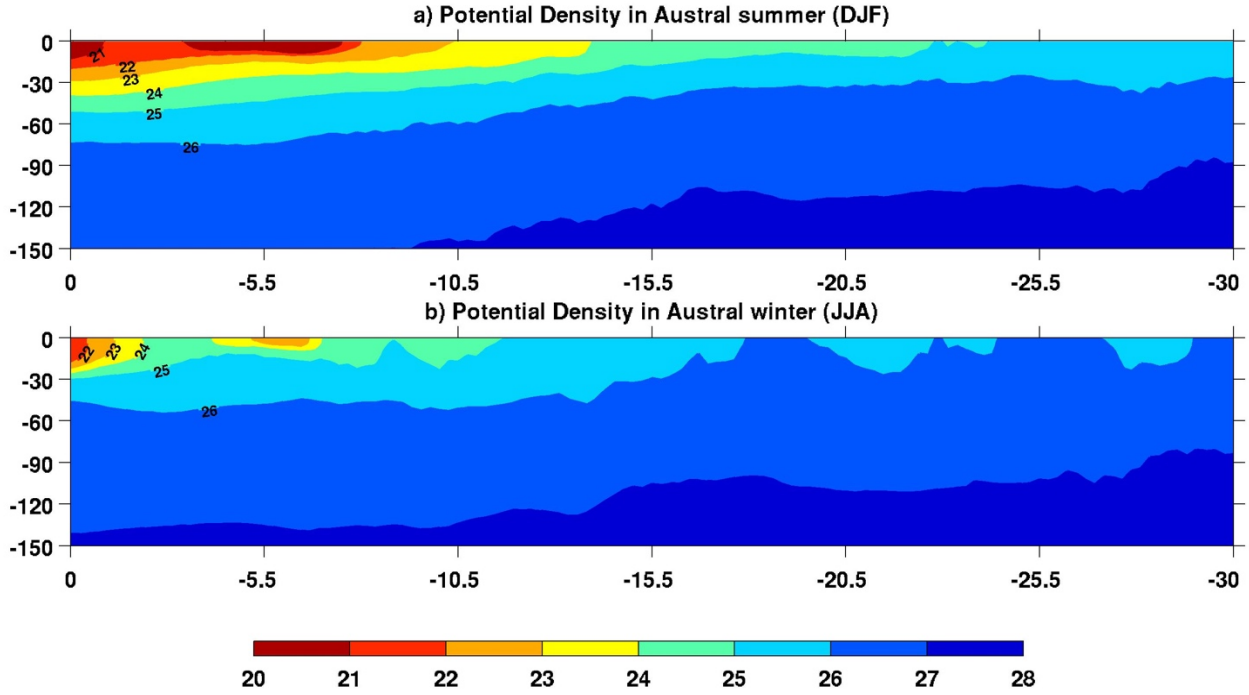

Figure 5.10: a) Vertical section of potential density derived from OGCM temperature and salinity, averaged within 1° coastal fringe from 30°S to 0°S and presented in the upper 150 m during: a) austral summer (DJF). From the red to blue means from less dense to denser waters. b) Same as a) but for austral winter (JJA). The seasonal cycle of potential density is computed from 1958 to 2015. Contours represent every 1 sigma layer.

remotely forced via equatorial Kelvin waves propagations [*Bachèlery et al.,* 2016a; *Imbol Koungue et al.,* 2017]. Forced downwelling or upwelling coastal trapped waves propagate

poleward along the southwest African coastal strengthening or reducing the local current magnitude. These coastal trapped waves could also change the vertical density gradient (vertical stratification). Depending on the season, the vertical stratification could modulate the signature of the coastal trapped waves at the sea surface. It has been suggested by *Bachèlery et al.* [2016a] and *Imbol Koungue et al.* [2017] that local stratification could modulate the major coastal events (*cf.* **Chapter 3**). As argued in **Chapter 3 (section 3.2.4),** most of the major and minor coastal events occurred between October and April (**Figures 3.8 and 4.3**) and the occurrences of these coastal events were attributed to the local stratification which was favourable to the imprint of these coastal events at the surface during this season. Hence, it is important to quantify the local vertical stratification at seasonal scale.

Figure 5.10 shows the nearshore potential density (averages within the 1°-width coastal fringe) derived from OGCM temperature and salinity during two seasons (the austral summer and the austral winter) along the southwest African coast from 30°S to 0°S. The seasonal cycle of potential density was first computed over 1958 – 2015. Less dense water layers are found at the top of the dense colder waters associated with lower densities (isopycnals 20 - 25) in austral summer than in austral winter. The lowest value of the potential density $\sigma = 20$ is found in austral summer (**Figure 5.10a**) at the surface around 6°S location of the Congo River. This low potential density is associated with the runoff discharge of the Congo River in the Atlantic Ocean. Note that the realism of this model simulation with regards to the prescribed river runoff has already been proved by the study of *Hernandez et al.* [2016] with the same resolution. A well-structured and stratified water column in austral summer compared to the one in austral winter. In December-January-February (**Figure 5.10a**), a rise of isopycnals tilted poleward and outcropping South of 23°S is observed. This allows cooler and denser upwelled waters to be at the surface marking the signature of the upwelling regime. Also, according to *Bachèlery et al*. [2016a], the Lüderitz upwelling cell causes abrupt change in stratification south of 26°S.

During austral winter (**Figure 5.10b**), the Congo River signature associated with low density waters in the upper layers at ~ 6°S, is not well marked as in austral summer (**Figure 5.10a**). The isopycnal $\sigma = 26$ outcrops 3 times (around 18°S, 25.5°S and 28°S) and the less dense water is located in the upper 30 m at ~ 0°S and 5.5°S. This could lead to affirm that the nearshore water column along the southwest African coast is more stable and stratified in austral summer than in austral winter. To better appreciate the water column stratification along the southwest

Atlantic Ocean, the Brunt Väisälä Frequency (N) is calculated using the formula:

$$N = \sqrt{\frac{g}{\rho_0}\frac{\partial \rho}{\partial z}}$$

where g is the gravity acceleration 9.8 $m.s^{-2}$, ρ_0 is the reference density taken at 1025 $kg.m^{-3}$ and $\partial\rho/\partial z$ is the vertical density gradient. The mean austral summer (DJF) and austral winter (JJA) seasons are shown in **Figure 5.11** similarly to **Figure 5.10**. It is important to remind that the Brunt-Väisälä frequency (N), is often used to express the degree of stratification [*Väisälä*, 1925],

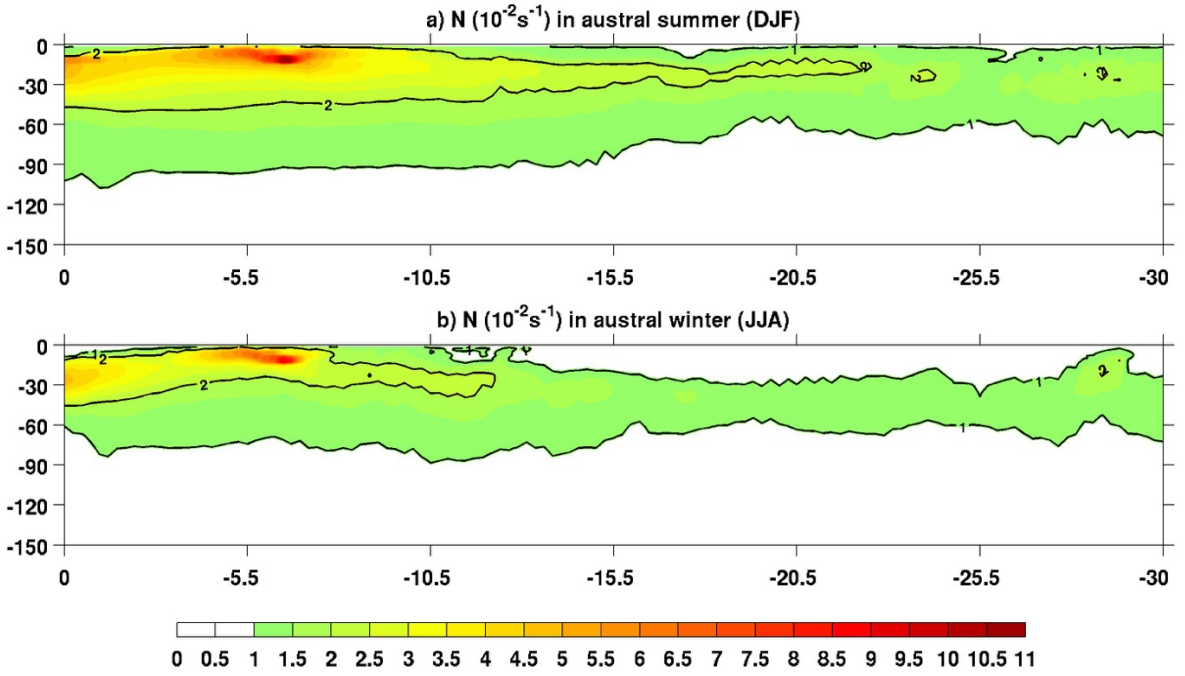

Figure 5.11: Vertical section of Brunt Väisälä Frequency given by N in $10^{-2}s^{-1}$ computed from OGCM over 1958 to 2015 averaged within 0.5° coastal fringe from 30°S to 0°S and presented in the upper 150 m during: a) Austral summer (DJF) b) Same as a) but for Austral winter (JJA). Contours represent 0.01 s^{-1} and 0.02 s^{-1}. Values between 0 and 0.01 s^{-1} are negligible.

or more precisely, the natural frequency of oscillation for a water parcel displaced adiabatically from its rest position. The largest vertical density gradient through the water column will imply

high values of *N*. In **Figure 5.11a** high values of *N* are located in the upper 100 m with maximum of 0.11 s^{-1} around 6°S in the upper 10 m. Note that maximum values of *N* are found within the thermocline as they are associated with strong temperature gradients. This latitude (6°S) corresponds to the place where the runoff (less dense fresher water) from the Congo River flows into the Atlantic Ocean (**Figure 5.10a**). The wind stress is weak throughout the year in the Southern Angola domain (**Figure 5.3**), also north of it, which induces weak vertical mixing in the upper ocean, increasing the local coastal surface stratification with the presence of warm tropical waters at the surface. This might explain the presence of strong stratification north of 12°S during the two seasons. The iso-contour 0.02 s^{-1} can be observed from the 0°S in the upper 40 m continuously up to around the latitude of 23°S in the upper 15 m and twice separately south of 24°S. The iso-contour 0.02 s^{-1} is close to the surface around 23°S, suggesting the end of the strong stratification. Notably, at this latitude (~23°S), **Figure 5.10a** shows that the isopycnal σ = 25 reaches the surface. Note the presence of iso-contour 0.01s^{-1} from the surface to 100 m depth at 0°S all the way to 30°S, where it is observed in the upper 70 m. The presence of the iso-contour 0.02 s^{-1} continuously up to 23°S where it is close to the surface and the presence of the iso-contour 0.01 s^{-1} up to 30°S suggests that south of 23°S, the stratification is weak either in austral summer or in austral winter as it is an upwelling area. The upper ocean layers are permanently mixed, and this suggests that south of 25°S, it is difficult to track the CTW at the sea surface. However, in austral winter (**Figure 5.11b)**, the highest value of *N* (0.09 s^{-1}) is observed around the Congo River area (~6°S) as in **Figure 5.11a**. South of 13°S, the 0.01 s^{-1} contour deepens to around 30 m and in the upper 30 m, there is no stratification. *Bachèlery et al.* [2016a] suggested that the stratification of the water column along the southwest African coast controls the efficiency by which CTW can trigger temperature anomalies through vertical advection process. A strong and well stratified water column is observed in austral summer up to ~23°S meaning that change in water column characteristics during the propagation of CTW will be more effective in austral summer than in austral winter. In austral summer vertical stratification will be more prone to track the CTW at the sea surface at least up to around 23°S. After quantifying the seasonal vertical stratification of the water column and arguing its seasonal influence on the CTW propagations, the vertical stratification variations at interannual timescales is investigated. Note that it is difficult to disentangle the signature of the CTW onto the stratification from the modulation of the CTW signature due to the variations of the vertical

stratification at interannual timescales. Therefore, time series of vertical temperature gradient, vertical stratification and correlation table between parameters shown below are computed at lag

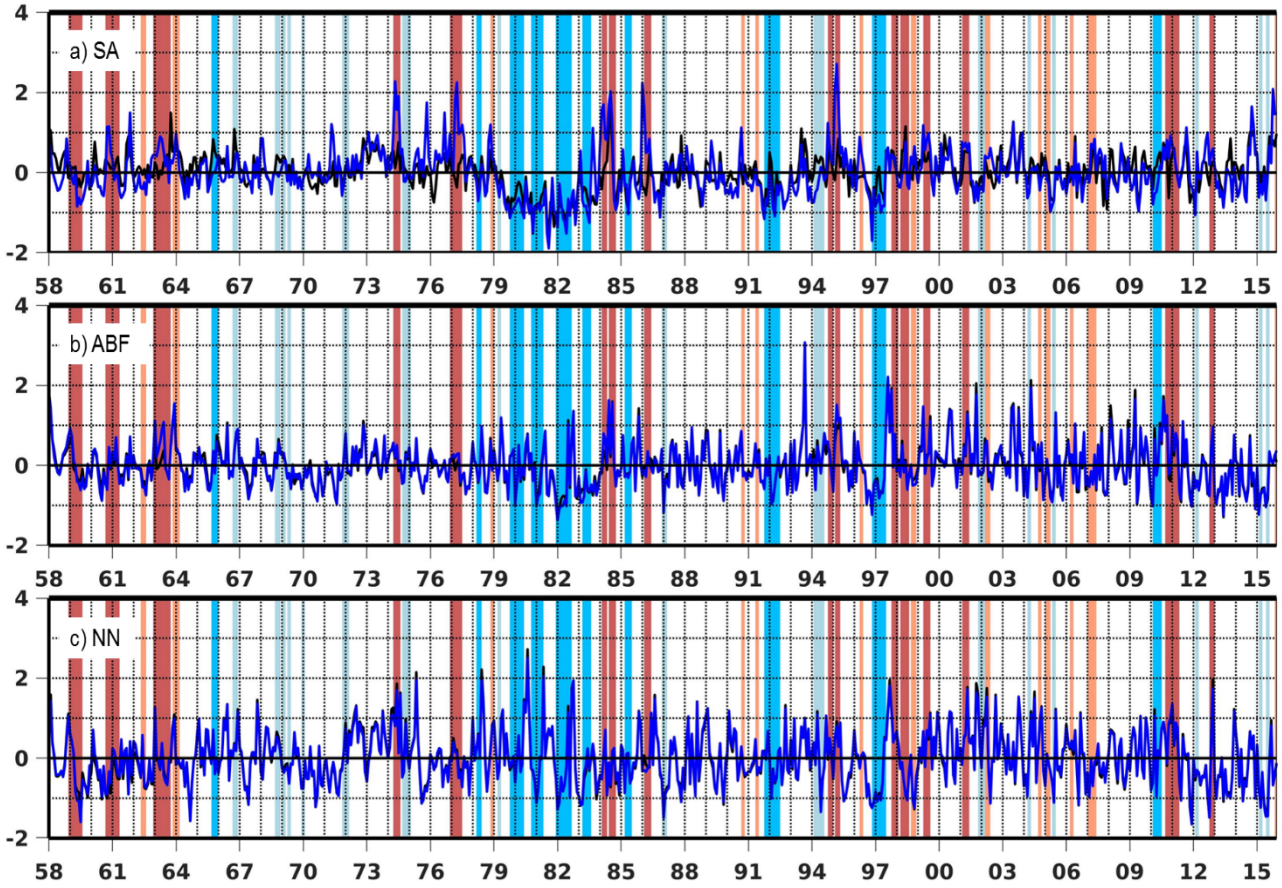

Figure 5.12: OGCM Monthly detrended normalized anomalies from 1958 to 2015 of N (blue line) and Vertical Temperature Gradient (VTG) (black line) averaged in the upper 50 m in a) Southern Angola averaged from 10°S to 15°S and from the coast to 1°offshore; b) Angola Benguela Front region averaged from 16.5°S to 17.5°S and from the coast to 1° offshore; c) Northern Namibia averaged from 19°S to 24°S and from the coast to 1° offshore. Red (blue) and light red (light blue) rectangles represent extreme warm (cold) and moderate warm (cold) coastal events respectively along the Angolan-Namibian coastlines identified in **Figure 4.1**.

0. **Figure 5.12** presents the detrended normalized anomalies of vertical temperature gradient *(-∂T/∂z)* and the Brunt Väisälä frequency *N* averaged within the upper 50 m in the three coastal

zones of interest at lag 0. The term *(-∂T/∂z)* is computed because I did not consider the (-) in the calculation of the Brunt Väisälä frequency. From the top to the bottom panels, most of the positive or negative anomalous coastal events are linked to positive or negative anomalies of vertical temperature gradient and the Brunt Väisälä frequency respectively. This result indicates that mostly during the anomalous warm and cold coastal events, the water column stratification given by the Brunt Väisälä frequency tends to anomalously increase and decrease respectively. This means that the water column and the vertical stratification move together. Also, this anomalous increase or decrease of the vertical stratification will depend on the season (**Figure 5.11**). Similarly, the vertical temperature gradient anomalies averaged in the upper 50 m seems to vary concomitantly with the anomalies of Brunt Väisälä frequency according to positive or negative coastal events.

Correlations	Southern Angola	ABF	Northern Namibia
VTG - N	0.67	0.98	0.99
N - T10	0.64	0.39	0.48

Table 5.2: Correlation between vertical temperature gradient (VTG), Brunt Väisälä frequency N, both averaged in the upper 50 m and T10 monthly detrended normalized anomalies averaged in Southern Angola, ABF zone and Northern Namibia).

The fact that the vertical gradient of temperature and the Brunt Väisälä frequency seem to vary in the same way in general, means that as vertical temperature gradient anomalously increases and decreases during positive and negative coastal events, the local stratification anomalously increases and decreases in the upper 50 m respectively. This is because the Brunt Väisälä frequency is function of the vertical temperature gradient. Moreover, vertical temperature gradient and Brunt Väisälä frequency anomalies vary similarly in the ABF and Northern Namibia zones. This is confirmed in **Table 5.2** (1st row) where the correlations between the 2 parameters are almost 1. However, in Southern Angola, there is a correlation of 0.67 between vertical temperature gradient and Brunt Väisälä frequency anomalies. This low correlation in

Southern Angola compared to ABF and Northern Namibia zones is due to the Brunt Väisälä frequency anomalies which is not only function of vertical temperature gradient anomalies. Brunt Väisälä frequency in Southern Angola could be highly impacted by intrusion of anomalous salinity waters coming from the surrounding river runoffs during warm or cold events. Also, in Southern Angola, T10 anomalies are more correlated with the Brunt Väisälä frequency (0.64) compared to vertical temperature gradient (0.39). This coherence between the two parameters is expected since the negative vertical temperature gradient is proportional to the vertical density gradient. For the interannual variations of local vertical stratification, it is important to mention that it is not possible to know if it is the local vertical stratification which is at the origin of the signature of the coastal events or if it is the coastal events which modify the local vertical stratification, and at which level the modification of the vertical stratification will influence the coastal events.

5.5 SUMMARY

In this section, OGCM T10 interannual anomalies are used to compute a composite analysis using 5 extreme coastal warm and cold events that peak in March – April and look at the large-scale wind stress pattern during the onset and the development of these extreme coastal events. Results suggest that significant maximum warming and cooling areas extend from the equatorial Atlantic to the southeastern Atlantic up to ~25°S along the Namibian coastline for both categorized events. However, cooling spatial pattern during the cold coastal event covers a larger area than the warming one in the tropical Atlantic. Also, Benguela Niña events seem to persist more than Benguela Niños. A tendency of Atlantic Niño or Niña to follow Benguela Niño or Niña is observed. Lagged composites of temperature at 10 m and wind stress anomalies reveal that both local and remote forcings develop simultaneously 1-2 months before the peak of Benguela Niños or Niñas (**Figures 5.1bc** and **5.2bc**). Evidences of ocean-atmosphere coupling were also depicted south of the equator mainly during the extreme warm and cold events. For example, Wind-Evaporation-SST feedback seemed to be at work 1 month before the peak of warm (cold) events (**Figure 5.1c** (**Figure 5.2c**)) with weakened (strengthened) southeasterly trade wind in the southern tropic impacting the wind stress circulation along the Angolan coast.

The role played by local wind stress as part of the large-scale wind stress circulation is also investigated. Results suggest that during most of the warm or cold anomalous coastal events, northerly or southerly wind stress anomalies are observed along the west African coast **(Figure 5.4 and 5.5)**, but mainly in Southern Angola (**Table 5.1**) despite the total absence of upwelling favourable winds in Southern Angola. Local meridional wind stress anomalies could favour the development of anomalous coastal events.

OGCM outputs (temperature and salinity) have been used to quantify the seasonal vertical stratification of the water column between 1958 and 2015. Results showed that local stratification is stronger in austral summer than austral winter (**Figure 5.11**), mostly north of 12°S where we find river discharges into the Atlantic Ocean (Congo river at around 6°S). Therefore, austral summer vertical stratification will be more prone to imprint the signature of the coastal trapped wave at the sea surface at least up to around 23°S. This is in agreement with the suggestion of *Bachèlery et al*. [2016a] and confirms the results of **Chapter 3 (section 3.2.4)**. In Southern Angola, local vertical stratification could be under the influence of intrusion of salinity anomalies from surrounding river runoffs.

CHAPTER 6

6 DISCUSSION, CONCLUSIONS AND PERSPECTIVES

The tropical southeastern Atlantic variability is examined at interannual timescales from 1958 to 2015 with a focus on the variability in the Benguela upwelling system, along the coast of Angola, Namibian and South Africa. The thesis objectives aim to understand the processes associated with the phenology of the Benguela Niños and Benguela Niñas events, their links with the equatorial Atlantic Ocean and the potential contribution of the local forcing in the southeastern Atlantic Ocean.

A first analysis is conducted from 1998 to 2012 period (15 years) because 1) PIRATA program provides in situ data from September 1997 only and 2) surface wind forcing is available to us until end of 2012. This study is the first to use a long time series (15 years) of PIRATA data to systematically detect equatorial Kelvin wave propagations along the equatorial Atlantic. This emphasizes the originality and uniqueness of this thesis. Additionally, satellite altimetry and outputs of an Ocean Linear Model were used.

Most of our results are obtained through time series analysis predominantly composed of monthly anomalies relative to the seasonal cycle. Note that interannual and intraseasonal variabilities are present in the time series when the monthly seasonal cycle is removed from the monthly time series to calculate the anomalies. *Bachèlery et al*. [2016a] showed that along the Angola – Namibia coastline only interannual coastal variability is associated with remote equatorial forcing, while intraseasonal timescales are mostly triggered by local atmospheric forcing (in agreement with *Goubanova et al.* [2013]). Considering SSHA equatorial propagations with amplitude exceeding 1 standard deviation of the time series for at least two consecutive months, allows filtering out most of the intraseasonal variability. It is the same for anomalous SSTA coastal events for which the amplitude exceeds 1 standard deviation of the time series during at least three consecutive months. This also ensures that the analysed timescales of variability lies in the same time-frequency range as the one of *Bachèlery et al*. [2016a] or longer period (18 months) as reported by *Florenchie et al*. [2004] when analysing

coastal SSTA time series.

Over the 1998-2012 period, the interannual OLM SSH outputs agree well with the equatorial observations emphasizing the dominance of the equatorial wave propagation signal on the equatorial variability over this period. This result allows us to extend the results from *Illig et al.* [2004] over a more recent period. 18 strong eastward equatorial Kelvin wave episodes in PIRATA and altimetric observations: 12 strong downwelling and 6 strong upwelling Kelvin waves are detected when using a methodology based on temporal and spatial coherence is applied to the OLM outputs. Note that not removing the linear trend in all the time series of anomalies would have impacted our results during the identification of the anomalous coastal events. Removing the trend also favours better comparison between the different products (in situ, satellite data, and model outputs). In the equatorial band, the second baroclinic mode of IEKW is the most energetic mode in agreement with findings of *Illig et al.* [2004]. Strong equatorial Kelvin wave signals are linked to Benguela Niño or Benguela Niña events along the western African coast. As illustrated in **Table 3.3**, performing correlations between time series of anomalies of IEKW mode 2 and coastal SST over the periods of strong interannual equatorial activities (removed uncorrelated equatorial propagations with coastal variability) increases the correlation values. Moreover, the seasonal cycle of the 5-month running correlation between equatorial activity and coastal variability over the identified strong equatorial propagation periods shows that values of the lag correlation between equatorial variability and SSTA in Southern Angola and in the Angola Benguela Front region reaches 0.75 in austral summer from October – April (**Figure 3.8b**). This result is encouraging to set up an early warning system for the Benguela Niño and Niña along the west African coast between Angola and Namibia. Along the west African coast, 12 out of 18 strong equatorial propagation of IEKW appear to be well connected with the warm or cold events This implies that 1/3 of strong equatorial propagations of IEKW mode 2 (positive episodes 2002 (March–May), 2007 (September–December), 2008 (April–July), 2009 (April–June) and negative episodes 2009 (June–September) and 2011 (May–August)) are not correlated with the coastal events. These uncorrelated events occur mostly in austral winter and could be due to the impact of local forcing (wind forcing) or the modulation of the signature of the anomalous coastal events by the local coastal stratification. The variability associated with the local surface forcing can be in phase or out of phase with the equatorial remote forcing and consequently could increase or weaken the signature of the remote equatorial

forcing along the western coast of Africa respectively. The local stratification being weak in Austral winter, it would be inefficient to imprint the SSTA or hinder the CTW signature at the surface during the onset of warm or cold coastal events.

A correlation of 0.65 statistically significant at 95% (**Table 3.1**) between PIRATA dynamic height anomalies and OLM SSHA at [0°E; 0°N] allows the exploitation of the OLM in combination with an OGCM to investigate all the anomalous equatorial propagations and coastal events from 1958 to 2015. Following the methodology developed in *Imbol Koungue et al.* [2017], 55 anomalous coastal events are depicted, divided into 26 extreme events (16 warm, 10 cold) and 29 moderate (13 warm and 16 cold) anomalous events over the period 1958 to 2015. 8 newly identified warm interannual coastal events have been recorded; namely, the extreme warm events 1958/1959 (December – July), 1960/1961 (September - April), 1974 (April - July). Similarly, undocumented extreme cold events are identified in 1965 (September - December), 1978 (March – May), 1979/1980 (October - May), 1980/1981 (October - April), 1985 (March - June). Most of these extreme warm and cold events occurred in the 3 coastal zones of interest excluding extreme cold events 1965 (September - December), 1978 (March – May) which develop only in Southern Angola and ABF zone. Note that few differences are observed in terms of period of the events (start and end) with the identified events in **Chapter 3**. For example, it was the case of the 2010/2011 (November – April) anomalous extreme coastal warm event in **Chapter 3** and the 2010/2011 (September – April) using the OGCM in **Chapter 4**. This has to be attributed to the difference in length of the time series (58 years for OGCM *vs*. 15 years for the PIRATA period) which yields different monthly climatology, standard deviations and then different normalized anomalies. Also, the fact that OGCM does not perfectly agree with observations and the presence of warm bias along the Angola Benguela Current system could impact the time series by increasing or reducing the duration of a coastal event. This could also justify the fact that some anomalous coastal events identified in **Chapter 3** are missing in **Chapter 4** for example, coastal warm events 2003 (July – December), 2008/2009 (November–January) which do not fulfil the criterion over the 1958-2015 period.

Over the 1958 to 2015 period, most of the extreme and moderate coastal warm or cold events are linked to downwelling or upwelling IEKW mode 2 propagations in agreement with **Chapter 3**. There is a 1-month lag when detrended anomalies of IEKW mode 2 leads surface temperature anomalies in Southern Angola and the ABF zone. Peak distributions of each

category of anomalous coastal events show that coastal events tend to peak during austral spring and late summer between October and April which is consistent with findings of **Chapter 3**. A poleward flow dominates the seasonal cycle of modelled meridional transport across the ABF in the upper 120 m with a minimum in October (~-1.4 Sv). This result does not fully agree with the finding of *Rouault* [2012] who used a different OGCM from 1982 – 2002 and found a bi-annual cycle in the modelled meridional transport across the ABF in the upper 250 m with two minima (February and October) and a reversal flow (equatorward flow) in June. This discrepancy has to be attributed to the different modelled meridional velocities (maximum or minimum meridional velocities position) provided by both simulations. At interannual timescales, meridional transport anomalies across the ABF might contribute to the development of anomalous coastal events as meridional transport anomalies could be linked to the passage of CTW at the ABF. Surprisingly, a lag of 2 months is found when detrended anomalies of net mass transport across the ABF lead surface temperature anomalies in the Northern Namibia zone which is consistent with the study of *Rouault* [2012] who reported a lag ranging between 2 – 4 months. As observed in **Figure 4.9,** the correlation at lag -1 month in Northern Namibia **(**~-0.15) is also significant at 95%, like for the equatorial forcing (**Figure 4.5**). The fact that maximum anti-correlation occurs at 2 month-lag (one month before the IEKW mode 2 forcing) could be due to the contribution of higher-order IEKW modes which propagate slower than IEKW mode 2 or to the effect of the large-scale wind stress forcing. **Figure 4.9** displays lags of 1 to 6 months when detrended normalized anomalies of meridional transport across the ABF lead detrended normalized anomalies of surface temperature in Northern Namibia. This range of lags (1 – 6 months) could be attributed to the slow advection of tropical waters in the Northern Benguela upwelling domain as found by *Rouault* [2012] or the speed or strength of the poleward undercurrent [*Mohrholz et al.,* 2008]. Across the ABF, the estimation of meridional temperature transport compared to the estimation of the mass transport across ABF zone does not allow to strengthen the statistics used to highlight the connexion between the dynamics in the ABF region and the coastal temperature variability. It implies that the advection of anomalous warm or cold waters across the ABF and its link to anomalous coastal events in Northern Namibia can be well explained by the net mass transport across the ABF. February-March-April composite analysis (**Figures 4.13** and **4.14**) of detrended surface temperature anomalies performed along with December-January-February average meridional transport anomalies across the ABF and January-February-March average of

IEKW mode 2 anomalies along the equatorial reveals that all the extreme warm or cold events are linked to downwelling or upwelling propagations of IEKW along the equatorial wave guide during JFM, except the newly identified extreme warm events 1958/1959, 1960/1961 and extreme warm event 2010/2011. As agreed earlier, meridional transport anomalies across the ABF in DJF are not always associated with anomalies of surface temperature in Northern Namibia in FMA. This was the case for the Benguela Niñas 1985, 2010 and Benguela Niños 1962/1963 and 1974. The strongest poleward flow across the ABF occurs in DJF 2000/2001 compared to the other 8 extreme warm events (**Table 4.3**) and the strongest equatorward or weakest poleward flow across the ABF is recorded during DJF 1979/1980 compared to the other 7 extreme cold events (**Table 4.4**). The strongest amplitude of downwelling EKW occurs in JFM 1984 (**Table 4.3**). Conversely, the strongest amplitude of upwelling EKW occurs in JFM 1997 (**Table 4.4**).

In the tropical Atlantic Ocean, composite maps of T10 surface temperature and wind stress anomalies of extreme coastal events that peak in March – April show that cooling or warming pattern is observed up to ~25°S along the Namibian coastline. This latitude corresponds to the southernmost latitude where the coastal trapped wave propagations can be detected on coastal the surface temperature signal [*Bachèlery et al.,* 2016a] being linked to anomalous coastal events. Benguela Niña events seem to persist more than Benguela Niño which agrees with the finding of *Florenchie et al.* [2004]. A tendency of Atlantic Niño or Niña to follow Benguela Niño or Niña is observed and is consistent with the previous findings of *Richter et al.* [2010] and *Lübbecke et al.* [2010]. Lagged composite maps of temperature at 10 m depth and wind stress anomalies reveal that local alongshore wind stress anomalies (local atmospheric forcing) occur concomitantly with remote forcing. Both local and remote forcing develop simultaneously 1-2 months before the peak of Benguela Niño or Niña in the tropical Atlantic Ocean and in North of the ABF. The analysis of these composite maps also reveals that wind stress anomalies along the equator are linked to coastal wind stress anomalies, which means that there is a large-scale pattern of wind stress. This large-scale circulation of wind stress persists during the peak of Benguela Niño or Niña. This suggests that both forcings (local and remote) are part of basin-scale weakening or strengthening of the wind stress during Benguela Niño or Niña respectively. This is consistent with the modelling study of *Lübbecke et al.* [2010] from 1958 to 2000 in which correlation map between April SST and February wind stress revealed

that the whole SAA weakens prior to the Benguela warming and comprises weak trade winds and coastal winds. Ocean-atmosphere coupling process seems to be at work (1 month before the peak and during the peak of the event) as northwesterly or southeasterly wind stress anomalies are present over the warming or cooling area south of the equator (**Figures 5.1c, d** and **5.2c, d**). At the monthly scale, local atmospheric forcing (part of the large-scale wind) is more correlated with anomalous coastal events occurring in Southern Angola (**Table 5.1**) despite the total absence of upwelling favourable winds in Southern Angola. This could be explained by, the ocean-atmosphere coupling south of the equator up to ~10°S which can lead to an intensification of northerly wind stress anomalies in Southern Angola. This could also explain the strong anti-correlation observed in Southern Angola (**Figure 5.6a** and **5.7**) when local meridional wind stress anomalies lead surface temperature anomalies by 1 month compared to the other coastal zones of interest. However, a potential contribution of the local surface heat fluxes has not been investigated in Southern Angola. Past studies [*Florenchie et al.,* 2004; *Rouault et al.,* 2007; *Bachèlery et al.*, 2016a] showed that local surface heat fluxes tend to damp the anomalous events in the ABA box. Along the west African coast, the austral summer vertical stratification is more prone to imprint the signature of the coastal trapped wave at the sea surface at least up to around 23°S. This agrees with the suggestion of *Bachèlery et al*. [2016a] and confirms the results of **Chapter 3 (section 3.2.4)**. Results show that in Southern Angola, the local vertical stratification could be under the influence of intrusion of salinity anomalies created by the surrounding river runoffs. Moreover, local vertical stratification anomalies are found to be more correlated with the vertical temperature gradient anomalies in the ABF zone and Northern Namibia at lag 0.

In conclusion, an OLM can be easily run using real-time satellite wind estimates or atmospheric model outputs. PIRATA parameters such as dynamic height and Z20, altimetry data are very important since they are available at real-time and could be used to set up an early warning system for anomalous coastal events in the southeast Atlantic Ocean (Benguela Niños or Niñas) or in the eastern equatorial Atlantic (Atlantic Niños). This could enable the creation of a bulletin for the Tropical Atlantic, as in the Pacific for El Niño or La Niña. The PIRATA array of moorings is very important for the monitoring of the Equatorial Kelvin wave activities and needs to be maintained. Across the ABF, the advection of warm or cold waters in the Northern Benguela upwelling system is a key factor for the development of anomalous coastal events. Composite maps revealed that during the peak season of Benguela Niño and Niña (March –

April), warming or cooling pattern was observed up to ~25°S along the Namibian coastline and Benguela Niña events last more than Benguela Niños. A tendency of Atlantic Niño or Niña to follow Benguela Niño or Niña has been observed. Both forcing (local and remote) could be part of basin-scale weakening or strengthening of the wind stress 1-2 months before the peak of Benguela Niño or Niña. Ocean-atmosphere coupling seems to be at work as northwesterly or southeasterly wind stress anomalies are observed over the warming or cooling area south of the equator East of 20°W. Local atmospheric forcing is more correlated with most of the anomalous warm and cold coastal events in Southern Angola (a non-upwelling wind-driven zone). This might be explained by the possible amplification of local wind stress in the Southern Angola through the ocean-atmosphere coupling process abovementioned which leads to contribute to the development of major warm and cold coastal events. Lastly, the results from this thesis open the possibility to predict Benguela Niños and Niñas, especially from October to April when the coastal water column is well stratified, using an Ocean Linear Model forced by wind speed, and altimetry and PIRATA data. Tide gauge and current meter available in real time in Angola and Namibia would complete the system and are much needed.

Further work will involve a study of the specific coastal events for which the equatorial index failed to explain the coastal interannual variability, although some answers can already be found in the literature. The link between the Southern Angola and Northern Namibia domains needs to be better ascertain. Also, this study stresses out the importance to better ascertain the role of local variability (strength of local stratification, cloud cover, and turbulent fluxes) for each Benguela Niño and Benguela Niña event over 1958–2015. The role of the near coastal wind stress curl which drives the poleward boundary current will be analyzed. Moreover, possible correlation between meridional wind stress anomalies further equatorward with T10 anomalies further poleward will be performed. For this matter, the OGCM outputs provide each term of the heat budget calculated in the subsurface. This will be done in continuation of this study. In particular, more work is needed regarding the impact of the vertical ocean stratification on the coastal trapped wave thermodynamical signature and the impact of coastal interannual events on the coastal vertical stratification. The link between the surface detrended normalized temperature anomalies in Northern Namibia and the detrended normalized anomalies of meridional transport across the ABF needs to be investigated, in order to be able to explain the lags of 8 to 10 months

found when coastal surface temperature anomalies lead meridional transport anomalies.

BIBLIOGRAPHY

Bachèlery, M. L., Illig, S., Dadou, I. (2016a). Interannual variability in the South-East Atlantic Ocean, focusing on the Benguela Upwelling System: Remote versus local forcing. *Journal of Geophysical Research: Oceans*, *121*(1), 284-310.

Bachèlery, M. L., Illig, S., Dadou, I. (2016b). Forcings of nutrient, oxygen, and primary production interannual variability in the southeast Atlantic Ocean. *Geophysical Research Letters*, *43*(16), 8617-8625.

Bachèlery, M-L., (2016). Variabilité cotière physique et biogéochimique en Atlantique Sud-Est : rôle du forçage atmosphérique local versus téléconnexion océanique. PhD thesis, University of Toulouse, Toulouse, France, 219 pp.

Bakun, A., Black, B. A., Bograd, S. J., Garcia-Reyes, M., Miller, A. J., Rykaczewski, R. R., Sydeman, W. J. (2015). Anticipated effects of climate change on coastal upwelling ecosystems. *Current Climate Change Reports*, *1*(2), 85-93.

Belmadani, A., Echevin, V., Dewitte, B., Colas, F. (2012). Equatorially forced intraseasonal propagations along the Peru-Chile coast and their relation with the nearshore eddy activity in 1992–2000: A modeling study. *Journal of Geophysical Research: Oceans*, *117*(C4).

Berrit, G. R., and C. A. Dias (1977). Hydroclimatologie des Régions Côtières de L'Angola. Cahiers ORSTOM, Séries Océanographie, 15: 181– 196.

Best, D. J., Roberts, D. E. (1975). Algorithm AS 89: the upper tail probabilities of Spearman's rho. *Journal of the Royal Statistical Society. Series C (Applied Statistics)*, *24*(3), 377-379.

Binet, D., Gobert, B., Maloueki, L. (2001). El Niño-like warm events in the Eastern Atlantic (6 N, 20 S) and fish availability from Congo to Angola (1964–1999). *Aquatic Living Resources*, *14*(2), 99-113.

Bourlès, B., Lumpkin, R., McPhaden, M. J., Hernandez, F., Nobre, P., Campos, E., Yu, L., Planton, S., Busalacchi, A., Moura, A. D., Servain, J. (2008). The PIRATA program: history, accomplishments, and future directions. *Bulletin of the American Meteorological Society*, *89*(8), 1111-1125.

Boyd, A. J., Salat, J., Masó, M. (1987). The seasonal intrusion of relatively saline water on the shelf off northern and central Namibia. *South African Journal of Marine Science*, *5*(1), 107-120.

Boyer, D. C., Hampton, I. (2001). An overview of the living marine resources of Namibia. *African Journal of Marine Science*, *23*, 5-35.

Boyer, D. C., Boyer, H. J., Fossen, I., Kreiner, A. (2001). Changes in abundance of the northern Benguela sardine stock during the decade 1990–2000, with comments on the relative importance of fishing and the environment. *African Journal of Marine Science*, *23*, 67-84.

Brandt, P., Funk, A., Tantet, A., Johns, W. E., Fischer, J. (2014). The Equatorial Undercurrent in the central Atlantic and its relation to tropical Atlantic variability. *Climate dynamics*, *43*(11), 2985-2997.

Bubnov, V. A. (1972). Structure and characteristics of oxygen minimum layer in southeastern Atlantic. *OCEANOLOGY-USSR*, *12*(2), 193-201.

Burmeister, K., Brandt, P., Lübbecke, J. F. (2016). Revisiting the cause of the eastern equatorial Atlantic cold event in 2009. *Journal of Geophysical Research: Oceans*, *121*(7), 4777-4789.

Cane, M. A., Sarachik, E. S. (1976). Forced baroclinic ocean motions. 1. Linear equatorial unbounded case. *Journal of Marine Research*, *34*(4), 629-665.

Cane, M. A., Sarachik, E. S. (1979). Forced baroclinic ocean motions. III- The linear equatorial basin case. *Journal of Marine Research*, *37*, 355-398.

Cane, M. A., Patton, R. J. (1984). A numerical model for low-frequency equatorial dynamics. *Journal of physical oceanography*, *14*(12), 1853-1863.

Carton, J. A., Huang, B. (1994). Warm events in the tropical Atlantic. *Journal of Physical Oceanography*, *24*(5), 888-903.

Chassot, E., Bonhommeau, S., Dulvy, N. K., Mélin, F., Watson, R., Gascuel, D., Le Pape, O. (2010). Global marine primary production constrains fisheries catches. *Ecology letters*, *13*(4), 495-505.

Chavez, F. P., Messié, M. (2009). A comparison of eastern boundary upwelling ecosystems. *Progress in Oceanography*, *83*(1-4), 80-96.

Clarke, A. J. (1983). The reflection of equatorial waves from oceanic boundaries. *Journal of Physical Oceanography*, *13*(7), 1193-1207.

Colas, F., Capet, X., McWilliams, J. C., Shchepetkin, A. (2008). 1997–1998 El Niño off Peru: A numerical study. *Progress in Oceanography*, *79*(2-4), 138-155.

Colberg, F., Reason, C. J. C. (2006). A model study of the Angola Benguela Frontal Zone: Sensitivity to atmospheric forcing. *Geophysical research letters*, *33*(19).

Colberg, F., Reason, C. J. C. (2007). Ocean model diagnosis of low-frequency climate variability in the South Atlantic region. *Journal of Climate*, *20*(6), 1016-1034.

Dai, A., Trenberth, K. E. (2002). Estimates of freshwater discharge from continents: Latitudinal and seasonal variations. *Journal of hydrometeorology*, *3*(6), 660-687.

Dee, D. P., Uppala, S. M., Simmons, A. J., Berrisford, P., Poli, P., Kobayashi, S., Andrae, U., Balmaseda, M. A., Balsamo, G., Bauer, P., Bechtold, P., Beljaars, A. C. M., van de Berg, L., Bidlot, J., Bormann, N., Delsol, C., Dragani, R., Fuentes, M., Geer, A. J., Haimberger, L., Healy, S. B., Hersbach, H., Hólm, E. V., Isaksen, L., Kållberg, P., Köhler, M., Matricardi, M., McNally, A. P., Monge-Sanz, B. M., Morcrette, J.-J., Park, B.-K., Peubey, C., de Rosnay, P., Tavolato, C., Thépaut, J.-N., and Vitart, F. (2011). The ERA-Interim reanalysis: configuration and performance of the data assimilation system. *Q.J.R. Meteorol. Soc.,* 137(656):553–597.

Diaconis, P., Efron, B. (1983). Computer-intensive methods in statistics. *Scientific American*, *248*(5), 116-131.

Dias, C. A. (1983a). Note on the evidence of a permanent southward flow of the upper oceanic tropospheric waters off Angola at 12° S. *Collection of Scientific Papers International Commission for the Southeast Atlantic Fisheries*, *10*, 99-102.

Dias, C. A. (1983). Preliminary report on the physical oceanography off southern Angola, March and July 1971. *Collection of Scientific Papers International Commission for the Southeast Atlantic Fisheries*, *10*, 103-116.

Ding, H., Keenlyside, N. S., Latif, M. (2009). Seasonal cycle in the upper equatorial Atlantic Ocean. *Journal of Geophysical Research: Oceans*, *114*(C9).

Doi, T., Tozuka, T., Sasaki, H., Masumoto, Y., Yamagata, T. (2007). Seasonal and interannual variations of oceanic conditions in the Angola Dome. *Journal of Physical Oceanography*, *37*(11), 2698-2713.

Du Penhoat, Y., Treguier, A. M. (1985). The seasonal linear response of the tropical Atlantic Ocean. *Journal of physical oceanography*, *15*(3), 316-329.

Ducet, N., Le Traon, P. Y., Reverdin, G. (2000). Global high-resolution mapping of ocean circulation from TOPEX/Poseidon and ERS-1 and-2. *Journal of Geophysical Research: Oceans*, *105*(C8), 19477-19498.

Dussin, R., Barnier B., Brodeau L. (2016). The making of Drakkar forcing set DFS5, DRAKKAR/MyOcean Rep. 01–04-16, Laboratoire de Glaciologie et Géophysique de l'Environnement, Grenoble, France.

Efron, B., (1977). Bootstrap methods: another look at the jackknife. *Ann. Statist.* 7 1-26.

Eisma, D., Van Bennekom, A. J. (1978). The Zaire river and estuary and the Zaire outflow in the Atlantic Ocean. *Netherlands Journal of Sea Research*, *12*(3-4), 255-272.

Enfield, D. B., Cornejo-Rodriguez, M. D. P., Smith, R. L., Newberger, P. A. (1987). The Equatorial source of propagating variability along the Peru coast during the 1982–1983 El Niño. *Journal of Geophysical Research: Oceans*, *92*(C13), 14335-14346.

Field, J. G., Shillington, F. A. (2006). Variability of the Benguela current system (16, E). *The sea: The global coastal ocean: Interdisciplinary regional studies and syntheses*, *14*, 835-863.

Florenchie, P., Lutjeharms, J. R., Reason, C. J. C., Masson, S., Rouault, M. (2003). The source of Benguela Niños in the south Atlantic Ocean. *Geophys. Res. Lett. 30 (10), 1505.* http://dx.doi.org/10.1029/2003GL017172.

Florenchie, P., Reason, C. J. C., Lutjeharms, J. R. E., Rouault, M., Roy, C., Masson, S. (2004). Evolution of interannual warm and cold events in the southeast Atlantic Ocean. *Journal of Climate*, *17*(12), 2318-2334.

Foltz, G. R., McPhaden, M. J. (2010a). Interaction between the Atlantic meridional and Niño modes. *Geophysical Research Letters*, *37*(18).

Foltz, G. R., McPhaden, M. J. (2010b). Abrupt equatorial wave-induced cooling of the Atlantic cold tongue in 2009. *Geophysical Research Letters*, *37*(24).

Fréon, P., Barange, M., Aristegui, J. (2009). Eastern boundary upwelling ecosystems: integrative and comparative approaches. Preface. *Progress in Oceanography*, *83*(1-4), 1-14.

Fu, L. L. (1981). The general circulation and meridional heat transport of the subtropical South Atlantic determined by inverse methods. *Journal of Physical Oceanography*, *11*(9), 1171-1193.

Gammelsrød, T., Bartholomae, C. H., Boyer, D. C., Filipe, V. L. L., O'toole, M. J. (1998). Intrusion of warm surface water along the Angolan Namibian Coast in February–March 1995: the 1995 Benguela niño. *African Journal of Marine Science*, *19*.

García-Reyes, M., Sydeman, W. J., Schoeman, D. S., Rykaczewski, R. R., Black, B. A., Smit, A. J., Bograd, S. J. (2015). Under pressure: Climate change, upwelling, and eastern boundary upwelling ecosystems. *Frontiers in Marine Science*, *2*, 109.

Garzoli, S. L., Gordon, A. L. (1996). Origins and variability of the Benguela Current. *Journal of Geophysical Research: Oceans*, *101*(C1), 897-906.

Gordon, A. L., Bosley, K. T. (1991). Cyclonic gyre in the tropical South Atlantic. *Deep Sea Research Part A. Oceanographic Research Papers*, *38*, S323-S343.

Goubanova, K., Illig, S., Machu, E., Garçon, V., Dewitte, B. (2013). SST subseasonal variability in the central Benguela upwelling system as inferred from satellite observations (1999–2009). *Journal of Geophysical Research: Oceans*, *118*(9), 4092-4110.

Grotjahn, R., Faure, G. (2008). Composite predictor maps of extraordinary weather events in the Sacramento, California, region. *Weather and Forecasting*, *23*(3), 313-335.

Hardman-Mountford, N. J., Richardson, A. J., Agenbag, J. J., Hagen, E., Nykjaer, L., Shillington, F. A., Villacastin, C. (2003). Ocean climate of the South East Atlantic observed from satellite data and wind models. *Progress in Oceanography*, *59*(2-3), 181-221.

Hazeleger, W., de Vries, P., Friocourt, Y. (2003). Sources of the Equatorial Undercurrent in the Atlantic in a high-resolution ocean model. *Journal of Physical Oceanography*, *33*(4), 677-693.

Hernandez, O., Jouanno, J., Durand, F. (2016). Do the Amazon and Orinoco freshwater plumes really matter for hurricane-induced ocean surface cooling? *Journal of Geophysical Research: Oceans*, *121*(4), 2119-2141.

Hernandez, O., Jouanno, J., Echevin, V., Aumont, O. (2017). Modification of sea surface temperature by chlorophyll concentration in the Atlantic upwelling systems. *Journal of Geophysical Research: Oceans, 122(7), 5367-5389*.

Hirst, A. C., Hastenrath, S. (1983). Atmosphere-ocean mechanisms of climate anomalies in the Angola-tropical Atlantic sector. *Journal of Physical Oceanography*, *13*(7), 1146-1157.

Hormann, V., Brandt, P. (2009). Upper equatorial Atlantic variability during 2002 and 2005 associated with equatorial Kelvin waves. *Journal of Geophysical Research: Oceans*, *114*(C3).

Hu, Zeng-Zhen, and Bohua Huang. "Physical processes associated with the tropical Atlantic SST gradient during the anomalous evolution in the southeastern ocean." *Journal of climate* 20.14 (2007): 3366-3378.

Illig, S., Dewitte, B., Ayoub, N., Du Penhoat, Y., Reverdin, G., De Mey, P., Bonjean, F., Lagerloef, G. S. E. (2004). Interannual long equatorial waves in the tropical Atlantic from a high-resolution ocean general circulation model experiment in 1981–2000. *Journal of Geophysical Research: Oceans*, *109*(C2).

Illig, S., Dewitte, B. (2006). Local coupled equatorial variability versus remote ENSO forcing in an intermediate coupled model of the tropical Atlantic. *Journal of climate*, *19*(20), 5227-5252.

Imbol Koungue, R., A., Illig, S., Rouault, M. (2017). Role of interannual Kelvin wave propagations in the equatorial Atlantic on the Angola Benguela Current system. *Journal of Geophysical Research: Oceans*, *122*(6), 4685-4703.

Junker, T., Schmidt, M., Mohrholz, V. (2015). The relation of wind stress curl and meridional transport in the Benguela upwelling system. *Journal of Marine Systems*, *143*, 1-6.

Junker, T., Mohrholz, V., Siegfried, L., van der Plas, A. (2017). Seasonal to interannual variability of water mass characteristics and currents on the Namibian shelf. *Journal of Marine Systems*, *165*, 36-46.

Kalnay, E., Kanamitsu, M., Kistler, R., Collins, W., Deaven, D., Gandin, L., Iredel, M., Saha, S., White, G., Woollen, J., Zhu, Y., Chelliah, M., Ebisuzaki, W., Higgins, W., Janowiak, J., Mo, K. C., Ropelewski, C., Wang. J., Leetmaa, A., Reynolds, R., Jenne, R., Joseph, D. (1996). The NCEP/NCAR 40-year reanalysis project. *Bulletin of the American meteorological Society*, *77*(3), 437-471.

Katz, E. J. (1977). Zonal pressure-gradient along equatorial Atlantic. *Journal of Marine Research*, *35*(2), 293-307.

Kopte, R., Brandt, P., Dengler, M., Tchipalanga, P. C. M., Macuéria, M., Ostrowski, M. (2017). The Angola Current: Flow and hydrographic characteristics as observed at 11° S. *Journal of Geophysical Research: Oceans*, *122*(2), 1177-1189.

Kopte, R. (2017). The Angola Current in a Tropical Seasonal Upwelling System Seasonal Variability in Response to Remote Equatorial and Local Forcing. PhD thesis, Christian-Albrechts-University, Kiel, Germany, 151 pp.

Koseki, S., Keenlyside, N., Demissie, T., Toniazzo, T., Counillon, F., Bethke, I., Ilicak, M., and Shen, M. L. (2017). Causes of the large warm bias in the Angola–Benguela Frontal Zone in the Norwegian Earth System Model. *Climate Dynamics*, 1-20.

Laing, A., Evans, J. L. (2011). Introduction to tropical meteorology. *Educational material from The COMET Program*.

Large, W. G., Yeager, S. G. (2009). The global climatology of an interannually varying air–sea flux dataset. *Climate dynamics*, *33*(2-3), 341-364.

Lass, H. U., Schmidt, M., Mohrholz, V., Nausch, G. (2000). Hydrographic and current measurements in the area of the Angola–Benguela Front. *Journal of Physical Oceanography*, *30*(10), 2589-2609.

Lass, H. U., Mohrholz, V. (2008). On the interaction between the subtropical gyre and the Subtropical Cell on the shelf of the SE Atlantic. *Journal of Marine Systems*, *74*(1-2), 1-43.

Le Clus, F. (1985). Effects of a warm water intrusion on the anchovy fishery in Namibia. *Collection of Scientific Papers International Commission for the Southeast Atlantic Fisheries*, *12*(1), 99-106.

Le Traon, P. Y., Nadal, F., Ducet, N. (1998). An improved mapping method of multisatellite altimeter data. *Journal of atmospheric and oceanic technology*, *15*(2), 522-534.

Leth, O., Middleton, J. F. (2006). A numerical study of the upwelling circulation off central Chile: Effects of remote oceanic forcing. *Journal of Geophysical Research: Oceans*, *111*(C12).

Li, G., Xie, S. P. (2012). Origins of tropical-wide SST biases in CMIP multi-model ensembles. *Geophysical Research Letters*, *39*(22).

Liu, W. T., Tang, W., Polito, P. S. (1998). NASA scatterometer provides global ocean-surface wind fields with more structures than numerical weather prediction. *Geophysical Research Letters*, *25*(6), 761-764.

Locarnini, R. A., Mishonov, A. V., Antonov, J. I., Boyer, T. P., Garcia, H. E., Baranova, O. K., Zweng, M. M., Paver, C. R., Reagan, J. R., Johnson, D. R., Hamilton, M., and Seidov, D. 00 (2013). World Ocean Atlas 2013, Volume 1: Temperature. S. Levitus, Ed., A. Mishonov Technical Ed.; NOAA Atlas NESDIS 73, 40 pp.

Lübbecke, J. F., Böning, C. W., Keenlyside, N. S., Xie, S. P. (2010). On the connection between Benguela and equatorial Atlantic Niños and the role of the South Atlantic Anticyclone. *Journal of Geophysical Research: Oceans*, *115*(C9).

Lutz, K., Jacobeit, J., Rathmann, J. (2015). Atlantic warm and cold water events and impact on African west coast precipitation. *International Journal of Climatology*, *35*(1), 128-141.

Madec, G. (2014). NEMO ocean engine (Draft edition r5171), Note du Pole de modelisation 27, Institut Pierre-Simon Laplace, France, ISSN No 1288-1619.

Maraldi, C., Chanut, J., Levier, B., Ayoub, N., De Mey, P., Reffray, G., Lyart, F., Cailleau, S., Drévillon, M., FanJul, E., Sotillo, M. G., Marsaleix, P., and Mercator Team. (2013). NEMO on the shelf: assessment of the Iberia-Biscay-Ireland configuration. *Ocean Science*, *9*, 745-771.

Marchesiello, P., McWilliams, J. C., and Shchepetkin, A. (2003). Equilibrium Structure and Dynamics of the California Current System. J. Phys. Oceanogr., 33(4):753–783.

Marin, F., Caniaux, G., Giordani, H., Bourlès, B., Gouriou, Y., Key, E. (2009). Why were sea surface temperatures so different in the eastern equatorial Atlantic in June 2005 and 2006?. *Journal of Physical Oceanography*, *39*(6), 1416-1431.

Materia, S., Gualdi, S., Navarra, A., Terray, L. (2012). The effect of Congo River freshwater discharge on Eastern Equatorial Atlantic climate variability. *Climate dynamics*, *39*(9-10), 2109-2125.

Meeuwis, J. M., Lutjeharms, J. R. E. (1990). Surface thermal characteristics of the Angola-Benguela front. *South African Journal of Marine Science*, *9*(1), 261-279.

Mercier, H., Arhan, M., Lutjeharms, J. R. (2003). Upper-layer circulation in the eastern Equatorial and South Atlantic Ocean in January–March 1995. *Deep Sea Research Part I: Oceanographic Research Papers*, *50*(7), 863-887.

Merle, J. (1978). Atlas hydrologique saisonnier de l'océan Atlantique intertropical. *Paris : ORSTOM, (82),* 184 p. (Travaux et Documents de l'ORSTOM ; 82). ISBN 2-7099-0493-4.

Mohrholz, V., Schmidt, M., Lutjeharms, J. R. E. (2001). The hydrography and dynamics of the Angola-Benguela Frontal Zone and environment in April 1999: BENEFIT Marine Science. *South African Journal of Science*, *97*(5-6), 199-208.

Mohrholz, V., Bartholomae, C. H., Van der Plas, A. K., Lass, H. U. (2008). The seasonal variability of the northern Benguela undercurrent and its relation to the oxygen budget on the shelf. *Continental Shelf Research*, *28*(3), 424-441.

Monteiro, P. M., and van der Plas, A. K. (2006). 5 Low oxygen water (LOW) variability in the Benguela system: Key processes and forcing scales relevant to forecasting. In *Large Marine Ecosystems* (Vol. 14, pp. 71-90). Elsevier.

Moroshkin, K. V., Bubnov, V. A., Bulatov, R. P. (1970). Water circulation in the eastern South Atlantic Ocean. *OCEANOLOGY, VOL 10, NO 1, P 27-34, 1970. 8 P, 4 FIG, 13 REF.*

Muller, A. A., Reason, C. J. C., Schmidt, M., Mohrholz, V., Eggert, A. (2014). Computing transport budgets along the shelf and across the shelf edge in the northern Benguela during summer (DJF) and winter (JJA). Journal of Marine Systems, 140, 82-91.

Nelson, G. (1989). Poleward motion in the Benguela area. In *Poleward flows along eastern ocean boundaries* (pp. 110-130). Springer, New York, NY.

Okumura, Y., Xie, S. P. (2004). Interaction of the Atlantic equatorial cold tongue and the African monsoon. *Journal of Climate*, *17*(18), 3589-3602.

Ostrowski, M., Da Silva, J. C., Bazik-Sangolay, B. (2009). The response of sound scatterers to El Niño-and La Niña-like oceanographic regimes in the southeastern Atlantic. *ICES Journal of Marine Science*, *66*(6), 1063-1072.

Penven, P., Echevin, V., Pasapera, J., Colas, F., & Tam, J. (2005). Average circulation, seasonal cycle, and mesoscale dynamics of the Peru Current System: A modeling approach. Journal of Geophysical Research: Oceans, 110(C10).

Peterson, R. G., Stramma, L. (1991). Upper-level circulation in the South Atlantic Ocean. *Progress in oceanography*, *26*(1), 1-73.

Philander, S. G. H., Pacanowski, R. C. (1986). A model of the seasonal cycle in the tropical Atlantic Ocean. *Journal of Geophysical Research: Oceans*, *91*(C12), 14192-14206.

Pizarro, O., Clarke, A. J., Van Gorder, S. (2001). El Niño sea level and currents along the South American coast: Comparison of observations with theory. *Journal of Physical Oceanography*, *31*(7), 1891-1903.

Pizarro, O., Shaffer, G., Dewitte, B., Ramos, M. (2002). Dynamics of seasonal and interannual variability of the Peru-Chile Undercurrent. *Geophysical Research Letters*, *29*(12).

Polo, I., Lazar, A., Rodriguez-Fonseca, B., Arnault, S. (2008). Oceanic Kelvin waves and tropical Atlantic intraseasonal variability: 1. Kelvin wave characterization. *Journal of Geophysical Research: Oceans*, *113*(C7).

Poole, R., Tomczak, M. (1999). Optimum multiparameter analysis of the water mass structure in the Atlantic Ocean thermocline. *Deep Sea Research Part I: Oceanographic Research Papers*, *46*(11), 1895-1921.

Reason, C. J. C., Florenchie, P., Rouault, M., Veitch, J. (2006). 10 Influences of large scale climate modes and agulhas system variability on the BCLME region. In *Large marine ecosystems* (Vol. 14, pp. 223-238). Elsevier.

Reffray, G., Bourdalle-Badie, R., Calone, C. (2015). Modelling turbulent vertical mixing sensitivity using a 1-D version of NEMO. *Geoscientific Model Development*, *8*(1), 69.

Reverdin, G., and McPhaden, M. J. (1986). Near-surface current and temperature variability observed in the equatorial Atlantic from drifting buoys. Journal of Geophysical Research: Oceans, 91(C5), 6569-6581.

Reynolds, R. W., and Smith, T. M. (1994). Improved global sea surface temperature analyses using optimum interpolation. *Journal of climate*, *7*(6), 929-948.

Reynolds, R. W., Rayner, N. A., Smith, T. M., Stokes, D. C., Wang, W. (2002). An improved in situ and satellite SST analysis for climate. *Journal of climate*, *15*(13), 1609-1625.

Richter, I., Xie, S. P. (2008). On the origin of equatorial Atlantic biases in coupled general circulation models. *Climate Dynamics*, *31*(5), 587-598.

Richter, I., Behera, S. K., Masumoto, Y., Taguchi, B., Komori, N., Yamagata, T. (2010). On the triggering of Benguela Niños: Remote equatorial versus local influences. *Geophys. Res. Lett. 37, L20604.* http://dx.doi.org/10.1029/2010GL0444461.

Richter, I., Xie, S. P., Wittenberg, A. T., Masumoto, Y. (2012). Tropical Atlantic biases and their relation to surface wind stress and terrestrial precipitation. *Climate dynamics*, *38*(5-6), 985-1001.

Richter, I., Xie, S. P., Behera, S. K., Doi, T., Masumoto, Y. (2014). Equatorial Atlantic variability and its relation to mean state biases in CMIP5. *Climate dynamics*, *42*(1-2), 171-188.

Risien, C. M., Chelton, D. B. (2008). A global climatology of surface wind and wind stress fields from eight years of QuikSCAT scatterometer data. *Journal of Physical Oceanography*, *38*(11), 2379-2413.

Rouault, M., Florenchie, P., Fauchereau, N., Reason, C.J.C. (2003). South East tropical Atlantic warm events and southern African rainfall. *Geophys. Res. Lett. 30*. http://dx. doi.org/10.1029/2003GL014840.

Rouault, M., Illig, S., Bartholomae, C., Reason, C. J. C., Bentamy, A. (2007). Propagation and origin of warm anomalies in the Angola Benguela upwelling system in 2001. *Journal of Marine Systems*, *68*(3-4), 473-488.

Rouault, M., Servain, J., Reason, C. J. C., Bourlès, B., Rouault, M. J., Fauchereau, N. (2009). Extension of PIRATA in the tropical South-East Atlantic: an initial one-year experiment. *African Journal of Marine Science*, *31*(1), 63-71.

Rouault, M. (2012). Bi-annual intrusion of tropical water in the northern Benguela upwelling. *Geophys. Res. Lett. 39, L12606.* http://dx.doi.org/10.1029/2012GL052099.

Rouault, M., Illig, S., Lübbecke, J., Imbol, Koungue, R., A. (2017). Origin, development and demise of the 2010–2011 Benguela Niño. *Journal of Marine Systems*, in press. https://doi.org/10.1016/j.jmarsys.2017.07.007.

Schott, F. A., Mccreary, J. P., Johnson, G. C. (2004). Shallow overturning circulations of the tropical-subtropical oceans. *Earth's Climate*, 261-304.

Schouten, M. W., Matano, R. P., Strub, T. P. (2005). A description of the seasonal cycle of the equatorial Atlantic from altimeter data. *Deep Sea Research Part I: Oceanographic Research Papers*, *52*(3), 477-493.

Schülein, F. H., Boyd, A. J., Underhill, L. G. (1995). Oil-to-meal ratios of pelagic fish taken from the northern and the southern Benguela systems: seasonal patterns and temporal trends, 1951–1993. *South African Journal of Marine Science*, *15*(1), 61-82.

Seager, R., Murtugudde, R., Naik, N., Clement, A., Gordon, N., Miller, J. (2003). Air–sea interaction and the seasonal cycle of the subtropical anticyclones. *Journal of climate*, *16*(12), 1948-1966.

Servain, J., Busalacchi, A. J., McPhaden, M. J., Moura, A. D., Reverdin, G., Vianna, M., Zebiak, S. E. (1998). A pilot research moored array in the tropical Atlantic (PIRATA). *Bulletin of the American Meteorological Society*, *79*(10), 2019-2031.

Shannon, L. V. (1985). The Benguela ecosystem Part 1. Evolution of the Benguela, physical features and processes. *Oceanogr. Mar. Biol. Ann. Rev.*, *23*, 105-182.

Shannon, L. V., Boyd, A. J., Brundrit, G. B., Taunton-Clark, J. (1986). On the existence of an El Niño-type phenomenon in the Benguela system. *Journal of Marine Research*, *44*(3), 495-520.

Shannon, L. V., Agenbag, J. J., Buys, M. E. L. (1987). Large-and mesoscale features of the Angola-Benguela front. *South African Journal of Marine Science*, *5*(1), 11-34.

Shannon, L. V., Nelson, G. (1996). The Benguela: large scale features and processes and system variability. In *The South Atlantic* (pp. 163-210). Springer, Berlin, Heidelberg.

Stander, G. H., De Decker, A. H. B. (1969). Some physical and biological aspects of an oceanographic anomaly off South West Africa in 1963. *Investigational Report 81,* Division of Sea Fisheries, South Africa, 46 pp.

Stramma, L., Peterson, R. G. (1989). Geostrophic transport in the Benguela Current region. *Journal of Physical Oceanography*, *19*(10), 1440-1448.

Stramma, L., Schott, F. (1999). The mean flow field of the tropical Atlantic Ocean. *Deep Sea Research Part II: Topical Studies in Oceanography*, *46*(1-2), 279-303.

Taylor, K. E. (2001). Summarizing multiple aspects of model performance in a single diagram. *Journal of Geophysical Research: Atmospheres*, *106*(D7), 7183-7192.

Tchipalanga, P., Dengler, M., Brandt, P., Kopte, R., Macuéria, M., Coelho, P., Ostrowoski, M., Keenlyside, N. S. (2018). Eastern boundary circulation and hydrography off Angola–building Angolan oceanographic capacities. Bulletin of the American Meteorological Society, (2018).

Toniazzo, T., Woolnough, S. (2014). Development of warm SST errors in the southern tropical Atlantic in CMIP5 decadal hindcasts. *Climate dynamics*, *43*(11), 2889-2913.

Trzaska, S., Robertson, A. W., Farrara, J. D., Mechoso, C. R. (2007). South Atlantic variability arising from air–sea coupling: Local mechanisms and tropical–subtropical interactions. *Journal of climate*, *20*(14), 3345-3365.

Umlauf, L., Burchard, H. (2003). A generic length-scale equation for geophysical turbulence models. *Journal of Marine Research*, *61*(2), 235-265.

Vaisala, V. (1925). Uber die Wirkung der Windschwankungen auf die Pilot beobachtungen. *Soc. Sci. Fennica, Commentationes Phys.-Math. II*, *19*, 37.

Veitch, J. A., Florenchie, P., Shillington, F. A. (2006). Seasonal and interannual fluctuations of the Angola–Benguela Frontal Zone (ABFZ) using 4.5 km resolution satellite imagery from 1982 to 1999. *International Journal of Remote Sensing*, *27*(05), 987-998.

Veitch, J., Penven, P., Shillington, F. (2010). Modeling equilibrium dynamics of the Benguela Current System. *Journal of Physical Oceanography*, *40*(9), 1942-1964.

Verstraete, J. M. (1992). The seasonal upwellings in the Gulf of Guinea. *Progress in Oceanography*, *29*(1), 1-60.

Voituriez, B., Herbland, A. (1982). Comparaisons des systèmes productifs de l'Atlantique Tropical Est: Dômes thermiques, upwellings côtiers et upwelling équatorial. *Rapports et Procès-Verbaux des Réunions Conseil International pour l'Exploration de la Mer*, *180,* 114-130.

Wacongne, S. H. (1988). Dynamics of the equatorial undercurrent and its termination. PhD thesis, Massachusetts Institute of Technology and Woods Hole Oceanographic Institution, Cambridge, USA, 366 pp.

Wacongne, S., Piton, B. (1992). The near-surface circulation in the northeastern corner of the South Atlantic Ocean. *Deep Sea Research Part A. Oceanographic Research Papers*, *39*(7-8), 1273-1298.

Walker, N. D. (1987). Interannual sea surface temperature variability and associated atmospheric forcing within the Benguela system. *South African Journal of Marine Science*, *5*(1), 121-132.

Walter, H. 1937. Die ökologischen verhältnisse in der Namib-nebelwiiste (Siidwestafrika) unter auswertung de aufzeichnungen des Dr G. Boss (Swakopmund), in JahrbUcher fUr Wissen-schaftliche Botanik, N. Pringsheim, ed., Verlag von GebrUder Bortraeger, Leipzig, 58-222.

Wedepohl, P. M., Lutjeharms, J. R. E., Meeuwis, J. M. (2000). Surface drift in the south-east Atlantic Ocean. *African Journal of Marine Science*, *22*.

Zebiak, S. E., Cane, M. A. (1987). A Model El Niño–Southern Oscillation. *Monthly Weather Review*, *115*(10), 2262-2278.

Zebiak, S. E. (1993). Air–sea interaction in the equatorial Atlantic region. *Journal of Climate*, *6*(8), 1567-1586.